BIOKIMIKA II

Applied Chemistry

Faculty of Chemistry

Donostia

eman ta zabal zazu

Universidad del País Vasco   Euskal Herriko Unibertsitatea

Copper Homeostasis in the Filamentous Ascomycete

Aspergillus nidulans.

Applied Chemistry and Polymeric Materials PhD program

Martzel Antsotegi Uskola

2021

Supervisor:

Unai Ona Ugalde Martinez

Senior Lecturer

Faculty of Chemistry

EHU/UPV

Hauts hartatikan ustekabean

Hor agertzen da… Txirritaa

Ur pistol batez...

Fuuurra fuurraaa...

Soineko txuriz jantzita!!

Momentu zailenetan ere barre bat

atera didazuen guztiontzat...

Zuen alde

Acknowledgment

Bueno, ba iritsi da hainbestetan amestutako momentua, iritsi da abentura honen bukaera. Bost urte pasatxoren ostean, iritsi da tesia entregatu eta bizitzako etapa honi bukaera emateko unea. Prozesu guzti honen parte izan zareten guztioi edo gehienoi behintzat eskerrak emateko tartea hartu nahiko nuke hurrengo lerro hauetan.

Lehenik eta behin, prozesu honetan ezinbestekoak izan diren bi pertsonetaz oroitzea dagokit, Unai eta Ane. Unai, bide guzti honetan zure gidaritza, aholkuak eta bideak zabaltzeko ahalegina asko estimatzen dut. Tesi gidari bezala nire lan erritmoak errespetatu dituzu beti, edozein arazoren aurrean zure bulegoko ateak ireki dizkidazu eta bulegotik ateratzerakoan beti lasaiago eta gauzak argiago nituela atera izan naiz. Benetan, mila esker. Ane, "my mentor", zuri zer esango dizut ba. Urteak dira laborategia utzi zenuenetik, baina denok oroitzen gara zutaz. Zure alaitasuna, lanerako grina, beti laguntzeko prest bueltan ezer espero gabe… askotan pentsatu izan dut, "nondik ateratzen ote du emakume honek hainbesteko energia?". Nire partetik esan behar dut nik tesi hau aurrera atera izanaren merituaren zati haundi bat zurea dela. Zurekin ikasi nuen zer zen laborategiko lana, lanarekiko konpromezua eta lan ona egitearen garrantzia. Askok pentsa lezakeena baino eragin handiagoa izan duzu nire bizitzan. Zerua irabazia duzu, Ane.

Bueno, eta laborategiko beste jendilajeaz ere ezin ahaztu. Nahiz eta proiektu berean aritu ez, zuek ere guzti honen parte zarete. DJ Oilier, zuri ere gauza asko eskertu behar dizkizut, aholku eske joan naizenean beti izan duzu erantzun zintzo bat eta animo hitzak egoera edozein delarik ere. Summer lab day eta soziedadeko bazkari guztien saltsa. Hi haiz hi tipoa! Eli O eta Eli P, zuek ere aspalditxo utzi zenuten laborategia eta badakit nire laborategiko hasiera hartan txotxolo samarra nintzela, baina zuengandik ere asko ikasi nuen. Azkenik, nola ez, "mis compañeros de armas", Mikel eta Ainara, a ze bi. Zuekin dena izan da

Acknowledgment

eramangarriagoa, momentu on eta ez hain onetan ere beti elkarri adarra jotzeko prest, laneko tentsioak baretzeko barre terapia lagunak. Bakoitzak orain bere bidea hartuko dugu, baina beti izango dugu lotura estu bat. Biologiako laborategiko jendeaz ere ezingo naiz ahaztu. Maite, Goretti eta Ana plazer bat izan da zuek ezagutzea.

I would also like to remember everyone that has been part of my journeys abroad. Roberta, Emiliano, Mattia, Mickey, Anton and many more… It's been a pleasure and an honor to meet you, work with you and learn from and with you.

Lantokitik kanpoko jendeaz oroitu nahiko nuke. Gurasoek ezin aipatu gabe utzi. Beraien esku dagoen guztia eta gehiago egingo luketela behin baino gehiagotan erakutsi didate. Milioi bat aldiz eskerrak emanagatik ere labur geldituko nintzateke. Koadrilakoei ere eskerrak, dena eramangarriagoa egiten duzue, zuekin egote hutsak barrua pozten dit eta arazoak ahaztarazi. And last but not least, Ainho. Eskerrik asko zaren bezalakoa izateagatik, ura eta olioa nahastu daitezkeela erakusteagatik eta nire aurpegi zurbilean argitasuna sortzeko duzun gaitasunagatik.

Bizitako guztiagatik, bihotz-bihotzez, eskerrak denoi!!!

Abbreviations

ACM	Aspergillus complete medium
A	Alanine
AMBER	Assisted Model Building with Energy Refinement
AMM	Aspergillus minimal medium
AspGD	Aspergillus Genome Database
ATP	Adenosine Triphosphate
BCS	Bathocuproinedisulfonic acid
BLASTp	Basic Local Alignment Search Tool for proteins
bp	Base pair
^{o}C	Celsius degrees
C-term	Carboxy-terminal
Cat	Catalase
CDF	Cation Diffusion Facilitator
CHARMM	Chemistry at Harvard Macromolecular Mechanics
cm	Centimeter
Co	Cobalt
Crp	Copper response P-type ATPase
Ctr	Copper Transporter
Cu	Copper
C/Cys	Cysteine
DIG	Digoxigenin
DNA	Deoxyribonucleic Acid
EDTA	Ethylenediaminetetraacetic acid
ER	Endoplasmic Reticulum
Fe	Iron
g	gram
g	*g*-force
G1	Growth
G2	Growth & Mitosis preparation
gDNA	genomic DNA
GFP	Green Fluorescent protein
GO	Gene Onthology
GROMACS	GROningen MAchine for Chemical Simulations
Gsp	Gene specific primer
h	hours
HA	Residues 98-106 of the human flu virus hemagglutinin
HBB	5aS,10aS)-1,3,8,10a-tetrahydroxy-2-[hydroxy(methyl)BLAHyl]-5a-(3-methylbut-2-enyl)benzofuro[3,2-b]c
Hg	Mercury
H/His	Histidine
HS	Hot Start

Abbreviations

K	Potassium
kDa	kiloDalton
l	liter
M	Molar
M	Mitosis
MD	Molecular Dynamics
min	minutes
µg	microgram
µl	microliter
µm	micrometer
mg	milligram
mJ	milliJoule
ml	milliliter
mm	millimeter
Mn	manganese
MOPS	3-(N-Morpholino)-propanesulfonic acid
MRE	Metal Response/Regulatory Element
mRFP	monomeric Red Fluorescent Protein
mRNA	messenger RNA
MT	metallothionein
MVB	Multivesicular Body
NE	Nuclear Envelope
Ni	nickel
N-terminal	Amino-terminal
PCR	Polymerase Chain Reaction
PEG	Polyethylene glycol
PM	Plasma Membrane
PREG	pregn-5-ene-3-ol derivative
OPM	Orientations of Proteins in Membranes
qPCR	quantitative Polymerase Chain Reaction
RT-PCR	Real-Time PCR
RMM	Regeneration Minimal Medium
RMM-TOP	Regeneration Minimal Medium-TOP
RMSD	Root Mean Square Deviation
RNA:	Ribonucleic acid
RNase	Ribonuclease
RNA-seq	RNA-sequencing
ROS	Reactive Oxygen Species
rpm	Revolutions per minute
rRNA	ribosomal RNA
S	DNA synthesis
s	seconds
SDS	Sodium dodecyl sulfate
Sod	Superoxide Dismutase

TCA	Trichloroacetic acid
TGN	Trans-Golgi Network
TM	Transmembrane
TMD	Transmembrane domain
TF	Transcription factor
t_o	Time zero
Tris	Tris(hydroxymethyl)aminomethane
UTR	Untranslated Region
UV	Ultraviolet
WMM	Watch Minimal Medium
WT	wild-type
Zn	Zinc
ZINC	Zinc Is Not Commercial

Index

Introduction

1- *Aspergillus nidulans*

Aspergillus nidulans (*Emericella nidulans*) is a filamentous fungus that belongs to the Ascomycota division. Vegetative cells, denominated hyphae, have a tubular shape and grow in a hyperpolarized manner by apical extension and lateral branching, forming an interconnected cellular network denominated mycelium (Harris *et al.*, 2005;Lee and Adams, 1994). The extension of hyphae results in radial expansion of the fungal colony (Harris and Momany, 2004) (Figure 1B & C). The clearest images of a fungal mycelium have been obtained in *Neurospora crassa*, as shown in Figure 1B & C. The fact that *A. nidulans* mycelium is very compact makes it difficult to obtain clear images; however the mycelium organization follows a comparable pattern in both organisms. The *Aspergillus* mycelium is coenocytic, meaning that its hyphae are multinucleated syncytia, generally haploid, and divided by perforated septa that permit the selective exchange of nutrients and effectors between cellular compartments (Glass *et al.*, 2004;Hickey *et al.*, 2002;Momany, 2002;Riquelme *et al.*, 2003).

The *A. nidulans* life cycle is constituted by four different stages: vegetative growth, asexual development, sexual development and the parasexual cycle (Todd *et al.*, 2007). The cycle is initiated by uninucleate haploid asexual spore or sexual ascospore germination. The spores are metabolically dormant cells retained in phase G1 (Growth) (Bergen and Morris, 1983). *A. nidulans* has a relatively short cell-cycle and the timing of the distinct phases of the cell cycle follow as stated: G1 (Growth), 15 minutes; S (Synthesis), 25 minutes; G2 (Growth and Mitosis preparation), 30 minutes; and M (Mitosis), around 5 minutes at 37 ºC (Bergen & Morris, 1983). Depending on environmental conditions the duration of the G1 and G2 phases is variable (Doonan, 1992). After spore germination, with an isotropic expansion and establishment of the polarity of the cell, the addition of new cellular material to the polarized tip of the germling leads to the mature vegetative cell, denominated hypha (Harris and Momany, 2004) (Figure 1A).

Introduction
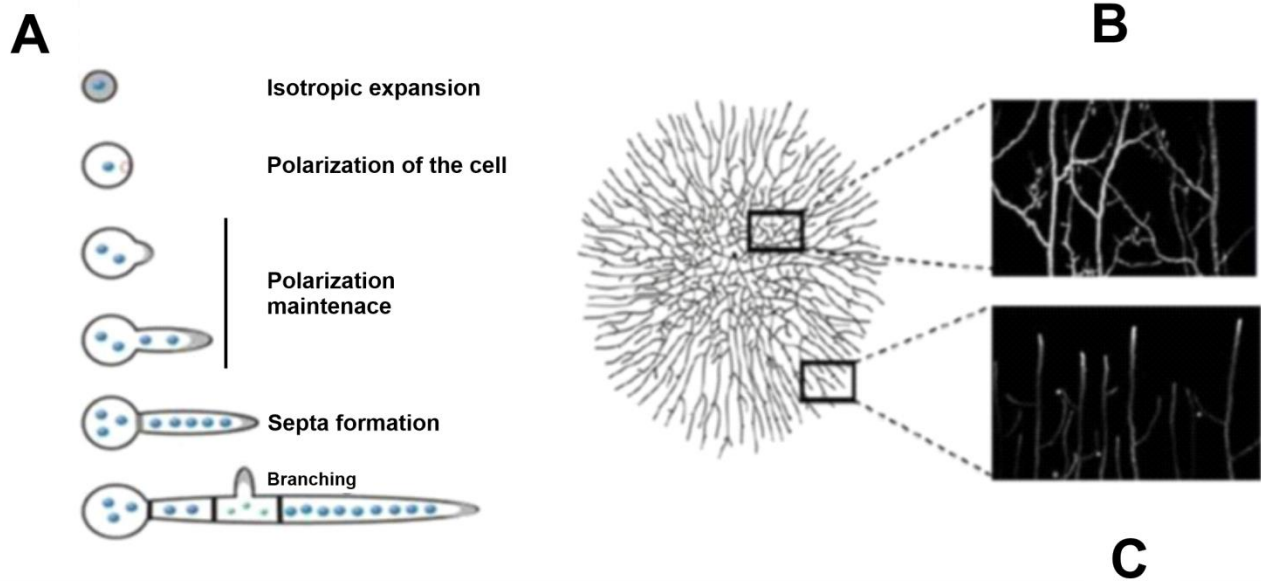
Figure 1: Colony morphology depicting vegetative growth: **(A)** Germination and vegetative growth scheme. The growth of the cell is localized at a discrete region of the cell and cells start to grow in a polarized way. Polarization is maintained and as the hypha grows bigger, septa formation and branching happens (modified from Momany, 2002). **(B)** In the inner part of the colony, hyphae are interconnected by anastomosis. **(C)** In the periphery, hyphae repel each other. Images B & C correspond to *Neurospora crassa* (Hickey *et al.,* 2002*)*.

A. nidulans can reproduce sexually or asexually and both developmental pathways are functionally interconnected (Adams *et al.*, 1998). Asexual development requires the formation of a fruiting body denominated conidiophore. It takes about 24 h to complete the asexual development cycle from spore germination to the generation of the first spore. Sixteen hours (16 h) after germination the first cell specialization events take place as foot cells are formed in the center of the colony giving rise to conidiophores in 6-8 h (Adams *et al.*, 1998;Bayram and Braus, 2012;Lee and Adams, 1994).
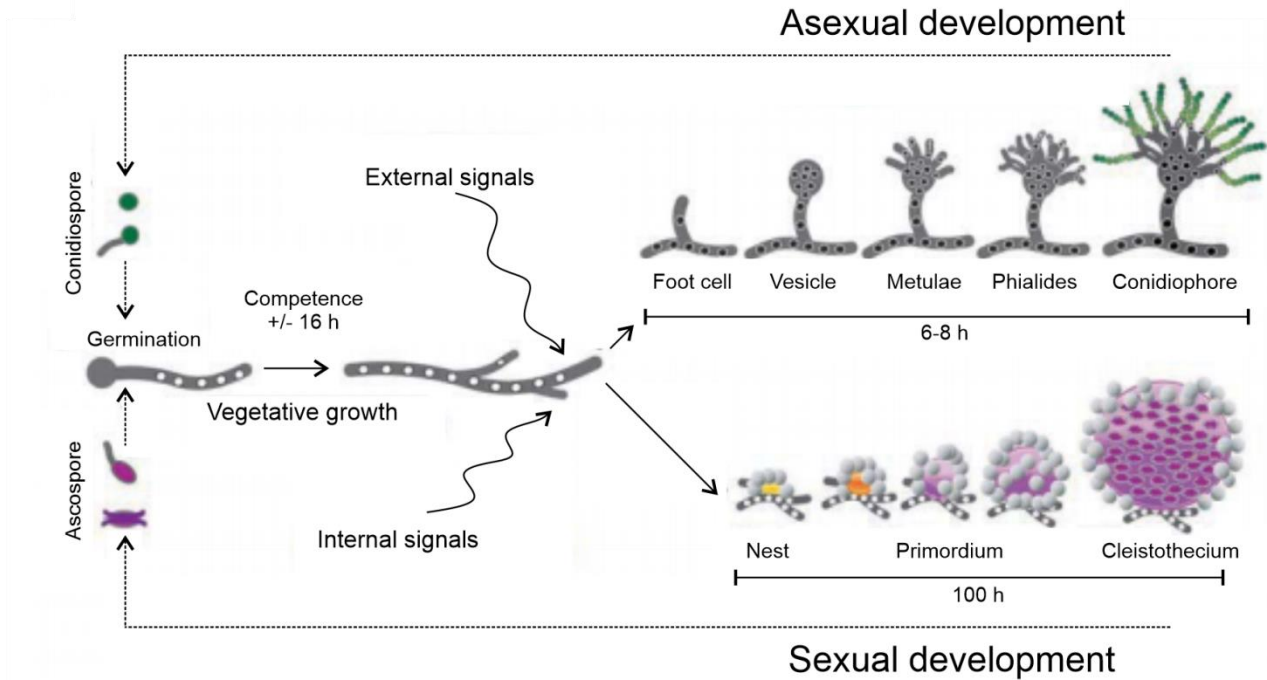
Figure 2: *A. nidulans* life cycle scheme from vegetative growth to sexual or asexual development. Image modified from Bayram and Braus, (2012).

Conidiophore formation is a complex structural process comprising different stages (Timberlake, 1990). The first step is the generation of a foot cell, a thick-walled cell that will be the backbone that will sustain the conidiophore. The process continues with the growth of the stalk. This structure will be the trunk of the conidiophore and grows by apical extension reaching a height of 100 μm. The apical side of the stalk begins to swell forming a structure known as the vesicle. The nuclei in the vesicle then undergo a synchronous division process followed by budding process of the vesicle, giving rise to metulae; a primary layer of sterigmata that keeps growing apically until forming specialised cells known as phialides. Finally, the phialides give rise to the uninucleate spores that will be segregated. Microscopic analyses indicate that around 60 metulae are formed per conidiophore vesicle, from each metula two phialides are generated and each phialide can make up to 100 spores; which means that the total number of conidia surpasses 10,000 for each conidiophore (Figure 2) (Adams *et al.*, 1998).

Introduction

A. nidulans spores possess a characteristic dark green pigment. Spore pigmentation is a multistep process ending in a yellow pigment precursor turning into dark green pigment. This step is catalyzed by laccase AnYA, which, as other members of the laccase family, requires copper ions as a cofactor (Aramayo and Timberlake, 1990;Clutterbuck, 1972;Scherer and Fischer, 2001).

Conidiophore production is a very demanding process, both materially and energetically speaking. The fungus goes from vegetative hyphae of 2-3 μm in diameter to a complex structure that is larger than 100 μm tall and this process takes place repeatedly and simultaneously at distal locations of the colony in synchrony with vegetative growth at the colony margin (Adams *et al.*, 1998). The colony largely provides for the requirements of conidiogenesis by recycling autophagy (Kikuma *et al.*, 2007;Richie and Askew, 2008). Autophagy is a self-degradation process that proves to be very important to obtain energy sources in response to nutrient stress and it is a widespread response to nutrient limitation in eukaryotic organisms (Cebollero and Reggiori, 2009). The organelles and cytoplasm are taken up into vacuoles to obtain reusable nutrients from them (Pollack *et al.*, 2009;Talbot and Kershaw, 2009). The hydrolyzed materials of the cells are transferred to adjacent cells serving as a nutrient source. Then, these nutrients can be transported wherever necessary, for example to conidiophore production points (Darrah *et al.*, 2006). One of the main objectives of autophagy is to provide nutrients for sporulation (Kikuma *et al.*, 2007;Richie and Askew, 2008). When speaking about nutrients, we don't mean carbon or nitrogen exclusively; it is documented that autophagy is also connected to metal ion homeostasis (Richie and Askew, 2008), which means that also pigmentation could be related to autophagy. Thus, the lack of a specific nutrient in a secondary level might not only compromise sporulation, it might also compromise other processes like pigmentation. In conditions of lack of first level supply, colony development itself will be severely limited.

Sexual development is an alternative path to asexual development but may be brought about at the end of the asexual development (Adams *et al.*, 1998). *A. nidulans* is a homotalic organism that possesses the two mating genes (HMG & α). This makes possible the sexual crossing between two different strains, but also between two different cells within a colony (homothallism) in *A. nidulans*. Sexual reproduction begins when two homokaryotic hyphae fuse by anastomosis constituting a heterokaryon cell. The different nuclei are fused and a transitory diploid nucleus is formed. This nucleus is then divided by meiosis followed by mitosis resulting in 8 ascospores. During the ascospore maturation process, another nuclear division happens giving birth to binucleate haploid ascospores (Bokor *et al.*, 2019;Han, 2009;Yager, 1992). Sexual development occurs within specific fruiting bodies termed cleistothecia (which means, a closed container) and these structures are surrounded by specialized protective cells named Hülle cells (Han, 2009). A vegetative hypha will emerge from each germinated ascospore (Adams *et al.*, 1998).

Finally, the parasexual cycle comprises the fusion of two vegetative hyphae resulting in an exchange of genetic material by anastomosis (Glass *et al.*, 2004). As a result, a heterokaryon with haploid genomic dotation is generated. A fusion between two haploid nuclei can also happen giving birth to diploid nuclei. The chromosomic dotation is restored by a haploidization (PONTECORVO *et al.*, 1953).

A. nidulans has been subjected to numerous live microscopy studies which have led to the detailed assessment of its cellular structures. *A. nidulans* is a multinucleated organism and these nuclei are spaced through the whole length of hyphae. The polar growth of hyphae conditions the distribution of structures and organelles within the cell. As the colony is developing, the organism needs a good communication system to keep the whole colony growing in an organized manner as the distances between the different growing tips increase (Markina-Inarrairaegui *et al.*, 2013;Pantazopoulou and Penalva, 2009). For that purpose, *A.*

Introduction

nidulans possesses a bidirectional endosome trafficking system that relies on microtubules (Penalva, 2005;Zekert and Fischer, 2009). The Golgi apparatus of *A. nidulans* shows a distinct shape from animals and plants. Rather than stacks, the *A. nidulans* Golgi resembles a strongly polarized network of tubules and cisternae (Hubbard and Kaminskyj, 2008;Momany, 2002). The Golgi receives biosynthetic cargo from the Endoplasmic Reticulum (ER) to be delivered, but it also receives recycling cargo from the endo-lysosomal system. It is thus considered a crossroad between exocytosis and endocytosis (Markina-Inarrairaegui *et al.*, 2013;Pantazopoulou, 2016). The *A. nidulans* ER has two main parts. The first resembles a nucleus cover, the Nuclear Envelope (NE). The second part is the Peripheral ER, a network of tubular membrane strands that expand throughout the whole hypha and are significantly polarized in the tip region (Markina-Inarrairaegui *et al.*, 2013) (Figure 3).

N- Nucleus   NE- Nuclear Envelope   PER-Peripheral ER   G-Golgi apparatus

B- Biosinthetic cargo   R- Recycling cargo   M- Microtubules
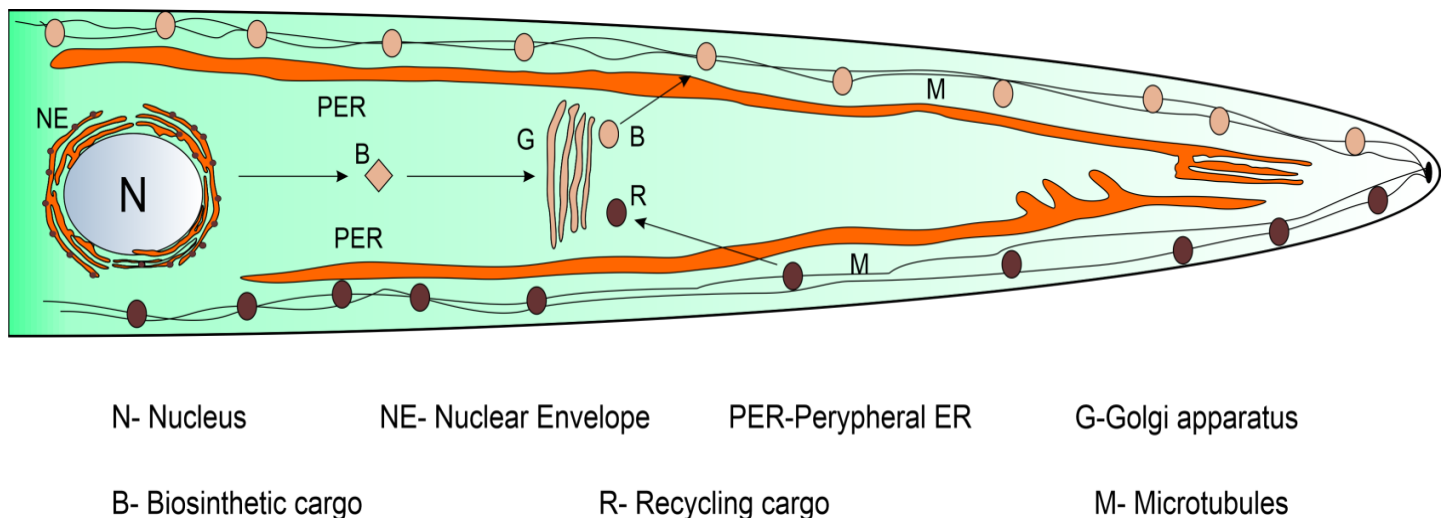
Figure 3: *A. nidulans* organelle distribution scheme focusing on the ER and Golgi. The Nuclear Envelope (NE) is the ER fraction around the nuclei. The Peripheral Endoplasmic Reticulum (PER) extends throughout the whole length of the hypha polarizing in the tip. The Golgi apparatus (G) is situated between the ER and the final destination of the cargo. The cargo is post-translationally modified (B) and sorted to the final destination, in this case the endosomes that travel through microtubules (M). The Golgi apparatus also receives recycling cargo (R).

The *A. nidulans* genome contains 30 million base pairs, approximately 10,982 genes distributed in eight chromosomes (Galagan *et al.*, 2005). The multiple molecular techniques applied in this fungus give the possibility to study biological questions with many different experimental approaches like gene replacement (Nayak *et al.*, 2006), protein tagging, subcellular localization analysis of proteins (Yang *et al.*, 2004) or proteomic analysis. This is one of the reasons why it has been used as a model organism to study stress-related cellular responses in eukaryotes for more than 30 years.

2- Copper an Essential Element for Life

All organisms depend on metal ions as catalysts, structural elements in proteins, in electron transfer reactions, or as messengers. The first-row transition metals cobalt (Co), copper (Cu), iron (Fe), manganese (Mn), and nickel (Ni), possess the appropriate Redox potential characteristics for key biological processes (Gerwien *et al.*, 2018;Nevitt *et al.*, 2012). The intracellular concentration of these metals is tightly controlled, as an excess of unbound metal would result in uncontrolled and deleterious side-reactions (Blatzer and Latge, 2017). Thus, tightly regulated mechanisms are in place to control to intracellular metal fluctuations of each metal ion species. This is achieved through accurate sensing of intracellular and extracellular metal levels coupled with the activation of various mechanisms that maintain free intracellular metal levels within a safety range (Nevitt *et al.*, 2012).

Copper (Cu) is an indispensable trace element for living organisms. Its capacity to adopt an oxidized (Cu^{2+}) and a reduced (Cu^+) state is exploited by many enzymes to act as Redox cofactors in enzyme-catalyzed processes (Nevitt *et al.*, 2012); cytochrome c, a key component of mitochondrial cellular respiration process; superoxide dismutase, for ROS neutralization; and laccases, an abovementioned protein family involved in fungal pigment synthesis (Ding *et al.*, 2014;Lutsenko, 2010;Scherer and Fischer, 2001;Smith *et al.*, 2017). However, free intracellular copper can interfere with Redox processes generating Reactive Oxygen Species

Introduction

(ROS) or cause metalloprotein dysfunction by displacement of other bound metal ions (Besold *et al.*, 2016;Fridovich, 1983;Macomber and Imlay, 2009;Smith *et al.*, 2017). Hence, all organisms have elaborate mechanisms that secure copper bioavailability, yet maintain free copper levels below the toxicity threshold. They include copper uptake, intracellular traffic, storage, and detoxification processes (Balamurugan and Schaffner, 2006;Nevitt *et al.*, 2012).

Most studies on copper homeostasis have been carried out in mammalian cells, bacteria, and yeast model systems. The model yeast *Saccharomyces cerevisiae* has served as an important reference for other lower eukaryotes (Balamurugan and Schaffner, 2006), including pathogens like *Cryptococcus neoformans* and *Candida albicans* (Ballou and Wilson, 2016). In these models, copper is a recognized virulence factor (Zhang *et al.*, 2016). A number of recent publications have described copper import and export mechanisms in *Aspergillus fumigatus*, a common airborne fungal pathogen (Blatzer and Latge, 2017), responsible for severe invasive aspergillosis in immunocompromised patients (Cai *et al.*, 2017).

The following sections present an overview of recently published findings on the different aspects of copper homeostasis in filamentous fungi.

3- Copper Import Across Membranes

The lipid bilayer of the plasma membrane is impenetrable to charged ions, including copper and this generates the necessity for copper import machinery through the plasma membrane. A functional copper transporter is required to be highly specific, in order not to transport other heavy metal cations. On the other hand, it needs display high-affinity binding in order to scavenge the cation selectively under commonly low availability conditions (Smith *et al.*, 2017).

High-affinity transporters are denominated Copper Transporter (Ctr) proteins. They are omnipresent in eukaryotes and display high specificity for copper (Petris, 2004;Puig *et al.*, 2002).

Saccharomyces cerevisiae has long been the subject of many studies on copper metabolism. The high-affinity copper uptake system consists of two plasma membrane metalloreductases responsible for converting Cu^{2+} to Cu^+, ScFre1 and ScFre2, and two plasma membrane copper transporters, ScCtr1 and ScCtr3, that internalize the reduced extracellular copper (Balamurugan and Schaffner, 2006;Nevitt *et al.*, 2012;Smith *et al.*, 2017). The regulation of the high-affinity copper system is copper-dependent and relies on the TF ScMac1 (Pena *et al.*, 1999). After import, the reduced copper is delivered to specific target proteins by specific copper chaperones. ScAtx1 is a chaperone that delivers copper to the P-type ATPase ScCcc2, a protein responsible for intracellular copper delivery; ScCcs1 delivers copper to the Cu/Zn Superoxide dismutase (Sod); and finally, ScCox17 delivers copper to the mitochondria (Balamurugan and Schaffner, 2006;Nevitt *et al.*, 2012;Smith *et al.*, 2017).

Complementation studies in yeast for the *Scctr1* and *Scctr3* double mutant led the way to identify Ctr homologs in different species. In *Candida albicans* copper import is mediated by the high-affinity copper transporter CaCtr1 and the copper reductases CaFre7 and CaFre10. The expression of the protein is induced by the transcription factor CaMac1 under low copper availability conditions (Marvin *et al.*, 2004).

The high-affinity copper uptake system in filamentous fungi contains all the elements mentioned above. In *A. fumigatus*, four Ctr proteins have been identified: AfCtrA1, AfCtrA2, AfCtrB and AfCtrC (Park *et al.*, 2014). According to the authors, phylogenetic analysis showed that these four proteins are closely related to *S. cerevisiae* Ctr1. AfCtrB showed higher homology to ScCtr2, a copper transporter that pumps stored copper out of the vacuole in conditions of copper

scarcity (Rees *et al.*, 2004). AfCtrA2 and AfCtrC are able to complement the disruption of *ctr1* in *S. cerevisiae* (Park *et al.*, 2014) and their expression is under the control of the TF AfMac1 (Cai *et al.*, 2017;Kusuya *et al.*, 2017;Park *et al.*, 2017).

4- Copper Detoxification

Even if copper import is a strictly controlled process, there are circumstances in which intracellular copper levels may reach toxic levels. In these circumstances, detoxification/sequestration mechanisms are activated to restore cellular copper balance. In contrast to the similarity in proteins and mechanisms described for copper uptake in yeast and filamentous fungi, copper detoxification is conducted by two different mechanisms. The details of this division are as presented below.

The first method relies on copper sequestration by metallothioneins (MTs) and has been exhaustively described in *S. cerevisiae*. It involves two copper-specific MTs, ScCup1 and ScCrs5, and these two proteins are responsible for copper tolerance (Culotta *et al.*, 1994;Jensen *et al.*, 1996). Metallothioneins, cysteine (C)-rich low molecular weight polypeptides characterized by high-affinity for diverse metals (Cu, Zn, Cd, Hg, etc.), are found in all eukaryotes and some prokaryotes (Balamurugan and Schaffner, 2006;Sutherland and Stillman, 2011). The synthesis of these proteins is induced in response to high levels of exposure to metals. They bind metals with high-affinity, thereby buffering them and lowering their intracellular concentrations.

The second mechanism, termed detoxification, which is absent in *S. cerevisiae*, has been described in filamentous fungi. It relies on P_{IB}-type ATPases: ATP-dependent heavy metal translocators that are deeply conserved from archaea to mammals (Palmgren and Nissen, 2011). These copper extrusion pumps represent the main detoxification mechanism in bacteria (Ladomersky and Petris, 2015), and in eukaryotes, they are also involved in copper compartmentalization into

the secretory network where copper is incorporated into different Cu-dependent proteins as a cofactor. In humans, two P_{IB}-ATPases hATP7A (Menkes disease protein) and hATP7B (Wilson disease protein) are responsible for the delivery of copper to the trans-Golgi compartment (TGN) (Lutsenko *et al.*, 2007). In response to Cu toxicity, both transporters change their location from the TGN to the cell membrane to act as detoxification (export) pumps conferring copper resistance to the cell (Petris *et al.*, 1996;Suzuki and Gitlin, 1999). In the dimorphic fungus *C. albicans*, each task is fulfilled by a different P_{IB}-ATPase; CaCcc2 is involved in copper compartmentalization into the TGN and CaCrp1p is responsible for copper detoxification at the plasma membrane (Riggle and Kumamoto, 2000;Weissman *et al.*, 2000). Despite the predominance of the detoxification mechanism in *C. albicans*, it has been reported to possess metallothioneins which also contribute to copper homeostasis (Weissman *et al.*, 2000).

C. albicans has become a benchmark for recent studies in filamentous fungi. Aspergilli rely on copper extrusion pumps as the main heavy metal detoxification mechanism (Antsotegi-Uskola *et al.*, 2017;Wiemann *et al.*, 2017) and it has been recently described that some species of the *Aspergillus* possess two CaCrp1p homologs (Yang *et al.*, 2018). The presence of a metallothionein has been described in *A. nidulans* (Antsotegi-Uskola *et al.*, 2017;Cai *et al.*, 2018).

5- Genetic Regulation of Copper Homeostasis

Copper homeostasis is principally regulated at the transcriptional level. Metal responsive transcription factors are able to sense the copper concentration within the cell and orchestrate a response by activating the copper import or copper detoxification, as required. These two regulatory pathways are under the control of two separate transcription factors (Keller *et al.*, 2005) which were first discovered in *S. cerevisiae* as Mac1 and Ace1 (Balamurugan and Schaffner, 2006).

Introduction

The high-affinity copper uptake system is controlled by the transcription factor Mac1. Most ascomycetes possess the characteristic functional domains of this copper sensing TF. The N-terminal region contains an RGHR and GRP amino acid motifs and the "Cu fist" domain, all together, they are responsible for the Cu-dependent DNA binding of the TF (Cai *et al.*, 2017). A C-terminal copper-binding domain with two cysteine-rich motifs is responsible for copper sensing (Kusuya *et al.*, 2017). Site-directed mutagenesis studies in *A. fumigatus* and *A. nidulans* have demonstrated that Cys residues of the N-terminal "Cu fist" domain are essential for Mac1 DNA binding (Cai *et al.*, 2019). Under copper limitation, AfMac1 binds copper response elements 5'-TGTGCTCA-3' in the gene promoter regions and enables the transcription of the Ctr proteins for copper uptake. On the other hand, copper accumulation leads to AfMac1 inactivation. The C-terminal copper-binding domain acts as an auto-inhibitory domain (Park *et al.*, 2017).

The copper detoxification process is orchestrated by the transcription factor Ace1. In *A. fumigatus*, AfAce1 is also involved in zinc detoxification (Cai *et al.*, 2018). The characteristic domains that identify this TF are the "Cu fist" DNA binding domain, and the numerous cysteine residues arranged in CxC-CxxC segments through the protein sequence, identified as necessary for function in *S. cerevisiae* (Hu *et al.*, 1990). Within the DNA binding domain, two different motifs are found, a 3 x Cys-His zinc finger and the KGRP amino acid motif for DNA binding stabilization. A single cysteine-rich domain is located downstream of the DNA binding domain. Under excess copper conditions, four Cu^+ atoms bind the Cys-rich domain to form a tetra-copper-thiolate cluster (Dameron *et al.*, 1991). Cluster formation leads to a conformational change that enables Ace1-DNA binding.

LOW COPPER ENVIRONMENT
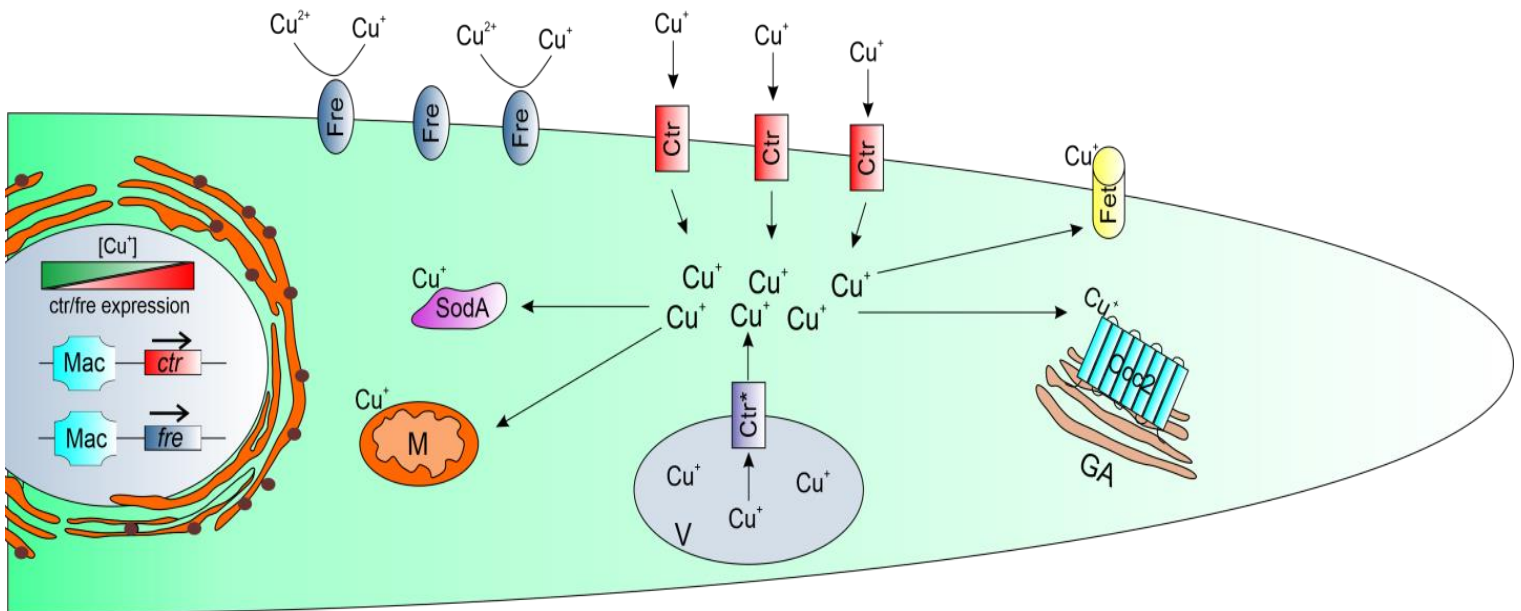
HIGH COPPER ENVIRONMENT
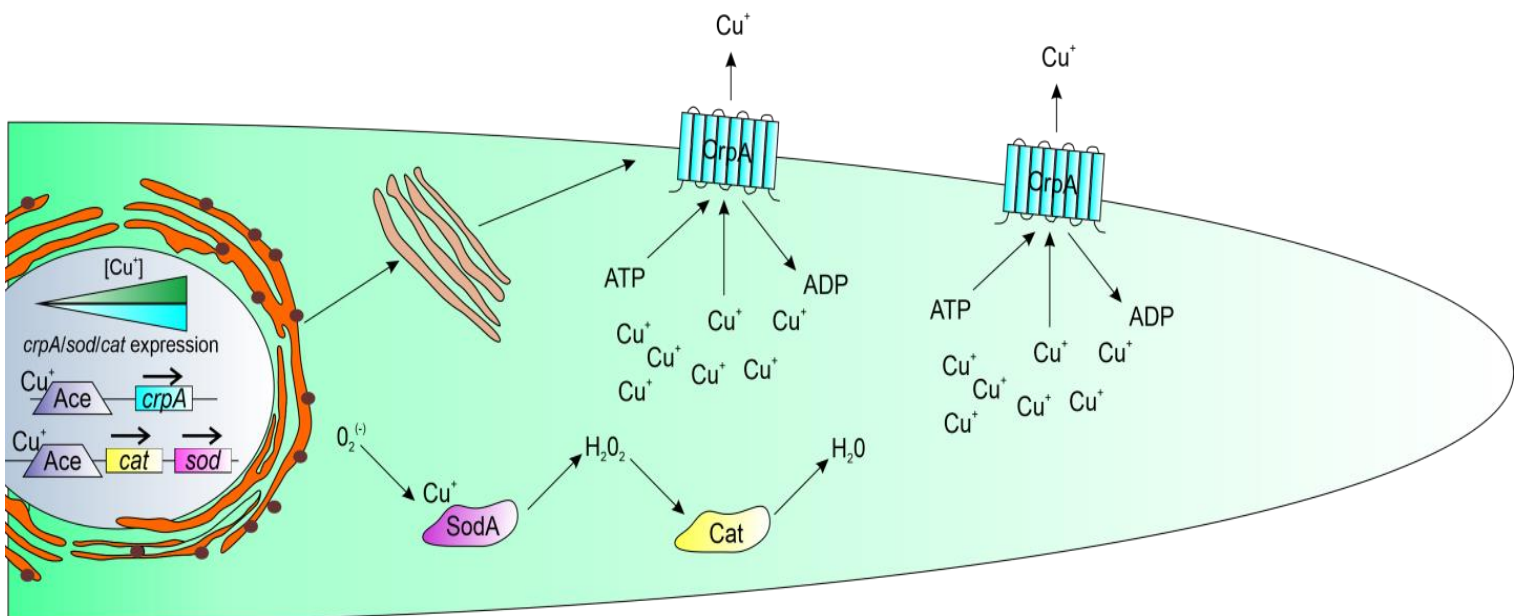
Introduction

Figure 4: LOW COPPER ENVIRONMENT. Copper homeostasis scheme for *A. nidulans* and *A. fumigatus*, under conditions of low copper availability. TF Mac1 binds to DNA enabling the transcription of the copper transporting proteins (*ctr*) and the plasma membrane copper reductase (*fre*) coding genes. The plasma membrane copper reductases (Fre) reduce environmental copper from Cu^{2+} to Cu^{+}. Subsequently, the copper transporting proteins (Ctr) introduce copper to the cell. Within the cell, Cu^{+} ions are distributed to the mitochondria (M) as cofactor of the electron transport chain enzymes, the Cu/Zn superoxide dismutase Sod1 (Sod) or the ferroxidase Fet (not present in *A. nidulans*), essential for Reductive Iron Assimilation (RIA). Copper is also distributed to the P-type ATPase Ccc2, responsible of Cu^{+} mobilization to the secretory compartment (GA). (*) The Ctr protein identified as the ScCtr2 ortholog is regulated in a Mac1-independent manner and pumps copper ions to the cytosol from the vacuole (V) compartment in copper scarcity conditions. **HIGH COPPER ENVIRONMENT.** Copper homeostasis scheme for *A. nidulans* and *A. fumigatus*, under copper toxicity conditions. The TF Ace1 binds copper forming a tetra-copper-thiolate cluster, thereby changing its conformation. By changing conformation, Ace1 is able to bind DNA and enables the transcription of the P-type ATPase crpA coding gene. The P-type ATPase CrpA is first synthesized in the endoplasmic reticulum and migrates to the plasma membrane passing through the Golgi apparatus. Once stabilized in the plasma membrane, CrpA pumps Cu^{+} ions out of the cell in order to reduce copper toxicity within the cell. Meanwhile, the superoxide dismutase *sod1* and catalase *cat1/2* coding genes experiment Ace1-mediated activation. Sod1 and Cat1/2 neutralize ROS generated by Cu+ toxicity or host organism defense mechanisms.

In summary, in most filamentous fungi, the copper homeostasis system is orchestrated by two transcription factors. The TF-termed Mac1 is responsible for regulating copper internalization elements and Ace1 controls copper detoxification. The characteristic features of these transcription factors are well conserved in filamentous fungi.

6- Copper in Fungal Biology and Justification for its Study

Fungal pathogens are responsible for harvest losses that are estimated to be around 33% of worldwide crops every year and post-harvest losses, around 40-50%. The single most important cause for these losses is the damage caused by

fungal pathogens (Alkan and Fortes, 2015). On the other hand, fungal infections affecting humans by organisms like *Candida*, *Aspergillus*, *Cryptococcus* or *Histoplasma* cause about half a million deaths each year (Brown *et al.*, 2012). In the bulk of the cases pathogenic fungi are filamentous or make use of the transient filamentous form to invade host cells. This is the case in human (*Aspergillus fumigatus*, *Hystoplasma capsulatum*, *Candida albicans*...) and plant pathogens (*Botrytis cinerea*, *Fusarium spp.* or *Alternaria spp.*, to name a few; Bastmeyer *et al.*, 2002;Doehlemann *et al.*, 2017).

Host organisms have developed defense strategies against fungal pathogens that target copper availability. By scavenging Cu^+ in the infection area, copper deprivation can be induced in the pathogen. On the contrary, host innate immune cells, such as macrophages, are able to mobilize copper to invade fungal tissue as a defense mechanism. The generation of Reactive Oxygen Species (ROS) is another defense mechanism employed by the innate immune system (Garcia-Santamarina and Thiele, 2015).

A. fumigatus is one of the notorious airborne fungal pathogens responsible for severe invasive aspergillosis (IA), especially in immunocompromised individuals (Cai *et al.*, 2017). Copper is a recognized virulence factor, as it is the cofactor of many enzymes that contribute to virulence, such as laccases or superoxide dismutase (Sod). Enzymes of the Sod family are copper-dependent enzymes responsible for neutralizing ROS. The Cu/Zn Sod enzyme is considered as an important virulence factor in pathogenic in organisms, like *C. albicans* and *C. neoformans* (Frohner *et al.*, 2009;Narasipura *et al.*, 2005). Laccases are involved in melanin biosynthesis and they are copper-dependent enzymes (Upadhyay *et al.*, 2013). Melanin confers a non-immunogenic status to the fungus and a protective layer to the action of host-derived ROS (Jahn *et al.*, 2000;Pihet *et al.*, 2009). When copper uptake is impaired, laccase and Sod activity are substantially reduced in *A. fumigatus* (Park *et al.*, 2014).

Introduction

The *A. fumigatus* Ace1 homolog deletion represses the expression of catalases such as *Afcat1* and *Afcat2* involved in hydrogen peroxide neutralization and the TF *AfatfA* which is known to be involved in spore maturation and ROS-response (Hagiwara *et al.*, 2014;Wiemann *et al.*, 2017). Moreover, it also inhibits the expression of the copper extrusion pump *AfcrpA* (Wiemann *et al.*, 2017), the main copper detoxification system in *A. fumigatus*, leaving the fungus exposed to copper mobilization to fungal tissue by host innate immune system cells. Thus, the copper detoxification machinery is a key factor in pathogen viability during infection.

Botrytis cinerea is a necrotrophic fungal plant pathogen of worldwide distribution, capable of infecting a wide range of hosts. Copper-dependent proteins play a central role in many aspects of the *B. cinerea*, including pathogenesis. The P-type ATPase BcCcc2, an ortholog of the *S. cerevisiae* Ccc2 copper transporting P-type ATPase that delivers Cu to the secretory compartment for subsequent protein modification (Smith *et al.*, 2017), is crucial for virulence in *B. cinerea* (Saitoh *et al.*, 2010). The absence of BcCcc2 results in a defective BcSod1 function (Lopez-Cruz *et al.*, 2017), as well as other proteins, proving the importance of the copper homeostasis system for *B. cinerea* virulence.

In summary, copper homeostasis plays an essential role in pathogenic fungi virulence development. The high-affinity copper uptake system enables the maturation of many copper-dependent enzymes for virulence. On the other hand, the detoxification system confers the organism with the necessary resistance for survival. In the case of phytopathogens, the intracellular copper delivery system is crucial for successful virulence development.

Copper has long been used as an antimicrobial agent in many different agricultural practices (Judet-Correia *et al.*, 2011) and the strategy based on the intensive use of fungicides based on copper is maintained. However, copper

accumulation causes harmful effects on soil and fresh water ecosystems, as well as drinking water quality. Moreover, this excessive use has also brought about increasing levels of copper resistance in microbial pathogens (Lamichane *et al.*, 2018;Santo *et al.*, 2010).

The mechanisms of copper resistance in fungi need a thorough assessment in order to find new and effective methods to complement or replace copper in the control of fungal disease. New details on the mechanism of copper toxicity on fungal cells may shed light on the potential use of synergists affecting copper homeostasis that could help lower the currently required copper dose. The acquisition of copper by fungi in the soil, and its exchange between microorganisms and plants in a symbiotic relationship is another aspect which should be considered, to ensure sustainable agricultural and environmental conservation programs.

A. nidulans is a model filamentous ascomycete that remains as one of the most studied lower eukaryotes. Gathering knowledge about the cellular response to copper concentrations in *A. nidulans* could be a significant step towards understanding the cellular response in related pathogenic fungi (*Alternaria*, *Botrytis*, *Magnaporthe*, etc.) and thus achieve the abovementioned objective. In this study, some key elements of copper homeostasis will be explained in *A. nidulans*. In the first chapter, the transcriptomic behavior of *A. nidulans* in copper toxicity conditions is discussed, along with a deep characterization of the high-affinity copper uptake proteins AnCtrA and AnCtrC. In the second chapter, the *A. nidulans* copper detoxification machinery will be exposed, focusing primarily on the P_{IB}-type ATPase AnCrpA. Finally, in the third chapter, a model of the CrpA protein generated by homology modelling will be presented. With this protein model virtual screening tests, followed by molecular docking and molecular dynamic tests were made to test possible inhibitors of the protein.

Objectives

Objectives

The objectives pursued by this thesis are the following ones:

- Characterization of the high-affinity copper transporters AnCtrA and AnCtrC in *A. nidulans*. Determine their function, hierarchy, expression dynamics, subcellular localization and possible regulation mechanisms.
- Characterization of the copper detoxification system in *Aspergillus nidulans*. Identify the main agents of the system, to study their impact on copper resistance and learn about their expression patterns, subcellular localization and the transcription factor regulating the system.
- To test molecular modelling techniques as new tools to search for inhibitory compounds of different targets of the copper homeostasis system of *A. nidulans.*

Materials & Methods

1- Strains, Primers and Plasmids

1.1- *Aspergillus nidulans* Strains

The genotypes of the *Aspergillus nidulans* strains used in this study are described in Table 1. The loci and nutritional selective markers used are described by Clutterbuck (1990).

Table 1: Stains used and generated throughout this study.

Strains	Genotype	Reference
MAD1427	*pyrG89, pabaA1; argB2; ΔnkuA::argB ; veA1, riboB2*	TN02A25 Oakley B.
MAD2731	*pabaA1; argB2; ΔnkuA::argB ; veA1, riboB2*	Markina-Iñarrairaegui *et al.* (2011)
MAD2733	*pabaA1; argB2; ΔnkuA::argB ; veA1*	Markina-Iñarrairaegui *et al.* (2011)
BD874	*pyrG89, pabaA1; ΔctrC::pyrG^{Af}; argB2; ΔnkuA::argB; veA1, riboB2*	This study
BD872	*pyrG89, pabaA1; ΔctrC::riboB^{Af}; argB2; ΔnkuA::argB; veA1, riboB2*	This study
BD878	*pyrG89, pabaA1; ctrC::gfp::riboB^{Af}; argB2; ΔnkuA::argB; veA1, riboB2*	This study
BD1160	*pyrG89, pabaA1; ctrC::gfp::riboB^{Af}; argB2; ΔnkuA::argB; ΔctrA::pyrG^{Af}; veA1, riboB2*	This study
BD880	*pyrG89, pabaA1; argB2; ΔnkuA::argB; ΔctrA::pyrG^{Af}; veA1, riboB2*	This study
BD1158	*pyrG89, pabaA1; argB2; ΔnkuA::argB; ctrA::gfp::riboB^{Af}; veA1, riboB2*	This study
BD1162	*pyrG89, pabaA1; ΔctrC::pyrG^{Af}; argB2; ΔnkuA::argB; ctrA::gfp::riboB^{Af}; veA1, riboB2*	This study

Materials & Methods

BD1064	*pyrG89, pabaA1; ΔctrC::riboB^{Af}; argB2; ΔnkuA::argB; ΔctrA::pyrG^{Af}; veA1, riboB2*	This study
BD1361	*pyrG89, pabaA1; ctrC^{C213A,C214A}::gfp::riboB^{Af}; argB2; ΔnkuA::argB; veA1, riboB2*	This study
BD1363	*pyrG89, pabaA1; ctrC^{201}::gfp::riboB^{Af1}; argB2; ΔnkuA::argB; ctrA::gfp::riboB^{Af}; veA1, riboB2*	This study
BD1357	*pyrG89, pabaA1; argB2; ΔnkuA::argB; ctrA^{C186A,C187A}::gfp::riboB^{Af}; veA1, riboB2*	This study
BD1359	*pyrG89, pabaA1; argB2; ΔnkuA::argB; ctrA^{164}::gfp::riboB^{Af}; veA1, riboB2*	This study
BD1365	*pyrG89, pabaA1; ctrC^{C213A,C214A}::gfp::riboB^{Af1}; argB2; ΔnkuA::argB; ctrA^{C186A,C187A}::ha$_3$::pyrG^{Af}; veA1, riboB2*	This study
BD1367	*pyrG89, pabaA1; ctrC^{201}::gfp::riboB^{Af1}; argB2; ΔnkuA::argB; ctrA^{164}::ha$_3$::pyrG^{Af}; veA1, riboB2*	This study
BD1369	*pyrG89, pabaA1; ctrC::gfp::riboB^{Af1}; argB2; ΔnkuA::arg; hhoA::mRFP::pyrG^{Af}; veA1, riboB2*	This study
BD1371	*pyrG89, pabaA1; argB2; ΔnkuA::argB; ctrA::gfp::riboB^{Af}, hhoA::mRFP::pyrG^{Af}; veA1, riboB2*	This study
BD888	*pyrG89, pabaA1; argB2; ΔnkuA::argB; ΔcrpA::pyrG^{Af}; veA1, riboB2*	This study
BD892	*pyrG89, pabaA1; argB2; ΔnkuA::argB; crpA::gfp::riboB^{Af}; veA1, riboB2*	This study
BD894	*pyrG89, pabaA1; argB2; ΔnkuA::argB; crpA::ha$_3$::pyrG^{Af}; veA1, riboB2*	This study
BD896	*pyrG89, pabaA1; argB2; crdA::ha$_3$::pyrG^{Af}, ΔnkuA::argB; ΔcrpA::riboB^{Af}; veA1, riboB2*	This study
BD898	*pyrG89, pabaA1; argB2; ΔcrdA::pyrG^{Af}, ΔnkuA::argB;; veA1, riboB2*	This study

BD900	*pyrG89, pabaA1; argB2; crdA::ha$_3$::pyrG^{Af}, ⊿nkuA::argB; veA1, riboB2*	This study
BD961	*pyrG89, pabaA1; argB2; ΔnkuA::argB; crpA::ha$_3$::pyrG^{Af}; ⊿aceA::riboB^{Af}; veA1, riboB2*	This study
BD963	*pyrG89, pabaA1; argB2;⊿crdA::pyrG^{Af}, ⊿nkuA::argB; ⊿crpA::riboB^{Af}; veA1, riboB2*	This study
BD965	*pyrG89, pabaA1; argB2; ΔnkuA::argB; ⊿aceA::pyrG^{Af}; veA1, riboB2*	This study
BD1062	*pyrG89, pabaA1; argB2; crdA::ha$_3$::pyrG^{Af}, ⊿nkuA::argB; ⊿aceA::riboB^{Af}; veA1, riboB2*	This study
BD1073	*pyrG89, pabaA1; argB2; ΔnkuA::argB; crpA^{An} (⊿crpA::pyrG^{Af}); veA1, riboB2*	This study

1.2- Plasmids

The plasmids shown in this report were used as a PCR template to generate null construct cassettes and cassettes for tagging proteins using fusion PCR method described in (Yang *et al.*, 2004).

- **p1503:** This plasmid was used to amplify the selection marker *pyrG^{Afum}* for knockout strain generation and GA$_5$-HA-pyrG^{Afum} cassette to generate strains expressing HA-tagged proteins. This plasmid is a TOPO based vector which contains a 5x glycine-alanine linker, followed by HA and *pyrG* locus from *A. fumigatus*.

- **p1548:** This plasmid was used to amplify the selection marker *riboB^{Afum}* for knockout strain generation and GA$_5$-GFP-riboB^{Afum} cassette to generate strains expressing GFP-tagged proteins. This plasmid is built like p1503.

Materials & Methods

1.3- Primers

The oligonucleotides used and designed for this study are listed in Table 2.

Table 2: Primers designed and used in this study

Oligo	Sequence (5´-3´)	Utility
CtrA-gsp1	GTTTGGCGTGTTGAAGTG	*ctrA* 5´ UTR
CtrA -gsp2	CTTGTCGAATGTCTGGATAC	*ctrA* 5´ UTR
CtrA -gsp3	CTTTGCTGTATATATTTTAAATGAAGCGC	*ctrA* 3´ UTR
CtrA -gsp4	GCTTATTTCACAGATTGGGATTTCC	*ctrA* 3´ UTR
CtrA -gsp5	AGTCTTCAAGAAGCGCTTTATCATTCT	*ctrA* 3´ ORF end
CtrA -gsp6	GCCACAACACTTGGTCGCTTCCTC	*ctrA* 3´ ORF end
CtrA -gsp2*	GTATCCAGACATTCGACAAGACCGGTCGCCTCAAACAATGCTCTTCACCCTC	*pyrG^{Af}/riboB^{Af}* cassette
CtrA -gsp3*	GCGCTTCATTTAAAATATATACAGCAAAGGTCTGAGAGGAGGCACTGATGC	*pyrG^{Af}/riboB^{Af} /gfp::riboB^{Af}* cassette
CtrA -gsp6*	GAGGAAGCGACCAAGTGTTGTGGCGGAGCTGGTGCAGGCGCTGGAGCC	*gfp::pyrG^{Af}* cassette
CtrC-gsp1	GGGAGTGATAGGTAAAAACA	*ctrC* 5´ UTR
CtrC -gsp2	CTTGTTAATGTCGTTTGTTG	*ctrC* 5´ UTR
CtrC -gsp3	TGTTTCACATACGCATATAA	*ctrC* 3´ UTR
CtrC -gsp4	ATCCTCTTTCATCTCTTTCC	*ctrC* 3´ UTR

CtrC -gsp5	CGTGCATCCAGTTCCAGCCTATCCATTC	*ctrC* 3′ ORF end
CtrC-gsp6	ACCGCAGCATTTCGTAACAGCCGTTGC	*ctrC* 3′ ORF end
CtrC -gsp2*	CAACAAACGACATTAACAAGACCGGTCGCCTCAAACAATGCTCTTCACCCTC	*pyrG^{Af}/riboB^{Af}* cassette
CtrC -gsp3*	GGATCTGAATTATATGCGTATGTGAAACACTGTCTGAGAGGAGGCACTGATG	*pyrG^{Af}/riboB^{Af}* /*gfp::pyrG^{Af}* cassette
CtrC -gsp6*	GCAACGGCTGTTACGAAATGCTGCGGTGGAGCTGGTGCAGGCGCTGGAGCC	*gfp::pyrG^{Af}* cassette
CtrA-fw	CTCTGTCGAGATGCTCTGGAACTG	*ctrA* forward primer for RT-PCR
CtrA- rev	GCAGGCTCTCTTCGTAATCCTTGG	*ctrA* reverse primer for RT-PCR
CtrC-fw	GTGTCATCTCGATGCTGTGGAA	*ctrC* forward primer for RT-PCR
CtrC- rev	CGAGGACTATGACGAGGCAGATG	*ctrC* reverse primer for RT-PCR
BenA-fw	AGATGCGCAACATCCAGAGC	*benA* forward primer. RT-PCR control
BenA-rev	CTGGTACTCGGAGACGAGATCG	*benA* reverse primer. RT-PCR control
CtrC-AA gsp 3	GCTGTTACGAAAGCCGCCGGTGGAGCTGGT	*ctrC* fordward primer for Cysteine mutation
CtrC-AA gsp 6	ACCAGCTCCACCGGCGGCTTTCGTAACAGC	*ctrC* reverse primer for Cysteine mutation
CtrC C-term gsp 3	CTCGTGGGAGTACATTGGGGGTGGAGGAGCTGGTGCAGGCGCTGGAGCCG	*ctrC* forward primer for C-term mutation
CtrC C-term gsp 6	TCCACCCCCAATGTACTCCCACGAG	*ctrC* reverse primer for C-term mutation
CtrA-AA gsp 3	GAAGCGACCAAGGCTGCTGGCGGAGCTGGT	*ctrA* fordward primer for Cysteine mutation
CtrA-AA gsp 6	ACCAGCTCCGCCAGCAGCCTTGGTCGCTTC	*ctrA* reverse primer for Cysteine mutation

Materials & Methods

CtrA C-term gsp 3	ACTCTTCTTCGACTGGGGGCAATATGGAGCTGGTGCAGGCGCTGGAGCCG	*ctrA* forward primer for C-term mutation
CtrA C-term-gsp 6	ATATTGCCCCCAGTCGAAGAAGAGT	*ctrA* reverse primer for C-term mutation
HhoA -gsp5	CTACAGTTGAGCCTATGCACAAG	*hhoA* 3´ ORF end
HhoA -gsp6	GGCCTTCTTGTTCTTAGCAGTC	*hhoA* 3´ ORF end
HhoA -gsp6*	GACTGCTAAGAACAAGAAGGCCGGAGCTGGTGCAGGCGCTGGAGCC	*mrfp::pyrG^{Af}* cassette
HhoA -gsp3*	CCAAGCCAGGCTGCCTGTCTGTCTGAGAGGAGGCACTGATGC	*mrfp::pyrG^{Af}* cassette
HhoA -gsp3	ACAGGCAGCCTGGCTTGG	*hhoA* 3´ UTR
HhoA -gsp4	GCAACAGTCGACAGCACAGC	*hhoA* 3´ UTR
CrpA-gsp1	CGTACATGGGTCTGGTCTTCCCC	*crpA* 5´ UTR
CrpA-gsp2	GACGAGTGGCGGCTAGTGTTCC	*crpA* 5´ UTR
CrpA-gsp3	TTATTTTTTTCTAGTTCCATGCATGC	*crpA* 3´ UTR
CrpA-gsp4	CCCTGAGCAGTCTCGATGAG	*crpA* 3´ UTR
CrpA-gsp5	CTTCAGCGGGTCGCAGATACG	*crpA* 3´ ORF end
CrpA-gsp6	CTCCTGTTGACGCGTAGTCCGG	*crpA* 3´ ORF end
CrpA-gsp2*	GGAACACTAGCCGCCACTCGTCACCGGTCGCCTCAAACAATGCTCTTCA	*pyrG^{Af}/riboB^{Af}* cassette
CrpA-gsp3*	CATCGCATGCATGGAACTAGAAAAAAATAACTGTCTGAGAGGAGGCACTGATGC	*pyrG^{Af}/riboB^{Af} /ha::pyrG^{Af}/gfp::riboB^{Af}* cassette
CrpA-gsp6*	CCGGACTACGCGTCAACAGGAGGGAGCTGGTGCAGGCGCTGGAGCC	*ha::pyrG^{Af}/gfp::riboB^{Af}* cassette

CrdA-gsp1	GGCTTCGAGAACTACCAGAACC	*crdA* 5′ UTR
CrdA-gsp2	ATTGAATGTTGTTTGAATGGTAG	*crdA* 5′ UTR
CrdA-gsp3	TGCGTTTGAATTCATGTTAATGAAGC	*crdA* 3′ UTR
CrdA-gsp4	CCAATCCGAGGTCGAGTACG	*crdA* 3′ UTR
CrdA-gsp5	ATGGTTCACCCCACCTCAACCTGCT	*crdA* 3′ ORF end
CrdA-gsp6	AGCCTTGGCCGTCGTAAAATCTGTCTC	*crdA* 3′ ORF end
CrdA-gsp2*	CTACCATTCAAACAACATTCAATACCGGTCGCCTCAAACAATGCTCT	*pyrG^{Af}/riboB^{Af}* cassette
CrdA-gsp3*	GCTTCATTAACATGAATTCAAACGCACTGTCTGAGAGGAGGCACTGATG	*pyrG^{Af}/riboB^{Af}/ha::pyrG^{Af}* cassette
CrdA-gsp6*	GAGACAGATTTTACGACGGCCAAGGCTGGAGCTGGTGCAGGCGCTGGAGC	*gfp::riboB^{Af}* cassette
AceA-gsp1	CCGATGATTCCTTCCACTGCCCAGACATAC	*aceA* 5′ UTR
AceA-gsp2	CGCCGCGGTTACTGGGATTGGCACATG	*aceA* 5′ UTR
AceA-gsp3	GGACAGCAAGGGCCTTAGAATCTT	*aceA* 3′ UTR
AceA-gsp4	ATACAAATAGAGAGGCGAAGGAATGGCG	*aceA* 3′ UTR
AceA-gsp2*	CATGTGCCAATCCCAGTAACCGCGGCGACCGGTCGCCTCAAACAATGCTCT	*pyrG^{Af}/riboB^{Af}* cassette
AceA-gsp3*	AAGATTCTAAGGCCCTTGCTGTCCCTGTCTGAGAGGAGGCACTGAT	*pyrG^{Af}/riboB^{Af}* cassette

Materials & Methods

2- Media and growth conditions

The different strains of *Aspergillus nidulans* were cultured according to the standard procedures for this fungus (PONTECORVO *et al.,* 1953). The Aspergillus minimal medium (AMM) or the Aspergillus complete medium (ACM) were used as culture media. For the solid culture medium, 1.5% of agar was added. Medium was supplemented with 1% glucose and 71 mM $NaNO_3$ and required 1x auxotrophies immediately before its use in the case of AMM, ACM, RMM (Regeneration Minimal Medium) and RMM-TOP. WMM (Watch Minimal Medium) was supplemented with 0.1 % glucose, 71 mM $NaNO_3$, 25 mM NaH_2PO_4 and required 1x auxotrophies. The media, solutions and stress inducing agents used through this thesis are listed in Tables 3 & 4.

Table 3: Media and solutions for *A. nidulans* culture.

Media and solutions	Elaboration (per litre)
Kaeffer trace element solution (1000x)	22 g $ZnSO_4$ x 7 H_2O
	11 g H_3BO_3
	5 g $MnCl_2$ x 4 H_2O
	5 g $FeSO_4$ x 7 H_2O
	1.6 g $CoCl_2$ x 6 H_2O
	1.6 g $CuSO_4$ x 5 H_2O
	1.1 g $(NH_4)_6Mo_7O_{24}$ x 4 H_2O
	Adjusted to pH= 6,8
	Sterilized by autoclave
	Store at 4 ^{o}C
Salt & trace element solution (50x)	26 g $MgSO_4$ x 7H_2O
	76 g KH_2PO4
	26 g KCl
	50 ml Kaeffer trace element solution
	Sterilized by autoclave

Aspergillus Minimal Medium (AMM)	20 ml salt & trace element solution 50x
	Adjusted to pH= 6.8
	Sterilized by autoclave
AMM solid	AMM
	15 g agar
	Adjusted to pH= 6.8
	Sterilized by autoclave
Aspergillus **Complete Medium (ACM)**	AMM
	5 g yeast extract
	Adjusted to pH= 6.8
	Sterilized by autoclave
ACM solid	ACM
	15 g agar
	Adjusted to pH= 6.8
	Sterilized by autoclave
Regeneration Minimal Medium (RMM)	20 ml salt & trace element solution 50x
	342 g sucrose
	15 g agar
	Adjusted to pH= 6.8
	Sterilized by autoclave
RMM-TOP	20 ml salt & trace element solution 50x
	342 g sucrose
	6 g agar
	Adjusted to pH= 6.8
	Sterilized by autoclave
Watch Minimal Medium (WMM)	1 ml Kaeffer trace element solution
	X g KCl
	X g $MgSO_4$ x 7 H_2O
	Adjusted to pH= 6.8
	Sterilized by autoclave

Materials & Methods

Glucose solution (20% p/v)	200 g D-glucose
	Sterilized by autoclave
Sodium Nitrate (100x)	603.46 g NaNO3
	Sterilized by autoclave
Biotin 10^4x	100 mg Biotin
	Filter sterilized
Uridine /Uracil	1.22 g /0.56 g
Riboflavin (100x)	250 mg Riboflavin
	Filter sterilized
p-aminobenzoic acid (1000x)	2 g p-aminobenzoic acid
	Sterilize by autoclave
5 M NaH$_2$PO$_4$	599.9 g NaH$_2$PO$_4$
	Sterilized by autoclave

Table 4: Metal salts and compounds used for stress induction.

Component	Medium concentration
CdNO$_3$	60-250 μM
FeSO$_4$	400 μM
CuSO$_4$	50-1000 μM
AgNO$_3$	0.5-5 μM
Bathocuproinedisulfonic acid (BCS)	100-600 μM

* Bathocuproinedisulfonic acid (BCS) is a copper chelator that selectively binds cuprous ions (Cu$^+$). Two molecules of BCS form a complex with a Cu$^+$ ion (2:1). This complex absorbs visible light at wavelengths between 400-550 nm (Koga *et al.*, 2019;Riha *et al.*, 2013).

3- Construction of Replacement Cassettes for Null and Tagged Protein Strain Generation

Different strains were generated by homologous recombination using linear constructions of DNA obtained by PCR amplification (Yang *et al.*, 2004). The enzyme used for this purpose was the Prime Star(R) HS DNA polymerase (Takara), with 3'-5'/5'-3' proofreading activity. The PCR conditions were set following Takara´s protocol, with some variations (time and annealing temperature) depending on the used primers and the size of the fragment amplified.

3.1- Construction of Replacement Cassettes for Null Mutant Strain Generation

The different steps of the cassette construction process are shown in Figure 5A. In the first step, by standard PCR reaction the promoter (5'-UTR) and the terminator (3'-UTR) regions flanking the target loci were amplified, using genomic DNA of the wild type strain (MAD1427) as template. The fragment corresponding to the promoter, obtained with the X-gsp1 and X-gsp2 primers, is approximately 1,500 bp long upstream of the gen. The terminator, around 1,500 bp long, corresponds to the downstream region starting immediately after the stop codon and was obtained with primers X-gsp3 and X-gsp4. For the construction of each knockout cassette the consequent nutritional selection marker, *pyrG*^{Afum} or *riboB*^{Afum}, was amplified with primers X-gsp2* and X-gsp3* from the corresponding plasmid (p1503 and p1548).

The amplicons have overlapping regions that permit their fusion, using primers X-gsp1 and X-gsp4, in a new PCR reaction. The resulting product is the replacement cassette used in the generation of the null strains.
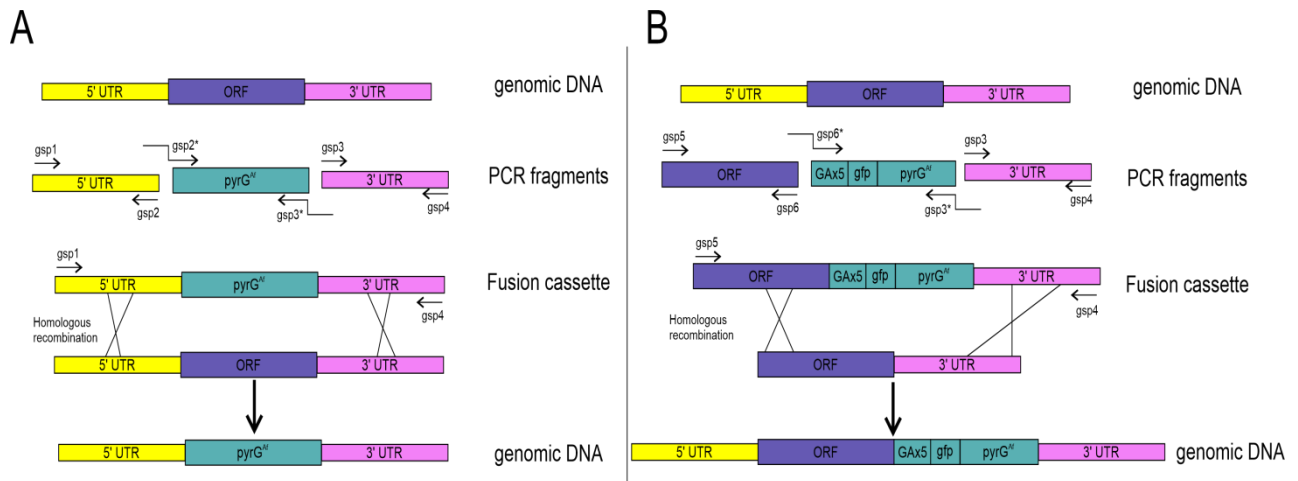
Figure 5: Fusion PCR strategy used to construct replacement cassettes to generate: **(A)** null and **(B)** tagged strains.

3.2- Construction of Replacement Cassettes for GFP/HA Tagged Protein Expressing Strain Generation

This technique was similar to the previous one; however, the approach required in-frame integration of GFP/HA/mRFP just before the stop codon of the target gene. Terminator region (3'-UTR) was amplified as described before. The 3´-coding region of the corresponding gene (without the stop codon) was amplified using X-gsp5 and X-gsp6 primers and genomic DNA of MAD1427 as template. The fragment coding GA5-GFP-pyrGAfum or GA5-HA-$pyrG^{Afum}$ were amplified from the corresponding plasmids (p1503 and p1548) using X-gsp6* and X-gsp3*. Primers located on both edges (X-gsp5 and X-gsp-4) of the cassette were used for the fusion PCR. The process is summarized in Figure 5B.

3.3- Construction of Replacement Cassettes to Generate Specific Cysteine Mutations and C-terminal Truncations of GFP Expressing Strains

The strains carrying mutations in the last cysteines of the C-terminal domain, CtrC$^{C213A;C214A}$ and AnCtrA$^{C186A;C187A}$ were constructed as follows: For each gene two specific complementary primers were designed, carrying the necessary nucleotide changes for cysteine modification. Two fragments with overlapping

tails were amplified using the GFP chimera of each gene as template; first fragment was gsp5-AAgsp6 and the second one AAgsp3-gsp4. Oligonucleotides gsp5 and gsp4 were used to fuse the fragments (Figure 6A). In the case of the C-terminally truncated mutants, other two primers were designed for each gene. The C-termgsp6 primer was placed upstream from the last amino-acid of interest and the C-termgsp3 primer had a 25 nucleotide tail complementary to the C-termgsp6 followed by the next nucleotide of the stop codon of the gene. Using the GFP chimera of each gene as a template, two overlapping fragments were amplified gsp5-C-termgsp6 and C-termgsp3-gsp4. Primers gsp5 and gsp4 were used for fragment fusion (Figure 6B). The cysteine mutants and the C-terminal deletion strains were tested by sequencing.
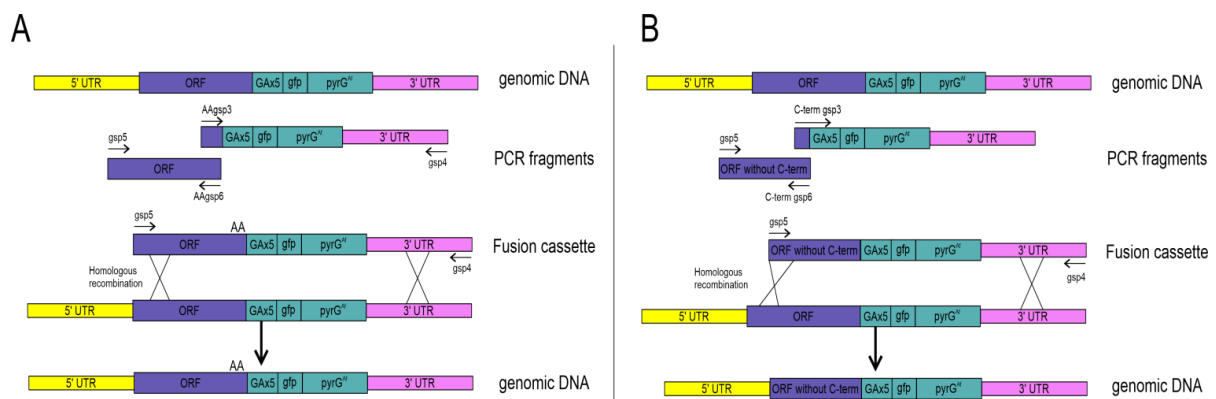
Figure 6: Fusion PCR strategy used to construct replacement cassettes to generate: **(A)** C-terminal cysteine mutants (cysteine to alanine) and **(B)** C-terminal truncated mutants.

4- Specific Protocols Applied in *Aspergillus nidulans*

4.1- *A. nidulans* Transformation

The transformation of *A. nidulans* was carried out following the protocol described in (Szewczyk *et al.*, 2006). *A. nidulans* conidia were scraped from a solid culture plate and resupended in 10 ml of Tween 20 %0.02 (v/v) detergent solution in a 50 ml Falcon tube by mixing thoroughly with a vortex. To remove impurities, the detergent and conidia solution was filtered into a new 50 ml

Materials & Methods

Falcon tube using sterile Miracloth (Calbiochem, 475855) and centrifuged at 4,000 rpm for 10 min. After centrifugation the supernatant was discarded and the conidia concentrated in the pellet was resuspended in fresh Tween 20 %0.02 (v/v) detergent solution. Conidia concentration was measured by counting with a hemocytometer (Thoma) under the microscope (Optihot, Nikon) using a 40x objective. 2.5×10^6 conidiospores/ml were inoculated in 150 ml of liquid ACM containing the carbon and nitrogen sources together with the required supplements. After 14 h of growth at 30 ^{o}C the mycelium was recollected by filtration. One gram (1g) of mycelium was resuspended in 16 ml of ACM containing the carbon and nitrogen sources together with the required supplements and 16 ml of Protoplasting solution (1.1 M KCl, 0.1 M citric acid, pH 5.5, 2.048 g of VinoTaste® (Novozymes)), an enzyme for digestion of the cell wall, was added. The mixture was incubated at 30 ^{o}C from 1 h to 2 h with gentle agitation. Protoplast formation was checked by observation of samples under an optical microscope.

During the protoplast formation process, two 50 ml falcon tubes with 16 ml of 1.2 M sucrose were prepared. The protoplast suspension was divided into equal volumes and gently added onto the 16 ml of 1.2 M sucrose solution to create two different phases. After centrifuging the biphasic solution at 4 ^{o}C for 15 min at 1,800 g, the protoplast fraction concentrated between the two phases was collected with a sterile Pasteur pipette. The collected protoplast fraction was diluted by adding two volumes of 0.6 M KCl. The suspension was again centrifuged at 4 ^{o}C for 10 min at 1,800 g. The pellet containing the protoplasts was washed three times with 0.6 M KCl and finally concentrated in 1 ml of 0.6 M KCl, 50 mM $CaCl_2$.

The transformation process starts when 100 µl protoplasts were mixed with DNA (transformation cassette, 1-3 µg of DNA) and 50 µl of Solution 8 (PEG 6,000 60% (p/v), 10 mM Tris-HCl pH 7.5, 10 mM $CaCl_2$). After incubating the mixture in ice for 20 min, 1 ml of Solution 8 was added and incubated at room temperature for

another 5 min. Finally, 5 ml of Solution 7 (1 M Sorbitol, 10 mM Tris-HCl pH 7.5, 10 mM $CaCl_2$) and 15 ml of warm RMM-TOP regeneration medium were added. The mixture was plated over the Petri plates containing selective regeneration minimal medium. The colonies grown from the transformed protoplasts were observed after 3-4 days of incubation at 37 ^{o}C. After conidia purification in selective medium, homokaryotic transformants were maintained. The presence of the recombinant nuclei was confirmed by PCR and Southern-blot technique as described in (Sambrook *et al.*, 1989).

4.2- Conidia Count

For conidia count experiments, the different strains were inoculated by point-inoculation in 55 mm Petri dishes in the selected conditions. Then they were incubated for 72 h at 37 ^{o}C. After the incubation time the area of the colonies was calculated using the Digimizer Image Analysis Software. Then the colony was collected into 50 ml falcon tubes in 40 ml Tween 20 0.02 % (v/v). The Falcon tube was agitated thoroughly using a vortex for approximately 2 min. The conidiospores were then counted using a hemocytometer (Thoma) under the microscope (Optihot, Nikon) using a 40x objective. Using the area measurements and calculated area of each strain, the conidia density per area was calculated (conidia/cm^{2}). Three replicates of each strain were made and the results were statistically treated. The mean values with their standard deviation values are shown in the graphs.

5- Molecular Biology, Biochemistry and Proteomic Techniques Applied in *Aspergillus nidulans*

5.1- Genomic DNA Extraction

DNA extraction was performed following the method described by Herrero-García (2013). In 100 ml Erlenmeyer flasks 30 ml of supplemented AMM were

Materials & Methods

prepared and inoculated with a 10^6 conidia/ml concentration (following the procedure explained in section 4.1). The inoculated media was then incubated at 37 ^{o}C at 250 rpm for 16 h. Approximately 300 mg of mycelium was collected by filtration using Miracloth and lyophilized for 10 h in a lyophilizer. The lyophilized mycelium was homogenyzed in a mini bead beater and resuspended in 1 ml of lysis buffer (25 mM Tris-HCl pH 8.0, 0.25 M sucrose and 20 mM EDTA). After the addition of 100 µl of 10% SDS the suspension was incubated at 65 ^{o}C for 15 min.

One milliliter (1 ml) of phenol/chloroform/isoamylalcohol (50:48:2) mix was added to the fungal extract. The suspension was shaken vigorously for 10 min and immediately after centrifuged for 5 min at 14,000 rpm. The aqueous phase was placed in a new Eppendorf. This procedure was repeated twice.

The genomic DNA of the aqueous phase was precipitated by adding 1/10 of the volume of Sodium Acetate (NaAc 3 M pH 6) and 0,6 volume of Isopropanol to the supernatant. The mixture was incubated for 15 min at room temperature. The mixture was centrifuged for 5 min at 14,000 rpm and the pellet was washed with 1 ml of 80% ethanol. After a second centrifugation, the supernatant was eliminated and the dried pellet was resuspended in 300-500 µl of milli-Q water. To prevent any RNA contamination every sample was treated with RNase-A (Roche) incubating the reaction at 37 ^{o}C for 1 h (mixing every 10-15 min). The genomic DNA was precipitated using NaAc and isopropanol and sedimented as mentioned above. The genomic DNA was washed again with 0.5 ml of ethanol 80% (v/v), as indicated before. Once the pellet was dry, the DNA was resuspended in 100-200 µl of milli-Q water and stored at -20 ^{o}C. The quality and concentration of the extracted DNA was tested by electrophoresis in a 0.8 % (w/v) agarose gel.

5.2- DNA Analysis by Southern-Blot

After the extracted gDNAs were digested with the appropriate restriction enzyme, the digestion products were run in a 0.8 % (w/v) agarose gel for 2 hours at 90 Volts.

After 10 min exposure to UV light (320nm, Vilber Lourmat), the gel was incubated for 45 min in denaturing solution (1.5 M NaCl, 0.5 M NaOH) and twice (2 x 30 min) in neutralizing solution (0.5 M Tris-HCl pH 7.5, 3 M NaCl). The gel was homogenized with 20x SSC solution (3 M NaCl, 300 mM Sodium Citrate, pH 7) it was transferred to a nylon membrane (Zeta-Probe® blotting, Bio-Rad) by following the standard protocol of capillarity transference (Sambrook *et al.*, 1989). The transferred DNA was fixed to the nylon membrane by exposing the membrane to two 120 mJ UV light pulses (Vilber Lourmat BLX-E254, 254 nm). The membrane was pre hybridized by incubating for 2 h at 42 ^{o}C in Church buffer (Church and Gilbert, 1984), before hybridizing with a specific DNA probe marked with Digoxigenin-dUTP prepared the day earlier (DIG High Prime DNA LABELLING AND DETECTION STARTER KIT II (Roche)).

For DNA probe generation, 1 μg were diluted in 16 μl. The DNA was first denatured by incubating for 10 min at 95 °C. Then it was cooled in ice for 5 min and finally, 4 μl of DIG High Prime were added and the probe was incubated at 37 ^{o}C overnight. The reaction was stopped by adding 2 μl of EDTA (0.2 M pH 8.0) and heating the sample for 10 min at 65 °C. For DNA hybridization, 5 μl of the probe were taken and denatured by incubating 5 min at 95 °C and then cooled in ice for 1 min before adding to the hybridization tube. The hybridization process was carried out at 42°C overnight.

The membrane was incubated with the marked probe for 16 h at 42 °C. To eliminate probe excess two washing steps (30 ml of 2x SSC, 0.1 % SDS) of 5 min and two more of 15 min at 65 ^{o}C (40 ml of 0.5x SSC, 0.1 % SDS) were carried out.

Materials & Methods

For the correct blocking the membrane was incubated for 30 min with 40 ml of blocking solution (stock 10x from the kit diluted in a maleic acid solution: 0.1 M Maleic acid, 0.15 M NaCl, pH 7.5). Two microliters (2 μl) of Anti-Digoxigenin-AP 1:10,000 were added to 20 ml of blocking solution and incubated for 30 min. The membrane was washed (two 20 min washing steps in 0.1 M Maleic acid, 0.15 M NaCl, 0.3% tween 20, pH 7.5 solution) and balanced with detection buffer (5 min balancing step in 0.1 M NaCl, 0.1 M Tris-HCl pH 9.5). The membrane was placed in a plastic surface. The chromogenic agent CSPD ready-to-use (Roche) was added on the DNA containing face of the membrane, expanded uniformly and incubated for 5 min. After the incubation the membrane was dried and incubated at 37 °C for 10 min to improve the luminescent reaction. The images of the detection were taken with a XR GelDoc chemiluminescence Analyzer and were processed with the ImageLab program.

5.3- Membrane Protein Extraction

Procedure described in Hervás-Aguilar and Peñalva (2010). Samples were incubated as described in section 5.1. The samples were collected by filtering with Miracloth, collected into an Eppendorf tube and immediately snap frozen by submerging in liquid nitrogen. Then, the frozen mycelium was lyophilized for 10 h. The lyophilized mycelium was crushed with a metal bead in a mini bead beater placed inside a fridge (4 ^{o}C). Approximately 6-7 mg of mycelium was resuspended in 1 ml of pre-cooled lysis buffer (0.2 M NaOH, 0.2% β-mercaptoethanol) by vigorous agitation for 1.5 min. To precipitate the proteins, 7.5% (w/v) TCA was added. The suspension was mixed gently and incubated for 10 min in ice. After the mixture was centrifuged at 4 ^{o}C for 5 min at 14,000 rpm the supernatant was taken away. A second centrifugation was performed in order to make sure that all TCA was removed. The pellet was partially resuspended by adding 100 μl of 1 M TrisBase and 200 μl of Laemmli buffer. Samples were stored at -20 ^{o}C.

5.4- Western-Blot

The precipitated protein samples were denatured at 95 ^{o}C and run in 10% (w/v) SDS-polyacrylamide gels (MiniProtean 3 system, Biorad) (Laemmli, 1970). The proteins of the gel were transferred to a nitrocellulose membrane. Prior to blocking the membrane a Ponceau staining was conducted as a loading control. The membrane was washed three times for 5 min with distilled water in agitation; then, the Ponceau stain (0.5% (w/v) Ponceau S dissolved in 1% (v/v) acetic acid) was added and incubated for 1 min. Multiple washes with water were carried out until the protein bands were visible. Then, a picture of the membrane was taken. To remove the Ponceau staining, the membrane was incubated in a 200 µM NaOH, 20% (v/v) acetonitrile solution for 1 min. After some additional washes with distilled water the membrane was ready to block. After blocking, tagged proteins were detected depending on the antigen or epitope, with their respective primary antibody (Table 5). In all the cases the secondary antibody was conjugated to horseradish peroxidase. The peroxidase activity was detected with Clarity TM Western chemiluminescence system (Biorad) in a XR GelDoc chemiluminescence Analyzer. ImageLab software was used to process and analyze the images taken.

Table 5: Antibodies used in the study

	ANTIBODY	DILUTION	SOURCE	REFERENCE
1º	α-GFP	1:5000	mouse	ROCHE
	α-HA	1:10000	mouse	Santa Cruz
	α-Hexokinase	1:80000	rabbit	Cemicon Intemat Inc
2º	α-mouse IgG	1:4000	goat	Jackson InmunoResearch
	α-rabbit IgG	1:10000	ass	Sigma

Materials & Methods

5.5- Fluorescence Microscopy

Aspergillus nidulans strains expressing CprA::GFP, CtrC::GFP-Hhoa::mRFP and CtrA::GFP-HhoA::mRFP in vegetative state were studied. A phosphate-supplemented of low phosphate minimal medium ("WATCH" minimal medium, WMM) version was used for culture. The basal medium containing 17 mM KCl, 5 mM MgSO4 and 1/400 of Kaeffer's trace element solution was supplemented with 0.1% glucose (w/v), 71 mM $NaNO_3$ and 25 mM NaH_2PO_4, which resulted in a pH of 5.5. Conidiospores were cultured on Ibidi-plates containing 3 ml of medium. Plates were incubated for 22 h at 25 °C before visualization under the microscope.

Fluorescence images were obtained from these in vivo cultures in an Axio Observer Z1 inverted microscope, equipped with a 63× Plan-Apochromat 1.4 oil immersion Lens, and fitted with filters number 38 (green fluorescence: excitation 470 nm; emission 525 nm. Red fluorescence: excitation 545/25; emission 605/70). The images were processed with ImageJ software.

5.6- RNA Extraction

Samples were incubated in the same conditions as described in section 5.1 with certain differences. The sample was incubated in a 2 L (liter) fermenter with an aeration rate of 1 volume per unit or medium volume per minute and agitation. The samples were collected by filtering with Miracloth, collected into cryovials and immediately submerged into liquid nitrogen to avoid heating of the sample. Then, the samples were crushed in a mortar with liquid nitrogen to avoid heating of the sample. About 150 mg of each sample were separated into an Eppendorf tube for total RNA extraction. For total RNA extraction, the Macherey-Nagel™ NucleoSpin™ RNA Plant Kit (Ref: 740949.50) was used following the manufacturer's instructions.

The quality and concentration of RNA was tested using two methods. First, the sample were run in a 1.2% (w/v) agarose gel and stained in ethidium bromide to check the integrity of the rRNA. Second, the purity and concentration of the samples was checked using the NanoDrop 2000c Spectrophotometer (Thermo Fisher Scientific) with 260 nm wavelength.

5.7- Northern-Blot

The RNA samples were run in a 1.2 % (w/v) agarose and 6.8% (v/v) formaldehyde gel. For a 200 ml gel, 2.4 g agarose were dissolved in 144 ml of RNase free water by boiling. Then 20 ml of MOPS 10x (0.4 M MOPS, Sigma-Aldrich; 0.1 M Sodium Acetate; 0.01 M EDTA) were added and left to cool down. When the mix was cooled (around 45 ^{o}C), 36 ml of formaldehyde 36.5-38 % (v/v; Sigma-Aldrich) were added. Finally, the whole mix was poured into the gel cuvette.

The samples to be loaded were prepared in the following steps: 7 μg of RNA were taken from each sample and diluted to 10 μl with RNase free water. Then to each sample 12.5 μl of N,N-dimethylformamide, 4 μl de formaldehyde (36,5-38% v/v), and 2.5 μl de MOPS 10x were added. The samples were incubated at 60 ^{o}C for 10 min. Then 3 μl of Gel Loading Buffer were added to each sample and samples were loaded. The gel was run at 10 Volts for 15-16 h. After the electrophoresis, the gel was stained in ethidium bromide to check the integrity and the concentration of the RNA samples. The gel was unstained by doing several washes in RNase free water and transferred to a nylon membrane following the protocol described in section 5.2. The transferred RNA was fixed to the nylon membrane (Zeta-Probe® blotting, Bio-Rad) by exposing the membrane to three 120 mJ UV light pulses (Vilber Lourmat BLX-E254, 254 nm).

After Cross-linking the RNA to the membrane the methylene blue staining was used as a loading control. The membrane was incubated in 5% (v/v) acetic acid for 15 minutes, then rinsed with RNase free water and incubated in a 0.04%

methylene blue in 0.5 M sodium acetate (pH 5.2) solution for 5 minutes; finally, the membrane was destained by washing the membrane with RNase free water until the rRNA bands were clearly visible. A picture of the rRNA bands was taken as a loading control of the membrane. After this we proceeded to the hybridization step.

For these experiments, DNA probes were generated as specified in section 5.2. The hybridization process was also identical except that it was carried out at 65 ^{o}C. The washing steps of the hybridized nylon membrane were the same as in section 5.2 except for two things, the 0.5x SSC, 0.1 % SDS buffer was changed for a 0.1x SSC, 0.1 % SDS and the last incubation at 37 ^{o}C was skipped due to background problems. The images of the detection were taken with a XR GelDoc chemiluminescence Analyzer and were processed with the ImageLab program.

5.8- cDNA

First strand cDNA of each sample was synthesized using the reverse transcriptase PrimeScriptTM RT reagent Kit (Takara) following manufacturer's instructions.

5.9- Real-Time PCR

qPCR assays were performed in an ABI 7500 system according to the manufacturer's instructions (Applied Biosystems, Foster, CA) using 5x PyroTaq EvaGreen qPCR Mix Plus (CMB, Cultek Molecular Bioline), an analog of SYBR Green. Three biological replicates of each condition and two technical replicates of each biological replicate were tested. Relative expression to the t_o sample was studied in each case and *AnbenA* was used as internal reference to normalize gene expression levels. The $2^{-\Delta\ CT}$ method was used to determine the relative expression level ratio. Oligonucleotides used in this assay are listed in Table 2.

6- Bioinformatics

Alignments were performed using the predicted protein sequences released in the National Centre for Biotechnology Information (NCBI) database. Multiple sequence alignments were performed and analyzed using Clustal Omega application in EBI (http://www.ebi.ac.uk/Tools/msa/clustalomega). Transmembrane domains were predicted using Hidden Markov Models (HMM) in the Institute Pasteur Mobyle server (http://mobyle.pasteur.fr). Phylogenetic analyses were carried out using the Molecular Evolutionary Genetics Analysis version 7 (MEGA 7) software (https://www.megasoftware.net/home). The used statistical method was neighbor-joining, with 500 bootstrap phylogeny test and p-distance as substitution model. For gene construct designing the VectorNTI 11.5 software was used.

To check Gene Onthology classification and possible gene function of our organism the Aspergillus Genome database (http://aspgd.org) and FungiDB (https://fungidb.org/fungidb/app) databases were mostly used. For gene homology relationship searches the Ensembl fungi (https://fungi.ensembl.org/index.html) database was used.

Other databases were also used assiduously, for example: Uniprot (https://www.uniprot.org/), GenBank (https://www.ncbi.nlm.nih.gov/genbank/) and RCSB Protein Data Bank (https://www.rcsb.org/).

I. Chapter-

The High-Affinity Copper Uptake System in *A. nidulans*

I. The High-Affinity Copper Uptake System in *A. nidulans*

1- Introduction

Previous studies have reported the high-affinity copper uptake system in eukaryotes to be composed of effectors denominated Copper Transporter (Ctr) proteins. They are relatively small proteins that contain up to three transmembrane domains (TMD) and show high copper specificity for reduced copper (Cu^+) (Petris, 2004;Puig *et al.*, 2002). ScCtr1 has multiple Cu-binding methionines arranged in MxM or MxxM motifs (Mets motifs) in the extracellular N-terminal for facilitated copper import (Dancis *et al.*, 1994). ScCtr3 on the other hand, has 11 cysteine residues, another Cu-binding ligand, throughout the sequence (Pena *et al.*, 2000). The conserved M-xxx-M motif in the transmembrane domain is essential for copper ion translocation (Puig *et al.*, 2002). In order to be internalized by Ctr proteins, environmental copper is reduced from Cu^{2+} to Cu^+ by cell surface metalloreductases ScFre1 and ScFre2 prior to uptake (Rees and Thiele, 2004;Rutherford and Bird, 2004). Cu^+ transport across membranes requires Ctr proteins to assemble as trimers and generate a pore in the plasma membrane (De Feo *et al.*, 2009). Cu^+ transport by Ctr proteins does not require ATP hydrolysis (Lee *et al.*, 2002), as Cu^+ enters the cell by a passive transport mechanism. Extracellular K^+ and the extremely low intracellular copper concentration facilitate copper import (Balamurugan and Schaffner, 2006).

The Ctr proteins responsible for high-affinity copper uptake were described in *A. fumigatus* by Park *et al.,* (2014). Studies also demonstrated that copper acquisition through the high-affinity copper uptake machinery was critical for growth and conidiation in low Cu environments (Kusuya *et al.*, 2017). As in many other pathogenic organisms, Cu uptake and virulence are also closely related in *A. fumigatus* (Cai *et al.*, 2017). Expression of Ctr proteins is up-regulated when *A. fumigatus* conidia are challenged by human neutrophils (Sugui *et al.*, 2008). Moreover, it has been reported that, in the absence of the Ctr proteins *A.*

I. The High-Affinity Copper Uptake System in *A. nidulans*

fumigatus fails to grow in infected tissues (Cai *et al.*, 2017), corroborating the importance of Ctr protein expression for virulence.

However, no high-affinity copper transporters had been reported in *A. nidulans*. With the RNA-seq data and previous data on copper homeostasis, two putative high-affinity copper transporters were identified, AN3209 and AN3813. While the characterization process of these putative copper transporters was ongoing, Cai *et al.,* (2019) reported AN3209 and AN3813 as Ctr proteins. Thus, the investigation was taken a step further in the characterization of the Ctr proteins.

The aim of this study was to gain insight on the effect of copper toxicity on gene expression, as well as to complement and expand the first characterization of the copper transport proteins by elucidating their role in general copper homeostasis in *Aspergillus nidulans*. For the first purpose, an RNA-seq experiment was performed which informed on gene expression changes in the most altered biological processes, structural components and molecular functions. For the second purpose, exhaustive functional analysis experiments permitted us to discern the individual roles of each Ctr protein in the copper uptake process. Apparently, AnCtrC plays a major role in high-affinity copper uptake in mild copper deficiency conditions. Its deletion causes secondary level copper limitation effects like spore and pigmentation deficiencies, most likely due to Cu deficiency of the conidial laccase AnYA, which can be ascribed to limiting copper stores in the cells due to impaired copper uptake (Scherer and Fischer, 2001). On the other hand, AnCtrA prevails as the most effective copper uptake protein in conditions of more extreme copper deficiency. Its deletion causes primary copper limitation effects like growth limitation and lack of pigmentation. Nevertheless, individual deletion of either Ctr protein reveals that both function in a complementary manner. To further complement the characterization of the high-affinity copper uptake system, a putative plasma membrane copper reductase is presented, AnFreC.

2- Results

2.1- Gene Expression Analysis Under Copper Toxicity Conditions

An RNA-seq analysis was performed to compare the transcriptome of vegetative hyphae grown for 16 h in liquid medium (nutritional condition; acronym NC) with that of a hyphae shifted to medium with 100 μM $CuSO_4$, a high enough concentration to activate the copper toxicity response (copper toxicity; acronym CT), 1 h before harvest. The reads of mRNAs expressed under NC and CT conditions mapped 87.4% and 89.7% of a total of 10,943 genes predicted by the AspGD, respectively. Based on the gene expression analysis criteria applied in this study ($\cong$2-fold change, p-value < 0.05) the expression of 13.7% (1,494) of genes was modified between the two conditions: 7.3% (796) of the genes were up-regulated (higher transcript levels in CT than in NT), while 6.4% (698) were down-regulated. The copper toxicity response therefore exhibited a balanced gene down-regulation and up-regulation rate (Figure 7A).

I. The High-Affinity Copper Uptake System in *A. nidulans*
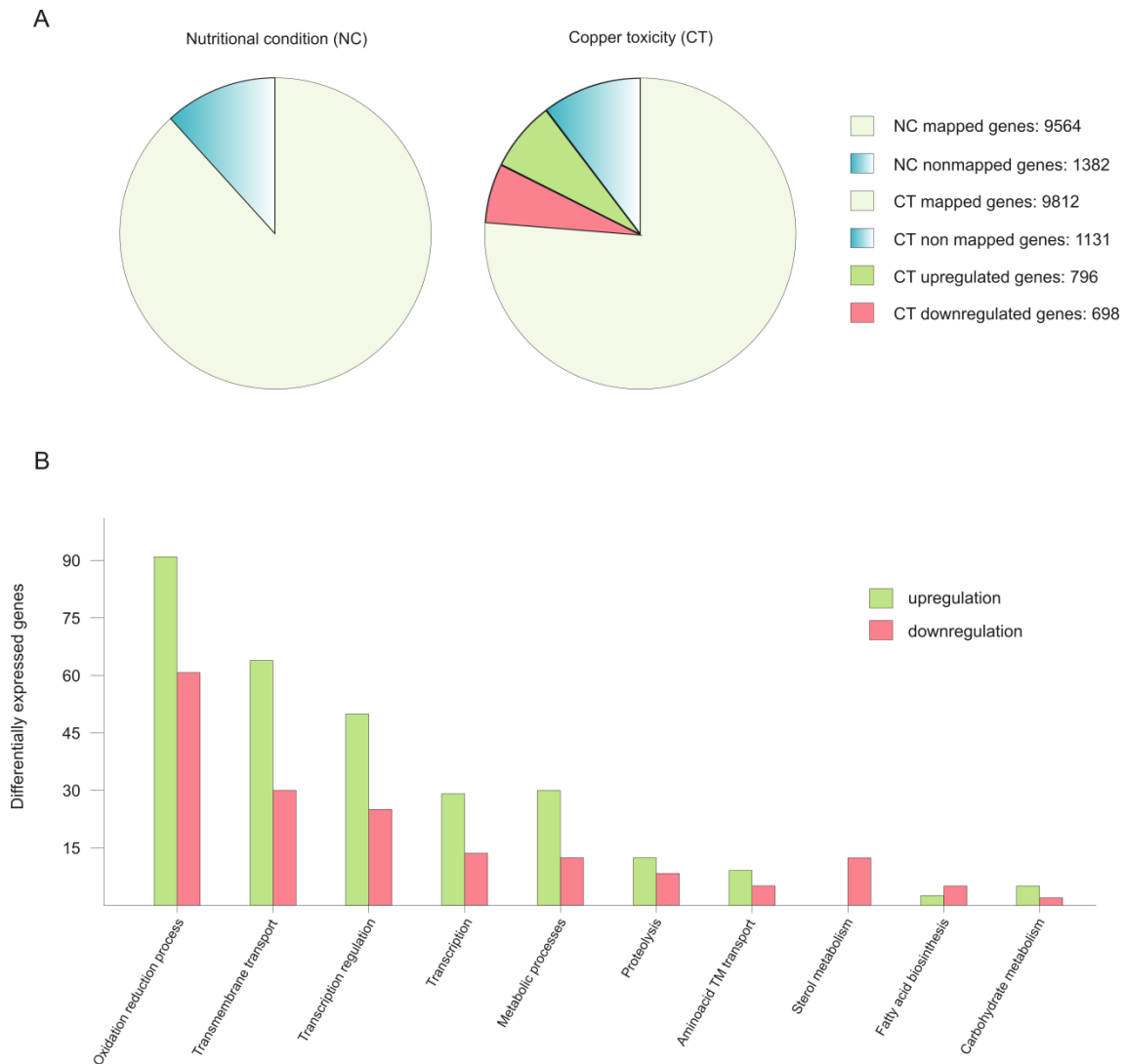
FIGURE 7: Graphic representation of the RNA-seq results. **(A)** To exemplify the number of mapped genes in each condition, the 10.943 genes predicted by the AspGD were considered as 100% and data was presented in percentages. The differentially expressed genes are represented in the copper toxicity pie chart divided in two colors in proportion to the number of up-regulated and down-regulated genes. **(B)** Representation of the up-regulated and down-regulated genes of the most affected biological processes.

I.The High-Affinity Copper Uptake System in *A. nidulans*

Table 6 shows the expression of most of the genes related to copper homeostasis, either characterized or predicted, and also some copper containing proteins. The TFs that orchestrate the copper homeostasis process, *AnaceA* and *Anmac1*, showed no significant variations in response to copper; however, the genes that code for copper mobilizing proteins, either uptake or detoxification, showed significant changes in their expression. The copper detoxification gene *AncrpA* was up-regulated in response to an external copper load. On the other hand, the already described Ctr protein coding genes *AnctrA* and *AnctrC* (elaborated on below) were significantly down-regulated under copper-toxicity condition; however, the putative Ctr protein coding gene, *AnctrB* (elaborated on below), was unaltered. Homology searches revealed the putative homologs of the *S. cerevisiae* Atx1, Cox17 and Ccs1 genes. A very important element for proper copper uptake is the plasma membrane oxidoreductase that reduces copper prior to internalization. In Table 6 a characterized metalloreductase, *AnfreA* is shown, along with two other predicted plasma membrane oxidoreductases, AN0773 and *AnfreC* (elaborated on below), which are co-regulated with the Ctr proteins and thus, could be possible metalloreductase candidates. Finally, the expression of the intracellular copper trafficking P-type ATPase *AnygA* shows significant up-regulation under excess copper conditions.

Besides copper homeostasis proteins, many other copper related proteins showed expression changes, as copper is a required cofactor of many enzymes (Table 6). The Cu/Zn superoxide dismutase *AnsodA* showed no difference in expression in response to the external copper load. On the other hand, laccases, a copper-containing enzyme-family required for melanin synthesis, displayed a divergent response: *AnyA* and *AnlccD* were down-regulated, while *AntilA* was up-regulated.

I. The High-Affinity Copper Uptake System in *A. nidulans*

Table 6: RNA-seq data of the copper homeostasis genes and the copper related protein coding genes.

Gene	log2 fold change	Value_1	Value_2	q value	Significant	Description
AN1924	-0,554556	250,162	170,327	0,269576	no	*AnaceA*. Copper detoxification TF
AN0658	0,417535	20,518	27,4048	0,503204	no	*Anmac1*. Copper uptake TF
AN3117	6,4078	11,9725	1016,54	0	yes	*AncrpA*. Copper-exporting P-type ATPase.
AN2934	-0,284851	71,0897	58,3523	0,686464	no	*AnctrB*. Copper ion transmembrane transporter activity.
AN3209	-4,18902	24,4975	1,34308	2,75E-08	yes	*AnctrA*. High-affinity copper transporter
AN3813	-2,97333	134,667	17,1475	3,34E-12	yes	*AnctrC*. High-affinity copper transporter.
AN3624	1,01501	20,1871	40,7964	0,015651	yes	*AnygA*. ScCcc2 homologue. Predicted copper transporter.
AN6045	1,95069	76,4666	295,588	2,09E-07	yes	Ccs1 Sod chaperone ortholog,
AN1390	0,137135	110,504	121,523	0,853005	no	Atx1 chaperone homologue.
AN4863	0,397399	78,3646	103,216	0,541532	no	Cox17 Cytochrome C oxidase chaperone homologue.
AN7662	-1,11534	35,8567	16,5508	0,018818	yes	*AnfreA*. Predicted iron metaloreductase.
AN0773	-2,14409	114,6	25,9269	4,15E-08	yes	Predicted metalloreductase.
AN3208	-4,54749	14,5531	0,622335	2,56E-14	yes	*AnfreC*. Predicted metalloreductase.
AN0241	-0,342918	1361,11	1073,16	0,57373	no	*AnsodA*. Cu/Zn-superoxide dismutase.
AN6635	-1,48008	4,56506	1,63643	0,034958	yes	*AnyA*. Conidial laccase involved in green pigment production.
AN6830	1,79e+308	0	0,145851	1	no	*AnlccA*. Putative laccase.
AN9170	0	0	0	1	no	*AnlccB.* Extracellular laccase.
AN5379	-0,611597	0,055515	0,0363333	1	no	*AnlccC.* Extracellular laccase.
AN0878	-1,92869	1,5301	0,401909	0,0384564	yes	*AnlccD.* Extracellular laccase.
AN0901	1,89527	6,9476	25,8445	6,10E-05	yes	*AntilA*. Hyphal tip laccase.

To interpret the biological significance of the registered changes in gene expression, we conducted a GO (Gene Onthology) classification analysis of the results. The identified changes in gene expression occurring in response to toxic copper levels were indicative of modifications in various processes (Figure 7B). Redox processes were the most affected. Copper has a relatively high reduction potential (E^o_0 = -0.34V), thus, it may interfere with ongoing oxidation-reduction processes, leading to changes in the expression levels of the corresponding enzymes. For example, seven oxidoreductases with predicted roles in sterol metabolism were significantly down-regulated (AN8907, AN4094, AN6506, AN6973, AN3638, AN10648, and AN3817). Catalases *AncatB*, *AncatC* and *AncpeA*/*AncatD* were slightly up-regulated. On the other hand, the expression of superoxide dismutases and the oxidative stress transcription factors *AnnapA* and

I.The High-Affinity Copper Uptake System in *A. nidulans*

AnatfA were not altered. Transmembrane (TM) transport of various substrates, as sugars, oligopeptides and metals was modified: the xylose transporters *AnxtrA* and *AnxtrB*, the putative high-affinity nickel uptake protein AN6115, the putative Cation Diffusion Facilitator (CDF) transporter. Finally, transcriptional regulation was also notably altered, based on the changes in the expression of transcription factors. Most of them were unidentified.

Analyzing the repercussion of copper-toxicity on gene expression, certain gene clusters were affected by copper addition. For example, the siderophore biosynthesis gene cluster (*AnsidA, AnsidC, AnsidD, AnsidF, AnsidG, AnsidH*, and *AnsidI*) was notably down-regulated, together with the iron homeostasis TF, *AnhapX*. Besides the siderophore biosynthesis cluster, most members of the Emericellamide antibiotic biosynthesis gene cluster were down-regulated (*AneasB, AneasC*, and *AneasD*). A set of genes (AN2558, AN2559, AN2560, AN2561, and AN2562) with no confirmed function was drastically up-regulated. However, by sequence analysis tools, we found that AN2562 was the homolog of the N-acetylglucosamine transporter Ngt1 from *C. albicans*; AN2560 was the homolog of the high-affinity methionine and cysteine transporter Mup1 from *S. cerevisiae* and *C. albicans*; AN2558 was the homolog of the flavin-containing monooxygenases CaIfk1 and ScFmo1; and AN2559 and AN2561 were a predicted oxidoreductase and a predicted methyltransferase, respectively (Table 7).

In summary, copper toxicity altered the expression of 13.7% of the genes with a balanced ratio between up-regulated and down-regulated genes (Figure 7A). Changes in copper concentration derived in a strong modification of the copper homeostasis system, the copper dependent enzymes and multiple biological processes, especially oxidation reduction processes and predictably, in cellular components such as biological membrane composition. As a remarkable feature, in most of these processes, more genes were up-regulated than down-regulated (Figure 7B).

I. The High-Affinity Copper Uptake System in *A. nidulans*

Table 7: RNA-seq data of differentially expressed genes.

Gene	log2 fold change	NC	CT	q value	Significant	Description
AN8251	-2,29289	212,998	43,4658	2,21E-10	yes	*AnhapX*. TF iron homeostasis
AN5823	-1,6464	2071,32	661,656	0,00046089	yes	*AnsidA*. Siderophore biosynthetic gene cluster member
AN8751	0,252704	33,0097	39,329	0,68274	no	*AnsidB*. Siderophore biosynthetic gene cluster member
AN0607	-0,957512	17,4648	8,99339	0,0248114	yes	*AnsidC*. Siderophore biosynthetic gene cluster member
AN6236	-1,68316	454,38	141,494	0,00026402	yes	*AnsidD*. Siderophore biosynthetic gene cluster member
AN6234	-0,91275	248,15	131,81	0,0336505	yes	*AnsidF*. Siderophore biosynthetic gene cluster member
AN8539	-1,19743	277,515	121,011	0,00473987	yes	*AnsidG*. Siderophore biosynthetic gene cluster member
AN6235	-1,19947	157,372	68,5252	0,00438479	yes	*AnsidH*. Siderophore biosynthetic gene cluster member
AN0609	-2,13608	394,676	89,7878	3,63E-09	yes	*AnsidI*. Siderophore biosynthetic gene cluster member
AN10080	-0,216896	22,965	19,7594	0,777446	no	*AnsidL*. Siderophore biosynthetic gene cluster member
AN7800	-0,267815	48,5357	40,3126	0,702964	no	*AnmirA*. Siderophore iron transporter
AN8540	-1,24341	1759,6	743,208	0,0167845	yes	*AnmirB*. Siderophore iron transporter
AN7485	-0,738315	101,585	60,894	0,103354	no	*AnmirC*. Siderophore iron transporter
AN8907	-3,85352	2257	156,138	0	yes	Putative sterol methyl oxidase
AN4094	-2,81214	478,501	68,131	2,56E-14	yes	Putative sterol reductase
AN6506	-2,63572	947,541	152,464	2,10E-11	yes	Putative sterol methyl oxidase
AN6973	-1,72893	1740,29	525,004	5,21E-05	yes	Putative sterol methyl oxidase
AN3638	-1,34834	382,258	150,129	0,00162595	yes	Putative sterol methyl oxidase
AN10648	-0,960416	76,6647	39,3987	0,0282487	yes	Sterol reductase activity, ergosterol biosynthetic process
AN3817	-0,929126	85,5385	44,9228	0,0288343	yes	Putative reductase, predicted role in sterol metabolism
AN6412	1,75949	4,36251	14,7705	0,00418067	yes	*AnxtrA*. Xylose transporter A
AN3264	1,44359	4,83779	13,1587	0,0126647	yes	*AnxtrB*. Xylose transporter B
AN2911	-0,0516925	117,662	113,521	0,95033	no	*AnatfA*. TF for response of conidia to stress.
AN7513	0,53883	117,309	170,426	0,298838	no	*AnnapA*. TF required for resistance to oxidative stress
AN8637	-1,56595	4,86518	1,64324	0,0317285	yes	*AncatA*. Catalase
AN9339	1,49778	18,7857	53,0525	0,00017666	yes	*AncatB*. Catalase
AN5918	1,24056	25,0035	59,0807	0,00396133	yes	*AncatC*. Catalase
AN7388	1,37382	12,0197	31,1495	0,00400481	yes	*AncpeA/AncatD*. Catalase
AN6115	1,89337	35,271	131,032	1,45E-06	yes	Cation Difusion Facilitator (CDF) transporter
AN2545	-1,46337	0,478858	0,173655	1	no	*AneasA*. Emericellamide biosynthetic gene cluster
AN2547	-2,25667	1,10672	0,231587	0,001229	yes	*AneasB*. Emericellamide biosynthetic gene cluster
AN2548	-4,52491	0,952086	0,0413563	0,0229756	yes	*AneasC*. Emericellamide (eas) biosynthetic gene cluster
AN2549	-2,98507	14,804	1,86976	1,06E-07	yes	*AneasD*. Emericellamide (eas) biosynthetic gene cluster
AN2558	6,95672	0,0388284	4,82314	5,62E-05	yes	CaIfk2 and ScFmo1 homologue
AN2559	8,11636	0,171753	47,662	2,56E-14	yes	Predicted oxidoreductase activity
AN2560	7,69094	0,0580346	11,992	6,81E-07	yes	ScMup1 and CaMup1 homologue
AN2561	7,98542	1,19049	301,7	0	yes	Putative methyltransferase
AN2562	7,07374	0,0340531	4,58737	0,00125881	yes	CaNgt1 homologue

2.2- Screening for Potential Copper Transport Proteins

In order to select putative copper transporters we searched for putative orthologs of *Saccharomyces cerevisiae* Ctr transporters among down-regulated genes under copper toxicity. Blastp searches using the full-length of the ScCtr protein sequences yielded three results, the already identified AN3209 and AN3813 and another putative copper transporter, AN2934, termed *AnctrB*. *AnctrB* is the top hit of the copper transporter ScCtr2, which encodes a vacuolar Cu transporter (Liu *et al.*, 2012;Qi *et al.*, 2012). Cai *et al.,* (2019) recently identified AN3209 and AN3813 as copper uptake proteins in *A. nidulans*, and AnMac1 as the TF controlling their expression. In this work, AN3209 and AN3813 were named AnCtrA2 and AnCtrC, respectively, claiming they were AfCtrA2 and AfCtrC homologs, but the protein sequence analysis results support a different interpretation. BLASTp analyses revealed that AnCtrA and AnCtrC are significant hits of AfCtrC (42% and 60% protein identity, respectively); however, there is no significant hit of AfCtrA2 (24% and 22% protein identity, respectively) in the *A. nidulans* proteome. Thus, instead of naming AN3209 as AnCtrA2, we considered the name AnCtrA.

Sequence data revealed that *AnctrA* and *AnctrC* share great similarity. Furthermore, out of the 127 species that possess an *AnctrA* ortholog, 94 also possess an *AnctrC* ortholog (Figure 14).

According to the phylogeny analyses shown in Figure 8, three major clusters can be differentiated. Most Ctr proteins of filamentous fungi are related to ScCtr3 (Red); *A. fumigatus*, *A. nidulans*, and *A. niger* possess Ctr proteins closely related to the vacuole Cu transporter ScCtr2 (Blue); Out of the 27 proteins of the phylogeny test, only four proteins are related to ScCtr1 (Green). The results reflect that ScCtr3 orthologs comprise the biggest group of proteins and in this group we can find most Ctr proteins of filamentous fungi.

I. The High-Affinity Copper Uptake System in *A. nidulans*
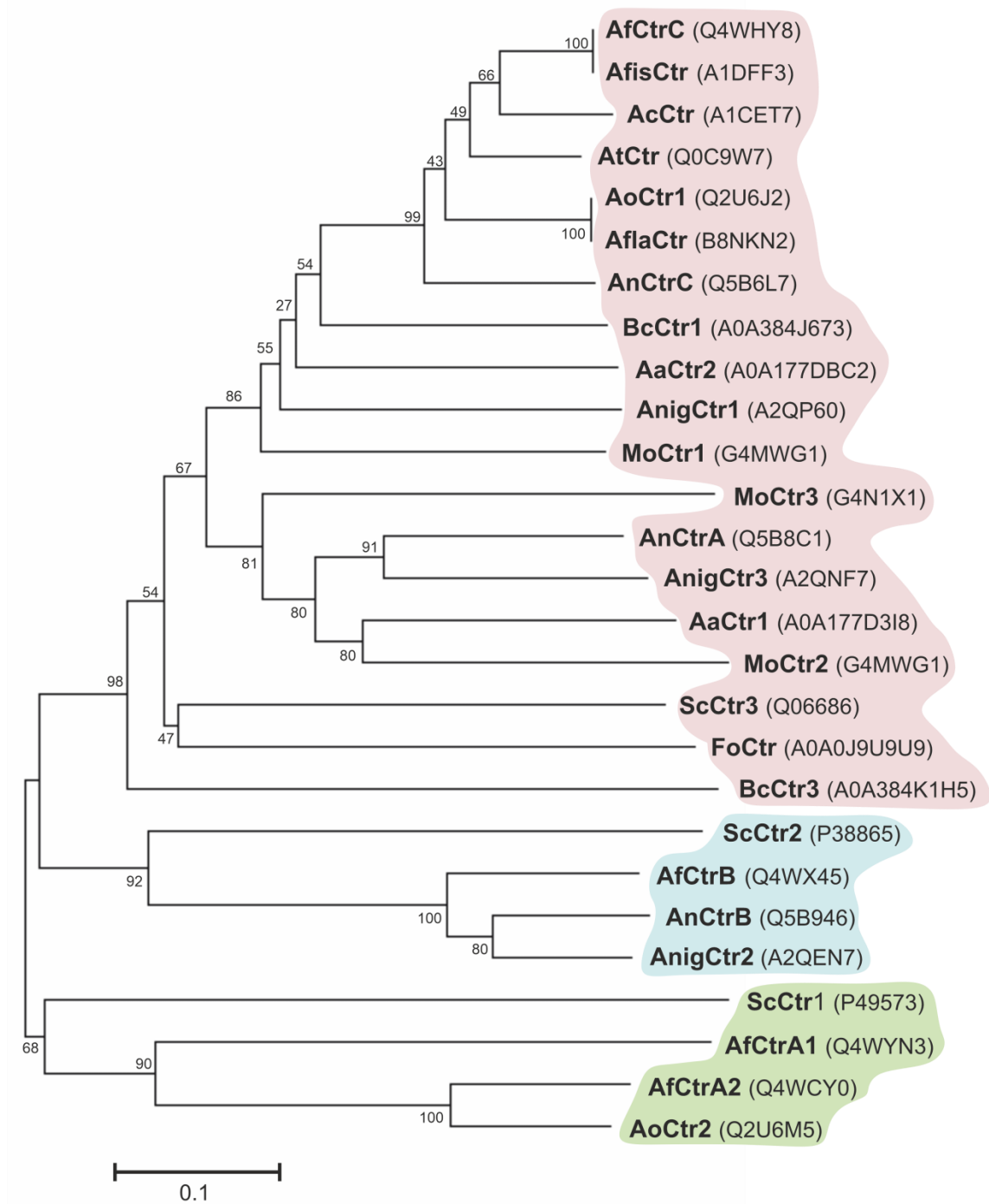
Figure 8: Phylogenetic analysis of Ctr proteins. Using MEGA7, a phylogenetic tree was generated by the Neighbor-Joining method with the Bootstrap method as phylogeny test. Analyzed organisms: *Alternaria alternata* (Aa), *Aspergillus nidulans* (An), *Aspergillus fumigatus* (Af), *Aspergillus fischeri* (Afis), *Aspergillus flavus* (Afla), *Aspergillus niger* (Anig), *Aspergillus oryzae* (Ao), *Aspergillus clavatus* (Ac), *Aspergillus terreus* (At), *Botrytis cinerea* (Bc), *Fusarium oxysporum* (Fo), *Magnaporthe oryzae* (Mo), and *Saccharomyces cerevisiae* (Sc).

I. The High-Affinity Copper Uptake System in *A. nidulans*

A multiple sequence alignment of *A. nidulans* Ctr proteins is shown in Figure 9. Strong similarities in amino acid sequences could be observed in certain regions of the N- and C-terminal, but not in the loop between transmembrane domains (TMD) 1 and 2, which showed higher variability. Detailed sequence analysis showed the presence of common conserved motifs predicted to code for copper binding. AnCtrA, AnCtrC, AfCtrC and CnCtr4 contain a Met motif arranged as M-xx-M-x-M in the amino-terminal region (Nt) (Met motif shown in blue box). Three additional methionine residues are conserved among the Ctr protein sequences aligned: a methionine in the amino-terminal, located $\cong$ 22 amino acids upstream from the TMD1 (M30 in AnCtrA, M23 in AnCtrC, M20 in ScCtr3, M58 in AfCtrC and M41 CnCtr4) and an M-xxx-M motif in the predicted TMD2 (M134-M138 in AnCtrA, M168-M172 in AnCtrC, M185-M189 in ScCtr3, M197-M201 in AfCtrC and M156-M160 CnCtr4). The methionine residue located prior to TMD1 is equidistant in *A. nidulans* and other fungi, as noted by Puig *et al.* (2002). As shown in Figure 9A, there are two conserved cysteine residues flanking this functional residue (Cys residues are highlighted in red for their copper handling capacity). Additional methionine and cysteine residues are widespread within the sequence. Finally, in all the proteins analyzed close to the terminus of the carboxy-terminal region, a putative copper handling motif that could be involved in copper coordination and transport was identified; a di-cystine motif in the case of ScCtr3, CnCtr4, AnCtrA and AnCtrC, and a M-x-C motif in the case of AfCtrC. Based on computer algorithms (TMHMM and HMMTOP predictions), as shown in Figure 9B, AnCtrA was predicted to contain two transmembrane regions while AnCtrC contained three. According to these predictions, the amino tail would be oriented to the outside of the cell and the carboxyl tail into the cytosol, in the case of AnCtrC. In the case of AnCtrA, however, both protein ends would be oriented to the outside.

I. The High-Affinity Copper Uptake System in *A. nidulans*

Figure 9: Sequence analysis of *Aspergillus nidulans* high-affinity copper transporters AnCtrA and AnCtrC. **(A)** Alignment of predicted full-length of *Saccharomyces cerevisiae* Ctr3, *Cryptococcus neoformans* Ctr4, *Aspergillus nidulans* CtrA and CtrC, and *Aspergillus fumigatus* CtrC sequences compared using the Clustal method. Identical residues are described with asterisk, and conservative and semi-conservative residues with double and single dots, respectively. Methionine residues are represented in green and cysteines in red. The length of each protein is indicated adjacent to the last amino acid. Protein accession numbers are reported as follows: ScCtr3 (Q06686), CnCtr4 (J9VLN4), AnCtrA (C8VIA1), AnCtrC (C8V6S8), and AfCtrC (Q4WHY8). **(B)** Proposed model of AnCtrA and AnCtrC describing the predicted membrane topology and the conserved methionine and cysteine residues. AnCtrA contains two transmembrane domains and AnCtrC three.

2.3- Functional Characterization of AnCtr Mutants

The function of AnCtrA and AnCtrC through mutant analysis was recently reported (Cai *et al.*, 2019); however, the individual role of each protein and their hierarchy in copper homeostasis remained unspecified. To gain further insight into this matter, single and double knock-outs of *AnctrA* and *AnctrC* were generated by gene replacement techniques (see list of strains).

I.The High-Affinity Copper Uptake System in *A. nidulans*

The capacity of these strains to grow under different copper availability conditions was tested. We first reproduced the experiment conducted by Cai *et al.,* (2019), by testing all generated mutant strains in 0 μM Cu media, with identical results: the single deletion mutants showed a WT-like phenotype and the only strain showing growth disruption was the double null mutant *ΔAnctrA-ΔAnctrC* (Figure 10A). These results provided evidence that, under copper deficiency conditions, AnCtrA and AnCtrC complemented each other. Addition of copper to the medium rescued the double deletion mutant defective phenotype. Similar results were obtained in liquid media as only the double null mutant showed a significantly lower growth rate than the WT strain (Figure 10B).
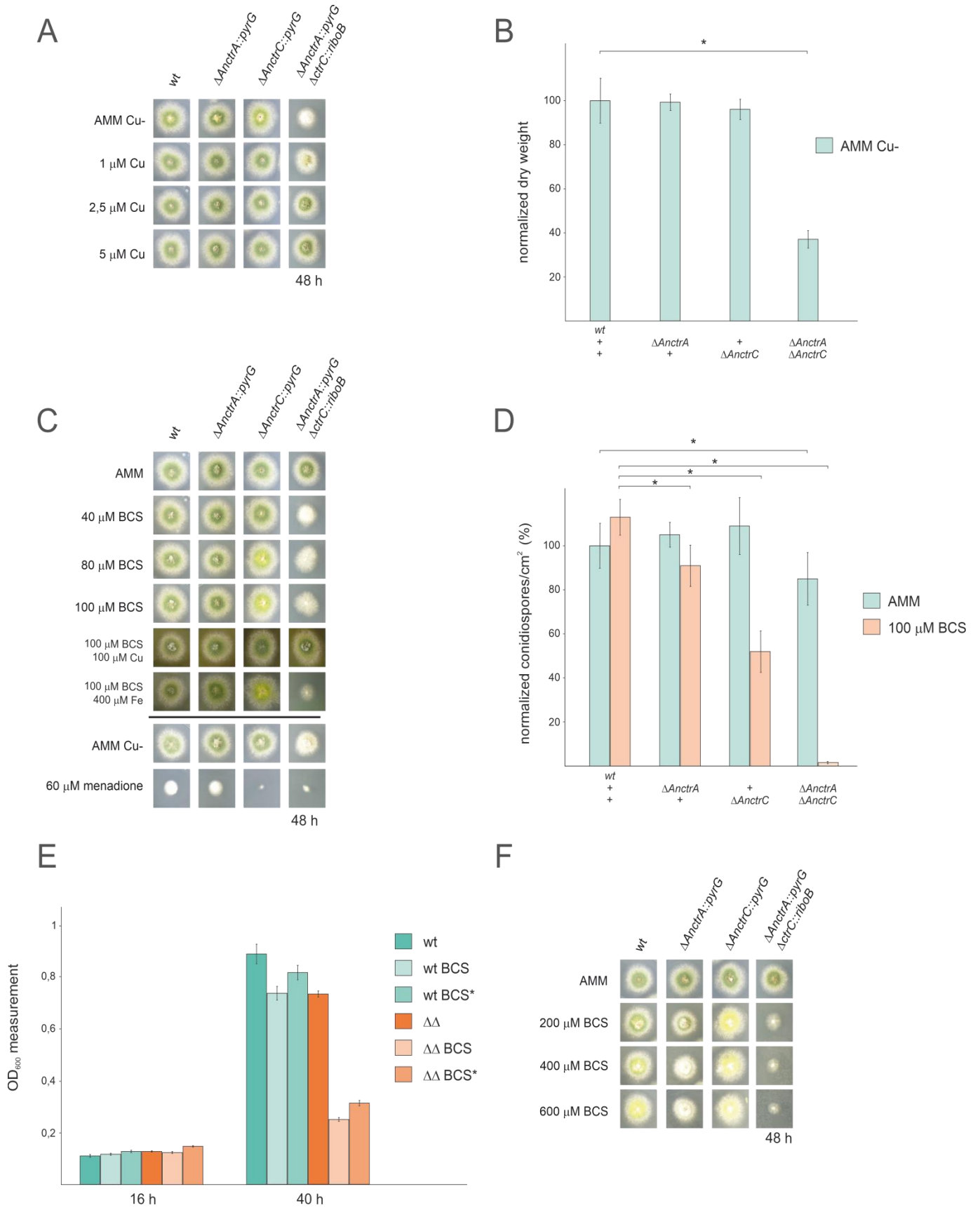
The above results showed that removing Cu from the trace element solution did not help discern phenotypic differences between single null mutants. Thus, we used the copper chelator Bathocuproinedisulfonic acid (BCS) in our experiments. As shown in Figure 10C, null mutant colonies did not exhibit appreciable alterations in radial growth or conidial pigmentation on regular solid minimal medium. Under copper starvation conditions (AMM supplemented with BCS), *ΔAnctrC* exhibited secondary level copper limitation effects at 80 μM concentration, displaying yellowish conidia which could be a result of the inactivity of the copper-dependent conidial laccase AnYA due to Cu deficiency (Scherer and Fischer, 2001). In contrast, the *ΔAnctrA* mutant presented no appreciable copper limitation effects. When both mutations were combined, primary level copper limitation effects were visible. Radial growth of the double knock-out strain was reduced to 40% and no pigmentation was appreciated. Upon Cu supplementation (100 μM BCS + 100 μM $CuSO_4$), normal growth and morphology were restored. It has been described that copper and iron metabolism are related in fungi, and iron can recover *Δmac1* colony morphology -very similar to the double knock-out strain shown in Figure 10C- to some extent in *A. fumigatus* (Cai *et al.*, 2017). Therefore, we tested whether addition of $FeSO_4$ could rescue the colony defects observed in *ΔAnctr* mutants grown under copper

starvation conditions. Fe supplementation (100 µM BCS + 400 µM FeSO₄) did not rescue the defects in null mutants (Figure 10C). Since Sods are also copper dependent enzymes, we hypothesized that a menadione (a widely used oxidative stress inducing agent) experiment could probably help clarify the nature of the differences observed so far between the two transporter null mutants. However, with 60 µM menadione, the phenotype was similar; the *ΔAnctrC* strain was visibly more affected by the oxidative damage generated by menadione, suggesting that in the condition tested Sod copper supply depended more on AnCtrC.

In addition to the above colony growth inhibition and pigmentation defects, hyphal growth in liquid medium and conidia production were also studied. To investigate the effect of the deletion of the *Anctr* coding genes on conidial production, we harvested and compared the number of conidiospores produced by each strain, under basal and low copper availability conditions (Figure 10D). Under basal conditions, single deletion of *Anctr* genes had no apparent effect on conidia production. Under copper deficiency conditions *AnctrA* deletion had a slight effect, but *AnctrC* deletion had a remarkable impact; conidia numbers were halved by comparison to the wild-type strain. Numbers of conidia are connected with the amount of biomass and the *ΔAnctrC* colony grown in solid AMM medium with 100 µM BCS was not smaller than the colony grown in AMM. Thus, copper scarcity had no effect on colony expansion, but on colony density, an effect that has also been described under other stresses conditions such as carbon or nitrogen starvation (Richie *et al.*, 2007). Deletion of both AnCtr proteins had a slight effect at control conditions. Under copper starvation conditions, conidia quantity was, 37-fold lower than the wildtype strain (Figure 10D).

A

B

C

D

E

F

I. The High-Affinity Copper Uptake System in *A. nidulans*

Figure 10: Functional analysis of *AnctrA* and *AnctrC* mutants. **(A)** Spores from the mutant strains were point-inoculated and images of colonies were taken after 48 h of incubation at 37 ^{o}C in 0 μM Cu AMM (Aspergillus minimal medium) and 0 μM Cu AMM with 1, 2.5, and 5 μM Cu. **(B)** Dry weight measurements of the mutant strains incubated for 16 h at 37 ^{o}C in 0 μM Cu AMM. **(C)** Spores from the mutant strains were point-inoculated and images of colonies were taken after 48 h of incubation at 37 ^{o}C in AMM and AMM with 100 μM CuSO$_4$, 100 μM BCS, 100 μM BCS with 100 μM CuSO$_4$ and 100 μM BCS with 400 μM FeSO$_4$. **(D)** Conidia production was determined by quantifying the number per unit of colony surface area (conidia/cm^2). In order to facilitate data comparison, growth of the WT strain at basal level was designated 100%, data was normalized and presented as percentages.*Significant conidiospore number reduction $p < 0.05$. **(E)** In liquid medium culture experiments, 6 x 10^4 spores of the WT and *ΔAnctrA-ΔAnctrC* strains were inoculated for 16 h and 40 h at 37 ^{o}C, under basal conditions (MMA), low copper availability conditions (BCS) and low copper availability conditions after 16 h of normal growth (BCS*). **(F)** Spores from the mutant strains were point-inoculated and images of colonies were taken after 48 h of incubation at 37 ^{o}C in AMM and AMM with 200, 400, and 600 μM BCS.

Hyphal growth studies were conducted with the WT stain and the *ΔAnctrA-ΔAnctrC* strain. At 16 h both strains presented very similar growth rates under all tested conditions. However, after 40 h, the double deletion strain presented a dramatically lower growth rate in low copper availability conditions compared to the WT and itself in basal copper conditions (28.1% and 35.2% compared to WT, for BCS and BCS* conditions, respectively) (Figure 10E). Thus, environmental copper deprivation had no apparent effect in the germination process but had a strong effect in the ensuing growth phase.

Since the addition of 100 μM BCS to media showed a secondary copper limitation phenotype in the *AnctrC* null mutant; but no characteristic phenotype was observed with the null *AnctrA* mutant and the WT strain, we increased the BCS concentration (400–600 μM). In these extremely low copper availability conditions, the WT strain presented secondary copper limitation symptoms like pigmentation deficiency, similar to that of the *ΔAnctrC* strain. In addition, the *ΔAnctrA* strain displayed primary level copper limitation effects as a reduced

radial growth and lack of pigmentation, similar to the double null strain albeit less aggravated (Figure 10F).

Taken together, the results support the interpretation that AnCtrA and AnCtrC are copper transporting proteins that complement each other. AnCtrC seems to be the principal copper transporting protein at nutritional and mild copper deficiency conditions, as the *AnctrC* deletion strain is more susceptible to oxidative damage and shows secondary copper limitation effects like defects in sporulation and spore pigmentation. However, the phenotypes of the WT strain and *ΔAnctrC* become very similar in extreme copper scarcity conditions, suggesting that the contribution of AnCtrC in those conditions is very limited. Although *AnctrA* deletion has no tangible effect under mild copper deficiency, primary level copper limitation effects are visible in extreme copper deficiency conditions. When both transporters were jointly deleted, pigmentation and colony growth defects were far greater than in the single null strains, as manifested by strongly reduced growth rate in liquid medium under low copper availability. This would support the view that both transporters cover an extended concentration range for environmental copper uptake.

2.4- AnCtr Protein Expression Dynamics

After identifying the copper uptake proteins involved in copper homeostasis, their expression patterns were investigated, with special interest in AnCtrA, which remained uncharacterized. Hence, the expression profiles of AnCtrA and AnCtrC throughout Cu and BCS treatments were examined in time course experiments.

We generated two fluorescent protein-tagged chimera strains: AnCtrA::GFP and AnCtrC::GFP. In order to test whether GFP tagging could alter protein function we verified that both strains followed wild-type like phenotypes under BCS treatments in plate experiments (Figure 11A).
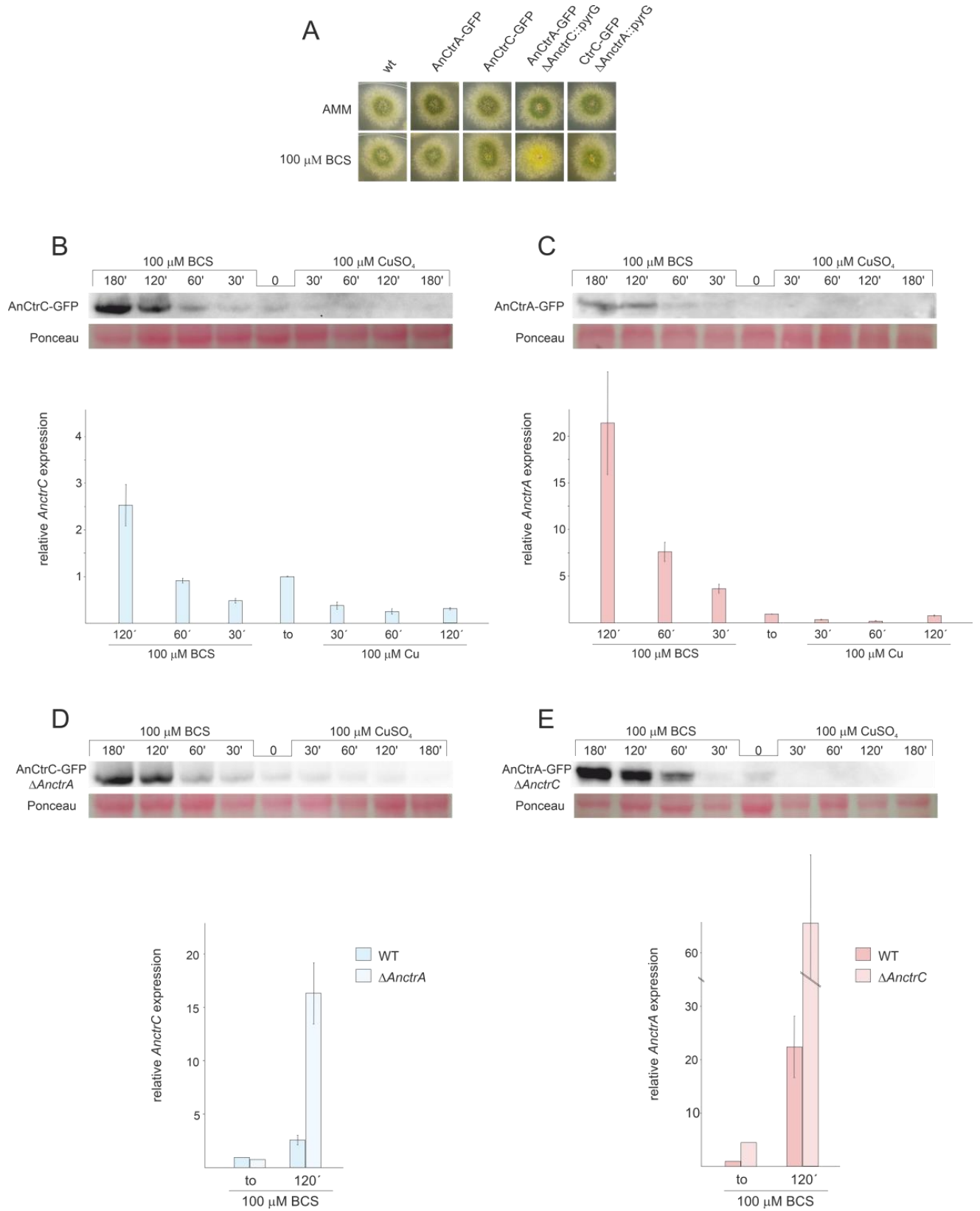
I. The High-Affinity Copper Uptake System in *A. nidulans*

RT-PCR experiments revealed that Cu and BCS addition caused opposite effects on *AnctrC* expression (Figure 11B). Shortly after 100 μM CuSO$_4$ addition, *AnctrC* transcript levels were reduced four-fold and this tendency was maintained throughout the experiment. On the other hand, upon addition of 100 μM BCS, initially presented lower relative expression of *AnctrC* transcript than at t$_o$, followed by a gradual increase, reaching the highest level at 120' (2.5-fold). Western-blot analyses were coherent with RT-PCR data. When BCS was added to the medium, a 50 kDa band coinciding with the AnCtrC::GFP monomer was visible. The signal detected at short incubation times was similar to the one detected at t$_o$. The signal grew stronger at longer exposures. After Cu addition, AnCtrC protein signal gradually faded through time.

The *AnctrA* transcript expression pattern showed a more specific pattern for copper deficiency conditions (Figure 11C). When copper was added, expression levels exhibited a five-fold decrease. However, upon BCS addition, expression increased up to 21.5-fold relative to the total RNA extract at t$_o$, substantially greater than observed in *AnctrC*. Western-blot analyses exhibited a 47 kDa band only visible in samples treated with BCS. Although the observed band was very faint at early incubation times, it grew stronger with increasing incubation times.

Phenotypic observation of the mutants showed that AnCtrC is effective under copper sufficiency or mild copper deficiency conditions, while AnCtrA function gains relevance under extreme copper deficiency conditions. Taking this into account, we decided to study the behavior of *AnctrA* and *AnctrC*, RNA and protein, in their respective null mutants and compared them with WT strain levels. *AnctrC* expression in a *ΔAnctrA* background was slightly lower at basal conditions.

I.The High-Affinity Copper Uptake System in *A. nidulans*

I. The High-Affinity Copper Uptake System in *A. nidulans*

Figure 11: AnCtrC and AnCtrA expression profiles with Cu and BCS. **(A)** Phenotypes of the strains used for expression analysis of AnCtrC and AnCtrA in AMM and AMM + BCS media. *(B)* Western-blot and RT-PCR data showing hanges in AnCtrC and AnctrC expression levels after addition of 100 μM CuSO$_4$ or 100 μM BCS. (C) Western-blot and RT-PCR data showing changes in AnCtrA and *AnctrA* expression levels after addition of 100 μM CuSO$_4$ or 100 μM BCS. **(D)** Western blot and RT-PCR data showing changes in AnCtrC and AnctrC expression levels in a *ΔAnctrA* genetic background, after addition of 100 μM CuSO$_4$ or 100 μM BCS. **(E)** Western-blot and RT-PCR data showing changes in AnCtrA and *AnctrA* expression levels in the *ΔAnctrC* genetic background, after addition of 100 μM CuSO$_4$ and 100 μM BCS.

However, at later times, expression levels grew 16.74-fold higher under copper deficiency conditions (Figure 11D). At the protein level, the expression profile was maintained. *AnctrA* expression on the other hand, was clearly different in a *ΔAnctrC* background. At basal levels *AnctrA* expression was 4.5-fold higher and 63.81-fold higher under copper starvations conditions (Figure 11E). At the protein level, t_o protein signal could be detected and with BCS incubation, the signal became considerably stronger compared to that in the wildtype background.

The results from this study demonstrated that *AnctrA* and *AnctrC* expression is copper dependent, albeit with some differences (Figure 11). *AnctrC* expression profile is more stable through time in line with a possible role of copper supply in nutritional and mild copper deficiency conditions. *AnctrA* expression on the other hand, experiences an outstanding induction after BCS addition, a fitting expression pattern for an extreme copper deficiency copper transporter. The implications of these results will be further elaborated when the relative contribution of each protein is discussed.

2.5- AnCtr Localization

AnCtrA and AnCtrC protein localization was conducted *in vivo* using strains expressing C-terminally GFP-tagged chimeric proteins, together with

I.The High-Affinity Copper Uptake System in *A. nidulans*

AnHhoA::mRFP marked strains. AnHhoA is Histone 1, a marker of the nuclear chromatin. Ctr proteins function as copper internalizing proteins. Considering the likely mobility upon changes in environmental copper concentration, we grew our GFP chimera expressing strains in regular WATCH medium, added BCS to the medium and observed protein dynamics within a 2 h period. In regular WATCH media without copper deprivation, AnCtrC::GFP was detected throughout the cytosol of hyphae (Figure 12A1). Many oval structures that co-localized with the red nuclei (white arrows) were distinguished, with some associated membranes displaying green fluorescence and the fluorescence signal was notably polarized (Figure 12A1.2).

After BCS addition fluorescence signal became more visible in the plasma membrane but no protein migration was appreciated. In the vicinity of the tip area, no fluorescence was localized in the plasma membrane and the signal inside the hyphae polarized toward the tip. After 2 h of BCS addition the presence of the protein in the plasma membrane became clearer along the hyphae but not in the tip region (Figure 12A2). Fluorescence signal was notably polarized in the tip region (Figure 12A2.2). Fluorescence was still visible in the perinuclear area and discrete fluorescence signals were detected elsewhere within hyphae but the identity of the organelles could not be specified (Figure 12A2.3). In the case of AnCtrA, throughout the course of the experiment, a gradual increase in fluorescence intensity was observed but protein localization remained quite stable. Without copper deprivation, the protein was mainly localized in irregular granules dispersed along the hyphae (Figure 12B1). Disperse fluorescence patches could be detected in the plasma membrane (Figure 12B1.2) and as with AnCtrC, close to the tip region no protein was localized in the membrane (Figure 12B1.3). After 2 h of BCS addition, the signal in the plasma membrane became more prominent (Figure 12B2). Besides the plasma membrane fluorescence signal numerous other structures were visible along the hyphae, possibly early endosomes (Figure 12B2.2). Even in copper deprivation

conditions, no protein was localized in the tip region (Figure 12B2.3). The subcellular localization of each protein will be analyzed further in the Discussion.
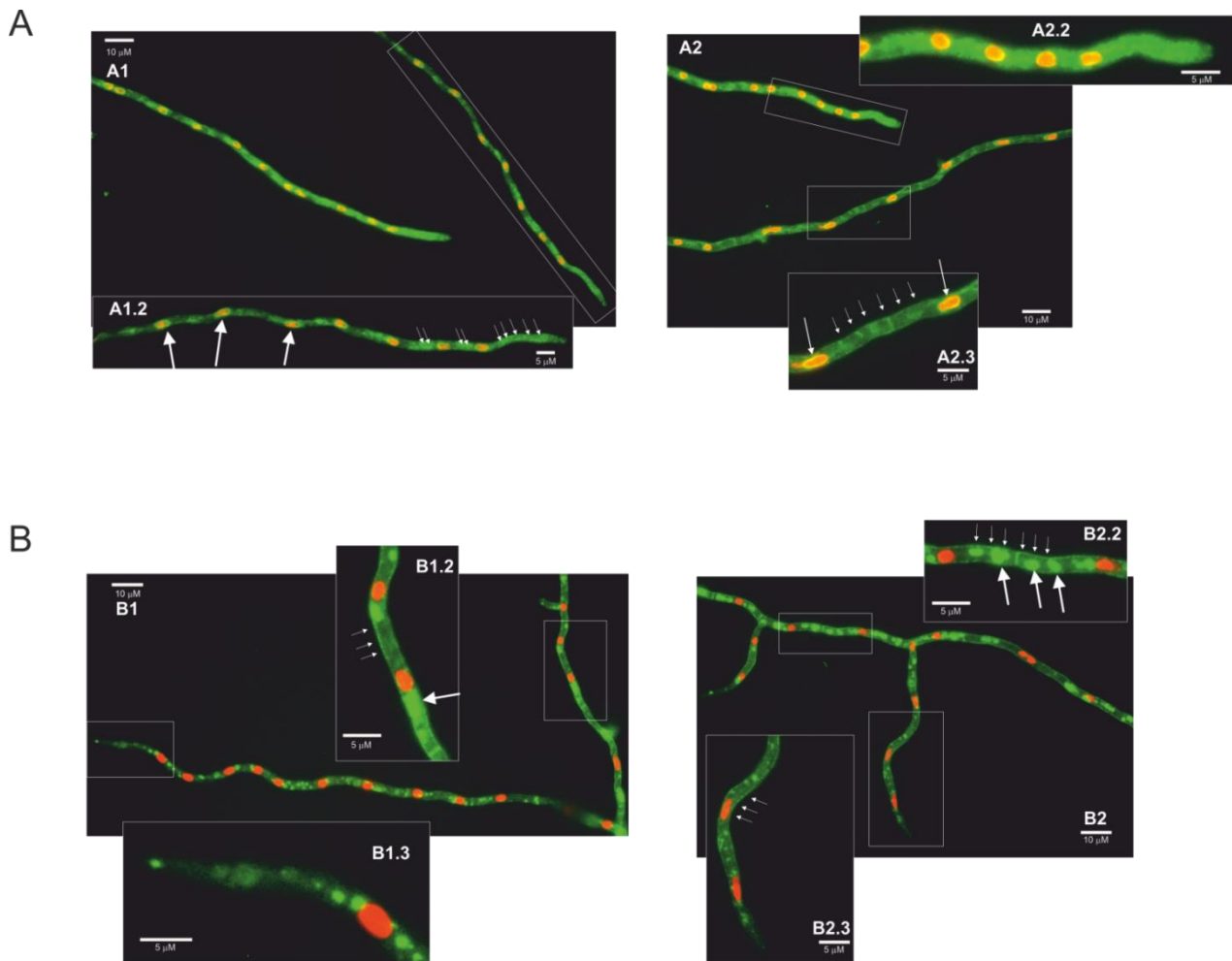
Figure 12: Fluorescence microscopy images of AnCtrC and AnCtrA chimeras. **(A)** AnCtrC::GFP-HhoA::mRFP protein expressing strains were grown in selective WATCH medium for 16 h at 30 °C. Images show the protein localization before BCS addition (A1) and 2 h after 100 mM BCS addition (A2). Pictures A1.2–A2.2–A2.3 show a closer look at the most interesting features. **(B)** AnCtrA::GFP-HhoA::mRFP protein expressing strains were grown in selective WATCH medium for 16 h at 30 °C. Images show the protein localization before BCS addition (B1) and 2 h after 100 mM BCS addition (B2). Pictures B1.2–B1.3–B2.2–B2.3 show a closer look at the most interesting features.

In conclusion, in the case of AnCtrC, the signal accumulated around nuclei associated membranes, most likely the nuclear envelope (Markina-Inarrairaegui *et al.*, 2013) and other structures; considering the polarization of the fluorescence signal possibly the peripheral ER. In low copper availability conditions, the fluorescence signal along the hyphae, except for the tip, partially shifted toward the membrane; nevertheless, most of the protein was still detected along the hyphae. In the case of AnCtrA the fluorescence signal was in the plasma membrane, but toward the tip region of the hyphae, the plasma membrane appeared free of fluorescence. The protein could be also detected in numerous morphologically heterogeneous compartments. These could be vacuolar compartments or early endosomes, considering the similarities between the role and expression pattern of AnCtrA and previously described copper uptake proteins.

2.6- C-Terminal Mutations of AnCtrA and AnCtrC

In organisms like *S. cerevisiae* and humans, Ctr protein C-terminals reportedly play a crucial role in shutting down copper uptake when intracellular copper concentrations reach a threshold (Schuller *et al.*, 2013). Certain copper binding residues, namely cysteines and histidines, are specifically involved in the mechanism, which is separate from copper uptake (Clifford *et al.*, 2016;Wu *et al.*, 2009). In the C-terminal of AnCtrA and AnCtrC there are two adjacent cysteines that are conserved in many other orthologs, flagging them as copper binding residues. In order to test this hypothesis, single and double mutants of the mentioned cysteine residues AnCtrA$^{C186;187A}$ and AnCtrC$^{C213;214A}$ were generated by alanine substitution. C-terminally truncated mutants, AnCtrA^{164} and AnCtrC^{201}, were also generated, in order to check if there was any difference in copper susceptibility compared to the cysteine mutants. The mutants were checked for a possible loss of function due to the inserted mutations. All mutants were proven to be functional, as the outcome of the C-terminal mutation in combination with a *ctr* deletion was not similar to the double null mutant (Figure

I. The High-Affinity Copper Uptake System in *A. nidulans*

13A). The mutants were grown in AMM with different concentrations of $CuSO_4$ and BCS as shown in Figure 13B.

Neither the deletion of the C-terminal domain nor the mutation of the cysteine residues resulted in added susceptibility toward copper. However, the mutants presented secondary level copper limitation effects in copper scarcity conditions, especially the double C-terminal deletant strain. The AnCtrA$^{164:}$:HA-AnCtrC^{201}::GFP strain phenotype was similar to the *ΔAnctrC* phenotype regarding conidial pigmentation deficiency at 125 μM BCS. The AnCtrC^{201}::GFP and AnCtrA$^{C186;187A}$::HA-AnCtrC$^{C213;214A}$::GFP also showed pigmentation deficiencies but to a lower degree.

Therefore, the broadly conserved di-cysteine motif was shown to have no impact on copper uptake shut-down under the conditions tested. However, this motif may be involved in copper uptake, since removing the C-terminal and the cysteine residues does appear to reduce uptake capacity as their deletion results in defective pigmentation, a secondary level copper limitation effect. This would mean that the copper uptake regulation mechanism of the *A. nidulans* Ctr proteins is different from the so far studied regulation mechanisms and that the contribution of the C-terminal is necessary for full capacity copper uptake.

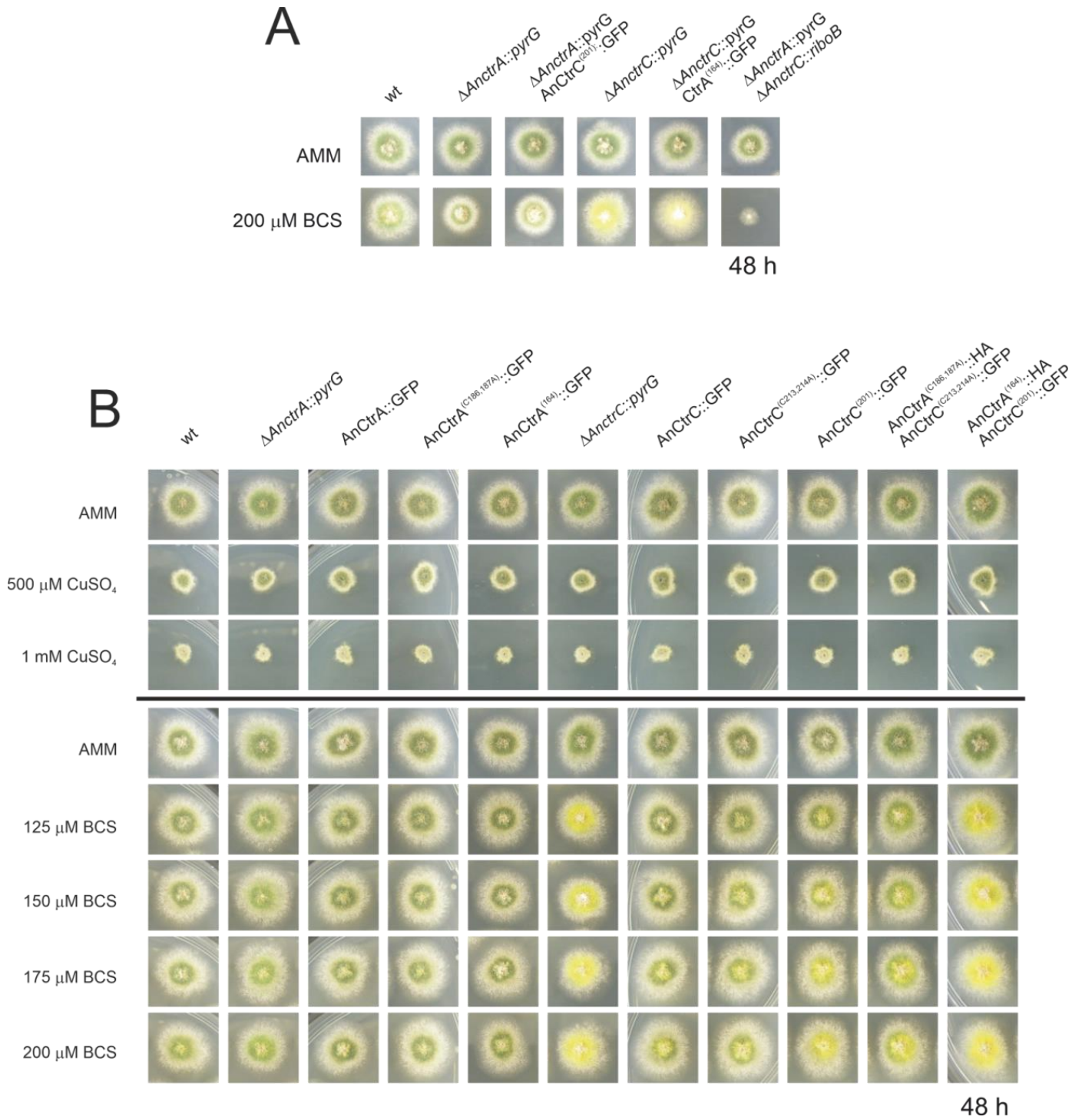**Figure 13:** Functional analysis of AnCtrA and AnCtrC C-terminal mutants. **(A)** Phenotypes of the AnCtrC and AnCtrA C-terminal mutants in AMM and AMM + BCS media to assess protein function. **(B)** Spores from the mutant strains were point-inoculated and images of colonies were taken after 48 h of incubation at 37 °C in AMM (*Aspergillus* minimal medium) and AMM with different concentrations of $CuSO_4$ and BCS.

I. The High-Affinity Copper Uptake System in *A. nidulans*

2.7- Screening for Cupric Metalloreductases

As mentioned in the RNA-seq analysis, the experiment offered the opportunity to search for Plasma Membrane metalloreductases, homologs to the Fre protein family. The expression of the copper metalloreductases reportedly follows the same expression pattern as Ctr proteins since both are under control of the TF Mac1 (Levitin and Whiteway, 2007;Yamaguchi-Iwai *et al.*, 1997). Our screen retrieved three candidates that were co-regulated with the Ctr protein out of ten members of the family of metalloreductases present in the *A. nidulans* genome: AnfreA, AN0773 and AN3208. AnfreA is a characterized iron reductase and it has no putative AnMac1 binding sequence. AN0773 and AN3208 are two uncharacterized putative copper reductases that possess a possible AnMac1 binding region in their respective promoter regions. However, a detail caught our attention. AN3208 is a putative cell surface metalloreductase adjacent to *AnctrA* and they share the promoter region where AnMac1 binds (Figure 14). This feature reinforces the idea that it may be a copper metalloreductase. Thus, it was named *AnfreC*. Synteny and multiple alignment data in the EnsemblFungi site revealed that the *AnctrA-AnfreC* ortholog's position and orientation is conserved in the majority of fungal species that contain an *AnctrA* ortholog. The majority of screened species (110/127) contain the putative plasma membrane high-affinity copper transporter and a metalloreductase located in tandem (Figure 14).

In summary, AN0773 and *AnfreC* fulfill the conditions to be copper metalloreductases. However, due to the unique features of *AnfreC* mentioned above it is a suitable candidate to be the main cupric metalloreductase in *A. nidulans*.

Figure 14: An image representing the chromosomal location of *AnfreC-AnctrA*, and a list of fungal organisms that possess an AnctrA ortholog are presented. (1) The organism possesses another Ctr protein ortholog of *AnctrC*. (2) The organism possesses an Ox-Red coding gene beside the *AnctrA* ortholog, just like *A. nidulans*. The color of the rectangles next to the organism represents: green (yes), red (no) and gray (unidentified).

Acaromyces ingoldii str.
Acremonium chrysogenum
Alternaria alternata str.
Anthracocystis flocculosa
Ascochyta rabiei str.
Aspergillus niger
Aureobasidium melanogenum
Aureobasidium namibiae
Aureobasidium pullulans
Aureobasidium subglaciale
Bipolaris maydis
Bipolaris oryzae
Bipolaris sorokiniana
Bipolaris victoriae
Bipolaris zeicola
Ceraceosorus guamensis
Chaetomium globosum
Chaetomium thermophilum
Cladophialophora carrionii
Cladophialophora yegresii
Claviceps purpurea
Colletotrichum gloeosporioides
Colletotrichum gloeosporioides
Colletotrichum graminicola
Colletotrichum graminicola
Colletotrichum higginsianum
Colletotrichum orbiculare
Coniella lustricola
Coniosporium apollinis
Cordyceps confragosa
Cordyceps sp.
Corynespora cassiicola
Cutaneotrichosporon oleaginosum
Cyphellophora europaea
Daldinia sp.
Diaporthe ampelina
Diaporthe helianthi
Drechmeria coniospora
Epicoccum nigrum
Eutypa lata
Exophiala aquamarina
Exophiala dermatitidis
Exophiala mesophila
Exophiala sideris
Exophiala spinifera
Exophiala xenobiotica
Exserohilum turcica
Fusarium culmorum
Fusarium fujikuroi
Fusarium graminearum
Fusarium oxysporum
Fusarium pseudograminearum
Fusarium solani
Fusarium verticillioides
Gaeumannomyces tritici
Grosmannia clavigera
Hypoxylon sp.
Jaminaea rosea
Kwoniella bestiolae
Kwoniella dejecticola
Kwoniella pini
Leptosphaeria maculans
Madurella mycetomatis
Magnaporthe oryzae

Magnaporthe poae
Meira miltonrushii
Metarhizium acridum
Metarhizium album
Metarhizium majus
Metarhizium majus
Metarhizium rileyi
Metarhizium robertsii
Microdochium bolleyi
Moelleriella libera
Moesziomyces antarcticus
Moesziomyces aphidis
Neonectria ditissima
Neurospora crassa
Neurospora tetrasperma
Ophiocordyceps australis
Ophiocordyceps camponoti-rufipedis
Paraphaeosphaeria sporulosa
Penicillium antarcticum
Penicillium brasilianum
Penicillium camemberti
Periconia macrospinosa
Periconia macrospinosa
Pestalotiopsis fici
Phaeosphaeria nodorum
Phialophora americana
Phialophora attae
Pseudomassariella vexata
Pseudomicrostroma glucosiphilum
Purpureocillium lilacinum
Pyrenochaeta sp.
Pyrenophora teres
Pyrenophora tritici-repentis
Ramularia collo-cygni
Rhinocladiella mackenziei
Rosellinia necatrix
Sordaria macrospora
Stachybotrys chartarum
Stachybotrys chlorohalonata
Stagonospora sp.
Stemphylium lycopersici
Thermothelomyces thermophila
Tilletiopsis washingtonensis
Tolypocladium paradoxum
Torrubiella hemipterigena
Trichoderma citrinoviride
Trichoderma parareesei
Trichoderma reesei
Trichosporon asahii
Ustilaginoidea virens
Ustilaginomycotina sp.
Ustilago maydis
Valsa mali
Verticillium dahliae
Verticillium dahliae
Verticillium longisporum
Verticillium longisporum
Verticillium longisporum
Verticillium longisporum
Verticillium longisporum
Verticillium longisporum
Zymoseptoria brevis
Zymoseptoria tritici

3- Discussion

This study provides additional information on the expression and function of the high-affinity copper uptake system reported in yeast and filamentous fungi of clinical interest. The study of gene expression profiles under basal copper availability conditions, copper deprivation and copper toxicity has shed new light on the overall adaptation of *A. nidulans* to copper fluctuations, as well as targeting the dynamics of copper transporters. The subsequent analysis through targeted mutagenesis of the principal copper transporters has enabled an interpretation of their individual contributions in the copper uptake process, their expression patterns and their subcellular localization dynamics. In addition, new inquiries into the role of transporter C-terminal domains together with the identification of putative membrane copper reductases have been initiated.

The response to copper toxicity in *A. nidulans* involves the differential expression of 13.7% of its genes. Significant changes were recorded on recognized copper homeostasis genes. Even though the expression of the TFs regulating the process was not significantly altered, that of proteins responsible of copper uptake and detoxification was very notable. The gene coding for the copper exporting P-type ATPase AnCrpA (Antsotegi-Uskola *et al.*, 2017;Levitin and Whiteway, 2007;Yamaguchi-Iwai *et al.*, 1997), was up-regulated. On the other hand, the two characterized copper transporter genes *AnctrA* and *AnctrC* (Cai et al., 2019) were down-regulated in line with the objective of reducing the copper uptake to the minimum. Finally, the significant up-regulation of the intracellular copper trafficking P-type ATPase *AnygA* (Clutterbuck, 1990) could be a response to the presence of high amounts of copper ions within the cell that have to be distributed or compartmentalized. Out of the identified three putative copper chaperones only the putative Cu/Zn Sod chaperone AN6045 was significantly up-regulated. The *S. cerevisiae* functional counterpart, chaperone Atx1, responsible for copper distribution within the cell, binds excess cytosolic copper (Lin and Culotta, 1995) and could act as a first level scavenger at low levels of toxicity.

This effect may have taken place under our experimental conditions, as discussed below.

Free cytoplasmic copper is known to produce ROS through Fenton-type reactions (Sutton and Winterbourn, 1989;Timoshnikov *et al.*, 2019). Superoxide dismutases, accept electrons from reduced metals or superoxides, yielding hydrogen peroxide, which, along with small organic peroxides, is the substrate of catalases (2 $H_2O_2 \longrightarrow 2\ H_2O + O_2$) (Zamocky *et al.*, 2008). Hence, the reported copper toxicity response involves the activation of both groups of enzymes (Wiemann *et al.*, 2017). In our experiments, however, we observed that catalases *AncatB* (2.82-fold), *AncatC* (2.36-fold) and *AncpeA/AncatD* (2.59-fold) were up-regulated, but the expression of the Cu/Zn superoxide dismutase *AnsodA* (Holdom *et al.*, 1996) (reported in Table 6), an enzyme activated in response to copper and zinc-derived ROS toxicity, remained unchanged, along with that of the ROS responsive transcription factors *AnatfA* and *AnnapA* (Table 7). These variations may stem from the differences in copper concentrations and the relative sensitivities of the strains used by (Wiemann *et al.*, 2017) and this study. In our experiments, 100 μM Cu concentrations were used, a dose that exerted no visible effect in *A. nidulans* colony development (Antsotegi-Uskola *et al.*, 2017). On the other hand, Wiemann *et al.,* (2017) used a 200 μM copper concentration, in an organism at which 50 μM already compromised colony development. It is therefore likely that, under conditions which elicit no phenotypic symptoms of copper toxicity, the AnCrpA detoxification system could have removed the free cytosolic copper, rendering ROS neutralization unnecessary. On the other hand, Wiemann *et al.,* (2017) combined higher copper concentrations and greater susceptibility may have overwhelmed the capacity of AfCrpA, thus triggering the up-regulation catalases to quench ROS and H_2O_2. Both results may depict the response to two different levels of copper toxicity. It may be hypothesized that catalases are heme-containing enzymes (Scherer *et al.*, 2002) and it is well known that intracellular free copper ions can displace

protein-bound iron. The selective up-regulation of the catalases in this case may be a response to this phenomenon, leading to the greater demand for functional catalases. More evidence will be required to confirm this interpretation.

Aside from catalases, the copper toxicity response also modified the expression of many other oxidoreductases. Laccases are blue-copper enzymes involved in lignin degradation or pigment biosynthesis (Scherer and Fischer, 2001). However, laccases don't show a specific expression pattern in response to copper toxicity (Table 6). Other oxidoreductases corresponded to membrane function-related metabolic processes such as sterol metabolism. Sterols, especially ergosterol, are the most abundant lipids in fungal cell membranes (Rodrigues, 2018), with roles in integral protein stabilization, membrane fluidity and permeability (Abe and Hiraki, 2009;Alvarez *et al.*, 2007). This could be a result of copper accumulation in the Plasma membrane (Cervantes and Gutierrez-Corona, 1994). Under copper toxicity, the expression of proteins involved in transmembrane traffic augmented; for example, many putative sugar transporters were up-regulated. This could be ascribed to a heightened requirement for energy (ATP) and reducing power (NADH), both principal products of aerobic sugar catabolism. For example, the ATP-dependent copper detoxification protein AnCrpA was highly up-regulated in this study, in line with earlier observations (Antsotegi-Uskola *et al.*, 2017). Changes in differential expression of various heavy metal transporters may indicate that a change of copper concentration could cause an imbalance in heavy metal homeostasis, as described in *A. fumigatus* (Cai *et al.*, 2017). Finally, a stress mechanism with such a wide ranging impact on cellular metabolism should also alter the regulation of a core regulatory process as transcription. A TF that experienced notable lower expression under copper toxicity conditions was *Anhap*X and this, in turn, is consistent with the down-regulation of the siderophore biosynthesis cluster that it has been reported to regulate (Schrettl *et al.*, 2004). The same result was obtained with the antimicrobial compound emericellamide biosynthesis cluster (Table 7). Finally, analyzing the data of the RNA-seq we found out a highly up-regulated set of genes. The up-regulation of

I.The High-Affinity Copper Uptake System in *A. nidulans*

an N-acetylglucosamide transporter, AN2562, could be an adaptive response to the high copper environment as this compound proves to be important for survival in the phagosome (Vesely *et al.*, 2017) where copper toxicity is used to kill by the innate immune system (Li *et al.*, 2019). Secondly, it is very convenient that a cysteine and methionine transporter, AN2560, would be up-regulated in such conditions as they are two amino-acids that participate in copper binding motifs (Pena *et al.*, 2000). The flavin-containing monooxygenase might play an important role in creating an optimal Redox environment threatened by the presence of copper in the cytosol (Suh *et al.*, 2000). These three genes together with the predicted oxidoreductase AN2559 and the putative methyltransferase AN2561 might comprise a defensive gene cluster against copper toxicity.

The phylogenetic characteristics of two *A. nidulans* Ctr proteins, AnCtrA and AnCtrC, have been examined in this study. Although the reference Ctr sequence used to screen for orthologs in fungi had been ScCtr1, none were found in the *A. nidulans* genome with that criterion. According to the Ensembl fungi ortholog predictions, homologs of ScCtr1 are only found in the Saccharomycetales order. Moreover, most Ctr proteins of filamentous fungi shared higher similarity with ScCtr3 (Figure 8). Unfortunately, *Scctr3* is poorly documented as it is disrupted by a Ty2 transposon in many laboratory strains (Knight *et al.*, 1996). AnCtrC showed phylogenetic relationship with numerous Ctr orthologs in *A. fumigatus*, *S. cerevisiae* and various other fungi. On the other hand, AnCtrA showed similarity with other putative Ctr proteins that have not been characterized.

Both proteins possess the characteristic features of Ctr proteins (Petris, 2004;Rees and Thiele, 2004;Zhou *et al.*, 2003). Ctr family members generally harbor three putative TMDs (Puig *et al.*, 2002), but according to topology software predictions, AnCtrA has only two TMDs. This has also been reported in *A. fumigatus* and *C. neoformans* (Park *et al.*, 2014;Waterman *et al.*, 2012). Cysteine residues are present throughout the sequence and cysteines are known for their affinity to copper (Pena *et al.*, 2000). Both proteins contain two cysteine

I. The High-Affinity Copper Uptake System in *A. nidulans*

residues flanking the methionine residue adjacent to TMD1. This soft Lewis base may be important to coordinate copper since it has been described that metal binding residues located close to the plasma membrane seem to play a more important role in copper transport (Puig *et al.*, 2002).

Functional characterization analyses in this study showed that the two Ctr proteins worked independently and the range of copper concentrations they covered were partially complementary, as derived from the obtained phenotypes. The phenotypes observed were broadly interpreted in terms of acute or partial deficiencies as follows. Normal growth rates and WT-like green conidial pigmentation were interpreted as an indication of adequate copper supply for basic growth and developmental functions. Defects in spore pigmentation and sporulation that did not affect growth rate were interpreted as the result of a partial limitation in copper. Conidiogenesis is strongly reliant on autophagy-derived resources (Kikuma *et al.*, 2007;Richie and Askew, 2008). The yellowish spore pigmentation could be explained by the inactivity of the copper-dependent conidial laccase AnYA; the phenotype corresponds with the *yA2* phenotype (Hermann *et al.*, 1983;Scherer and Fischer, 2001). On the other hand, acute copper deficiency was interpreted to affect extracellular copper transport with direct consequences on vegetative growth. Following these criteria, we surmised that AnCtrC functions as the principal copper uptake protein under copper sufficiency and mild copper deficiency conditions. AnCtrA may complement the lack of AnCtrC at moderate copper deficiencies but is specifically required for extreme copper deficiency scenarios.

As shown in this study, conditions of low copper availability induce a gradual up-regulation in Ctr expression, while high copper levels induce the opposite effect. The rapid shutdown of the copper uptake system under high extracellular copper concentrations is of great importance to avoid copper toxicity (Bertinato and L'Abbe, 2004;Dong *et al.*, 2013). The expression patterns of AnCtrA and AnCtrC under similar testing conditions share certain similarities with *S. cer*evisiae Ctr

proteins; a Ctr protein with a more stable expression pattern (ScCtr3) and another one that is uniquely expressed under low copper availability conditions (ScCtr1) (Pena *et al.*, 2000). AnCtrC is the only high-affinity copper transporter expressed at basal copper levels, which means it is likely to cover for copper intake under ordinary copper availability (Figure 11B). On the other hand, AnCtrA expression pattern seems to be designed for extreme copper scarcity conditions, when AnCtrC transport cannot meet the cell's copper requirements. These results are in line with the conclusions from phenotypic analyses of selective null mutants discussed above.

In terms of protein localization dynamics, Ctr proteins are known to follow a very dynamic trafficking pathway. Pena *et al.,* (2000) described that ScCtr3 traveled to the plasma membrane through the Trans-Golgi network and the fluorescence signal of tagged proteins accumulated in the ER after inhibiting protein traffic from ER to Golgi. However, when copper concentration rose, Ctr proteins like ScCtr1, moved from the plasma membrane to the vacuole (Liu *et al.*, 2007), or early endosomes, as in the case of hCtr1 (Clifford *et al.*, 2016;Eisses and Kaplan, 2002). The predominant ER localization of AnCtrC (Markina-Inarrairaegui *et al.*, 2013) and its partial migration to the plasma membrane in copper deficiency conditions support its role as a copper uptake protein covering transport under copper sufficiency or mildly limiting conditions. The predominant plasma membrane and vesicular localization of AnCtrA is in line with reported data of other proteins that respond to extreme copper deficiency scenarios such as described for ScCtr1 or hCtr1 (Clifford *et al.*, 2016;Eisses and Kaplan, 2002;Liu *et al.*, 2007).

The shutdown of copper transport as a measure to avoid toxicity has been documented many instances. Previous reports on this toxicity-preventing mechanism refer to certain residues, mostly cysteines, in the C-terminus of Ctr proteins as key elements in uptake modulation (Liu *et al.*, 2007;Schuller *et al.*, 2013;Wu *et al.*, 2009). Copper has been postulated to bind C-terminal cysteines,

purportedly triggering the mechanism. The possible role of the Ctr proteins' C-terminal in activity modulation has not been studied in filamentous fungi. However, the C-terminal di-cysteine motif, a common heavy metal binding sequence (Lekeux *et al.*, 2018) can be found in Ctr proteins of *Alternaria alternata, Aspergillus fumigatus, Botrytis cinerea, Fusarium graminearum, Histoplasma capsulatum* and *Magnaporthe oryzae*. We first hypothesized that this di-cysteine motif could act as copper uptake modulator, as the ScCtr1 C-terminal cysteine residues or the hCtr1 HCH amino acid motif. However, our results do not indicate any copper dependent uptake modulation or internalization role. Moreover, unlike the C-terminus of ScCtr1, that is dispensable for full copper uptake capacity (Wu *et al.*, 2009), deletion of AnCtrC C-terminus results in secondary copper deficiency effects manifested as a pigmentation deficiency (Figure 13B). Thus, the C-terminus of the Ctr proteins plays some role in the copper uptake process. Further studies will be needed to clarify this question.

Plasma membrane metalloreductases are crucial components of the copper uptake process as they provide Ctr transporting proteins with the substrate in a transport-compatible reduced state (Labbe *et al.*, 1997;Petris, 2004). There are documented reductases that reduce iron and also copper (Georgatsou *et al.*, 1997); however, *AnfreA* was discarded for lacking a putative Mac1 binding sequence. AN0773 and *AnfreC* both shared copper reductase features, but the phylogenetically preserved genomic location of *AnfreC* in tandem with *AnctrA* tipped the scales in its favor. The genes coding for the reductive iron assimilation complex composed by the oxidoreductase FetC and the iron transporter FtrA (Schrettl *et al.*, 2004) are located in tandem, exactly like *AnfreC-AnctrA*, in *Fusarium* species (Park *et al.*, 2007;Wiemann *et al.*, 2012) and other *Aspergillus* species like *A. fumigatus, A. clavatus* and *A. fischeri* for example. This fact points out to *AnfreC* as the main copper oxidoreductase.

II. Chapter-

The Copper Detoxification System in *A. nidulans*

1- Introduction

Having covered the transport of copper into fungal cells in the previous chapter, we now turn our attention to the element of copper homeostasis dealing with the internalized fraction of the cation that may be exerting toxicity. This may be implemented through several mechanisms.

The RNA-seq data presented in the previous chapter offered the opportunity to identify putative actors of the copper detoxification process: metallothioneins, acting as copper quenching molecules and P-type ATPases that could pump the cation into specific compartments or out of the cell. Thus, we screened for genes that coded for metallothioneins and for P-type ATPases that could be up-regulated under copper toxicity conditions. Two P-type ATPase coding genes were identified in the screen.

P-type ATPases constitute a superfamily of membrane cargo transporters that transport different kinds of cargo, from cations to lipids. Phylogenetically, they are classified into 5 main subfamilies, from P_I to P_5, and in each family there are also subgroups divided. The heavy metal transporting ATPases belong to the P_{IB} subgroup. P_{IB}-type ATPases have peculiar terminal extensions (N- or C-terminal) which contain metal (copper) binding domains (MBDs), rich in Cys and sometimes His. P_{IB}-ATPases possess 6 to 8 transmembrane domains (TMDs), metal-binding sequences in their TMDs, regulatory MBDs, a structure involved in enzyme phosphorylation (P-domain), a nucleotide-binding domain (N-domain), and an energy transduction domain (A-domain) (Palmgren and Nissen, 2011).

One of the identified genes was an already annotated gene, *AnyA,* with intracellular copper delivery function (Clutterbuck, 1990). The other one, AN3117, had not been characterized yet. From previous work in *C. albicans* and humans, P-type ATPases are known to either change location to perform different functions within the copper homeostasis system, copper delivery and

II. The Copper Detoxification System in *A. nidulans*

detoxification (Lutsenko *et al.*, 2007;Petris *et al.*, 1996;Suzuki and Gitlin, 1999); or the two processes can be achieved by two different P-type ATPases (Riggle and Kumamoto, 2000;Weissman *et al.*, 2000). *A. nidulans* follows the second model and AN3117 was named AnCrpA, a putative detoxification protein.

Even though no metallothioneins were found among the up-regulated genes in the RNA-seq, a single putative metallothionein coding gene was identified by Blastp sequence analysis.

This chapter describes the identification and characterization of the major copper detoxification determinant in *A. nidulans*, the copper transporting P_I-type ATPase, AnCrpA. AnCrpA expression is highly inducible and dynamic in response to prolonged copper exposure and localizes close to the cellular surface as a result of an organized trafficking process. In addition, metal-dependent induction of AnCrpA is under the control of AnAceA, a transcription factor activator of genes involved in copper detoxification. A third gene encoding a metallothionein-like protein has been identified, AnCrdA, with as yet unidentified function. Our results indicate that copper detoxification in *A. nidulans*, as in the dimorphic fungus *C. albicans*, relies mainly in copper excretion.

2- Results

2.1- Identification of Copper Resistance Determinants in *A. nidulans*.

The RNA-seq experiment described in chapter one, provided a spectrum of up-regulated genes under copper toxicity. Detailed examination for candidates responsible for copper detoxification resulted in the identification of AN3117, a gene that encodes a 1211 amino acid (3636 bp) protein with all the signature motifs of heavy metal transporting P-type ATPases. The protein is encoded by a single exon containing gene located at chromosome VI. Blastp searches were

carried out in order to establish homology relations. AN3117 was classified as a homologue of the main copper detoxification determinant in *Candida albicans*, the P-type ATPase CaCrp1 (35% identity, 55% similarity and 95% query cover) (Riggle and Kumamoto, 2000;Weissman *et al.*, 2000). Thus, AN3117 was named AnCrpA (copper resistance P-type ATPase). An already annotated gene termed *AnygA* coding for a P-type ATPase was also detected within the up-regulated genes. The protein coded by this gene shared great homology with the ScCcc2 P-type ATPases from *C. albicans* and *S. cerevisiae* (Fu *et al.*, 1995;Weissman *et al.*, 2000). This P-type ATPase has been attributed the role of copper transport to the secretory pathway. The absence of this protein reportedly causes a pigmentation defect resulting in yellow conidia (Clutterbuck, 1990).

From literature references and bioinformatic tools, the signature domains identified in other copper transporting ATPases from human, bacteria, yeast and archaea (Barry *et al.*, 2010;Mandal *et al.*, 2002;Migocka, 2015;Rosenzweig and Argüello, 2012;Smith *et al.*, 2016;Solioz and Odermatt, 1995) were recognized in AnCrpA (Figure 15A). This kind of ATPases have 8 transmembrane helixes (TM), TM 1-5 belong to the denominated Transport domain, TMDs 6-8 belong to the Support domain and there is an invariant CPC copper translocation motif located within the 6th TMD. Five adjacent cysteine rich metal binding motifs (MBD) are present in the cytoplasmic N-terminal, two CxxC motifs and three GMxCxxC motifs. As shown in Figure 15A**,** the configuration of the N-terminal MBDs is very variable; however, AnCrpA and CaCrp1 share the same configuration. Finally, the three signature motifs present in all P-type ATPses, the aspartyl kinase domain (DKTG) containing the transiently phosphorylated aspartate residue during the catalytic cycle, the ATP binding sequence (GDGVND) and the phosphatase domain (TGES; Inesi *et al.*, 2014;Palmgren and Nissen, 2011).

II. The Copper Detoxification System in *A. nidulans*
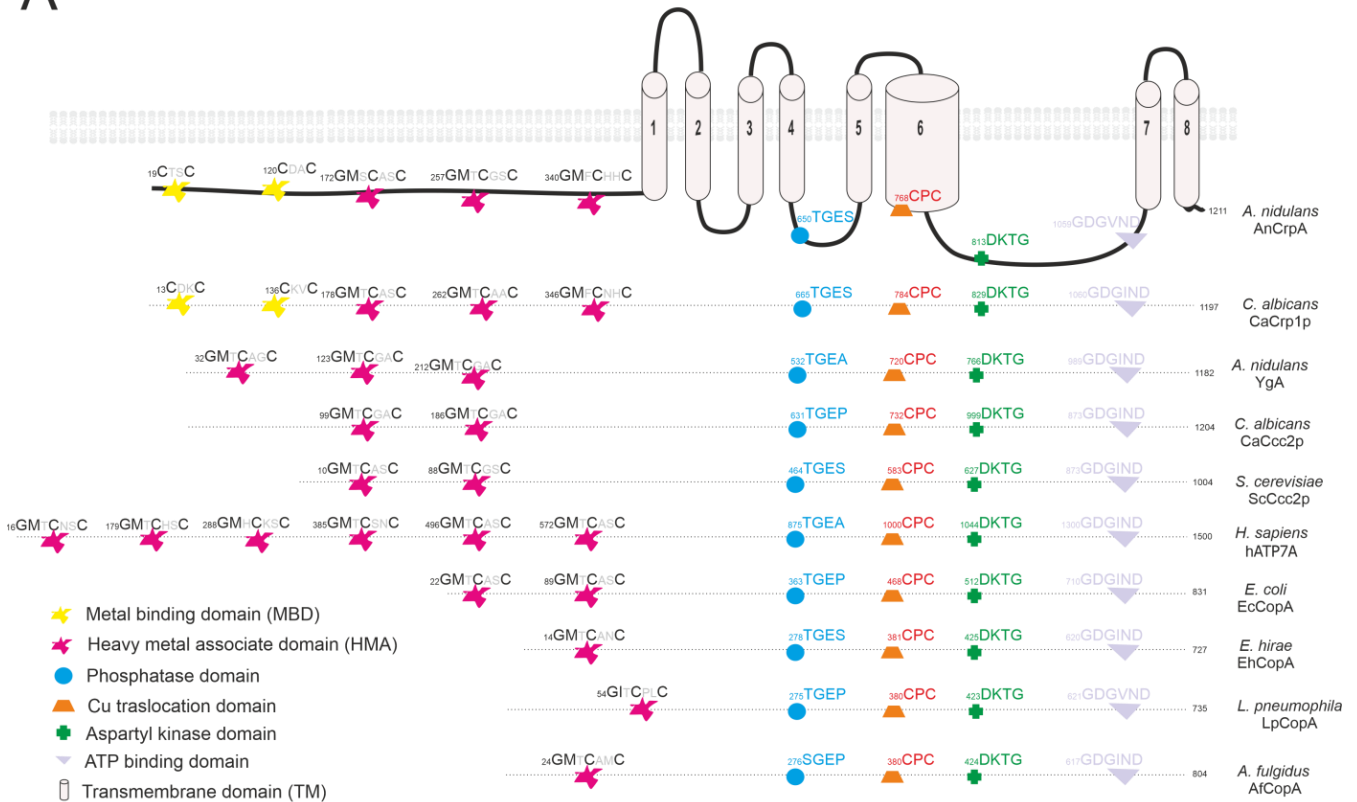
Figure 15: (A) Proposed two dimensional model of AnCrpA describing the predicted membrane topology and comparison of the conserved functional domains of PI-type ATPases and their position among different species. GenBank accession numbers are given in parentheses: *Aspergillus nidulans* AnCrpA (CBF83376.1) and AnYgA (CBF75750.1); Candida albicans CaCrp1p (AAF78958.1) and CaCcc2p (XP_720761.1); Saccharomyces cerevisieae ScCcc2p (AAC37425.1); Homo sapiens Menkes disease protein hATP7A (AAA35580.1); Escherichia coli EcCopA (CDL39203.1); *Enterococcus hirae* EhCopA (AAA61835.1); *Legionella pneumophila* copper-translocating P-type ATPase (WP_010947353.1); *Archaeoglobus fulgidus* copper-exporting P-type ATPase AfCopA (KUJ93751.1). **(B)** Alignment of predicted full-length of AnCrdA and CaCrd2p sequences compared using Clustal method. Asterisks describe identical, double and single dots, conservative and semi-conservative residues, respectively. CxC repeats are boxed in light blue. Protein accession numbers are reported as follows: *Aspergillus nidulans* CrdA (CBF79264.1) and *Candida albicans* CaCrd2p (AAF78959.1).

Previous studies in other organisms have proven that MTs are crucial for copper tolerance. Thus, an in silico search for possible MT coding genes using known *S. cerevisiae* and *C. albicans* MT coding genes as templates was performed. As a result, a possible orthologue of CaCrd2 was found, product of AN7011, termed AnCrdA. This 109 amino acid protein shared 44% similarity and 36% identity with CaCrdA. As shown in Figure 15B, MTs are abundant in cysteine residues arranged in clusters throughout the whole sequence for copper handling. AnCrdA possesses seven C-x-C clusters. The difference in length and presence cysteine residues between the compared proteins might be due to the great diversity in primary structure of MTs (Blindauer and Leszczyszyn, 2010). According to other signature characteristics of MTs, AnCrdA has only one aromatic residue, high Ser and Lys content (9 and 6% respectively) and lack of His (Riggle and Kumamoto, 2000).

2.2- Functional Characterization

In order to elucidate the contribution of each protein to the copper detoxification process single deletion mutants *ΔAncrpA* and *ΔAncrdA* were generated using gene replacement techniques (Materials and Methods). The generated mutant strains were subjected to copper tolerance assays together with the wild-type strain, by inoculating them in different $CuSO_4$ concentrations. Results showed that the *AncrpA* null strain was remarkably more susceptible to copper toxicity; at 150 µM $CuSO_4$ almost total growth inhibition was achieved (Figure 16A). At 100 µM $CuSO_4$ a very peculiar cellular morphology we named "copper phenotype" was distinguishable. The colony showed a wild-type like radial growth, but with a notably lower colony density (Figure 16B). In close up view images of *ΔAncrpA* inoculated in 150 µM $CuSO_4$ isolated hyphae covering the longitudinal area of wild-type colony size were detected (Figure 16B, magenta dotted line). With additional 24 h incubation the poor cellular growth within the colony gradually recovered (Figure 16C, magenta line). To assess the

nature of the susceptibility presented by *ΔAncrpA* the mutation was reverted. By doing this, the "copper phenotype" was rescued and so the involvement of the P_I-type ATPase in copper resistance was confirmed (Figure 16). On the contrary, no contribution in the copper resistance task was observed by AnCrdA, as the null *AncrdA* mutant displayed a wild-type phenotype over the tested concentration range (Figure 16A).

For further elucidations, a *ΔAncrpA*-*ΔAncrdA* double null mutant was generated and tested over the same copper concentration range. The copper sensitivity level shown by the double null mutant was identical to the *ΔAncrpA* strain, meaning that mutations of *AncrpA* and *AncrdA* showed no additive effect and AnCrdA was not required for copper resistance in the conditions tested.

The promiscuous nature of these of transporters, described in other organisms (Mandal *et al.*, 2002;Odermatt *et al.*, 1994), was also an issue to consider. The generated mutants were tested with different concentration ranges of $AgNO_3$ and $Cd(NO_3)_2$. The extreme sensitivity presented by the wild-type *A. nidulans* strain towards silver, 2.5 to 5 μM, was an unavoidable obstacle for accurate silver tolerance determination. However, with 150 μM $Cd(NO_3)_2$ cadmium the *ΔAncrpA* deletion mutant displayed a further aggravated phenotype (reduced growth $\sim$ 50%) than the wild-type strain. The colony morphology was certainly different to the above mentioned "copper phenotype" (Figure 16A). As in the previous case, deletion of *AncrdA* did not result in any phenotypic differences in heavy metal tolerance.

A

D

B

C
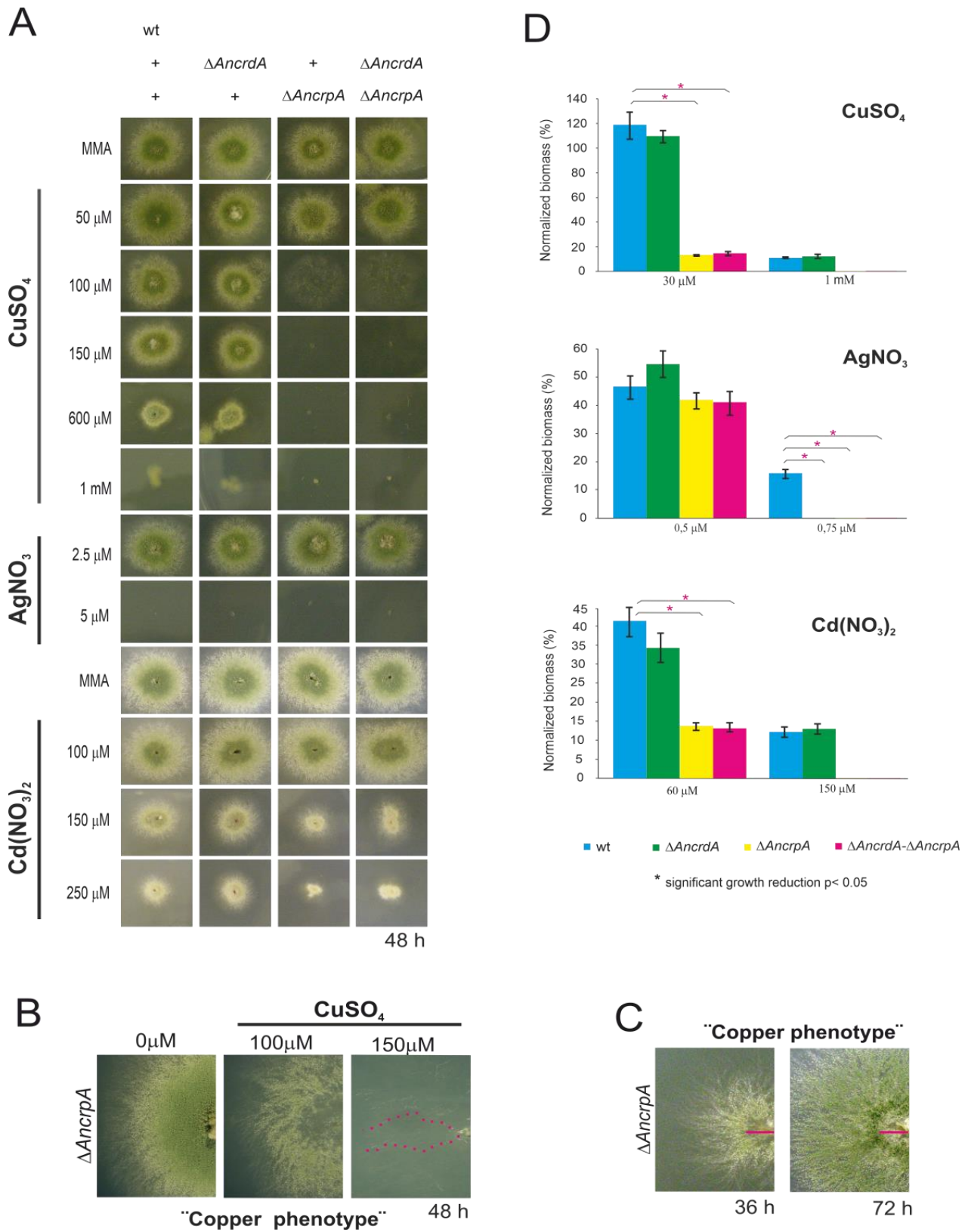
II. The Copper Detoxification System in *A. nidulans*

Figure 16: Phenotypic analysis of *AncrpA* and *AncrdA* mutant strains. Spores of strains having the indicated relevant genotypes were point-inoculated on standard MMA. Images of colonies were taken after 2 days of incubation at 37 °C. **(A)** Mutant characterization in solid medium supplemented with indicated concentrations of metal salts. **(B)** Close-up views of the morphological colony alterations in the central region of the colony caused by the deletion of *AncrpA* when exposed to 100 µM CuSO4, denominated "Copper phenotype." At 150 µM $CuSO_4$ isolated hyphae were observed (magenta dotted line). **(C)** Recovery of cellular growth in the central region of the colony over the time (magenta lines). Images of colonies were taken after 36 and 72 h of incubation. **(D)** Cellular growth in liquid MMA was monitored by determining the dry weight (biomass) of cells grown 24 h at 37 °C with the indicated concentrations of metal salts. In order to facilitate data comparison growth of each strain at basal level (no stress) was designated 100%, data was normalized and presented as percentages. Graphs show the means ± standard deviation (SD) of triplicate experiments (n = 3). * Significant growth reduction $p < 0.05$.

Liquid mycelial biomass experiments further corroborated the results obtained in solid medium. Cellular growth in the presence of cadmium and copper was strongly conditioned by *AncrpA* deletion, whereas in the case of *AncrdA* deletion, no significant difference was observed. Biomass production of *ΔAncrpA* and *ΔAncrpA-ΔAncrdA* decreased up to 15% and 14%, respectively, compared to the wild-type with 30 µM $CuSO_4$ and 60 µM $Cd(NO_3)_2$. In the case of silver, no differences were observed as all strains were unable to grow at 0.75 µM $AgNO_3$.

In conclusion, the obtained results highlight the importance of AnCrpA for copper resistance in *A. nidulans* and possibly other metals. On the other hand, in the conditions tested, the contribution of AnCrdA in metal ion toxicity resistance is negligible. The possible role of this protein remains to be elucidated.

2.3- Expression Dynamics

Earlier studies on these proteins reported that MT expression is boosted by a heavy metal load (Ehrensberger and Bird, 2011;García *et al.*, 2002;Liu and Thiele, 1997;Peña *et al.*, 1998) and copper detoxification by P-type ATPases is activated by either inducing expression (Riggle and Kumamoto, 2000;Weissman *et al.*,

2000) or changing their subcellular localization (Cobbold *et al.*, 2002;Suzuki and Gitlin, 1999).

To confirm whether *AncrpA* followed the premise, an AnCrpA::HA$_3$ chimera expressing strain was generated. In order to rule out any possible alterations in protein function due to HA$_3$ tagging, the copper and cadmium tolerance levels of the tagged strains were tested. The results showed that AnCrpA::HA$_3$ was functional (Fig 17). For the experiment, 16 h cultures were harvested according to the established sampling times. The t$_0$ sample was taken after 16 h of incubation, then 100 µM of CuSO$_4$ was added to the medium and samples were taken in the indicated times (15-360 min) (Fig 17B). Gene and protein expression results are presented in a graphic normalized with respect rRNA and hexokinase respectively (Fig 17C).

Northern-blot results show that *AncrpA* trasncripts were not detectable in resting cells. Gene expression was first detected, 15 min after Cu-addition reaching the peak of expression at 60 min. Then, the expression decreased gradually throughout the course of the experiment reaching similar expression level to that observed at 15 min (Fig 17B). These results reinforce the idea that *AncrpA* expression follows the abovementioned pattern: after copper addition, expression is transiently induced and in long copper exposures, low transcript levels are maintained. The gene expression pattern matched that of protein expression, except for the fact that the band corresponding to the chimera was first detected at 30 min after copper exposure (Figure 17B). Something worth mentioning is the presence of dispersed high molecular weight AnCrpA::HA$_3$ species and a barely visible smaller band in the 60 min sample, which could be indicative of post-translational modifications.

In order to assess the previously reported metal promiscuity of AnCrpA, the protein expression experiment was repeated with silver and cadmium stress. In the presence of 2.5 µM AgNO$_3$, the magnitude of the response was considerably

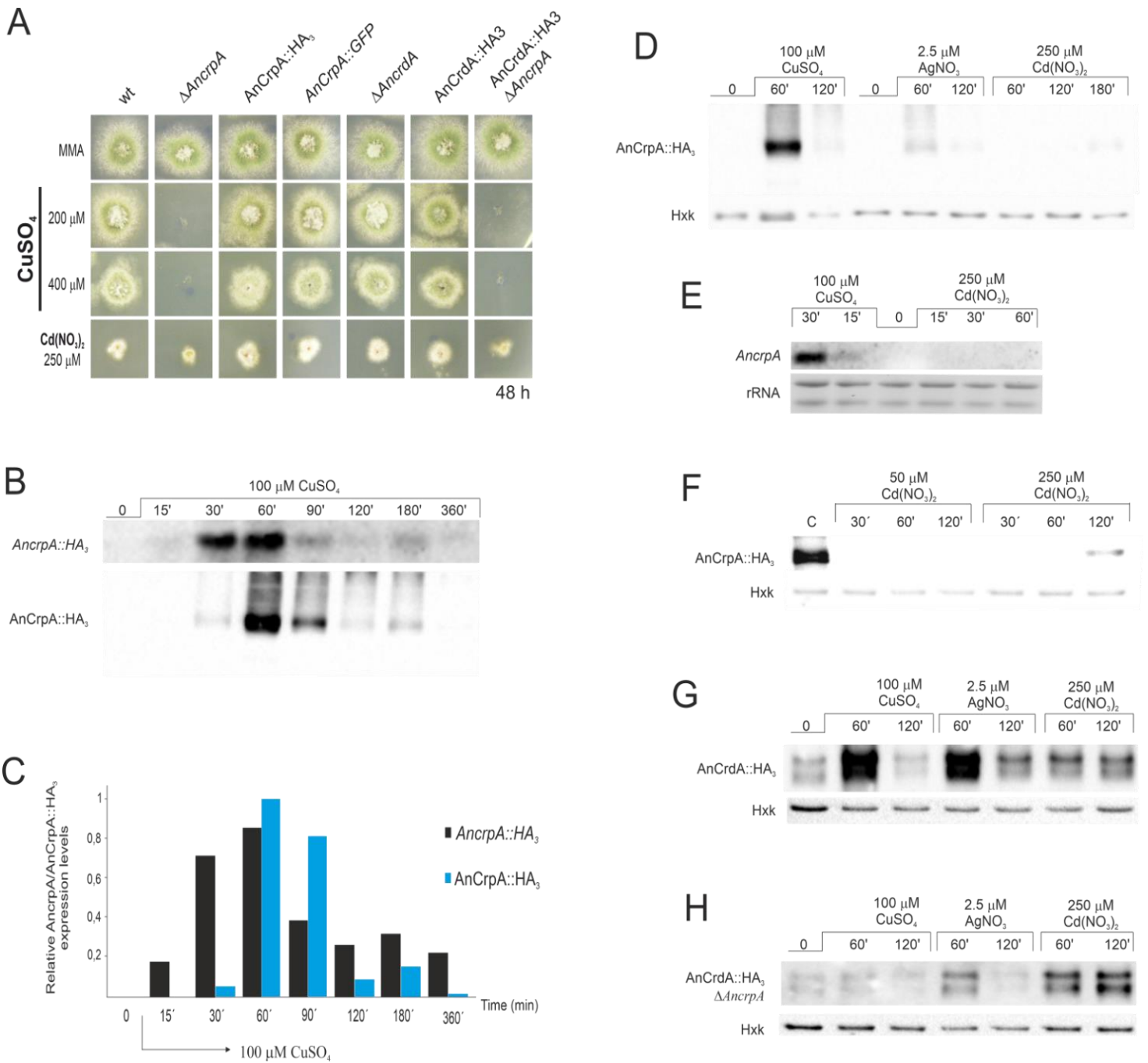# II. The Copper Detoxification System in *A. nidulans*

lower, but behavior of the protein matched the copper expression pattern with a maximum expression peak at 60 min followed by a considerable decline (Figure 17D). On the other hand, exposure to 250 μM Cd(NO$_3$)$_2$ resulted in a barely visible band at 2 h of exposure. This result was not consistent with the sensitivity to cadmium displayed by the Δ*AncrpA* strain in the functional characterization experiment; thus, another experiment was designed with longer exposure time. It was observed that protein expression was visible to some extent within the 120-180 min range (Figure 17D), showing that Cd triggers expression of AnCrpA at late instances, most likely as non-specific all-out response.

To discard a possible protein synthesis inhibition process due to heavy-metal toxicity (Matts *et al.*, 1991;Staneviciene *et al.*, 2008) as the reason for late AnCrpA detection in the presence of cadmium, *AncrpA* transcript expression was analyzed at earlier time points. No *Ancrp*A trancript was detected with early cadmium exposure, while *AncrpA* transcript was clearly visible at 15 min exposure time with copper (Figure 17E). For further proof, AnCrpA expression was compared between 50 and 250 μM Cd(NO$_3$)$_2$. No protein was detected with 50 μM and as mentioned above, with 250 μM protein was detected after 2 h of exposure.

AnCrdA function was first analyzed in solid medium after two days of culture and no significant results were obtained. However, studies conducted in *C. albicans* pointed out that the AnCrdA homologue CaCrd2 was implicated in initial copper ion buffering. Thus, protein expression analyses were conducted at short exposure times. These analyses revealed a $\sim$ 15 kDa band, in accordance with the expected AnCrdA::HA$_3$ fusion protein size and a second slower-migrating band $\sim$ 17 kDa. The relative expression levels of the mentioned bands were variable under different conditions. As shown in Figure 17G, basal AnCrdA expression was observed in the absence of metal exposition and protein levels were increased in the presence of the tested metals. Exposition to CuSO$_4$ and AgNO$_3$ yielded a similar response in pattern and intensity and Cd(NO$_3$)$_2$

exposition advanced protein expression by 1h after exposure and maintained the expression. The AnCrdA response to Cd was several times faster and stronger compared to AnCrpA.

II. The Copper Detoxification System in *A. nidulans*

FIGURE 17: AnCrpA-HA3 and AnCrdA-HA3 induction by heavy metal ions. (A) Copper sensibility assay of tagged AnCrpA and AnCrdA mutant strains. **(B)** Northern-blot and Western-blot showing changes in *AncrpA::HA$_3$* transcript and AnCrpA::HA$_3$ expression levels after addition of 100 µM of CuSO$_4$ and monitored at the indicated times. Images correspond to the area of interest. **(C)** The graph shows *AncrpA::HA$_3$* transcript and AnCrpA::HA$_3$ protein expressions relative to the corresponding loading controls, rRNA and hexokinase respectively. Average pixel intensity for each band was calculated with Image J (version 4.0; Fujifilm, Valhalla, NY). **(D)** Comparison of AnCrpA::HA$_3$ induction pattern by different metal salts [100 µM CuSO$_4$, 2.5 µM AgNO$_3$, and 250 µM Cd(NO$_3$)$_2$]. Images correspond to the area of interest. **(E)** Northern-blot showing changes in *AncrpA::HA$_3$* expression after addition of 100 µM of CuSO4 but not during 1 h treatment with 250 µM of Cd(NO3)2. **(F)** Western-blot comparing Cd-induced AnCrpA::HA$_3$ expression after 50 µM and 250 µM of Cd(NO$_3$)$_2$ addition. Western-blot showing changes in HA3 tagged version of AnCrdA in a wild-type **(G)** and null *AncrpA* **(H)** background induced by different metal ions.

Expression of AnCrdA was then studied in a *ΔAncrpA* genetic background, hypothesizing that the deletion of the major copper resistance determinant in the organism may result in heightened AnCrdA expression in order to increase the copper buffering capacity. For this purpose, a *ΔAncrpA* strain expressing the AnCrdA::HA$_3$ chimera was generated (Figure 17A). Comparing protein expression between the *ΔAncrpA* and the wild-type background, the signal detected in copper and silver exposure samples was significantly lower and, in the case of cadmium, it was similar. Taken together, the results indicate that AnCrdA expression is negatively affected by the absence of *AncrpA.*

Overall, the obtained results show that *AncrpA* has a dynamic expression pattern during long copper treatments, a strong early response followed by a notable decay reaching low expression levels that are maintained through time. The experiments performed with different metal salts suggest that this ATPase functions principally as a copper transporter, but it may also have a role in silver transport. On the other hand, AnCrdA responds to metal toxicity, but its role in heavy metal tolerance remains uncertain.

2.4- AnCrpA Dynamic Localization

The results obtained so far are consistent with at a copper extrusion role of the P-type ATPase AnCrpA; this implied plasma membrane (PM) localization, not excluding other compartments. To test this hypothesis, an AnCrpA::GFP fusion protein expressing strain was generated. The strain displayed a wild-type like phenotype in the tested conditions (Figure 18A) and the protein expression analyses revealed similar protein dynamics to those previously seen AnCrpA::HA$_3$ strain (Figure 18A).

For life *in vivo* microscopy experiments, cells were grown overnight without copper stress and then shifted to new media containing 100 μM CuSO$_4$. The protein was first visible at 30 min upon the medium shift. It was localized throughout the hyphae in structures reminiscent of the ER (Figure 18B.A1,A2; arrowed), surrounding oval structures that resembled the nucleus and strands associated to the PM (Markina-Inarrairaegui *et al.*, 2013). Taking a closer view to the tip region, a finger-like protrusion towards the tip could be distinguished (Figures 18B.A2,A4). After 1h of copper exposition, AnCrpA localization changed. A homogeneous fluorescence signal in the cytosol was detected, but the most notable feature was the strong fluorescence signal throughout the cellular periphery, suggesting a predominant PM localization of AnCrpA (Figures 18B.B1,B2). In addition, it was found that the fluorescence signal was polarized at the tip region in a large number of cells (Figures 18B.B3, B4). Linescan measures were made in order to quantify signal accumulation throughout the drawn lines and prove that the signal distribution is stronger in the PM and the tip region.

After two hours of copper exposition, AnCrpA distribution was again modified. A large part of the fluorescence remained at the PM. However, different aggregates of variable morphologies were visible: punctate and ring-shaped structures reminiscent of the Golgi body were dispersed in the cytosol

II. The Copper Detoxification System in *A. nidulans*

(Pantazopoulou and Penalva, 2009) (Figures 18B.C2, C3, yellow arrowheads). After three hours the aggregates turned noticeably bigger, akin to vacuolar compartments (Pantazopoulou *et al.*, 2007) (Figures 18B.C4, magenta arrows). The nature of the mentioned organelles has to be corroborated by colocalization experiments.
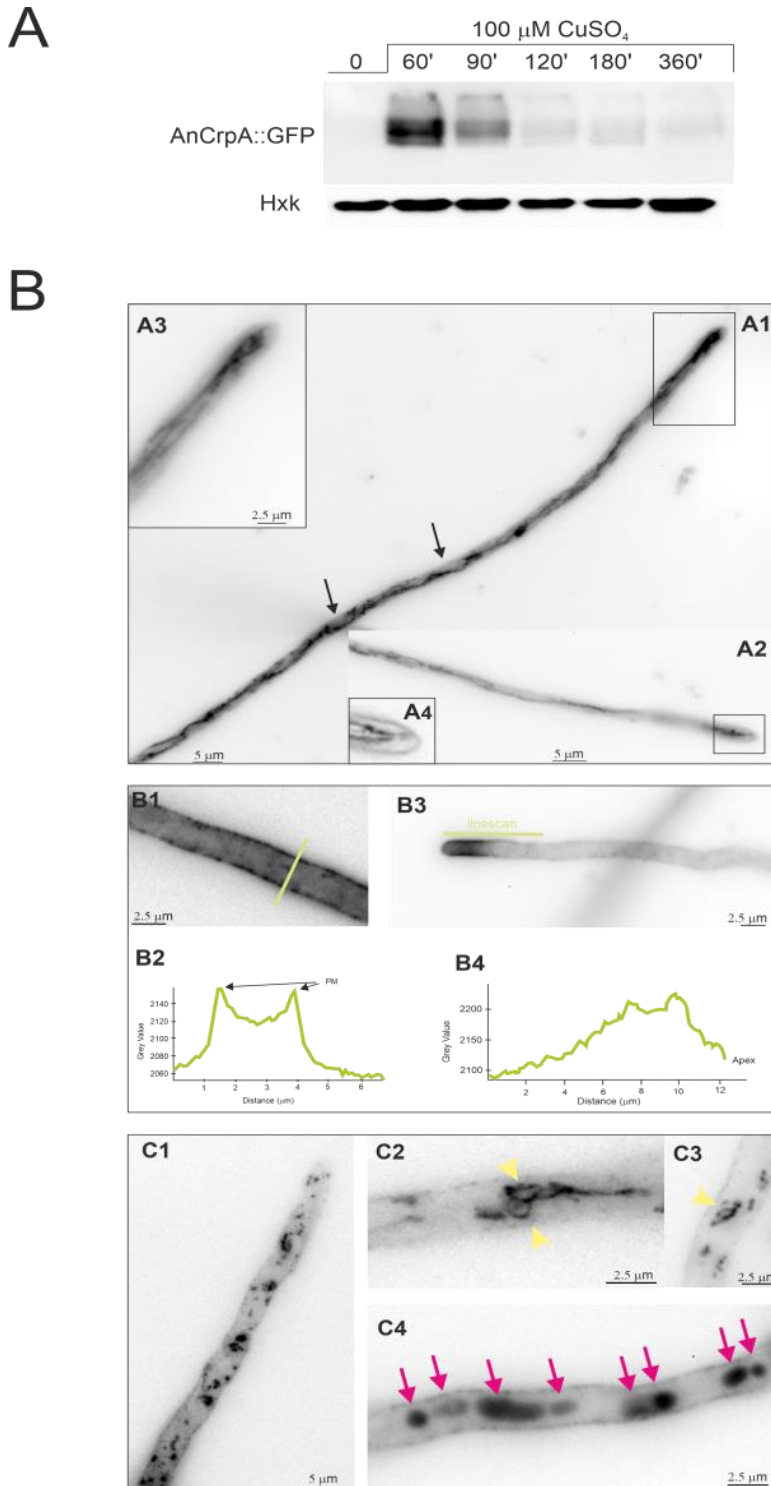

Figure 18: Effect of exposure to copper on intracellular localization of CrpA-GFP. (A) Western-blot confirming AnCrpA::GFP expression kinetics after addition of 100 μM of CuSO$_4$. (B) Cells of a strain expressing a AnCrpA::GFP fusion were grown in selective medium for microscopy for 16 h at 25 ^{o}C and shifted to medium containing 100 μM CuSO$_4$ for the indicated times. Images taken 30 min after the shift. (A1,A2) AnCrpA localized in a network of strands and tubules. (A3,A4) Images correspond to the rectangular region indicated in (A1,A3) showing a magnification of the tip region. (B1–B4) Images corresponding to 1 h after the shift. GFP fluorescence was accumulated predominately in the PM (B1) and polarized in the tip region (B3). Panels (B2,B4) correspond to the line scans of AnCrpA::GFP signal across the indicated lines. (C1–C4) Images taken 2–3 h after shifting. Panels (C1,C2,C3) are examples of ring-shaped structures (yellow arrowheads) and (C4) of abnormal aggregates (magenta arrows). Images were treated with sharp filter, shown in inverted gray contrast and represent average intensity projections of Z-stacks.

In conclusion, the results point to AnCrpA being synthesized in the presence of copper, as demonstrated in the protein analysis experiments. Then the protein is directed to the membrane, most likely for copper extrusion purposes and finally, the protein is gradually removed from the membrane in an apparently regulated trafficking process.

2.5- Expression Regulation of AnCrpA and AnCrdA by the Transcription Factor AnAceA

The rapid and regulated copper-inducible transcription of *AncrpA* suggested that it is under the control of a copper-dependent transcription factor (TF). Blastp searches using *S. cerevisiae* Ace1p (CAA96877.1)(Dameron *et al.*, 1991), *Candida glabrata* Amt1p (XP_447430.1) (Zhou *et al.*, 1992), and *Yarrowia lipolytica* Crf1p (XP_500631.1) (García *et al.*, 2002)) amino acid sequences allowed the identification of the putative transcription factor homologous in *A. nidulans*, a 525 amino acid long protein encoded by AN1924 ORF (1,689 bp) and referred to from now on as AnAceA.

AnAceA contains several features described for its orthologs, especially the N-terminal DNA-binding domain. This region (Figure 19A) showed the highest sequence conservation, especially the first subdomain (residues 1–39), copper-fist DNA-binding domain, which displayed 61% identity with 1–40 amino terminal amino acids of YlCrf1p (76% similarity), 55% with ScAce1p (73% similarity) and 45% identity with CgAmt1p (76% similarity). This whole region encompasses 11 of the 14 encoded cysteines arranged in CxC or CxxC clusters, conserved among the copper regulatory transcription factors mentioned. These cysteine residues are necessary for copper binding, which induces a conformational change of the protein. This, in turn, allows the interaction of the copper-activated DNA-binding region with the Metal Regulatory Elements (MRE) of the promoter of the target genes (Peña et al., 1998). AnAceA exhibits a serine (14%) and proline (12%) rich composition and unusual distribution (SSxSS, SSS, PPP clusters), especially in the

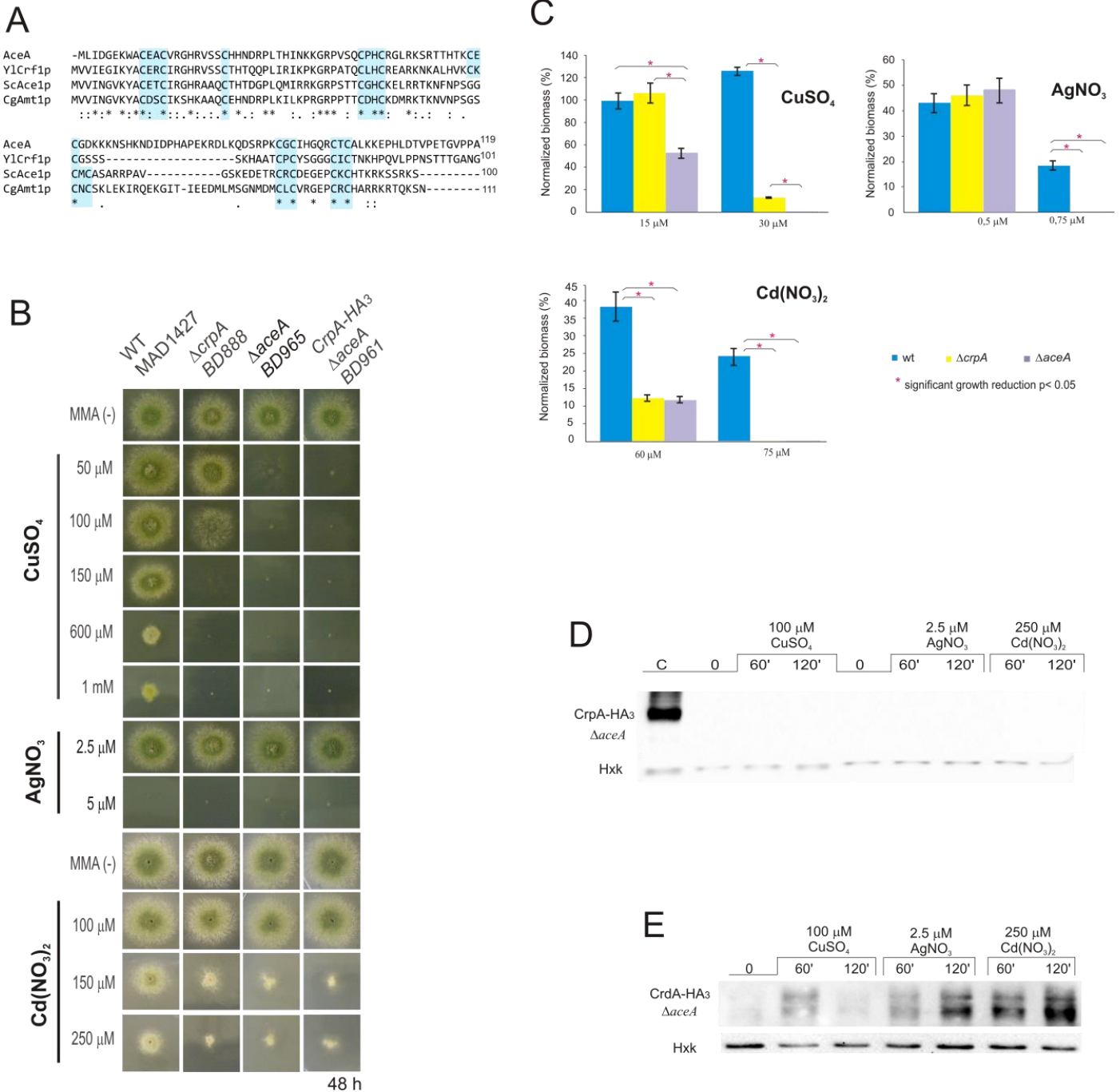## II. The Copper Detoxification System in *A. nidulans*

C-terminal half of the protein, similar to YlCrf1p of *Y. lipolytica* (García et al., 2002).

The conservation of motifs is consistent with the view that AnAceA may be the transcriptional factor involved in copper tolerance in *A. nidulans*. To investigate its role, a single-knockout mutant of *AnaceA* locus was generated (BD965) and tested in the same range of metal concentrations used before. Growth analyses demonstrated that not only did the *ΔAnaceA* strain display an identical "copper phenotype" to that observed in *ΔAncrpA*, but it also exhibited a more pronounced sensitivity response to $CuSO_4$, since colony defects were observed at lower concentration (Figure 19B). Elevated cadmium content provoked a reduction of colony growth, nevertheless in a similar degree to the previously observed in the *ΔAncrpA* strain. Biomass measurements supported these results (Figure 19C). The *ΔAnaceA* mutant strain was significantly more sensitive to $CuSO_4$ than *ΔAncrpA* strain ($p < 0.05$). In contrast, the tolerance to Cd^{+2} and Ag^+ was almost identical in both strains. These results confirm the implication of AnAceA in metal tolerance, playing a key role in copper resistance.

We hypothesized that AnAceA was the copper dependent transcriptional activator of genes involved in copper detoxification, thus the strain bearing a mutation in the *AnaceA* gene should be sensitive to copper primarily due to a defect in copper-inducible transcription. In order to prove this hypothesis, we analyzed by Western-blot extracts of strain BD961, which expressed the AnCrpA::HA$_3$ fusion protein in an *AnaceA*-deletant background (Figure 19B). Using anti-HA$_3$ antibody, we did not detect the 134 kDa band observed previously, as in extracts from the strain expressing AnCrpA::HA$_3$ and loaded as control (Figure 19D). The lack of AnCrpA::HA$_3$ detection demonstrated that AnAceA is necessary for metal induction of the P_{IB}-type pump transcription. Subsequently, the HA3 tagged metallothionein like protein in response to metal salts in the absence of *AnaceA* allele (BD1062) was analyzed. AnCrdA::HA$_3$ was detected in the *AnaceA* -deleted strain (Figure 19E). Moreover, results indicated

that AnCrdA expression levels and kinetics in the null *ΔAncrpA* and *ΔAnaceA* mutant strains were comparable. This result indicates that AnAceA is not essential for metal-induced activation of *AncrdA* and supports the possibility of a role different from metal ion detoxification.

II. The Copper Detoxification System in *A. nidulans*

FIGURE 19: Functional analysis of AnAceA. **(A)** Multiple alignment of the most conserved region, N-terminal half, of AnAceA, YlCrf1p, ScAce1p, and CgAmt1p, which contains the majority of cysteine residues arranged in clusters (indicated in light blue boxes). Protein alignments were performed using Clustal Omega. Genebank protein accesion numbers are as follows: *A. nidulans* AceA (CBF85835.1), *Y. lipolytica* YlCrf1p (XP_500631.1), *S. cerevisiae* ScAce1p (CAA96877.1), and *C. glabrata* CgAmt1p (XP_447430.1). **(B)** *AnaceA* mutant characterization in solid medium supplemented with indicated concentrations of $CuSO_4$, $AgNO_3$, and $Cd(NO_3)_2$. **(C)** Biomass measurement of WT, *ΔAnaceA* and *ΔAncrpA* strains grown at indicated conditions. Data was normalized and presented as percentages. Bars indicate means and error bars standard deviation. N = 3. Western-blot showing **(D)** AnCrpA::HA_3 and **(E)** AnCrdA::HA_3 induction by heavy metal ions in a null *AnaceA* background strain. Hexokinase and AnCrpA::HA_3 sample of cells treated for 1 h with copper were used as controls. *Significant growth reduction $p < 0.05$.

Taken together, these results confirm that AnAceA is the transcription factor responsible of regulating genes involved in copper detoxification, as *AncrpA*, and suggest the existence of an as yet unidentified gene responsible for the residual copper resistance in *A. nidulans*.

3- Discussion

Eukaryotes rely on accurately regulated mechanisms to maintain the balance between copper uptake, compartmentalization and detoxification. In this study we identified and characterized AnCrpA as a key element of the copper detoxification system in *A. nidulans*.

Sequence analysis identified AnCrpA as the putative homolog of CaCrp1p, which had been reported to confer high resistance to copper by ion extrusion (Riggle and Kumamoto, 2000;Weissman *et al.*, 2000). Both proteins proteins share an atypical structure and distribution of the N-terminal metal binding domains (MBD) (Figure 15). Since these motifs are likely involved in regulation, we postulate that AnCrpA and CaCrp1p may share similar ion specificities and biological functions. Studies carried out in *Y. lipolytica* strongly support the concept that copper resistance is not mediated by MT related Cu buffering but

by efflux in this species (García *et al.*, 2002;Ito *et al.*, 2007). Further blast searches in this dimorphic fungus revealed a putative homolog YALI0B02684p (GeneBank accession number XP_500433.1), which displayed a similar N-terminal extension. These results indicate that ATPase-based copper extrusion may be found in a wider range of fungi than those reported so far. It is also important to underscore the crucial role of copper resistance for virulence of clinically important fungal pathogens as *C. albicans* (Mackie *et al.*, 2016), *Cryptococcus neoformans* (Ding *et al.*, 2013a;Samanovic *et al.*, 2012) and *A. fumigatus* (Dietl *et al.*, 2016;Wiemann *et al.*, 2017).

Evidence of the direct participation of AnCrpA in copper resistance was obtained by the extreme sensitivity exhibited by AnCrpA null mutants. An atypical aspect of the phenotype of the null *AncrpA* mutation was the poor growth in the central region of the colony, which overcame toxicity over time. Similar adaptive growth patterns have been described previosuly (Valix *et al.*, 2001). As the colony matures, copper may bind to new cellular material locally, resulting in reduction of free copper concentration, and increased growth.

Besides copper, *ΔAncrpA* also exhibited sensitivity to cadmium; however, the divergent phenotype reflected either affinity of metals for different targets and/or distinct detoxification paths (Mendoza-Cózatl *et al.*, 2010). Neither *AncrpA* Cd-induction nor Cd-protein expression under low Cd concentration was observed. In addition, AnCrpA was detected only in the presence of high cadmium loads. Together, these results support an indirect PI-type ATPase activation taking place, possibly due to the saturation of the main cadmium detoxification system, a Cd^{2+} pump (Shiraishi *et al.*, 2000;Thorsen *et al.*, 2009) or glutathione-derived peptides denominated phytochelatins (Mendoza-Cózatl *et al.*, 2005;Mendoza-Cózatl *et al.*, 2010).

Regarding silver toxicity, our data showed that *A. nidulans* is sensitive to this metal at a very low (2.5–5 µM) concentration range. Biomass measurements

II. The Copper Detoxification System in *A. nidulans*

indicate that AnCrpA may participate in silver resistance. On the other hand, it was observed that silver induced expression of AnCrpA which matched copper kinetics, although to a lesser extent. Based on these results, we propose that copper is the principal substrate of the *A. nidulans* ATPase, however silver may also be transported. Indeed, this is consistent with the fact that the orthologs described above are also reported Cu^+/Ag^+ transporters. Although we did not ascertain it in this study, AnCrpA likely exports Cu^+ and not Cu^{2+} since; (a) in the reduced cytosolic environment Cu^{+2} is found in Cu^+ form and (b) substitution of Cu^+ by Ag^+ is possible in proteins with CxxC containing MBDs, but not Cu^{2+} (Petris *et al.*, 1996).

Long term copper exposure induces an early, strong, and transient expression followed by a basal maintenance expression level of AnCrpA. Regarding the effect of copper exposure on *AncrpA* expression over time, it has been demonstrated that *AncrpA* induction is rapid (within 15 min), transiently strong (57-fold increase in 1 h) and sustained throughout the period of exposure to copper, since mRNA levels were detectable along the whole experiment. Hypothesizing that *AncrpA* mRNA levels may reflect intracellular ion concentrations, it is plausible that, under long term high copper exposure, cells would firstly synthesize an elevated amount of Cu-exporter in order to rapidly reduce the initial burst of copper incorporated via high-affinity transporters. Subsequently, pump levels would be down-regulated and then maintained at a certain level during the period in which copper continues to enter chronically to the cell via low-affinity transporters, similar to *S. cerevisiae* (Yu *et al.*, 1996). Regulation studies are ongoing at present in our laboratory to verify whether AnCrpA post-translational modifications (PTM) are involved in AnCrpA activity control besides the transcriptional regulation described in this work.

AnCrpA localization to the cell membrane in response to copper addition sustains the expected copper extrusion role of this ATPase. Detailed evaluation of the subcellular distribution indicated that AnCrpA is under the control of a

highly orchestrated trafficking process that resembles membrane transporter regulation (Lauwers *et al.*, 2010;Pantazopoulou and Diallinas, 2007). It may be envisaged that, in response to increased cytosolic Cu^+, de novo synthesized AnCrpA may traffic from the ER to the Golgi compartment and then to the plasma membrane (PM). Upon a purported decrease in cytosolic copper concentration, a fraction of PM AnCrpA would be internalized by endocytosis and sorted to the multivesicular body (MVB). AnCrpA could then be recycled back to the PM via the TGN as reported in human cells (Pase *et al.*, 2004) where the PM AnCrpA pool could be the result of two different protein delivery pathways; a newly synthesized and a recycled AnCrpA pool. Post-translational modification and organelle trafficking mutant studies would be required to establish a model of AnCrpA sorting and regulation. Solving the molecular mechanism of the P_I-type ATPase trafficking in *A. nidulans* could provide novel insights into how cells with a polarized architecture regulate copper ATPase activity.

The active role of AnAceA in copper resistance gene regulation was demonstrated by the extreme copper-sensitive phenotype of the knock-out mutant and the absence of expression of AnCrpA in the *ΔAnaceA* strain. In fact, the increased sensitivity of *ΔAnaceA* with respect to *ΔAncrpA* mutants highlighted two major points: firstly, the participation of an additional element in the copper detoxification path and secondly, the predominant role of AnCrpA over the minor participation of the other player in the system. This second participant could be either a copper-metallothionein (MT) that has not been identified or a copper scavenging phytochelatin, like in *Schizosaccahoromyces pombe* (Clemens *et al.*, 1999). Identification of new metallothioneins, since the primary structure is highly diverse, could be a laborious task. It may be worthwhile to attempt a different approach: the characterization of the AnAceA binding metal-response element (MRE) on the AnCrpA promoter might propose a consensus MRE sequence for *A. nidulans* copper detoxification genes that could facilitate new searches.

II. The Copper Detoxification System in *A. nidulans*

AnCrdA expression was induced by copper, silver and cadmium within 1 h, indicating a role in metal homeostasis. In summary, we found that: (a) a $\Delta AncrdA$ strain did not exhibit a metal sensitivity phenotype, (b) a non-additive effect of *AncrpA* and *AncrdA* deletion was observed, (c) the deletion of *AncrpA* did not increase *AncrdA* expression, and (d) AnAceA was not required to activate AnCrdA expression. Taken together, these results do not support the participation of AnCrdA in AnCrpA-mediated metal detoxification. A likely role for this putative metallothionein may be as an antioxidant (Blindauer and Leszczyszyn, 2010;Palmiter, 1998). Further studies will confirm whether the principal AnAceA-regulated PI-type ATPase (AnCrpA) system is connected with AnCrdA mechanism in response to metal stress.

III. Chapter-

Molecular Modelling Approach to Screen for AnCrpA Inhibitors

III. Molecular Modelling Approach to Screen for AnCrpA Inhibitors

1- Introduction

The two previous chapters of this thesis cover the high-affinity copper uptake system and the copper detoxification system of *A. nidulans*. The original aim of this project was to gain insight on copper homeostasis in order to find possible ways to complement or replace copper as an agricultural fungicide.

There are some different approaches to improve the efficiency of antifungal preparations and one of them is by synergistic interaction, the use of an ingredient that complements or amplifies the antifungal activity of the active ingredient, the synergist. If the synergist can exert an impact on the functionality of the copper homeostasis system, this could lead to higher susceptibility to copper. Four processes where synergists could exert the desired effect on copper homeostasis are: uptake, delivery, buffering and detoxification. This chapter presents an attempt of a molecular modelling approach to find active compounds that interfere with copper detoxification as proof of concept.

Current knowledge on copper homeostasis is limited to the uptake and the detoxification systems. The Ctr proteins AnCtrA and AnCtrC are two possible targets. Their purpose is to bind Cu^+ with high-affinity and transport it inside the cell when the cell senses that copper reservoir is low. However, their expression profile is specific for low copper environments and the literature has provided evidence that these proteins shut down when copper concentrations rise in the environment. If more details of this mechanism were available, specific means to interfere with the mechanism could be attempted. This is not currently feasible.

The best understood target currently is AnCrpA. As shown in chapter 2, it is the main detoxification agent in *A. nidulans* and inhibiting its activity, either totally or partially could make a significant difference to potentiate the effect of copper-based fungicides. In addition, phylogenetic analyses have shown that a wide range of phytopathogenic fungi possess a homolog protein of AnCrpA.

III. Molecular Modelling Approach to Screen for AnCrpA Inhibitors

In this chapter the procedure followed to find inhibitory compounds for AnCrpA using computational techniques will be described. First, a structural model of AnCrpA was generated based on the crystal structure of the *Legionella pheumophila* copper extruding P-type ATPase LpCopA. This is called homology modelling (Waterhouse *et al.*, 2018). From the literature we determined the most interesting areas for AnCrpA inhibition and different compound libraries were screened by docking in the selected areas of the AnCrpA model. This process is called virtual screening, a high-throughput approach to find the best candidates according to their binding-energy values. From the virtual screening experiments a set of candidates were selected depending on the binding-energy (Jaghoori *et al.*, 2016). However, the virtual screening gives no information about the orientation of the molecule (binding pose) in the grid (delimited binding area) and being a process that manipulates a lot of information in short time is also prone to error. Thus, individual docking experiments were made to check the results of virtual screening and to obtain the orientation of the molecule that corresponds with the best binding energy possible (Rizvi *et al.*, 2013). Finally, molecular dynamics experiments were carried out with each molecule to check protein-ligand complex stability (Mangiaterra *et al.*, 2017).

The whole process was carried out under the supervision of Dr. Roberta Galeazzi at the Department of Live and Environmental Sciences (DiSVA) in "Università Politecnica delle Marche" for their experience in similar procedures (Mangiaterra *et al.*, 2017).

III. Molecular Modelling Approach to Screen for AnCrpA Inhibitors

2- Materials & Methods

2.1- Protein Preparation

The protein structure of AnCrpA was obtained by homology modelling. The PDB file of the template was downloaded from the Protein Data Bank (PDB). The *Legionella pneumophila* CopA protein structure "4bbj" obtained by protein crystallization was used as a template (35.8% identity). This structure has a 2.75 Å resolution and is delineated in the E2P state (Andersson *et al.*, 2014). The homology modelling was carried out in the fully automated protein structure homology-modelling server SWISS-MODEL using the "User template" option. Once the structure of the protein was obtained hydrogens were added to the new model and the template and the Root Mean Square Deviation (RMSD) between the template and our structure was calculated using Chimera software (Pettersen *et al.*, 2004;Waterhouse *et al.*, 2018).

Protein salinity was settled in pH 6.5, which corresponds to the internal pH of the organism (Caddick *et al.*, 1986). Then the macromolecule was minimized using a standardized protocol (Galeazzi *et al.*, 2014;Scire *et al.*, 2013) (Mohamadi *et al.*, 1990;Suite., 2011), using AMBER force field (Duan *et al.*, 2003). By doing this the software makes the net inter-atomic force closest to zero as possible.

2.2- Grid Generation

For the virtual screening experiments the area in which we want to dock the compound library has to be delimited. Each delimited area is called a receptor grid. To generate the receptor grids to test, "Receptor Grid Generation" tool from Autodock Vina software was used (Morris *et al.*, 2009;Sanner, 1999). For grid selection, data available on *Legionella pneumophila* CopA was used. Two sites were specifically selected: The ATP binding site and the putative chaperone binding region.

III. Molecular Modelling Approach to Screen for AnCrpA Inhibitors

Grid 1 (The ATP binding site): 70 x 70 x 76 Å.

Grid 2 (Putative chaperone binding site): 62 x 100 x 86 Å.

2.3- Virtual Screening and Focused Docking

Molecular docking experiments were carried out in the AutoDock Vina version 1.1.2 software (Trott and Olson, 2010). The in-house compound libraries were screened using the VINA software against the two selected receptor grids of the AnCrpA model (most compounds are from the database ZINC12). The PDB file of our model was converted to PDBQT and all compounds were docked in the selected grids using standard parameters. The procedure was repeated three times, each one in a different computer. Only the compounds that appear in the top 10 binding energy score on the three replicates of each library were used for further procedures (Jaghoori *et al.*, 2016).

After choosing the compounds with best binding energy score from the Virtual Screening, Autodock 4.2.1 (AD4) was used to check the virtual screening results and in case they were good, obtain the best binding pose (orientation of the molecule in the binding grid) and relative energy (Chang *et al.*, 2010;Morris *et al.*, 1998). The virtual screening process binds the compounds 10 times in the delimited grid and shows the best binding-energy of each compound, but it gives no information about how the molecule is oriented within the grid (binding pose) and the residues that it interacts with. With Autodock 4.2.1 the molecules are docked individually and the number of binding times was increased from 10 to 1000 within each grid. As a result of this process different binding poses of each molecule that would differ in binding-energy and frequency would be obtained. The binding pose with best energy and frequency ratio was chosen in each case (Rizvi *et al.*, 2013).

2.4- Molecular Dynamics

Molecular dynamics simulations are a tool to predict the behavior of the protein and the ligand when they are docked. This approach shows if they are likely to form a stable complex or not. As AnCrpA is localized in the plasma membrane, for the molecular dynamics simulation an AnCrpA-Plasma Membrane complex was designed. For such purpose, AnCrpA orientation in the membrane was obtained by the OPM server (https://opm.phar.umich.edu/ppm_server) and the Protein-Plasma membrane (PM) complex was built using CHARMM GUI (http://www.charmm-gui.org/). The membrane was composed of 25% ergosterol, 42% palmitoyl oleyl phosphaditylcholine and 33% N-palmitoyl sphingomyelin. The result was a Protein-PM complex with a 91 x 91 x 160 Å size, appropriately solvated with water and ionized (0.15 M NaCl). AMBER99SB-ILDN force field parameters were used for the proteins and lipids (Guy *et al.*, 2012) and the TIP3P model (Jorgensen, 1998) model for solvent as implemented in GROMACS 5 (Hess *et al.*, 2008). First the Protein-PM model was minimized, subjected to six equilibration steps and then the molecular dynamic simulation of 10 ns was carried out on its own. The same procedure was repeated with the Protein-PM complex with each compound docked in the grid with the best binding orientation obtained with Autodock 4.2.1. By doing this the stability of the ligand-receptor complex is studied (Mangiaterra *et al.*, 2017).

III. Molecular Modelling Approach to Screen for AnCrpA Inhibitors

3- Results & Discussion

3.1- The template Model LpCopA

As selected template for homology modelling was the *Legionella pheumophila* copper detoxification ATPase LpCopA. Up to date it is the copper transporting P-type ATPase that has been crystallized with highest resolution (Andersson *et al.*, 2014). These proteins need magnesium ion as a cofactor for ATP hydrolysis. As shown in Figure 20, the Mg ion is located at the catalytic site. The catalytic site of the protein, phosphorylation domain (P-domain), nucleotide-binding domain (N-domain) and energy transduction domain (A-domain), and the eight transmembrane domains are correctly resolved. However, the structure of the N-terminal first 72 residues was not resolved (Figure 21A).
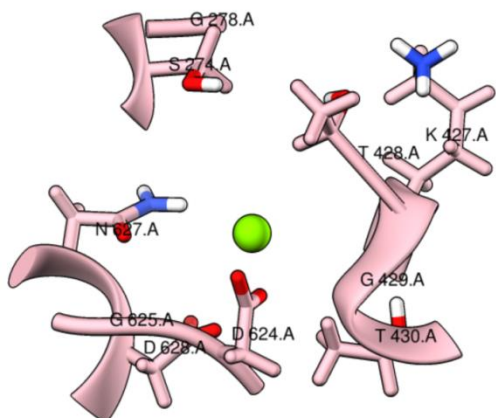

Figure 20: Close up view of the catalytic site of LpCopA.

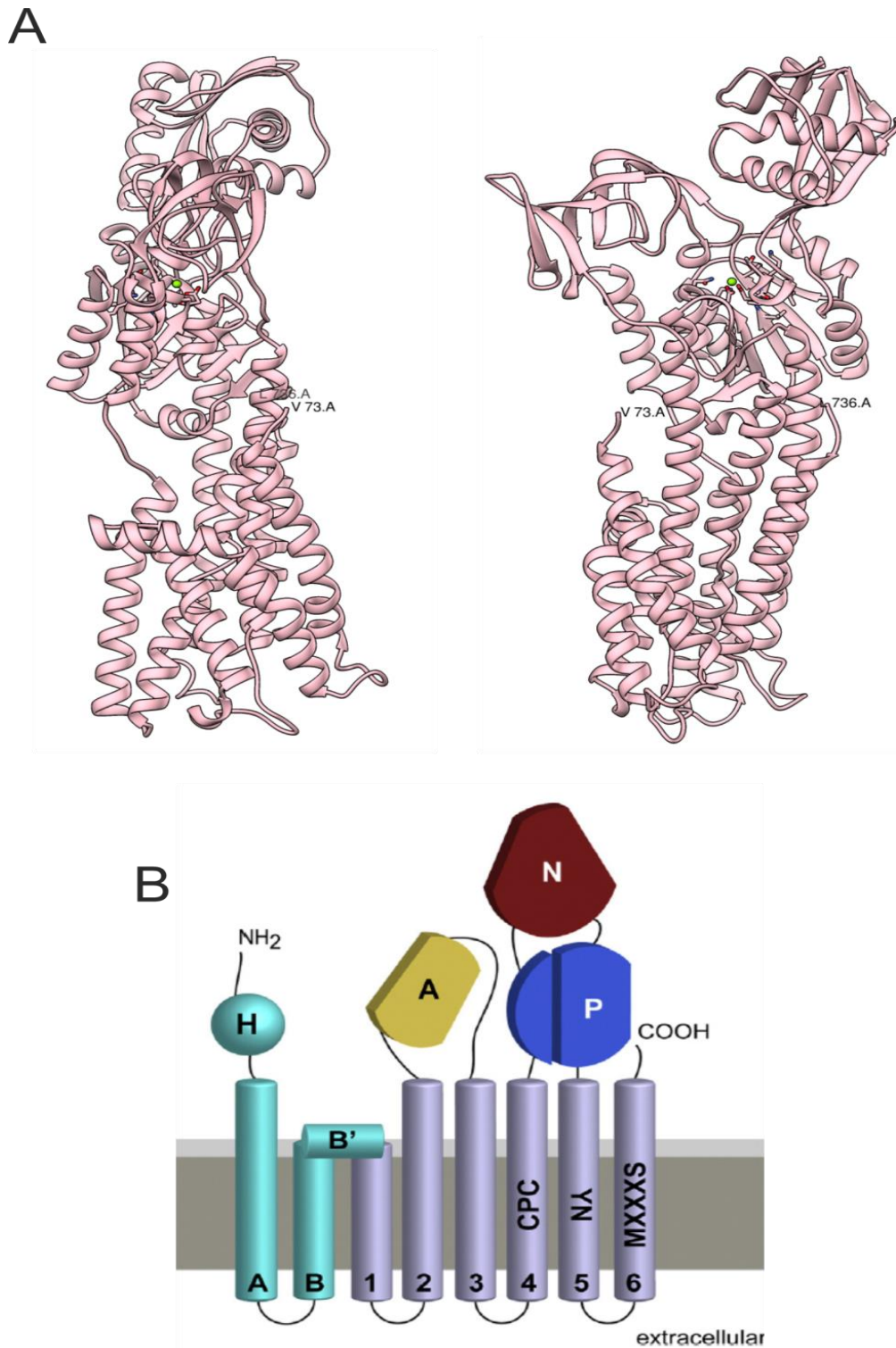**Figure 21:** LpCopA protein structure. **(A)** The backbone of the protein from Valine 73 to Leucine 736 with the Mg ion located in the catalytic cycle and the eight transmembrane domains. **(B)** The general structure scheme of P$_{IB}$-type ATPases (Mattle *et al.*, 2013). H represents the N-terminal Heavy Metal Binding Domain, P the phosphorylation domain, N the nucleotide-binding domain and A the energy transduction domain.

III. Molecular Modelling Approach to Screen for AnCrpA Inhibitors

PIB-type ATPases possess a structural peculiarity in the first two TMDs. The first two TMDs (MA-MB-MB´; Figure 21B) are not part of the transmembrane pore that drives Cu ions through the membrane as they sit beside the pore formed by TMDs 1-6. MA and MB are connected to the pore through the perpendicular amphipathic helix MB'. This helix has a positively charged surface and is connected to TMD 1. Basically, MB' is the entrance of the pore. According to Mattle and collaborators (2013), MB' is a putative chaperone docking area. The argument behind the statement is that the surface of the amphipatic helix is positively charged while copper-donating chaperones frequently contain a negatively charged surface. Its location in the pore entrance and the putative chaperone docking role make MB' a very interesting target for docking experiments.
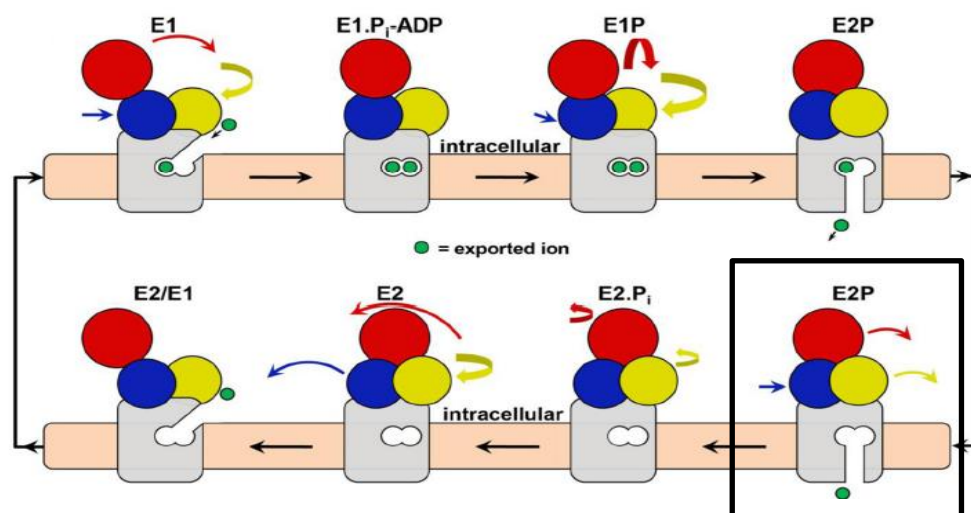
Figure 22: P-type ATPase reaction cycle (Andersson *et al.*, 2014). The intracellular A-, P- and N-domains are colored yellow, blue and red, respectively, while the M-domain is gray. Ions are transported accompanied by phosphate hydrolysis and structural rearrangements (arrows). The LpCopA crystal structure was resolved in E2P state (black box).

The transmembrane cargo-traffic of the P-type ATPases requires a great dynamism of structure of these proteins. During the transfer period the protein goes through different phases (illustrated in Figure 22). In the case of our

template LpCopA structure, it was captured in E2P state, meaning that the pore is opened to the extracellular side (Andersson et al., 2014).

The above described model (LpCopA) was used to obtain an AnCrpA model by homology modelling. The result of the homology modelling was an AnCrpA model with a resolved structure from ARG422 to GLU1187, eight transmembrane domains and one Mg ion in the catalytic site. The same as in LpCopA the N-terminal tail of the protein is not present in the model (Figure 23).
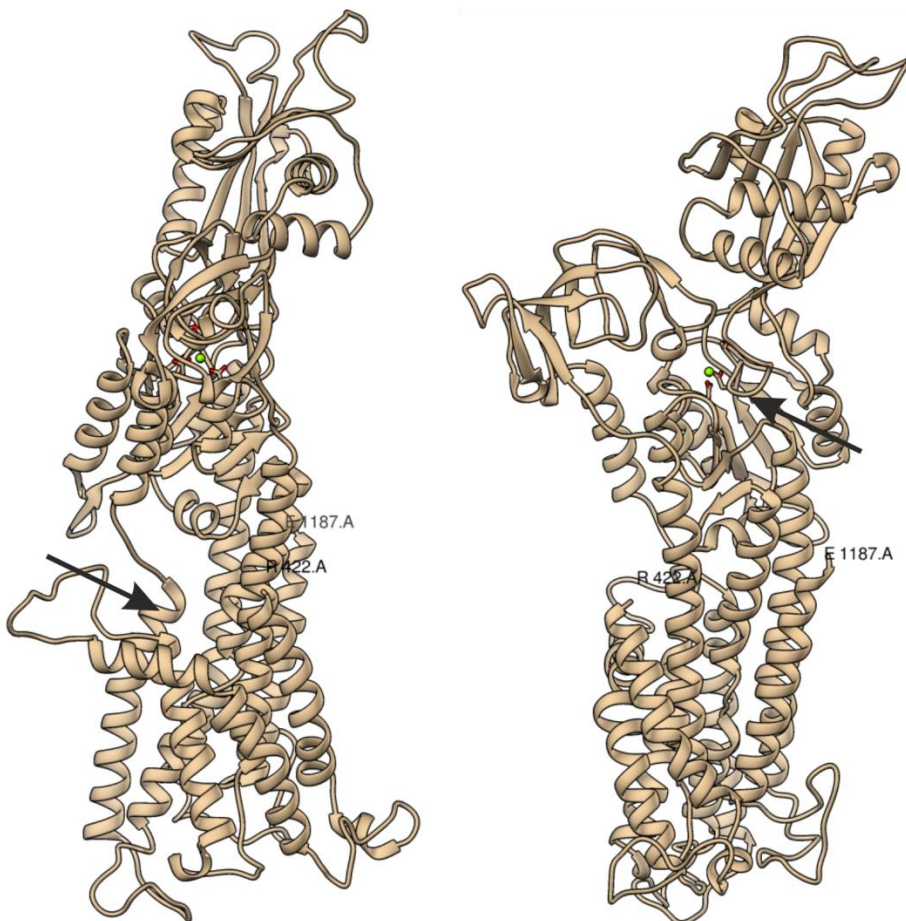
Figure 23: AnCrpA model obtained by homology modelling. The image in the left side shows the entrance of the pore past MB' helix (arrow). The image in the right side shows the catalytic site where the Mg ion is located (arrow).

In the catalytic site of the newly obtained AnCrpA model we verified that all important domains for the phosphorylation-dephosphorylation cycle (A, P and N domains) were all very close to the Mg ion (Figure 24).

III. Molecular Modelling Approach to Screen for AnCrpA Inhibitors
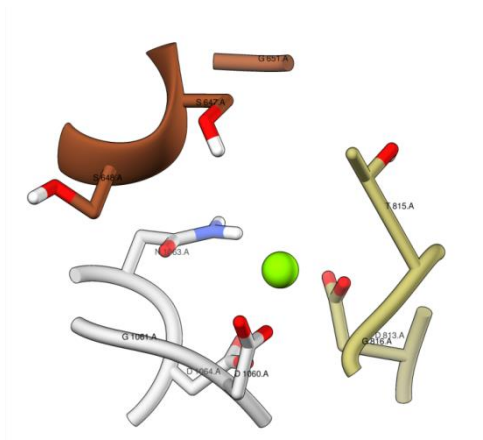
Figure 24: The catalytic site of AnCrpA. The Mg ion is surrounded by the three characteristic P-type ATPase domains for ATP hydrolysis. The phosphorylation domain (P-domain) in green; the nucleotide-binding domain (N-domain) in gray; and finally, the energy transduction or the phosphatase domain (A-domain) in brown.

After all necessary checking of the protein, the AnCrpA-plasma membrane complex was created for the molecular dynamics simulations as described in the Materials & Methods section (Figure 25).
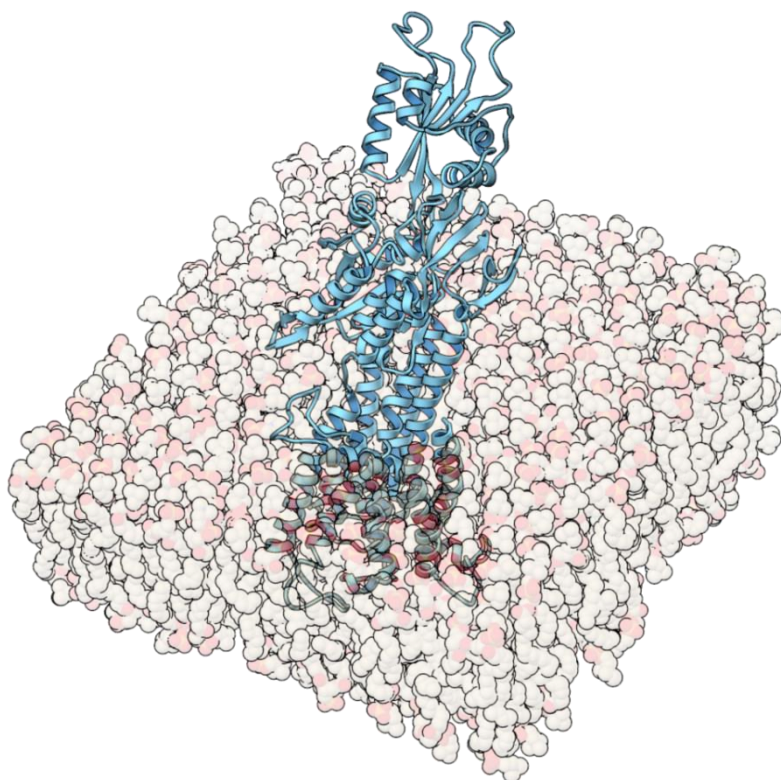
Figure 25: AnCrpA-plasma membrane complex generated using CHARMM GUI software. The plasma-membrane components have been made transparent to see the arrangement of the pore through the membrane. The amphipatic helix MB' is at the edge of the membrane.

III. Molecular Modelling Approach to Screen for AnCrpA Inhibitors

3.2- Model Validation

Grid 1 is the ATP binding site; thus, we decided to dock ATP first as a control.

As shown in Figure 26A ATP binds in the selected grid. The phosphate groups of the ATP molecule are situated very close to the catalytic domains of the P-type ATPase (Figure 26B): ASP1060, GLY1061, ASN1063 and ASP1064 of the nucleotide binding domain (gray); ASP645, SER647 and SER648 of the phosphorylation domain (green); finally, ASP813, THR815 and GLY816 from the phosphatase domain (brown) (Figure 26B).From this experiment we learned that the model was reliable.

Figure 26: Image of an ATP^{-4} molecule docked in Grid 1. **(A)** The backbone of AnCrpA is shown in surface mode. The three phosphate groups of ATP sneak in through a passway and interact with residues of the A, N and P domains. **(B)** The residues within a 5 Å distance from the ATP molecule are shown together with the predicted hydrogen bonds (blue lines).

III. Molecular Modelling Approach to Screen for AnCrpA Inhibitors

3.3- Virtual Screening

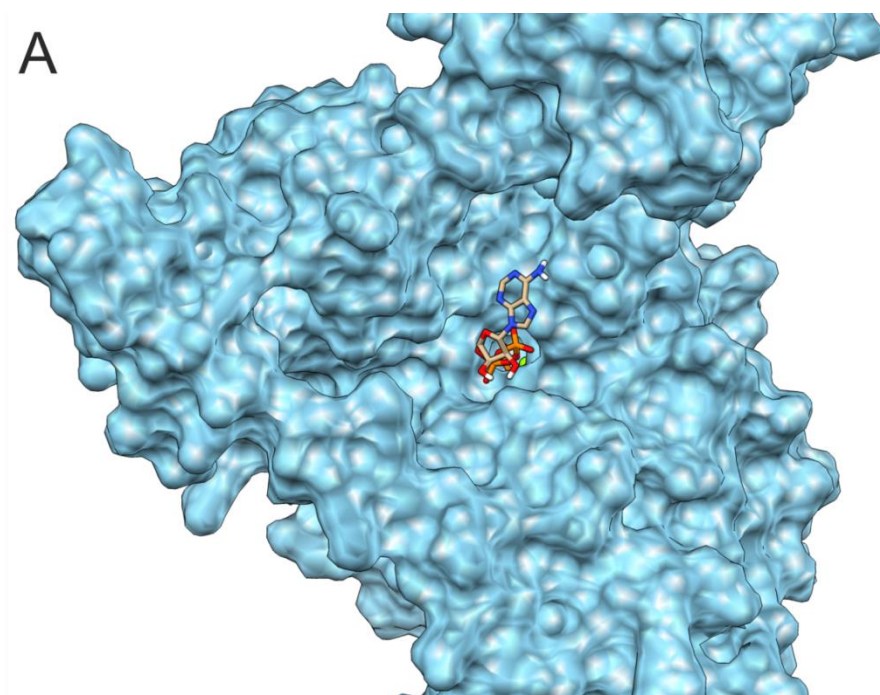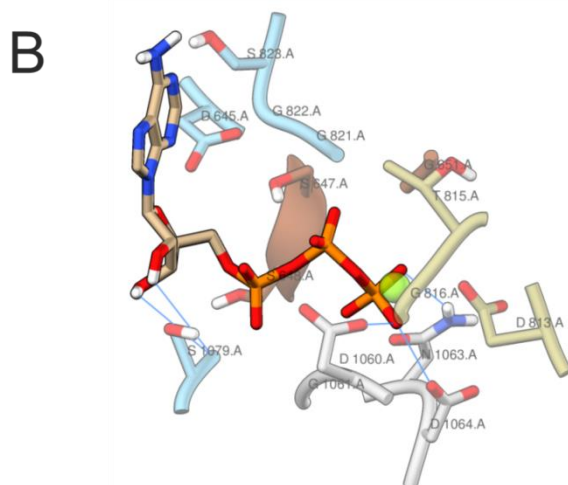After checking the new AnCrpA model everything was ready for the compound library screenings. Different in-house compound libraries were screened against our model in the two different grids we selected, the catalytic site and the entrance of the transmembrane pore.

The compounds with best binding energy are listed in tables 8 & 9. A binding energy below -9 kcal/mol corresponds to activity within the micromolar range (Mangiaterra *et al.*, 2017).

Table 8: Virtual screening results from Grid 1, the catalytic site. All compounds belong to the ZINC12 database and they are named ZINCXXXXXXXX.

ZINC	Compound name	Bind. energy
95099267	1,11,13-trihydroxy-6-methoxy-pentacene-5,7,12,14-tetrone	-8.98
08221225	Lutein	-7.8
14879959	lutein G	-8.25
14879961	Lutein	-7.7
95099399	(5aS,10aS)-1,3,8,10a-tetrahydroxy-2-[hydroxy(methyl)BLAHyl]-5a-(3-methylbut-2-enyl)benzofuro[3,2-b]c	-8.63

Table 9: Virtual screening results from Grid 2, the entrance of the transmembrane pore. All compounds belong to the ZINC12 database and they are named ZINCXXXXXXXX.

ZINC	Compound name	Bind. energy
95099267	1,11,13-trihydroxy-6-methoxy-pentacene-5,7,12,14-tetrone	-8.475
95099369	[dihydroxy-heptamethyl-[(2S,3R,4S,5R)-3,4,5-trihydroxytetrahydropyran-2-yl]oxy-BLAHyl]	-8.5
08221225	Lutein	-8.1
14879959	lutein G	-8.3
14879961	Lutein	-8.15
35877687	Pregn-5-ene-3-ol	-8.7

3.4- Focused Docking and Molecular Dynamics

The compounds with best binding energy were selected and further docking experiments were made using the software Autodock 4.0 in order to obtain the binding poses and more accurate binding-energy data. By doing this, the binding-energies obtained in the virtual screening process are also verified. If the results obtained in the individual docking don't coincide with the virtual screening results, the compounds are discarded.

Besides the compounds from the in-house compound libraries, other compounds found through the literature were subjected to docking experiments. We also tested an extra compound which has been subjected to some *in vivo* preliminary tests by a local company. Due to confidentiality matters this compound was named COMPOUND 1 (COMP1). COMP1 showed a very strong binding energy at grid 1, thus it was included for the molecular dynamics experiments.

Based on binding energy criteria, the following compounds were selected for molecular dynamics experiments:

Grid 1: COMP1, ZINC95099399, ZINC08221225.

Grid 2: ZINC95099267, ZINC95099369, ZINC35877687, ZINC08221225.

The following step was the molecular dynamics simulation with each compound. For the molecular dynamics simulation we used the AnCrpA-PM complex created by CHARMM-GUI software (Figure 25). We ran a molecular dynamics simulation of the complex on its own as a control and then another molecular dynamics (MD) simulation with each compound docked on the protein. With the molecular dynamics simulation we were able to determine the stability of the protein ligand complex (whether the compound moves away or remains in the binding-site), the development of the biding-energy and the structural behavior of our

III. Molecular Modelling Approach to Screen for AnCrpA Inhibitors

model during the simulation with and without compounds attached. The location of the two delimited binding grids is illustrated in Figure 27.

Figure 27: AnCrpA model showing the different binding regions selected for docking experiments. Grid 1, the ATP binding site is shown in black box. Grid 2, the entrance of the pore is shown in blue box.

3.5- Grid 1: ZINC95099399 (HBB)

HBB   (5aS,10aS)-1,3,8,10a-tetrahydroxy-2-[hydroxy(methyl)BLAHyl]-5a-(3-methylbut-2-enyl)benzofuro[3,2-b]c) was one of the compounds that showed the best binding energy in grid 1. The binding pose with best binding energy was selected with a binding energy value of (-8.84 kcal/mol).
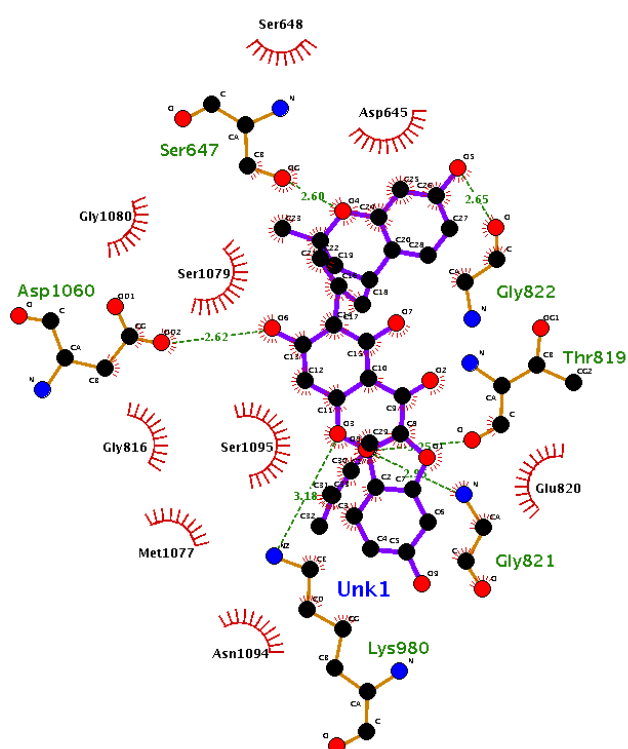
Figure 28: AnCrpA amino acids involved in interactions with HBB in grid 1 (Image obtained by Ligplus protein-ligand interaction online server).

Previously the binding of an ATP molecule was tested, so it was decided to check the binding poses of ATP and HBB together to see if there was significant overlapping between the two poses. The HBB molecule in the selected pose covered the ATP entry site and overlapped with the ATP molecule in the catalytic site (Figure 29).

III. Molecular Modelling Approach to Screen for AnCrpA Inhibitors
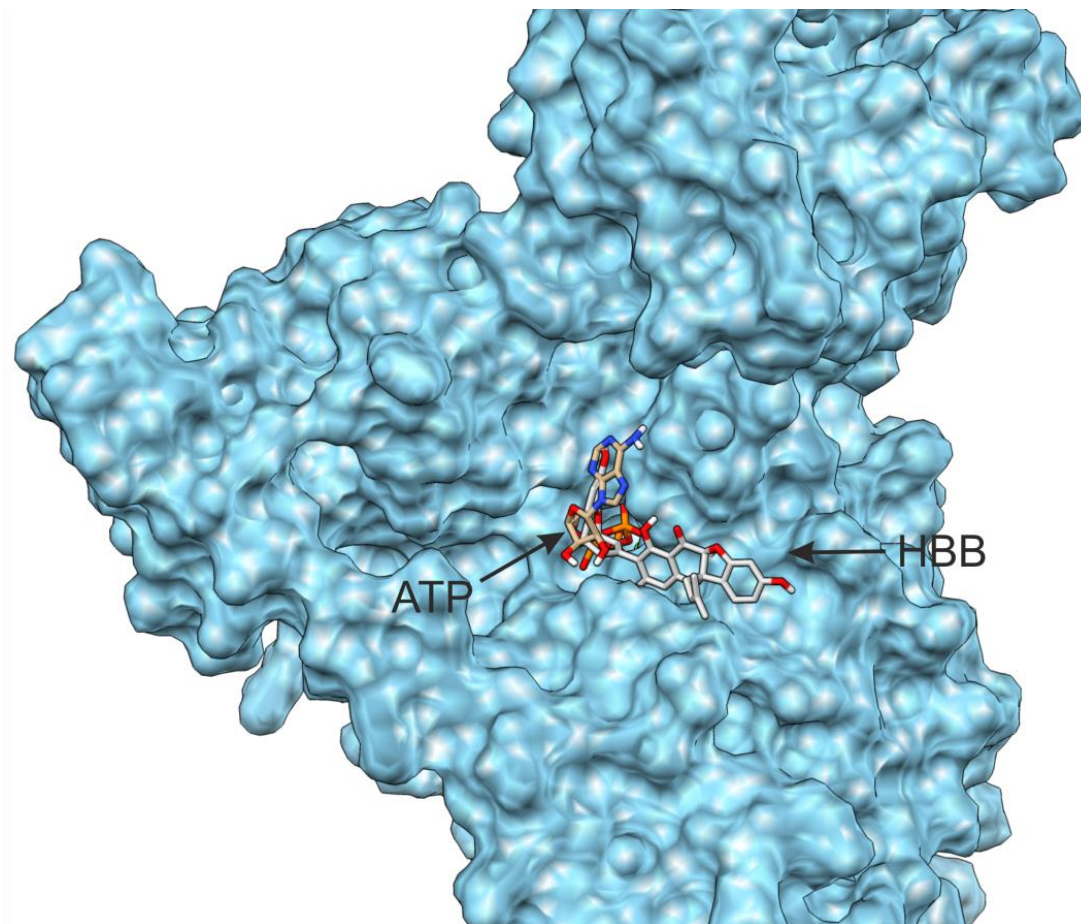
Figure 29: ZINC95099399 (HBB, light gray) and ATP^{-4} (ATP, dark gray) docked in Grid 1 of AnCrpA. The backbone of AnCrpA is shown in surface mode. The HBB molecule in this pose overlaps with ATP when it is bound to AnCrpA.

Once it was determined that the binding pose of the HBB could interfere with the ATP binding and the binding energy was sufficient, molecular dynamics simulations were undertaken to assess the stability of the protein-ligand complex. The MD simulation showed that the HBB molecule moved away from the stipulated binding grid and the protein structure was visibly disrupted, especially in the catalytic site. However, the RMSD graph showed that the dynamics of the protein did not differ substantially when the HBB molecule was bound (Figure 30).
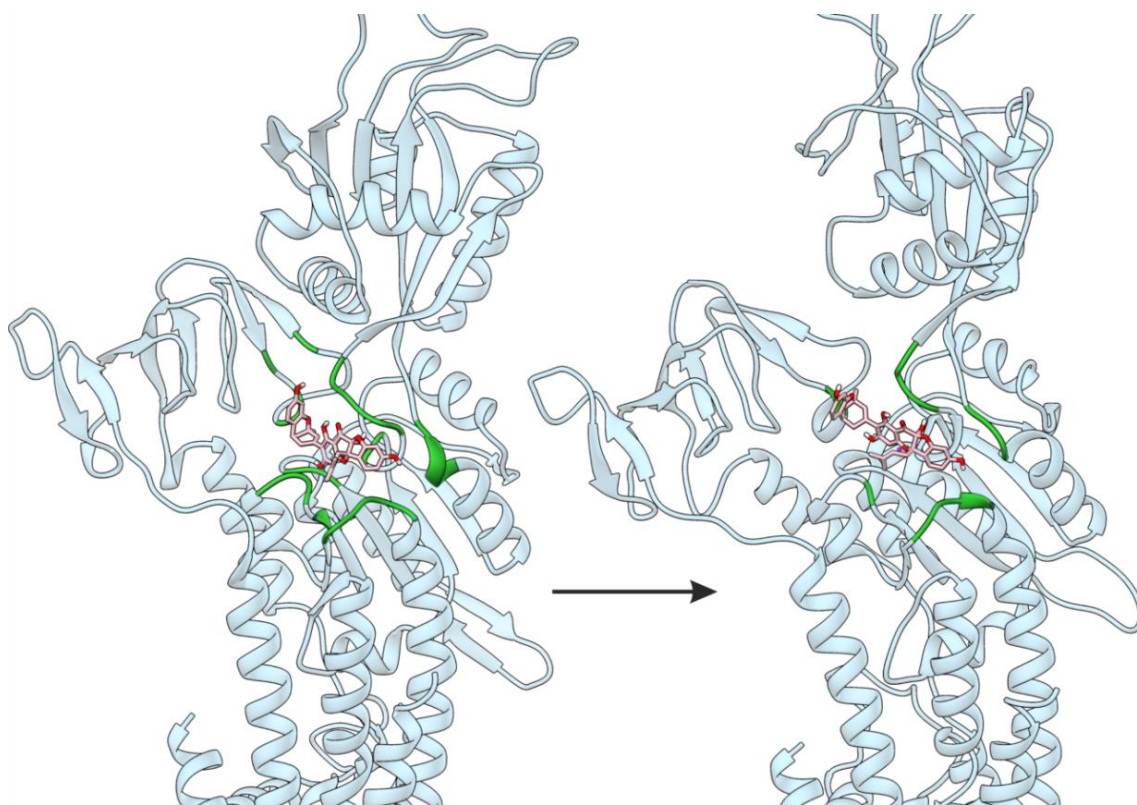
Figure 30: Before and after image of the MD simulation showing the HBB molecule pose along with the AnCrpA backbone. The residues within a 5 Å distance from the molecule are shown in green. The graph below compares the fluctuations of the protein-membrane complex throughout the time course of the MD simulation without ligand (NoLigand) and with ZINC95099399 (HBB).

III. Molecular Modelling Approach to Screen for AnCrpA Inhibitors

The same procedure was followed for the selected compounds to be tested in grid 1, COMP1 and ZINC08221225, and similar results were obtained. In both cases the initial docking energy was satisfactory; however, the molecular dynamics experiments showed that both compounds moved away from the docking sites. Figure 31 shows the evolution of binding energies of the tested compounds throughout molecular dynamics simulation. HBB shows the best binding energy in the beginning of the simulation (-275 kJ/mol) and even though the binding energy fluctuates until 5 ns, it is then stabilized in a value around -240 kJ/mol. The other two compounds showed a lower binding energy from the beginning (-150 kJ/mol). In the case of COMP1, the final binding energy was higher than the initial; however, it kept fluctuating throughout the simulation. In the case of ZINC08221225 (Lutein), the binding energy dipped, a sign that the molecule tends to move away from AnCrpA.

Figure 31: Graph showing the development of the protein-molecule binding energy throughout the course of molecular dynamics simulation. COMP1 is shown in blue (COM), ZINC95099399 in green (HBB) and ZINC08221225 in red (LUT).

3.6-Grid 2: ZINC35877687 (PREG)

The compound with best binding-energy in grid 2 was compound ZINC35877687. This compound is pregn-5-ene-3-ol, an alkaloid derivative. It was denominated PREG. The binding-energy of this compound after the focused docking experiments was -8.4 kcal/mol. It also interacted with putative residues predicted to be involved in the copper transport, MET521, and putative residues that interact with the chaperone docking, LYS497 (Mattle et al., 2013).
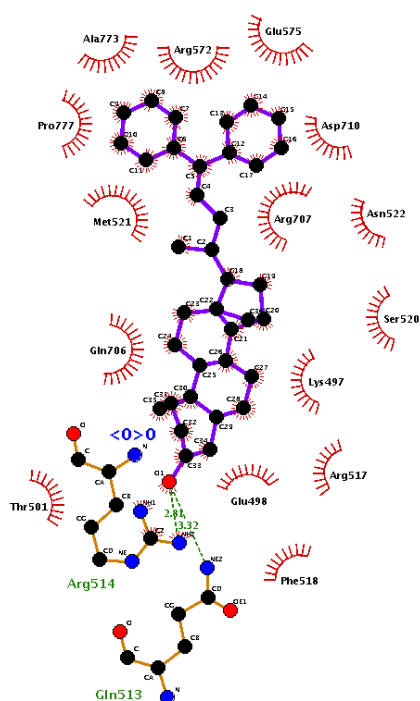
Figure 32: AnCrpA amino acids involved in interactions with PREG in grid 2 (Image obtained by Ligplus protein-ligand interaction online server).

After the best binding pose of the compound was found, as with the previous compound, a molecular dynamics simulation was performed using the same established parameters for the previous simulation. After the simulation time, the pose of the molecule did not seem to be notably altered, however the RMSD values showed an outstanding variation when the PREG molecule was bound and that is indicative of a non-stable complex.

III. Molecular Modelling Approach to Screen for AnCrpA Inhibitors
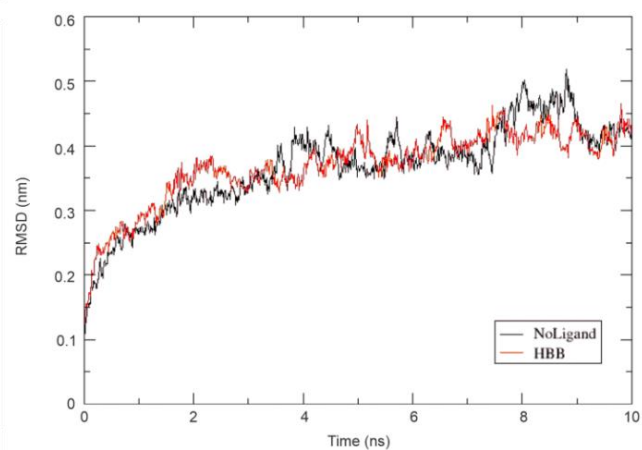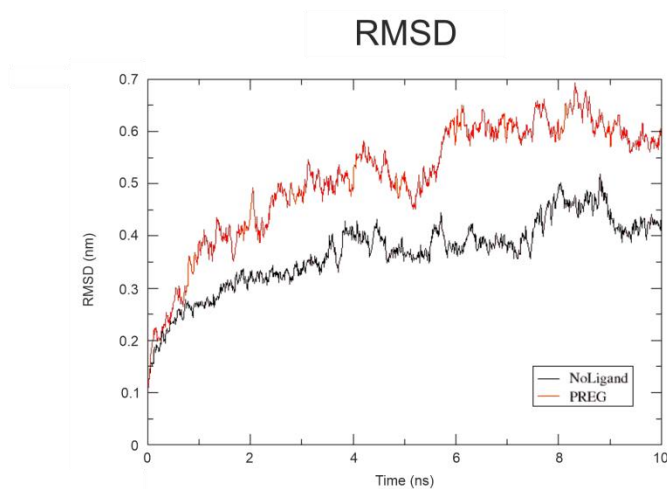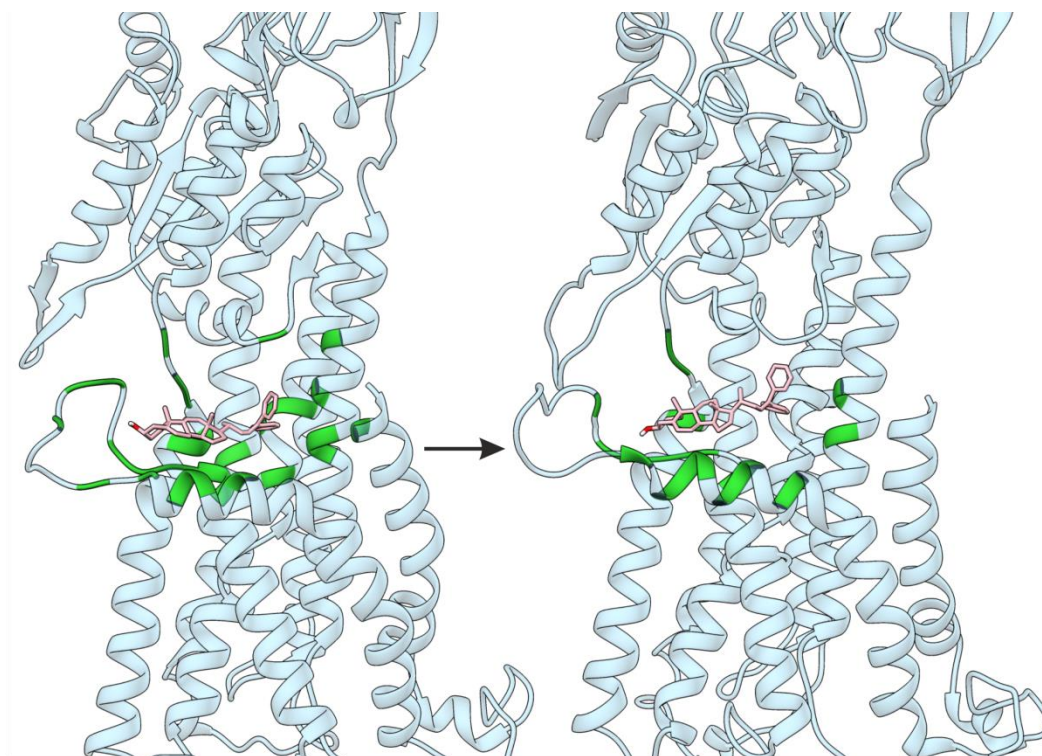

Figure 33: Before and after image of the MD simulation showing the PREG molecule pose along with the AnCrpA backbone. The residues within a 5 Å distance from the molecule are shown in green. The graph below compares the fluctuations of the protein-membrane complex throughout the time course of the MD simulation without ligand (NoLigand) and with ZINC35877687 (PREG).

The above described procedure was repeated with the remaining selected compounds of grid 2, ZINC95099267, ZINC95099369, and ZINC08221225. In the case of ZINC95099267 and ZINC95099369, the molecule was notably displaced

from the initial binding grid and the RMSD profile was also very unstable (Figure 33). Finally, ZINC08221225 had an outstanding initial binding energy but due to its non-polar nature and the proximity of the plasma membrane, it directly migrated to the lipid bilayer of plasma membrane. The same as the simulations carried out in grid 1, in Figure 34, we can see the evolution of the binding energies of the tested compounds throughout molecular dynamics simulation. ZINC35877687 (PREG) and ZINC08221225 (LUT), show the highest binding energy in the beginning of the simulation (-250 kJ/mol), then ZINC95099267 (ARO) (-230 kJ/mol) and last ZINC95099369 (SUG) (-200 kJ/mol). The binding energy of LUT drops before reaching 4 ns of simulations. The binding energy of the other three compounds fluctuates during the course of the simulation, and even if the decrease of the binding-energy values remains moderate, they are lower than the initial ones. These data reflect that the biding capacity of these compounds in the entry site of the pore is not satisfactory inhibition purposes.
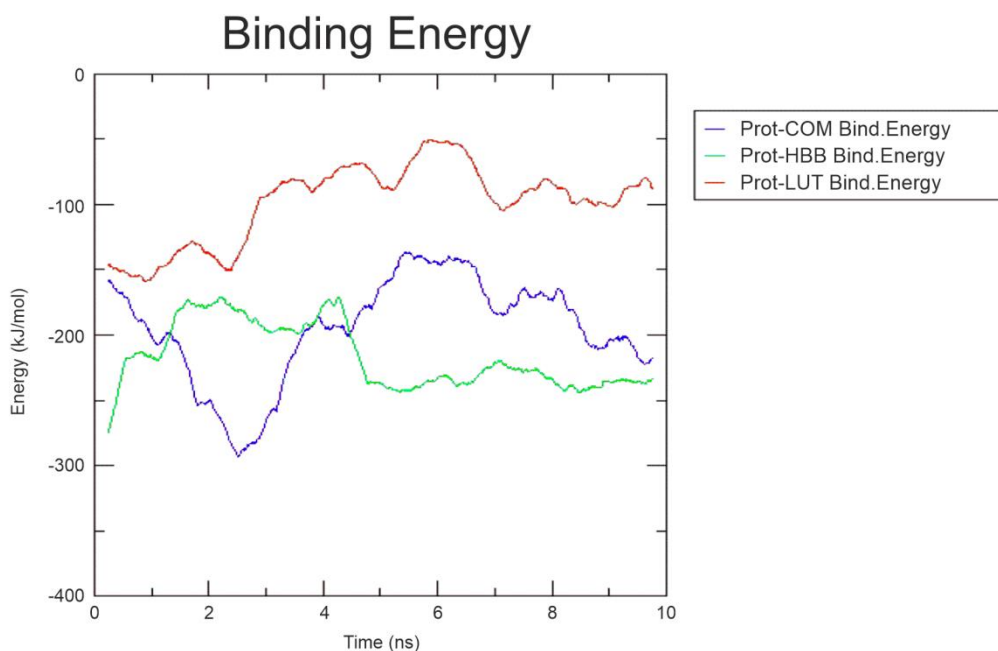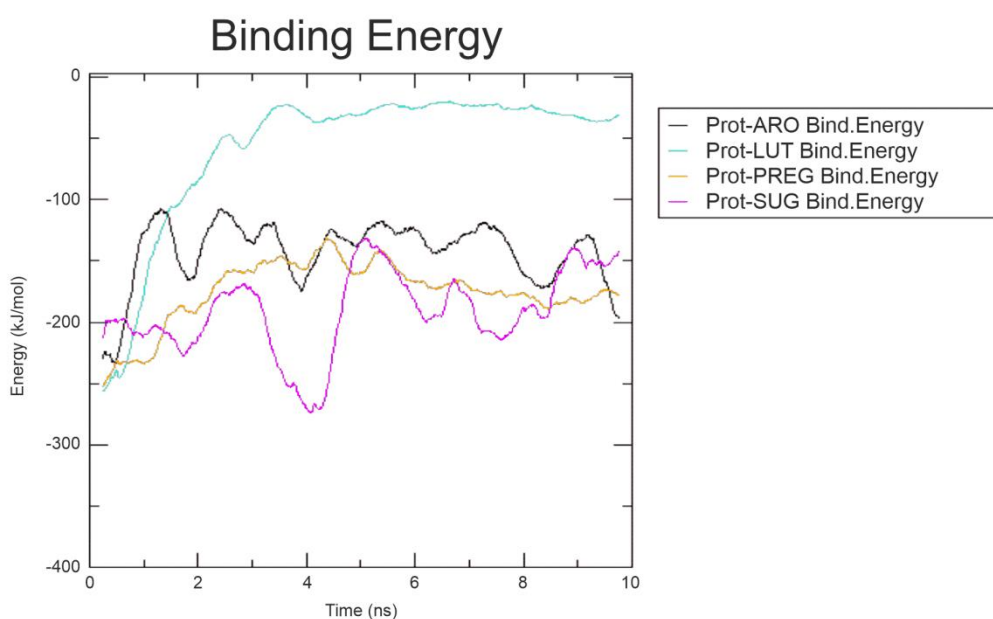

Figure 34: Graph showing the development of the protein-molecule binding energy throughout the course of molecular dynamics simulation. ZINC95099267 is shown in black (ARO), ZINC95099369 in pink (SUG), ZINC35877687 in yellow (PREG) and ZINC08221225 in light blue (LUT).

III. Molecular Modelling Approach to Screen for AnCrpA Inhibitors

The molecular dynamics simulations results in grid 2, the entrance of the pore, are not sufficient to justify continued efforts in their study. All tested compounds were displaced from the initial binding site and the binding poses are notably changed after the simulation time, the RMSD graphs show a substantial difference when the compound is bound to the AnCrpA-membrane complex, the binding energy values are low in comparison to required standards and they are not stable during molecular dynamics simulation. All this data together supports the interpretation that these compounds do not form a stable complex with the protein and thus they are not good candidates to achieve AnCrpA inhibition. The main reason could be that the template model was crystallized in the E2P conformation. This means the transmembrane pore is closed in the intracellular side, the docking site, and opened in the extracellular area, making it more difficult to access the residues of the pore from the intracellular side.

Out of these experiments the best results were obtained in grid 1, the catalytic site. HBB showed the most satisfactory results in terms of binding energy, RMSD profile and stability in the binding grid. However, is not a commercially available compound and it would have to be synthesized. COMP1 was the second best match. Even though the overall results of the compound were not as adequate as HBB, the fact that it is a commercially available compound, makes it a candidate worth further testing.

In conclusion, with the work conducted under the supervision of Dr. Galeazzi we accomplished our objectives: first, we can state that a molecular modelling approach is valid to find inhibitory compounds for our copper detoxification P-type ATPase AnCrpA and second, the doctorate student has been introduced to Molecular Modelling.

Final Discussion

Final Discussion

Copper homeostasis in *A. nidulans* has been the overall subject of this study, with special focus on uptake and detoxification of the cation. An RNA-seq experiment comparing the transcriptome under copper toxicity to standard laboratory nutritional conditions provided the starting point of the investigation. The obtained results allowed for the identification of genes and biological processes involved in the response to copper toxicity. Moreover, reference to previous literature and sequence analysis tools helped identify the genes involved in the copper homeostasis at different stages of the toxicity-response process, especially focusing on high-affinity uptake and detoxification.

The *A. nidulans* high-affinity copper uptake system shares similarities with counterparts in *Cryptococcus, Saccharomyces* and *A. fumigatus*. The uptake system is regulated by the transcription factor AnMac1 that exclusively controls the expression of copper uptake proteins. Plasma-membrane metalloreductases reduce environmental copper from Cu^{2+} to Cu^{+} (Cai *et al.,* 2019). Even though these elements have not been characterized, *A. nidulans* possesses nine putative plasma membrane reductases related to the *S. cerevisiae* metalloreductase family ScFre. Finally, two high-affinity copper transporters, one of which covers for the acquisition of copper under most environmental conditions (ScCtr3, CnCtr1 and AnCtrC) and the other specifically covers for in high copper-deficiency scenarios (ScCtr1, CnCtr4 and AnCtrA) (Antsotegi-Uskola *et al.*, 2020). Thus, our current understanding is that the high-affinity copper uptake system in fungi is conserved in the species so far examined*.*

Despite this apparent uniformity, there are specific aspects that need to be covered, such as details on the role of AnCtrB. According to the RNA-seq data obtained in this study, the expression of this gene is not significantly changed under copper toxicity conditions. In addition, there are some discrepancies on

<u>Final Discussion</u>

the regulation of different homologs of this protein. The first articles published in the *S. cerevisiae* homolog Ctr2 state that it is solely regulated by iron availability (Rees and Thiele, 2007); on the other hand, more recent articles report that the ScMac1 is involved in its regulation (Liu *et al.*, 2012;Qi *et al.*, 2012). Reports describing the *A. fumigatus* homolog AfCtrB claim that neither the environmental copper level nor the deletion of AfMac1 have any role in its regulation (Cai *et al.*, 2017;Kusuya *et al.*, 2017). Despite regulation controversies, the function of this protein is well specified in yeast as a copper transporter that mobilizes vacuolar copper to cytosolic copper chaperones (Balamurugan and Schaffner, 2006;Nevitt *et al.*, 2012;Smith *et al.*, 2017) and its single deletion makes no difference on colony development in high and low copper availability environments (Kampfenkel *et al.*, 1995). However, in filamentous fungi its function remains poorly understood and Cai and collaborators (2017) reported that deletion of AfCtrB renders the colony unable to develop, in high, regular and low copper availability conditions. Further work is necessary to accurately define AnCtrB function.

Some discrepancies on functional hierarchy of the Ctr proteins in the high-affinity copper uptake system have emerged in two different studies. Park and collaborators (2014) presented the first characterization of Ctr protein in *A. fumigatus* proposing that *AfctrA2* and *AfctrC* are functionally equivalent since individual deletion mutants exhibited a wild type–like phenotype with 100 µM BCS. On the other hand, Cai *et al.,* (2017) reported that the *Afctr*C deletion mutant showed defective colony morphology with 100 µM BCS, suggesting that this protein plays a dominant role in copper homeostasis. This thesis concludes that the lack of copper deficiency phenotype (in this case a secondary level) under mild copper deficiency conditions in a single deletion strain does not necessarily prove that any one of the Ctr proteins has a dominant role over the other(Page 67-68, Figure 10). The possibility still remains that one of the Ctr proteins may be more active under the tested conditions or that the other Ctr protein responds in more specific scenarios.

Copper addition reverted the defective phenotypes of the *Anctr* deletant strains, corroborating that the cause of the phenotypes was indeed copper deficiency. It is well known that copper and iron metabolism are closely related and a recent study in *A. fumigatus* has revealed that the TF Mac1, responsible for the regulation of the high-affinity copper uptake system, also plays a role in regulating iron homeostasis (Park *et al.*, 2018). Apparently, *Afmac1* deletion down-regulates the expression of siderophores and reductive iron transporters. Along with this, it has been described that iron can partially rescue the copper starvation phenotype generated by deletion of the TF *Afmac1* in *A. fumigatus* (Cai *et al.*, 2017). Usually, when the deletion of a transcription factor compromises the high-affinity uptake of a heavy metal, addition of this metal to the medium reverts or at least partially recovers the depletion phenotype via low-affinity transporters or other mechanisms. This is the case with the *A. nidulans* copper transporters and the *Anmac1* deletion phenotypes when copper is added (Cai *et al.*, 2019). However, in contrast to the *A. fumigatus Δmac1* phenotype, the *A. nidulans Δmac1* copper depletion phenotype (very similar to the double knock-out strain shown in Figure 10C, page 67-68) shows no recovery when iron is supplemented to the medium (not shown). The high-affinity iron uptake systems present substantial differences (Blatzer *et al.*, 2011;Eisendle *et al.*, 2003;Schrettl *et al.*, 2004) between these two organisms. Whether the regulation of iron uptake differs between *A. fumigatus* and *A. nidulans* remains to be investigated.

A common feature of AnCtrA that raised attention was the number of TM domains predicted by the TMHMM topology prediction software (Page 64, Figure 9B). These predictions need to be corroborated, but similar models have been documented for *A. fumigatus* and *C. neoformans* Ctr proteins (Park *et al.*, 2014;Waterman *et al.*, 2012). If these predictions were confirmed, it would imply that the oligomerization mechanism may differ from the one described by De Feo and collaborators (2012). Instead of a trimer with nine combined trans-membrane domains, the oligomer of Ctr monomers with an even number of

Final Discussion

Final Discussion

trans-membrane domains would always possess an even number of trans-membrane domains probably altering the oligomer formation.

Finally, our attempt to characterize the putative copper uptake shutdown mechanism of the AnCtr proteins had an unexpected outcome. Our C-terminal mutations did not have any effect on copper susceptibility; the only effect we were able to record was reduced copper uptake capacity as secondary level copper limitation effects were observed in mutant strains (Page 77, Figure 13B). Based on the observed results, we postulate that, in the conditions tested, the cysteines object of study and the C-terminal do not act as copper uptake modulators but they have a role in copper transport. The secondary level copper limitation effect, the yellow pigmentation, is most likely due to an impaired AnYA laccase function that correlates with an insufficient copper supply, as laccases are copper dependent enzymes (Hermann *et al.*, 1983;Scherer and Fischer, 2001). Considering the distal localization of this motif it is rather difficult for it to participate in transmembrane copper mobilization. The key for the copper deficiency phenotype might be that, mutating the di-cysteine motif or deleting the C-terminal might be taking away the linker for interaction between the Ctr protein and the chaperone as it has been described in human and yeast (Kahra *et al.*, 2016;Xiao and Wedd, 2002). Thus, the distribution effected by the chaperone route might be blocked or substantially altered, with the corresponding phenotypic manifestation of copper deficiency.

Following the Ctr protein regulation mechanism in *A. nidulans*, it is clear that the C-terminal deletion does not exert an impact on copper susceptibility, so it would be reasonable to consider whether there is any regulation mechanism at all that blocks or controls transmembrane copper traffic in the event of a copper fluctuation in the environment, since the only known mechanism relies solely on the C-terminal (Clifford *et al.*, 2016;Schuller *et al.*, 2013;Wu *et al.*, 2009).

In contrast with the conservation of the copper uptake system in fungi, resistance to copper appears to be achieved by two alternative mechanisms. The first mechanism is through metallothioneins. These cysteine-rich small proteins chelate free copper ions of the cytosol in organisms like *S. cerevisiae* and *C. neoformans* (Balamurugan and Schaffner, 2006;Ding *et al.*, 2013b;Nevitt *et al.*, 2012;Smith *et al.*, 2017). The second mechanism relies on heavy metal pumping P_{IB}-type ATPases. These heavy metal pumps extrude copper ions from the cytosol to the extracellular space in organisms like, *A. nidulans*, *A. fumigatus* and *C. albicans* (Antsotegi-Uskola *et al.*, 2017;Riggle and Kumamoto, 2000;Weissman *et al.*, 2000;Wiemann *et al.*, 2017). This divergence in metal detoxification mechanism by different fungal species may be the result of an adaptation to their respective ecological niches. *S. cerevisiae* has been isolated from a range of environments (Goddard and Greig, 2015), many of which are specific, such as fruits and flowers. In contrast, *C. albicans*, like most filamentous fungi, is an all-rounder found in environments ranging from the digestive tracts of animals to soils, where competition and antagonism are common. In these environments, P_{IB}-ATPase (CaCrp1p) mediated copper export confers superior tolerance in comparison to MTs, despite the greater cost in energy required to produce it and operate it. MTs, on the other hand, may allow for the immobilization of greater amounts of copper, as a resource, in media which may be especially poor in copper, such as flower nectar. In the same medium and growing conditions, *S. cerevisiae* is able to grow in up to 2 mM of $CuSO_4$, whereas *C. albicans* tolerates 20 mM of $CuSO_4$ (Weissman *et al.*, 2000).

The synthesis time of metallothioneins versus the P-type ATPases favours the metallothioneins. Actually the ScCup1 metallothionein synthesis time is almost half of AnCrpA. ScCup1 synthesis is clearly detectable 10 min after 100 µM $CuSO_4$ addition and by 25 min, the expression level is outstanding (Pena *et al.*, 1998). Thus, the reason behind P-type ATPases providing a superior tolerance is not an earlier reaction time, which leaves two different possibilities: firstly, that the amount of synthesized P-type ATPases outscores the metallothioneins and thus

Final Discussion

they confer a higher resistance; or secondly, that the strategy of pumping copper out is simply more effective against copper toxicity than the buffering strategy.

In this study, a single metallothionein coding gene was identified in *A. nidulans*, but its contribution to heavy metal toxicity resistance was not demonstrated. In the conditions tested, (Cu, Cd and Ag) the presence of the metallothionein did not confer resistance to heavy metal toxicity. In an article published by Cai and collaborators (2018), the authors found that the of AnCrdA homolog in *A. fumigatus* contributed minimally to Cu tolerance when AfAce1 and AfCrpA were both mutated and AfCrdA was overexpressed. Thus, CrdA contribution in laboratory conditions, where the organism is well accommodated, appears rather low or negligible. However, it might make a difference in the natural environment, where every resistance mechanism counts, as a second mechanism over the pump, for example.

Throughout this investigation, the obtained results were compared to data obtained by Wiemann and collaborators (2017) in *A. fumigatus*. This led to the realization that the level copper toxicity induced determined the characteristics of the response. This opened the possibility to envisage the existence of a multilevel resistance mechanism in Aspergilli. The first level of copper toxicity response would involve copper detoxification through P_{IB}-type ATPase CrpA. As described in this study, the fungus activates a rapid and intense expression of AnCrpA and the metallothionein AnCrdA at 100 μM $CuSO_4$. However, the expression is transient and the RNA-seq data indicate that other defense mechanisms like ROS neutralization are not activated, purportedly signaling that no uncontrolled ROS are intracellularly detected. The second level copper toxicity response would be the one described in *A. fumigatus* by Wienmann and collaborators (2017) at 200 μM $CuSO_4$. This would involve not only the activation of CrpA and CrdA but also the up-regulation of all the ROS neutralization machinery, catalase and superoxide dismutase. Having such and multilevel copper toxicity response would be an efficient system capable of deploying the

required cellular mechanisms to the level of toxicity encountered by the organism. This proposal would require experimental validation through experimentation at different copper toxicity levels, to verify the activation of the different response levels.

Finally, AnCrpA is clearly the principal copper detoxification agent in *A. nidulans*; however, AnCrpA is not exclusively activated by copper. Other studies have corroborated that the P-type ATPase CrpA and the TF AceA, also contribute to other heavy metal resistance, such as zinc in *A. fumigatus*. Thus, the P-type ATPase CrpA has versatile detoxification role as described in other organisms (Mandal *et al.*, 2002;Odermatt *et al.*, 1994).

This study started at the time when only a single publication was available about the copper homeostasis system in filamentous fungi. At the time of its final presentation, several contributions provide evidence to propose a preliminary model to describe the state of the cell in regular environmental conditions.

The average copper concentration in soil according to a study conducted in United States (Agency for Toxic Substances & Disease Registry, 2004) is about 50 parts per million (ppm) parts soil. According to the Geochemical Mapping of Agricultural and Grazing Land Soil in Europe (GEMAS) project that analyzed thousands of soil samples across Europe, the mean copper value was 20 ppm parts soil (Ballabio *et al.*, 2018). Analyzing these figures it seems that copper is generally available in sufficient concentration for a proper maintenance of life; however, the soil is the living niche for thousands or organisms that co-exist in the environment and have to compete for the available resources. Thus, high-affinity uptake mechanisms would be a consequence of such competition.

In this condition, the TF regulating *AnctrA* and *AnctrC* expression*,* AnMac1 would actively bind to their promoters, enabling transcription*,* as well as that of the plasma-membrane metalloreductase *AnfreC* (at least *AnfreC* and most likely

Final Discussion

other Fre protein coding genes). In this "regular" environmental situation one would expect a mild copper deficiency situation. Thus, *AnctrC* transcription would likely be very active and *AnctrA* transcription would be barely active. The plasma-membrane metalloreductases and the copper transporters would be located in the plasma-membrane to make sure that copper is internalized to the cell. Once the copper is internalized to the cell the copper chaperones AN6045, AN1390 and AN4863 would bind the internalized copper. These chaperones perform a double function: First, they bind the incoming ion preventing possible deleterious effects due to uncontrolled copper accumulation in the cytosol. Second, they are responsible for copper delivery within the cell. By homology based predictions we infer that: AN6045, homolog of the ScCcs1, would be responsible for copper delivery to the Cu/Zn Superoxide Dismutase AnSodA; AN1390, homolog of ScAtx1, would deliver copper to the P-type ATPase AnYgA responsible for delivery into the trans-Golgi network; AN4863, homolog of the ScCox17, would deliver copper to the cytochrome oxidase complex at the inner membrane of mitochondria (Balamurugan and Schaffner, 2006;Nevitt *et al.*, 2012;Smith *et al.*, 2017). Finally, the copper reservoir in the vacuoles also plays a role in a copper store management under scarcity conditions. Although the role of vacuolar AnCtrB is not yet fully understood, based on the literature it may be inferred that it may be actively pumping copper from within the vacuolar copper reservoir to supplement external copper import deficit (Figure 35).
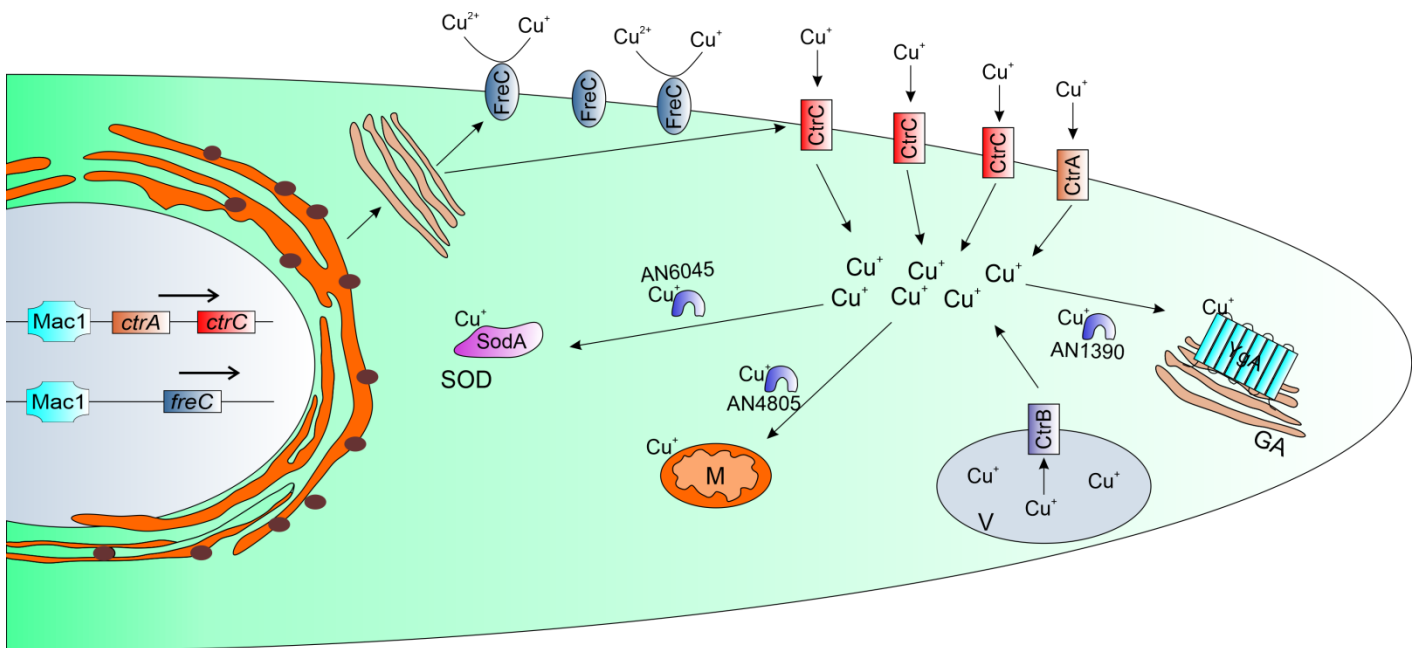
Figure 35: Copper homeostasis system model for environmental copper concentration in *A. nidulans*. TF Mac1 binds DNA enabling the transcription of the Ctr protein coding genes and Fre protein coding genes (in this case only *freC* is shown). These proteins will migrate to the plasma-membrane through the secretory pathway and stablish the high-affinity copper uptake complex constituted by copper reducing metalloreductases and high-affinity copper transporters. The internalized copper will be received by the different copper chaperones and distributed to their corresponding locations. AN6045, homolog of the ScCcs1, would be responsible for copper delivery to the Cu/Zn Superoxide Dismutase (Sod) AnSodA; AN1390, homolog of ScAtx1, would deliver copper to the P-type ATPase AnYgA responsible of copper delivery into the secretory compartments of the Golgi Apparatus (GA) for copper loading onto copper-requiring proteins; AN4863, homolog of the ScCox17, would deliver copper to the cytochrome oxidase complex at the inner membrane of mitochondria (M). Finally, the copper reservoir of the vacuole (V) will also contribute to fulfill the copper requirements of the organism.

As exposed throughout this thesis, the gratuitously abundant use of copper to combat fungal disease in modern agriculture has left a notable environmental footprint with imminent consequences like soil and aquifer contamination. When copper is applied in excess it can bind to organic material and other compounds, like clay or sand, and remain in the top layer of soil. On the other hand, when copper is dissolved in water it is carried in solution as free copper or bound to

<u>Final Discussion</u>

suspended particles and it can reach ground waters, riverbeds, lakes and estuaries (Agency for Toxic Substances & Disease Registry, 2004).

Moreover, copper-tolerances from the disease-causing strains have also been documented to steadily increase, making it clear that copper based antimicrobial preparations need a thorough reassessment.

Thus, the formulation of new antifungal preparations with lower copper doses has become an issue of growing importance to regulatory authorities. Different approaches to tackle the challenge of copper dose reduction have emerged in the recent years and one of the most notable ones is the encapsulation in nanoparticles. Metallic nanomaterials (silver, gold, copper and titanium) exhibit specific characteristics that result in enhanced antimicrobial activity (Vimbela *et al.*, 2017). Micron-size particles allow for the control of parameters such as density, malleability, stability and reactivity which make a significant difference to antimicrobial activity. Field studies in different environments with copper nanoparticles have been reported satisfactory results against bacteria and fungi (Carvalho *et al.*, 2019;Hermida-Montero *et al.*, 2019;Ingle and Rai, 2017;Munoz-Escobar and Reyes-Lopez, 2020). Thus, the application of copper in nanoscale format is a promising strategy and it could become a viable solution against multidrug resistant bacteria and fungi for surface treatment or medical purposes. However, the use of copper nanoparticles in agriculture may entail prohibitive manufacturing costs in comparison with traditional dissolved copper salt applications.

A different method to enhance copper toxicity could be the use of co-formulants that exert a synergistic interaction with copper. This strategy has been successfully used to fight antibiotic-resistant bacteria in the clinical field (Gomara and Ramon-Garcia, 2019;Rozenbaum *et al.*, 2019;Wittekind and Schuch, 2016;Zerweck *et al.*, 2017). We believe that finding a synergistic counterpart for

copper is plausible now that we have more knowledge about the copper homeostasis system in filamentous fungi.

We ourselves favored this second option and this was the reason for the visit to Dr. Galeazzi's laboratory was first proposed. It was proposed as to proof the concept that molecular modelling principles and techniques could be applied to find inhibitory compounds for certain elements of the copper homeostasis system. This would make the search of a synergistic counterpart for copper much easier because it can be done by a computational approach and then the candidates can be verified experimentally.

With AnCrpA we proved that this approach is valid by testing two compounds, ZINC95099399 and COMP1, as potential AnCrpA inhibitors. The objective of inhibiting AnCrpA is to deactivate the *A. nidulans* main copper detoxification mechanism that is also present in many phytopathogens (Antsotegi-Uskola *et al.*, 2017). We hypothesize that by doing this the necessary amount to kill the organism would be notably lower.

Apart from AnCrpA, there are some other possible targets that by inhibiting or modulating their activity could potentiate the toxic effect of copper. For example, copper chaperones can be an interesting target. According to some investigations in ScCtr1 and hCtr1 proteins (Kahra *et al.*, 2016;Xiao and Wedd, 2002), the copper chaperones receive copper ions directly from the Ctr proteins C-terminal avoiding the threat of free copper ions in the cytosol. By inhibiting or blocking the copper delivering chaperones we can create an opening to maximize the impact of free copper ions entered to the cell.

Another strategy to maximize copper damage would be to target the TFs controlling the copper homeostasis system. Out of the two TF the most interesting would be AnAce1, the one controlling the copper detoxification system (Antsotegi-Uskola *et al.*, 2017). ScAceA1 studies show that this TF has a

Final Discussion

cysteine-rich copper binding domain denominated the "DNA Binding Domain" that binds four copper ions forming a tetra-copper-thiolate cluster (Cai *et al.*, 2018;Smith *et al.*, 2017). The formation of this cluster triggers a conformational change that enables DNA binding and thus, the transcription of the whole copper detoxification machinery. This domain is largely conserved in *Aspergilli spp.* and other genera like *Botrytis*, *Magnaporthe* and *Fusarium*. A compound that would form a stable complex with AnAce1 would be likely to prevent DNA binding of the TF and thus the copper detoxification machinery would not be activated, maximizing the damage of internalized copper ions.

Finally, another hypothetical option would be related to the as yet undemonstrated Ctr copper uptake protein shutdown mechanism. In case there is such mechanism it could be a good possibility to exploit this avenue. By delaying the copper uptake shutdown the toxic effect of the copper present in the antifungal formulations would be increased. This approach would first require a full characterization of the Ctr protein regulation mechanism.

The development of resistance to copper by fungal strains has been long documented (Cervantes & Gutierrez-Corona, 1994; Ashida, 1965). Copper resistance in fungi is achieved by metal trapping by cell-wall components, altered copper uptake, extracellular chelation or precipitation by secreted metabolites, intracellular copper chelation by metallothioneins or phytochelatins; and finally intracellular copper extrusion by P-type ATPases (Antsotegi-Uskola *et al.*, 2017;Cervantes and Gutierrez-Corona, 1994;Kovacec *et al.*, 2017;Wiemann *et al.*, 2017). It has been reported that copper-resistant *S. cerevisiae* strains possess multiple ScCup1 metallothionein coding gene copies while regular copper-sensitive strains bear a single copy (Cervantes and Gutierrez-Corona, 1994). However, taking it to agriculture, where copper-resistant phytopathogens are a real problem, the cause or causes of these resistances remain unclear. Judet-Correia and collaborators (2011) documented the MIC (Minimal Inhibitory Concentration) values of two *Botrytis cinerea* strains demonstrating that some

isolates of these molds can develop resistance. Following the *S. cerevisiae* example it might be that these copper-resistant phytopathogens possess more than one copy of the AnCrpA homolog as documented in *Aspergillus* species (Yang *et al.*, 2018). Otherwise it could be an overall improvement of all above commented defense mechanisms that confers these strains an unusual capacity to resist copper. Whatever the case is, it would be a key point to know the source of these resistances in order to find the right target.

While this thesis was ongoing, apart from our contributions in the model organism *A. nidulans,* there have been some contributions in the pathogenic fungus *A. fumigatus,* but many details remain to be uncovered. Considering the repercussion of copper homeostasis on fungal biology, it is a topic worth studying in more depth and a wider range of species. The copper uptake and detoxification mechanisms and their respective transcription factors have been the focus of recent publications (Antsotegi-Uskola *et al.*, 2017;Antsotegi-Uskola *et al.*, 2020;Cai *et al.*, 2019;Cai *et al.*, 2017;Kusuya *et al.*, 2017;Park *et al.*, 2017;Park *et al.*, 2014;Wiemann *et al.*, 2017), identifying the principal participants of each process, but the copper buffering and intracellular distribution mechanisms remain practically unknown. Phylogenetic analyses have revealed the presence of proteins that act as copper scavenging and trafficking vehicles in other organisms (Ding *et al.*, 2014), but so far, those proteins have not been investigated. This evidence calls for further investigation covering intracellular copper trafficking and storage in oncoming years.

Conclusions

Conclusions

The main conclusions extracted from this work are the following:

- Three proteins involved in copper homeostasis have been identified in *Aspergillus nidulans*: a P_{IB}-type ATPase, AnCrpA, and two copper transporter (Ctr) proteins, AnCtrA and AnCtrC.

- AnCtrA and AnCtrC are copper transporting proteins taking part in the high-affinity copper uptake system. AnCtrC covers copper uptake for nutritional requirements and AnCtrA is more important in high copper deficiency scenarios; however, the two proteins work in a complementary manner.

- AnCrpA is the major copper resistance determinant in *A. nidulans* and is expressed tightly and transiently in the presence of high copper levels.

- AnAceA is a TF which regulates copper tolerance key elements. Besides activating *AncrpA* expression, regulates an additional element which has a minor role in copper detoxification process that has not been yet identified.

- The molecular modelling approach is suitable to find AnCrpA inhibitors. ZINC95099399 and COMP1 showed the most satisfactory results. These compounds have to be tested experimentally.

References

References

Abe,F. and Hiraki,T. (2009). Mechanistic role of ergosterol in membrane rigidity and cycloheximide resistance in Saccharomyces cerevisiae. Biochim. Biophys. Acta *1788*, 743-752.

Adams,T.H., Wieser,J.K., and Yu,J.H. (1998). Asexual sporulation in Aspergillus nidulans. Microbiol. Mol. Biol. Rev. *62*, 35-54.

Agency for Toxic Substances & Disease Registry (2004). Public Health Statement. In: Toxicological Profile for Copper.

Alkan,N. and Fortes,A.M. (2015). Insights into molecular and metabolic events associated with fruit response to post-harvest fungal pathogens. Front Plant Sci. *6*, 889.

Alvarez,F.J., Douglas,L.M., and Konopka,J.B. (2007). Sterol-rich plasma membrane domains in fungi. Eukaryot. Cell *6*, 755-763.

Andersson,M., Mattle,D., Sitsel,O., Klymchuk,T., Nielsen,A.M., Moller,L.B., White,S.H., Nissen,P., and Gourdon,P. (2014). Copper-transporting P-type ATPases use a unique ion-release pathway. Nat. Struct. Mol. Biol. *21*, 43-48.

Antsotegi-Uskola,M., Markina-Inarrairaegui,A., and Ugalde,U. (2017). Copper Resistance in Aspergillus nidulans Relies on the PI-Type ATPase CrpA, Regulated by the Transcription Factor AceA. Front Microbiol. *8*, 912.

Antsotegi-Uskola,M., Markina-Inarrairaegui,A., and Ugalde,U. (2020). Copper Homeostasis in Aspergillus nidulans Involves Coordinated Transporter Function, Expression and Cellular Dynamics. Front Microbiol. *11*, 555306.

Aramayo,R. and Timberlake,W.E. (1990). Sequence and molecular structure of the Aspergillus nidulans yA (laccase I) gene. Nucleic Acids Res. *18*, 3415.

Balamurugan,K. and Schaffner,W. (2006). Copper homeostasis in eukaryotes: teetering on a tightrope. Biochim. Biophys. Acta *1763*, 737-746.

Ballabio,C., Panagos,P., Lugato,E., Huang,J.H., Orgiazzi,A., Jones,A., Fernandez-Ugalde,O., Borrelli,P., and Montanarella,L. (2018). Copper distribution in European topsoils: An assessment based on LUCAS soil survey. Sci. Total Environ. *636*, 282-298.

Ballou,E.R. and Wilson,D. (2016). The roles of zinc and copper sensing in fungal pathogenesis. Curr. Opin. Microbiol. *32*, 128-134.

Barry,A.N., Shinde,U., and Lutsenko,S. (2010). Structural organization of human Cu-transporting ATPases: learning from building blocks. J. Biol. Inorg. Chem. *15*, 47-59.

Bastmeyer,M., Deising,H.B., and Bechinger,C. (2002). Force exertion in fungal infection. Annu. Rev. Biophys. Biomol. Struct. *31*, 321-341.

References

Bayram,O. and Braus,G.H. (2012). Coordination of secondary metabolism and development in fungi: the velvet family of regulatory proteins. FEMS Microbiol. Rev. *36*, 1-24.

Bergen,L.G. and Morris,N.R. (1983). Kinetics of the nuclear division cycle of Aspergillus nidulans. J. Bacteriol. *156*, 155-160.

Bertinato,J. and L'Abbe,M.R. (2004). Maintaining copper homeostasis: regulation of copper-trafficking proteins in response to copper deficiency or overload. J. Nutr. Biochem. *15*, 316-322.

Besold,A.N., Culbertson,E.M., and Culotta,V.C. (2016). The Yin and Yang of copper during infection. J. Biol. Inorg. Chem. *21*, 137-144.

Blatzer,M., Binder,U., and Haas,H. (2011). The metalloreductase FreB is involved in adaptation of Aspergillus fumigatus to iron starvation. Fungal. Genet. Biol. *48*, 1027-1033.

Blatzer,M. and Latge,J.P. (2017). Metal-homeostasis in the pathobiology of the opportunistic human fungal pathogen Aspergillus fumigatus. Curr. Opin. Microbiol. *40*, 152-159.

Blindauer,C.A. and Leszczyszyn,O.I. (2010). Metallothioneins: unparalleled diversity in structures and functions for metal ion homeostasis and more. Nat. Prod. Rep. *27*, 720-741.

Bokor,E., Amon,J., Keisham,K., Karacsony,Z., Vagvolgyi,C., and Hamari,Z. (2019). HMGB proteins are required for sexual development in Aspergillus nidulans. PLoS. One. *14*, e0216094.

Brown,G.D., Denning,D.W., Gow,N.A., Levitz,S.M., Netea,M.G., and White,T.C. (2012). Hidden killers: human fungal infections. Sci. Transl. Med. *4*, 165rv13.

Caddick,M.X., Brownlee,A.G., and Arst,H.N., Jr. (1986). Regulation of gene expression by pH of the growth medium in Aspergillus nidulans. Mol. Gen. Genet. *203*, 346-353.

Cai,Z., Du,W., Liu,L., Pan,D., and Lu,L. (2019). Molecular Characteristics of the Conserved Aspergillus nidulans Transcription Factor Mac1 and Its Functions in Response to Copper Starvation. mSphere. *4*.

Cai,Z., Du,W., Zeng,Q., Long,N., Dai,C., and Lu,L. (2017). Cu-sensing transcription factor Mac1 coordinates with the Ctr transporter family to regulate Cu acquisition and virulence in Aspergillus fumigatus. Fungal. Genet. Biol. *107*, 31-43.

Cai,Z., Du,W., Zhang,Z., Guan,L., Zeng,Q., Chai,Y., Dai,C., and Lu,L. (2018). The Aspergillus fumigatus transcription factor AceA is involved not only in Cu but also in Zn detoxification through regulating transporters CrpA and ZrcA. Cell Microbiol. e12864.

Carvalho,R., Duman,K., Jones,J.B., and Paret,M.L. (2019). Bactericidal Activity of Copper-Zinc Hybrid Nanoparticles on Copper-Tolerant Xanthomonas perforans. Sci. Rep. *9*, 20124.

Cebollero,E. and Reggiori,F. (2009). Regulation of autophagy in yeast Saccharomyces cerevisiae. Biochim. Biophys. Acta *1793*, 1413-1421.

Cervantes,C. and Gutierrez-Corona,F. (1994). Copper resistance mechanisms in bacteria and fungi. FEMS Microbiol. Rev. *14*, 121-137.

Chang,M.W., Ayeni,C., Breuer,S., and Torbett,B.E. (2010). Virtual screening for HIV protease inhibitors: a comparison of AutoDock 4 and Vina. PLoS. One. *5*, e11955.

Church,G.M. and Gilbert,W. (1984). Genomic sequencing. Proc. Natl. Acad. Sci. U. S. A *81*, 1991-1995.

Clemens,S., Kim,E.J., Neumann,D., and Schroeder,J.I. (1999). Tolerance to toxic metals by a gene family of phytochelatin synthases from plants and yeast. EMBO J. *18*, 3325-3333.

Clifford,R.J., Maryon,E.B., and Kaplan,J.H. (2016). Dynamic internalization and recycling of a metal ion transporter: Cu homeostasis and CTR1, the human Cu(+) uptake system. J. Cell Sci. *129*, 1711-1721.

Clutterbuck,A.J. (1972). Absence of laccase from yellow-spored mutants of Aspergillus nidulans. J. Gen. Microbiol. *70*, 423-435.

Clutterbuck,A.J. (1990). The genetics of conidiophore pigmentation in Aspergillus nidulans. J. Gen. Microbiol. *136*, 1731-1738.

Cobbold,C., Ponnambalam,S., Francis,M.J., and Monaco,A.P. (2002). Novel membrane traffic steps regulate the exocytosis of the Menkes disease ATPase. Hum. Mol. Genet. *11*, 2855-2866.

Culotta,V.C., Howard,W.R., and Liu,X.F. (1994). CRS5 encodes a metallothionein-like protein in Saccharomyces cerevisiae. J. Biol. Chem. *269*, 25295-25302.

Dameron,C.T., Winge,D.R., George,G.N., Sansone,M., Hu,S., and Hamer,D. (1991). A copper-thiolate polynuclear cluster in the ACE1 transcription factor. Proc. Natl. Acad. Sci. U. S. A *88*, 6127-6131.

Dancis,A., Haile,D., Yuan,D.S., and Klausner,R.D. (1994). The Saccharomyces cerevisiae copper transport protein (Ctr1p). Biochemical characterization, regulation by copper, and physiologic role in copper uptake. J. Biol. Chem. *269*, 25660-25667.

Darrah,P.R., Tlalka,M., Ashford,A., Watkinson,S.C., and Fricker,M.D. (2006). The vacuole system is a significant intracellular pathway for longitudinal solute transport in basidiomycete fungi. Eukaryot. Cell *5*, 1111-1125.

De Feo,C.J., Aller,S.G., Siluvai,G.S., Blackburn,N.J., and Unger,V.M. (2009). Three-dimensional structure of the human copper transporter hCTR1. Proc. Natl. Acad. Sci. U. S. A *106*, 4237-4242.

References

Dietl,A.M., Amich,J., Leal,S., Beckmann,N., Binder,U., Beilhack,A., Pearlman,E., and Haas,H. (2016). Histidine biosynthesis plays a crucial role in metal homeostasis and virulence of Aspergillus fumigatus. Virulence. *7*, 465-476.

Ding,C., Festa,R.A., Chen,Y.L., Espart,A., Palacios,Ò., Espin,J., Capdevila,M., Atrian,S., Heitman,J., and Thiele,D.J. (2013a). Cryptococcus neoformans copper detoxification machinery is critical for fungal virulence. Cell Host. Microbe *13*, 265-276.

Ding,C., Festa,R.A., Chen,Y.L., Espart,A., Palacios,O., Espin,J., Capdevila,M., Atrian,S., Heitman,J., and Thiele,D.J. (2013b). Cryptococcus neoformans copper detoxification machinery is critical for fungal virulence. Cell Host. Microbe *13*, 265-276.

Ding,C., Festa,R.A., Sun,T.S., and Wang,Z.Y. (2014). Iron and copper as virulence modulators in human fungal pathogens. Mol. Microbiol. *93*, 10-23.

Doehlemann,G., Okmen,B., Zhu,W., and Sharon,A. (2017). Plant Pathogenic Fungi. Microbiol. Spectr. *5*.

Dong,K., Addinall,S.G., Lydall,D., and Rutherford,J.C. (2013). The yeast copper response is regulated by DNA damage. Mol. Cell Biol. *33*, 4041-4050.

Doonan,J.H. (1992). Cell division in Aspergillus. J. Cell Sci. *103 (Pt 3)*, 599-611.

Duan,Y. *et al.* (2003). A point-charge force field for molecular mechanics simulations of proteins based on condensed-phase quantum mechanical calculations. J. Comput. Chem. *24*, 1999-2012.

Ehrensberger,K.M. and Bird,A.J. (2011). Hammering out details: regulating metal levels in eukaryotes. Trends Biochem. Sci. *36*, 524-531.

Eisendle,M., Oberegger,H., Zadra,I., and Haas,H. (2003). The siderophore system is essential for viability of Aspergillus nidulans: functional analysis of two genes encoding l-ornithine N 5-monooxygenase (sidA) and a non-ribosomal peptide synthetase (sidC). Mol. Microbiol. *49*, 359-375.

Eisses,J.F. and Kaplan,J.H. (2002). Molecular characterization of hCTR1, the human copper uptake protein. J. Biol. Chem. *277*, 29162-29171.

Fridovich,I. (1983). Superoxide radical: an endogenous toxicant. Annu. Rev. Pharmacol. Toxicol. *23*, 239-257.

Frohner,I.E., Bourgeois,C., Yatsyk,K., Majer,O., and Kuchler,K. (2009). Candida albicans cell surface superoxide dismutases degrade host-derived reactive oxygen species to escape innate immune surveillance. Mol. Microbiol. *71*, 240-252.

Fu,D., Beeler,T.J., and Dunn,T.M. (1995). Sequence, mapping and disruption of CCC2, a gene that cross-complements the Ca(2+)-sensitive phenotype of csg1 mutants and encodes a P-type ATPase belonging to the Cu(2+)-ATPase subfamily. Yeast *11*, 283-292.

Galagan,J.E. *et al.* (2005). Sequencing of Aspergillus nidulans and comparative analysis with A. fumigatus and A. oryzae. Nature *438*, 1105-1115.

Galeazzi,R., Massaccesi,L., Piva,F., Principato,G., and Laudadio,E. (2014). Insights into the influence of 5-HT2c aminoacidic variants with the inhibitory action of serotonin inverse agonists and antagonists. J. Mol. Model. *20*, 2120.

García,S., Prado,M., Dégano,R., and Domínguez,A. (2002). A copper-responsive transcription factor, CRF1, mediates copper and cadmium resistance in Yarrowia lipolytica. J. Biol. Chem. *277*, 37359-37368.

Garcia-Santamarina,S. and Thiele,D.J. (2015). Copper at the Fungal Pathogen-Host Axis. J. Biol. Chem. *290*, 18945-18953.

Georgatsou,E., Mavrogiannis,L.A., Fragiadakis,G.S., and Alexandraki,D. (1997). The yeast Fre1p/Fre2p cupric reductases facilitate copper uptake and are regulated by the copper-modulated Mac1p activator. J. Biol. Chem. *272*, 13786-13792.

Gerwien,F., Skrahina,V., Kasper,L., Hube,B., and Brunke,S. (2018). Metals in fungal virulence. FEMS Microbiol. Rev. *42*.

Glass,N.L., Rasmussen,C., Roca,M.G., and Read,N.D. (2004). Hyphal homing, fusion and mycelial interconnectedness. Trends Microbiol. *12*, 135-141.

Goddard,M.R. and Greig,D. (2015). Saccharomyces cerevisiae: a nomadic yeast with no niche? FEMS Yeast Res. *15*.

Gomara,M. and Ramon-Garcia,S. (2019). The FICI paradigm: Correcting flaws in antimicrobial in vitro synergy screens at their inception. Biochem. Pharmacol. *163*, 299-307.

Guy,A.T., Piggot,T.J., and Khalid,S. (2012). Single-stranded DNA within nanopores: conformational dynamics and implications for sequencing; a molecular dynamics simulation study. Biophys. J. *103*, 1028-1036.

Hagiwara,D., Suzuki,S., Kamei,K., Gonoi,T., and Kawamoto,S. (2014). The role of AtfA and HOG MAPK pathway in stress tolerance in conidia of Aspergillus fumigatus. Fungal. Genet. Biol. *73*, 138-149.

Han,K.H. (2009). Molecular Genetics of Emericella nidulans Sexual Development. Mycobiology. *37*, 171-182.

Harris,S.D. and Momany,M. (2004). Polarity in filamentous fungi: moving beyond the yeast paradigm. Fungal. Genet. Biol. *41*, 391-400.

Harris,S.D., Read,N.D., Roberson,R.W., Shaw,B., Seiler,S., Plamann,M., and Momany,M. (2005). Polarisome meets spitzenkorper: microscopy, genetics, and genomics converge. Eukaryot. Cell *4*, 225-229.

Hermann,T.E., Kurtz,M.B., and Champe,S.P. (1983). Laccase localized in hulle cells and cleistothecial primordia of Aspergillus nidulans. J. Bacteriol. *154*, 955-964.

Hermida-Montero,L.A., Pariona,N., Mtz-Enriquez,A.I., Carrion,G., Paraguay-Delgado,F., and Rosas-Saito,G. (2019). Aqueous-phase synthesis of nanoparticles of copper/copper

References

oxides and their antifungal effect against Fusarium oxysporum. J. Hazard. Mater. *380*, 120850.

Herrero-García,E. Desarrollo asexual en *Aspergillus nidulans*: regulación molecular y celular de la actividad del bZIP FlbB. 2013.
Ref Type: Thesis/Dissertation

Hervás-Aguilar, A. and Peñalva, M.A. (2010). Endocytic machinery protein SlaB is dispensable for polarity establishment but necessary for polarity maintenance in hyphal tip cells of *Aspergillus nidulans*. Eukaryot Cell. *9*, 1504–1518.

Hess,B., Kutzner,C., van der Spoel,D., and Lindahl,E. (2008). GROMACS 4: Algorithms for Highly Efficient, Load-Balanced, and Scalable Molecular Simulation. J. Chem. Theory. Comput. *4*, 435-447.

Hickey,P.C., Jacobson,D., Read,N.D., and Glass,N.L. (2002). Live-cell imaging of vegetative hyphal fusion in Neurospora crassa. Fungal. Genet. Biol. *37*, 109-119.

Holdom,M.D., Hay,R.J., and Hamilton,A.J. (1996). The Cu,Zn superoxide dismutases of Aspergillus flavus, Aspergillus niger, Aspergillus nidulans, and Aspergillus terreus: purification and biochemical comparison with the Aspergillus fumigatus Cu,Zn superoxide dismutase. Infect. Immun. *64*, 3326-3332.

Hu,S., Furst,P., and Hamer,D. (1990). The DNA and Cu binding functions of ACE1 are interdigitated within a single domain. New Biol. *2*, 544-555.

Hubbard,M.A. and Kaminskyj,S.G.W. (2008). Rapid tip-directed movement of Golgi equivalents in growing Aspergillus nidulans hyphae suggests a mechanism for delivery of growth-related materials. Microbiology (Reading.) *154*, 1544-1553.

Inesi,G., Pilankatta,R., and Tadini-Buoninsegni,F. (2014). Biochemical characterization of P-type copper ATPases. Biochem. J. *463*, 167-176.

Ingle,A.P. and Rai,M. (2017). Copper nanoflowers as effective antifungal agents for plant pathogenic fungi. IET. Nanobiotechnol. *11*, 546-551.

Ito,H., Inouhe,M., Tohoyama,H., and Joho,M. (2007). Characteristics of copper tolerance in Yarrowia lipolytica. Biometals *20*, 773-780.

Jaghoori,M.M., Bleijlevens,B., and Olabarriaga,S.D. (2016). 1001 Ways to run AutoDock Vina for virtual screening. J. Comput. Aided Mol. Des *30*, 237-249.

Jahn,B., Boukhallouk,F., Lotz,J., Langfelder,K., Wanner,G., and Brakhage,A.A. (2000). Interaction of human phagocytes with pigmentless Aspergillus conidia. Infect. Immun. *68*, 3736-3739.

Jensen,L.T., Howard,W.R., Strain,J.J., Winge,D.R., and Culotta,V.C. (1996). Enhanced effectiveness of copper ion buffering by CUP1 metallothionein compared with CRS5 metallothionein in Saccharomyces cerevisiae. J. Biol. Chem. *271*, 18514-18519.

References

Jorgensen,W.L. (1998). Temperature dependence of TIP3P, SPC, and TIP4P water from NPT Monte Carlo simulations: seeking temperatures of maximum density. J. Comput. Chem. *19*, 1179-1186.

Judet-Correia,D., Charpentier,C., Bensoussan,M., and Dantigny,P. (2011). Modelling the inhibitory effect of copper sulfate on the growth of Penicillium expansum and Botrytis cinerea. Lett. Appl. Microbiol. *53*, 558-564.

Kahra,D., Kovermann,M., and Wittung-Stafshede,P. (2016). The C-Terminus of Human Copper Importer Ctr1 Acts as a Binding Site and Transfers Copper to Atox1. Biophys. J. *110*, 95-102.

Kampfenkel,K., Kushnir,S., Babiychuk,E., Inze,D., and Van,M.M. (1995). Molecular characterization of a putative Arabidopsis thaliana copper transporter and its yeast homologue. J. Biol. Chem. *270*, 28479-28486.

Keller,G., Bird,A., and Winge,D.R. (2005). Independent metalloregulation of Ace1 and Mac1 in Saccharomyces cerevisiae. Eukaryot. Cell *4*, 1863-1871.

Kikuma,T., Arioka,M., and Kitamoto,K. (2007). Autophagy during conidiation and conidial germination in filamentous fungi. Autophagy. *3*, 128-129.

Knight,S.A., Labbe,S., Kwon,L.F., Kosman,D.J., and Thiele,D.J. (1996). A widespread transposable element masks expression of a yeast copper transport gene. Genes Dev. *10*, 1917-1929.

Koga,T., Sakata,Y., and Terasaki,N. (2019). Accumulation and Analysis of Cuprous Ions in a Copper Sulfate Plating Solution. J. Vis. Exp.

Kovacec,E., Regvar,M., van Elteren,J.T., Arcon,I., Papp,T., Makovec,D., and Vogel-Mikus,K. (2017). Biotransformation of copper oxide nanoparticles by the pathogenic fungus Botrytis cinerea. Chemosphere *180*, 178-185.

Kusuya,Y., Hagiwara,D., Sakai,K., Yaguchi,T., Gonoi,T., and Takahashi,H. (2017). Transcription factor Afmac1 controls copper import machinery in Aspergillus fumigatus. Curr. Genet. *63*, 777-789.

Labbe,S., Zhu,Z., and Thiele,D.J. (1997). Copper-specific transcriptional repression of yeast genes encoding critical components in the copper transport pathway. J. Biol. Chem. *272*, 15951-15958.

Ladomersky,E. and Petris,M.J. (2015). Copper tolerance and virulence in bacteria. Metallomics. *7*, 957-964.

Lamichane,J.R., Osdaghi,E., Behlau,F., et al. (2018). Thirteen decades of antimicrobial copper compounds applied in agriculture. Agron. Sustain. Dev. *38*.

Lauwers,E., Erpapazoglou,Z., Haguenauer-Tsapis,R., and André,B. (2010). The ubiquitin code of yeast permease trafficking. Trends Cell Biol. *20*, 196-204.

References

Lee,B.N. and Adams,T.H. (1994). Overexpression of flbA, an early regulator of Aspergillus asexual sporulation, leads to activation of brlA and premature initiation of development. Mol. Microbiol. *14*, 323-334.

Lee,J., Pena,M.M., Nose,Y., and Thiele,D.J. (2002). Biochemical characterization of the human copper transporter Ctr1. J. Biol. Chem. *277*, 4380-4387.

Lekeux,G. *et al.* (2018). di-Cysteine motifs in the C-terminus of plant HMA4 proteins confer nanomolar affinity for zinc and are essential for HMA4 function in vivo. J. Exp. Bot. *69*, 5547-5560.

Levitin,A. and Whiteway,M. (2007). The effect of prostaglandin E2 on transcriptional responses of Candida albicans. Microbiol. Res. *162*, 201-210.

Li,C., Li,Y., and Ding,C. (2019). The Role of Copper Homeostasis at the Host-Pathogen Axis: From Bacteria to Fungi. Int. J. Mol. Sci. *20*.

Lin,S.J. and Culotta,V.C. (1995). The ATX1 gene of Saccharomyces cerevisiae encodes a small metal homeostasis factor that protects cells against reactive oxygen toxicity. Proc. Natl. Acad. Sci. U. S. A *92*, 3784-3788.

Liu,J., Sitaram,A., and Burd,C.G. (2007). Regulation of copper-dependent endocytosis and vacuolar degradation of the yeast copper transporter, Ctr1p, by the Rsp5 ubiquitin ligase. Traffic. *8*, 1375-1384.

Liu,L., Qi,J., Yang,Z., Peng,L., and Li,C. (2012). Low-affinity copper transporter CTR2 is regulated by copper-sensing transcription factor Mac1p in Saccharomyces cerevisiae. Biochem. Biophys. Res. Commun. *420*, 600-604.

Liu,X.D. and Thiele,D.J. (1997). Yeast metallothionein gene expression in response to metals and oxidative stress. Methods *11*, 289-299.

Lopez-Cruz,J., Oscar,C.S., Emma,F.C., Pilar,G.A., and Carmen,G.B. (2017). Absence of Cu-Zn superoxide dismutase BCSOD1 reduces Botrytis cinerea virulence in Arabidopsis and tomato plants, revealing interplay among reactive oxygen species, callose and signalling pathways. Mol. Plant Pathol. *18*, 16-31.

Lutsenko,S. (2010). Human copper homeostasis: a network of interconnected pathways. Curr. Opin. Chem. Biol. *14*, 211-217.

Lutsenko,S., Barnes,N.L., Bartee,M.Y., and Dmitriev,O.Y. (2007). Function and regulation of human copper-transporting ATPases. Physiol Rev. *87*, 1011-1046.

Mackie,J., Szabo,E.K., Urgast,D.S., Ballou,E.R., Childers,D.S., MacCallum,D.M., Feldmann,J., and Brown,A.J. (2016). Host-Imposed Copper Poisoning Impacts Fungal Micronutrient Acquisition during Systemic Candida albicans Infections. PLoS. One. *11*, e0158683.

Macomber,L. and Imlay,J.A. (2009). The iron-sulfur clusters of dehydratases are primary intracellular targets of copper toxicity. Proc. Natl. Acad. Sci. U. S. A *106*, 8344-8349.

Mandal,A.K., Cheung,W.D., and Argüello,J.M. (2002). Characterization of a thermophilic P-type Ag+/Cu+-ATPase from the extremophile Archaeoglobus fulgidus. J. Biol. Chem. *277*, 7201-7208.

Mangiaterra,G., Laudadio,E., Cometti,M., et al. (2017). Inhibitors of multidrug efflux pumps of Pseudomonas aeruginosa from natural sources: An in silico high-throughput virtual screening and in vitro validation. Med. Chem. Res. *26*, 414-430.

Markina-Inarrairaegui,A., Pantazopoulou,A., Espeso,E.A., and Penalva,M.A. (2013). The Aspergillus nidulans peripheral ER: disorganization by ER stress and persistence during mitosis. PLoS. One. *8*, e67154.

Marvin,M.E., Mason,R.P., and Cashmore,A.M. (2004). The CaCTR1 gene is required for high-affinity iron uptake and is transcriptionally controlled by a copper-sensing transactivator encoded by CaMAC1. Microbiology *150*, 2197-2208.

Mattle,D., Sitsel,O., Autzen,H.E., Meloni,G., Gourdon,P., and Nissen,P. (2013). On allosteric modulation of P-type Cu(+)-ATPases. J. Mol. Biol. *425*, 2299-2308.

Matts,R.L., Schatz,J.R., Hurst,R., and Kagen,R. (1991). Toxic heavy metal ions activate the heme-regulated eukaryotic initiation factor-2 alpha kinase by inhibiting the capacity of hemin-supplemented reticulocyte lysates to reduce disulfide bonds. J. Biol. Chem. *266*, 12695-12702.

Mendoza-Cózatl,D., Loza-Tavera,H., Hernández-Navarro,A., and Moreno-Sanchéz,R. (2005). Sulfur assimilation and glutathione metabolism under cadmium stress in yeast, protists and plants. FEMS Microbiol. Rev. *29*, 653-671.

Mendoza-Cózatl,D.G. *et al.* (2010). Tonoplast-localized Abc2 transporter mediates phytochelatin accumulation in vacuoles and confers cadmium tolerance. J. Biol. Chem. *285*, 40416-40426.

Migocka,M. (2015). Copper-transporting ATPases: The evolutionarily conserved machineries for balancing copper in living systems. IUBMB. Life *67*, 737-745.

Mohamadi,G., Richard,N.G., Guida,W.C., Liskamp,R., Lipton,M., Caufield,C., Chang,G., Hendrickson,T., and Still,W.C. (1990). MacroModel - an integrated software system for modeling organic and bioorganic molecules using molecular mechanics. J. Comput. Chem. *11*, 440-467.

Momany,M. (2002). Polarity in filamentous fungi: establishment, maintenance and new axes. Curr. Opin. Microbiol. *5*, 580-585.

Morris,G.M., Goodsell,D.S., Halliday,R.S., Huey,R., Hart,W.E., Belew,R.K., and Olson,A.J. (1998). Automated docking using a Lamarckian genetic algorithm and an empirical binding free energy function. J. Comput. Chem. *19*, 1639-1662.

Morris,G.M., Huey,R., Lindstrom,W., Sanner,M.F., Belew,R.K., Goodsell,D.S., and Olson,A.J. (2009). AutoDock4 and AutoDockTools4: Automated docking with selective receptor flexibility. J. Comput. Chem. *30*, 2785-2791.

References

Munoz-Escobar,A. and Reyes-Lopez,S.Y. (2020). Antifungal susceptibility of Candida species to copper oxide nanoparticles on polycaprolactone fibers (PCL-CuONPs). PLoS. One. *15*, e0228864.

Narasipura,S.D., Chaturvedi,V., and Chaturvedi,S. (2005). Characterization of Cryptococcus neoformans variety gattii SOD2 reveals distinct roles of the two superoxide dismutases in fungal biology and virulence. Mol. Microbiol. *55*, 1782-1800.

Nayak,T., Szewczyk,E., Oakley,C.E., Osmani,A., Ukil,L., Murray,S.L., Hynes,M.J., Osmani,S.A., and Oakley,B.R. (2006). A versatile and efficient gene-targeting system for Aspergillus nidulans. Genetics *172*, 1557-1566.

Nevitt,T., Ohrvik,H., and Thiele,D.J. (2012). Charting the travels of copper in eukaryotes from yeast to mammals. Biochim. Biophys. Acta *1823*, 1580-1593.

Odermatt,A., Krapf,R., and Solioz,M. (1994). Induction of the putative copper ATPases, CopA and CopB, of Enterococcus hirae by Ag+ and Cu2+, and Ag+ extrusion by CopB. Biochem. Biophys. Res. Commun. *202*, 44-48.

Palmgren,M.G. and Nissen,P. (2011). P-type ATPases. Annu. Rev. Biophys. *40*, 243-266.

Palmiter,R.D. (1998). The elusive function of metallothioneins. Proc. Natl. Acad. Sci. U. S. A *95*, 8428-8430.

Pantazopoulou,A. (2016). The Golgi apparatus: insights from filamentous fungi. Mycologia. *108*, 603-622.

Pantazopoulou,A. and Diallinas,G. (2007). Fungal nucleobase transporters. FEMS Microbiol. Rev. *31*, 657-675.

Pantazopoulou,A., Lemuh,N.D., Hatzinikolaou,D.G., Drevet,C., Cecchetto,G., Scazzocchio,C., and Diallinas,G. (2007). Differential physiological and developmental expression of the UapA and AzgA purine transporters in Aspergillus nidulans. Fungal. Genet. Biol. *44*, 627-640.

Pantazopoulou,A. and Penalva,M.A. (2009). Organization and dynamics of the Aspergillus nidulans Golgi during apical extension and mitosis. Mol. Biol. Cell *20*, 4335-4347.

Park,Y.S., Kang,S., Seo,H., and Yun,C.W. (2018). A copper transcription factor, AfMac1, regulates both iron and copper homeostasis in the opportunistic fungal pathogen Aspergillus fumigatus. Biochem. J. *475*, 2831-2845.

Park,Y.S., Kim,J.H., Cho,J.H., Chang,H.I., Kim,S.W., Paik,H.D., Kang,C.W., Kim,T.H., Sung,H.C., and Yun,C.W. (2007). Physical and functional interaction of FgFtr1-FgFet1 and FgFtr2-FgFet2 is required for iron uptake in Fusarium graminearum. Biochem. J. *408*, 97-104.

Park,Y.S., Kim,T.H., and Yun,C.W. (2017). Functional characterization of the copper transcription factor AfMac1 from Aspergillus fumigatus. Biochem. J. *474*, 2365-2378.

Park,Y.S., Lian,H., Chang,M., Kang,C.M., and Yun,C.W. (2014). Identification of high-affinity copper transporters in Aspergillus fumigatus. Fungal. Genet. Biol. *73*, 29-38.

Pase,L., Voskoboinik,I., Greenough,M., and Camakaris,J. (2004). Copper stimulates trafficking of a distinct pool of the Menkes copper ATPase (ATP7A) to the plasma membrane and diverts it into a rapid recycling pool. Biochem. J. *378*, 1031-1037.

Peña,M.M., Koch,K.A., and Thiele,D.J. (1998). Dynamic regulation of copper uptake and detoxification genes in Saccharomyces cerevisiae. Mol. Cell Biol. *18*, 2514-2523.

Pena,M.M., Koch,K.A., and Thiele,D.J. (1998). Dynamic regulation of copper uptake and detoxification genes in Saccharomyces cerevisiae. Mol. Cell Biol. *18*, 2514-2523.

Pena,M.M., Lee,J., and Thiele,D.J. (1999). A delicate balance: homeostatic control of copper uptake and distribution. J. Nutr. *129*, 1251-1260.

Pena,M.M., Puig,S., and Thiele,D.J. (2000). Characterization of the Saccharomyces cerevisiae high affinity copper transporter Ctr3. J. Biol. Chem. *275*, 33244-33251.

Penalva,M.A. (2005). Tracing the endocytic pathway of Aspergillus nidulans with FM4-64. Fungal. Genet. Biol. *42*, 963-975.

Petris,M.J. (2004). The SLC31 (Ctr) copper transporter family. Pflugers Arch. *447*, 752-755.

Petris,M.J., Mercer,J.F., Culvenor,J.G., Lockhart,P., Gleeson,P.A., and Camakaris,J. (1996). Ligand-regulated transport of the Menkes copper P-type ATPase efflux pump from the Golgi apparatus to the plasma membrane: a novel mechanism of regulated trafficking. EMBO J. *15*, 6084-6095.

Pettersen,E.F., Goddard,T.D., Huang,C.C., Couch,G.S., Greenblatt,D.M., Meng,E.C., and Ferrin,T.E. (2004). UCSF Chimera--a visualization system for exploratory research and analysis. J. Comput. Chem. *25*, 1605-1612.

Pihet,M., Vandeputte,P., Tronchin,G., Renier,G., Saulnier,P., Georgeault,S., Mallet,R., Chabasse,D., Symoens,F., and Bouchara,J.P. (2009). Melanin is an essential component for the integrity of the cell wall of Aspergillus fumigatus conidia. BMC. Microbiol. *9*, 177.

Pollack,J.K., Harris,S.D., and Marten,M.R. (2009). Autophagy in filamentous fungi. Fungal. Genet. Biol. *46*, 1-8.

PONTECORVO,G., ROPER,J.A., HEMMONS,L.M., MACDONALD,K.D., and BUFTON,A.W. (1953). The genetics of Aspergillus nidulans. Adv. Genet. *5*, 141-238.

Puig,S., Lee,J., Lau,M., and Thiele,D.J. (2002). Biochemical and genetic analyses of yeast and human high affinity copper transporters suggest a conserved mechanism for copper uptake. J. Biol. Chem. *277*, 26021-26030.

Qi,J., Han,A., Yang,Z., and Li,C. (2012). Metal-sensing transcription factors Mac1p and Aft1p coordinately regulate vacuolar copper transporter CTR2 in Saccharomyces cerevisiae. Biochem. Biophys. Res. Commun. *423*, 424-428.

References

Rees,E.M., Lee,J., and Thiele,D.J. (2004). Mobilization of intracellular copper stores by the ctr2 vacuolar copper transporter. J. Biol. Chem. *279*, 54221-54229.

Rees,E.M. and Thiele,D.J. (2004). From aging to virulence: forging connections through the study of copper homeostasis in eukaryotic microorganisms. Curr. Opin. Microbiol. *7*, 175-184.

Rees,E.M. and Thiele,D.J. (2007). Identification of a vacuole-associated metalloreductase and its role in Ctr2-mediated intracellular copper mobilization. J. Biol. Chem. *282*, 21629-21638.

Richie,D.L. and Askew,D.S. (2008). Autophagy: a role in metal ion homeostasis? Autophagy. *4*, 115-117.

Richie,D.L., Fuller,K.K., Fortwendel,J., Miley,M.D., McCarthy,J.W., Feldmesser,M., Rhodes,J.C., and Askew,D.S. (2007). Unexpected link between metal ion deficiency and autophagy in Aspergillus fumigatus. Eukaryot. Cell *6*, 2437-2447.

Riggle,P.J. and Kumamoto,C.A. (2000). Role of a Candida albicans P1-type ATPase in resistance to copper and silver ion toxicity. J. Bacteriol. *182*, 4899-4905.

Riha,M., Karlickova,J., Filipsky,T., Macakova,K., Hrdina,R., and Mladenka,P. (2013). Novel method for rapid copper chelation assessment confirmed low affinity of D-penicillamine for copper in comparison with trientine and 8-hydroxyquinolines. J. Inorg. Biochem. *123*, 80-87.

Riquelme,M., Fischer,R., and Bartnicki-Garcia,S. (2003). Apical growth and mitosis are independent processes in Aspergillus nidulans. Protoplasma *222*, 211-215.

Rizvi,S.M., Shakil,S., and Haneef,M. (2013). A simple click by click protocol to perform docking: AutoDock 4.2 made easy for non-bioinformaticians. EXCLI. J. *12*, 831-857.

Rodrigues,M.L. (2018). The Multifunctional Fungal Ergosterol. MBio. *9*.

Rosenzweig,A.C. and Argüello,J.M. (2012). Toward a molecular understanding of metal transport by P(1B)-type ATPases. Curr. Top. Membr. *69*, 113-136.

Rozenbaum,R.T. *et al.* (2019). Antimicrobial synergy of monolaurin lipid nanocapsules with adsorbed antimicrobial peptides against Staphylococcus aureus biofilms in vitro is absent in vivo. J. Control Release *293*, 73-83.

Rutherford,J.C. and Bird,A.J. (2004). Metal-responsive transcription factors that regulate iron, zinc, and copper homeostasis in eukaryotic cells. Eukaryot. Cell *3*, 1-13.

Saitoh,Y., Izumitsu,K., Morita,A., and Tanaka,C. (2010). A copper-transporting ATPase BcCCC2 is necessary for pathogenicity of Botrytis cinerea. Mol. Genet. Genomics *284*, 33-43.

Samanovic,M.I., Ding,C., Thiele,D.J., and Darwin,K.H. (2012). Copper in microbial pathogenesis: meddling with the metal. Cell Host. Microbe *11*, 106-115.

Sambrook,J., Fritsch,E.F., and Maniatis,T. (1989). *Molecular Cloning: A Laboratory Manual*, Cold Spring Harbor Laboratory Press.

Sanner,M.F. (1999). Python: a programming language for software integration and development. J. Mol. Graph. Model. *17*, 57-61.

Santo,C.E., Morais,P.V., and Grass,G. (2010). Isolation and characterization of bacteria resistant to metallic copper surfaces. Appl. Environ. Microbiol. *76*, 1341-1348.

Scherer,M. and Fischer,R. (2001). Molecular characterization of a blue-copper laccase, TILA, of Aspergillus nidulans. FEMS Microbiol. Lett. *199*, 207-213.

Scherer,M., Wei,H., Liese,R., and Fischer,R. (2002). Aspergillus nidulans catalase-peroxidase gene (cpeA) is transcriptionally induced during sexual development through the transcription factor StuA. Eukaryot. Cell *1*, 725-735.

Schrettl,M., Bignell,E., Kragl,C., Joechl,C., Rogers,T., Arst,H.N., Jr., Haynes,K., and Haas,H. (2004). Siderophore biosynthesis but not reductive iron assimilation is essential for Aspergillus fumigatus virulence. J. Exp. Med. *200*, 1213-1219.

Schuller,A., Auffermann,G., Zoschke,K., Schmidt,U., Ostermann,K., and Rodel,G. (2013). Overexpression of ctr1Delta300, a high-affinity copper transporter with deletion of the cytosolic C-terminus in Saccharomyces cerevisiae under excess copper, leads to disruption of transition metal homeostasis and transcriptional remodelling of cellular processes. Yeast *30*, 201-218.

Scire,A., Baldassarre,M., Galeazzi,R., and Tanfani,F. (2013). Fibrillation properties of human alpha(1)-acid glycoprotein. Biochimie *95*, 158-166.

Shiraishi,E., Inouhe,M., Joho,M., and Tohoyama,H. (2000). The cadmium-resistant gene, CAD2, which is a mutated putative copper-transporter gene (PCA1), controls the intracellular cadmium-level in the yeast S. cerevisiae. Curr. Genet. *37*, 79-86.

Smith,A.D., Logeman,B.L., and Thiele,D.J. (2017). Copper Acquisition and Utilization in Fungi. Annu. Rev. Microbiol. *71*, 597-623.

Smith,N., Wei,W., Zhao,M., Qin,X., Seravalli,J., Kim,H., and Lee,J. (2016). Cadmium and Secondary Structure-dependent Function of a Degron in the Pca1p Cadmium Exporter. J. Biol. Chem. *291*, 12420-12431.

Solioz,M. and Odermatt,A. (1995). Copper and silver transport by CopB-ATPase in membrane vesicles of Enterococcus hirae. J. Biol. Chem. *270*, 9217-9221.

Staneviciene,I., Sadauskiene,I., Lesauskaite,V., Ivanoviene,L., Kasauskas,A., and Ivanov,L. (2008). Subacute effects of cadmium and zinc ions on protein synthesis and cell death in mouse liver. Medicina (Kaunas.) *44*, 131-138.

Sugui,J.A., Kim,H.S., Zarember,K.A., Chang,Y.C., Gallin,J.I., Nierman,W.C., and Kwon-Chung,K.J. (2008). Genes differentially expressed in conidia and hyphae of Aspergillus fumigatus upon exposure to human neutrophils. PLoS. One. *3*, e2655.

References

Suh,J.K., Poulsen,L.L., Ziegler,D.M., and Robertus,J.D. (2000). Redox regulation of yeast flavin-containing monooxygenase. Arch. Biochem. Biophys. *381*, 317-322.

Suite. (2011). MacroModel, Version 9.9. Schrödinger, LLC, New York, NY.

Sutherland,D.E. and Stillman,M.J. (2011). The "magic numbers" of metallothionein. Metallomics. *3*, 444-463.

Sutton,H.C. and Winterbourn,C.C. (1989). On the participation of higher oxidation states of iron and copper in Fenton reactions. Free Radic. Biol. Med. *6*, 53-60.

Suzuki,M. and Gitlin,J.D. (1999). Intracellular localization of the Menkes and Wilson's disease proteins and their role in intracellular copper transport. Pediatr. Int. *41*, 436-442.

Szewczyk,E., Nayak,T., Oakley,C.E., Edgerton,H., Xiong,Y., Taheri-Talesh,N., Osmani,S.A., and Oakley,B.R. (2006). Fusion PCR and gene targeting in Aspergillus nidulans. Nat. Protoc. *1*, 3111-3120.

Talbot,N.J. and Kershaw,M.J. (2009). The emerging role of autophagy in plant pathogen attack and host defence. Curr. Opin. Plant Biol. *12*, 444-450.

Thorsen,M., Perrone,G.G., Kristiansson,E., Traini,M., Ye,T., Dawes,I.W., Nerman,O., and Tamás,M.J. (2009). Genetic basis of arsenite and cadmium tolerance in Saccharomyces cerevisiae. BMC. Genomics *10*, 105.

Timberlake,W.E. (1990). Molecular genetics of Aspergillus development. Annu. Rev. Genet. *24*, 5-36.

Timoshnikov,V.A., Kobzeva,T., Selyutina,O.Y., Polyakov,N.E., and Kontoghiorghes,G.J. (2019). Effective inhibition of copper-catalyzed production of hydroxyl radicals by deferiprone. J. Biol. Inorg. Chem. *24*, 331-341.

Todd,R.B., Davis,M.A., and Hynes,M.J. (2007). Genetic manipulation of Aspergillus nidulans: heterokaryons and diploids for dominance, complementation and haploidization analyses. Nat. Protoc. *2*, 822-830.

Trott,O. and Olson,A.J. (2010). AutoDock Vina: improving the speed and accuracy of docking with a new scoring function, efficient optimization, and multithreading. J. Comput. Chem. *31*, 455-461.

Upadhyay,S., Torres,G., and Lin,X. (2013). Laccases involved in 1,8-dihydroxynaphthalene melanin biosynthesis in Aspergillus fumigatus are regulated by developmental factors and copper homeostasis. Eukaryot. Cell *12*, 1641-1652.

Valix,M., Tang,J.Y., and Malik,R. (2001). Heavy metal tolerance of fungi . Minerals engineering *14*, 499-505.

Vesely,E.M., Williams,R.B., Konopka,J.B., and Lorenz,M.C. (2017). N-Acetylglucosamine Metabolism Promotes Survival of Candida albicans in the Phagosome. mSphere. *2*.

Vimbela,G.V., Ngo,S.M., Fraze,C., Yang,L., and Stout,D.A. (2017). Antibacterial properties and toxicity from metallic nanomaterials. Int. J. Nanomedicine. *12*, 3941-3965.

Waterhouse,A. *et al.* (2018). SWISS-MODEL: homology modelling of protein structures and complexes. Nucleic Acids Res. *46*, W296-W303.

Waterman,S.R., Park,Y.D., Raja,M., Qiu,J., Hammoud,D.A., O'Halloran,T.V., and Williamson,P.R. (2012). Role of CTR4 in the Virulence of Cryptococcus neoformans. MBio. *3*.

Weissman,Z., Berdicevsky,I., Cavari,B.Z., and Kornitzer,D. (2000). The high copper tolerance of Candida albicans is mediated by a P-type ATPase. Proc. Natl. Acad. Sci. U. S. A *97*, 3520-3525.

Wiemann,P., Albermann,S., Niehaus,E.M., Studt,L., von Bargen,K.W., Brock,N.L., Humpf,H.U., Dickschat,J.S., and Tudzynski,B. (2012). The Sfp-type 4'-phosphopantetheinyl transferase Ppt1 of Fusarium fujikuroi controls development, secondary metabolism and pathogenicity. PLoS. One. *7*, e37519.

Wiemann,P. *et al.* (2017). Aspergillus fumigatus Copper Export Machinery and Reactive Oxygen Intermediate Defense Counter Host Copper-Mediated Oxidative Antimicrobial Offense. Cell Rep. *19*, 2174-2176.

Wittekind,M. and Schuch,R. (2016). Cell wall hydrolases and antibiotics: exploiting synergy to create efficacious new antimicrobial treatments. Curr. Opin. Microbiol. *33*, 18-24.

Wu,X., Sinani,D., Kim,H., and Lee,J. (2009). Copper transport activity of yeast Ctr1 is down-regulated via its C terminus in response to excess copper. J. Biol. Chem. *284*, 4112-4122.

Xiao,Z. and Wedd,A.G. (2002). A C-terminal domain of the membrane copper pump Ctr1 exchanges copper(I) with the copper chaperone Atx1. Chem. Commun. (Camb.) 588-589.

Yager,L.N. (1992). Early developmental events during asexual and sexual sporulation in Aspergillus nidulans. Biotechnology *23*, 19-41.

Yamaguchi-Iwai,Y., Serpe,M., Haile,D., Yang,W., Kosman,D.J., Klausner,R.D., and Dancis,A. (1997). Homeostatic regulation of copper uptake in yeast via direct binding of MAC1 protein to upstream regulatory sequences of FRE1 and CTR1. J. Biol. Chem. *272*, 17711-17718.

Yang,K., Shadkchan,Y., Tannous,J., Landero Figueroa,J.A., Wiemann,P., Osherov,N., Wang,S., and Keller,N.P. (2018). Contribution of ATPase copper transporters in animal but not plant virulence of the crossover pathogen Aspergillus flavus. Virulence. *9*, 1273-1286.

Yang,L., Ukil,L., Osmani,A., Nahm,F., Davies,J., De Souza,C.P., Dou,X., Perez-Balaguer,A., and Osmani,S.A. (2004). Rapid production of gene replacement constructs and

References

generation of a green fluorescent protein-tagged centromeric marker in Aspergillus nidulans. Eukaryot. Cell *3*, 1359-1362.

Yu,W., Farrell,R.A., Stillman,D.J., and Winge,D.R. (1996). Identification of SLF1 as a new copper homeostasis gene involved in copper sulfide mineralization in Saccharomyces cerevisiae. Mol. Cell Biol. *16*, 2464-2472.

Zamocky,M., Furtmuller,P.G., and Obinger,C. (2008). Evolution of catalases from bacteria to humans. Antioxid. Redox. Signal. *10*, 1527-1548.

Zekert,N. and Fischer,R. (2009). The Aspergillus nidulans kinesin-3 UncA motor moves vesicles along a subpopulation of microtubules. Mol. Biol. Cell *20*, 673-684.

Zerweck,J., Strandberg,E., Kukharenko,O., Reichert,J., Burck,J., Wadhwani,P., and Ulrich,A.S. (2017). Molecular mechanism of synergy between the antimicrobial peptides PGLa and magainin 2. Sci. Rep. *7*, 13153.

Zhang,P., Zhang,D., Zhao,X., Wei,D., Wang,Y., and Zhu,X. (2016). Effects of CTR4 deletion on virulence and stress response in Cryptococcus neoformans. Antonie Van Leeuwenhoek *109*, 1081-1090.

Zhou,H., Cadigan,K.M., and Thiele,D.J. (2003). A copper-regulated transporter required for copper acquisition, pigmentation, and specific stages of development in Drosophila melanogaster. J. Biol. Chem. *278*, 48210-48218.

Zhou,P., Szczypka,M.S., Sosinowski,T., and Thiele,D.J. (1992). Expression of a yeast metallothionein gene family is activated by a single metalloregulatory transcription factor. Mol. Cell Biol. *12*, 3766-3775.

Appendices

Copper Homeostasis in *Aspergillus nidulans* Involves Coordinated Transporter Function, Expression and Cellular Dynamics

Martzel Antsotegi-Uskola*, Ane Markina-Iñarrairaegui and Unai Ugalde

Microbial Biochemistry Laboratory, Department of Applied Chemistry, Faculty of Chemistry, University of the Basque Country, San Sebastian, Spain

Copper ion homeostasis involves a finely tuned and complex multi-level response system. This study expands on various aspects of the system in the model filamentous fungus *Aspergillus nidulans*. An RNA-seq screen in standard growth and copper toxicity conditions revealed expression changes in key copper response elements, providing an insight into their coordinated functions. The same study allowed for the deeper characterization of the two high-affinity copper transporters: AnCtrA and AnCtrC. In mild copper deficiency conditions, the null mutant of *AnctrC* resulted in secondary level copper limitation effects, while deletion of *AnctrA* resulted in primary level copper limitation effects under extreme copper scarcity conditions. Each transporter followed a characteristic expression and cellular localization pattern. Although both proteins partially localized at the plasma membrane, AnCtrC was visible at membranes that resembled the ER, whilst a substantial pool of AnCtrA accumulated in vesicular structures resembling endosomes. Altogether, our results support the view that AnCtrC plays a major role in covering the nutritional copper requirements and AnCtrA acts as a specific transporter for extreme copper deficiency scenarios.

Keywords: copper toxicity response, copper uptake, *Aspergillus nidulans*, copper homeostasis, copper transporters, Ctr, di-cysteine

INTRODUCTION

Copper (Cu) is an indispensable trace element for most living organisms. Its capacity to adopt an oxidized (Cu^{2+}) and a reduced (Cu^+) state is exploited by many enzymes to act as redox cofactor in enzyme catalyzed processes (Nevitt et al., 2012); cytochrome c, a key component of mitochondrial cellular respiration process; superoxide dismutase, for ROS neutralization; laccases, a protein family with great biotechnology implications which are involved in fungal pigment synthesis; and lysil oxidase for collagen maturation, for example (Scherer and Fischer, 2001; Lutsenko, 2010; Ding et al., 2011; Smith et al., 2017). However, free intracellular copper can interfere with red-ox processes generating reactive oxygen species (ROS) or cause metalloprotein dysfunction by displacement of other bound metal ions (Fridovich, 1983; Macomber and Imlay, 2009; Besold et al., 2016). Hence, all organisms have elaborate mechanisms that secure copper bioavailability, yet maintain free copper levels below the toxicity threshold.

They include copper uptake, intracellular traffic, storage, and detoxification processes (Balamurugan and Schaffner, 2006; Nevitt et al., 2012).

Homeostasis studies in *Saccharomyces cerevisiae*, first lead to the identification of genes responsible for Cu uptake, distribution to cellular compartments and detoxification (Culotta et al., 1994; Lin et al., 1997; Pena et al., 1998). An efficient copper uptake system has been proved to be critical to cover basic cellular needs of the cation. The expression of the high affinity Cu uptake system is transcriptionally regulated by a copper metalloregulatory transcription factor (CuMRTF) named ScMac1 (Labbe et al., 1997; Keller et al., 2005). In the absence of copper, ScMac1 is able to bind DNA, thereby activating the expression of the high affinity Cu uptake system. High Cu concentrations, in turn, result in ScMac1 inactivation (Zhu et al., 1998).

Copper is transported inside the cell by two high affinity copper transporter proteins (Ctr) localized at the plasma membrane, ScCtr1 and ScCtr3 (Pena et al., 2000). They are relatively small proteins that contain up to three transmembrane domains (TM) and show high copper specificity for reduced copper (Cu$^+$) (Puig et al., 2002; Petris, 2004). ScCtr1 has multiple Cu-binding methionines arranged in MxM or MxxM motifs (Mets motifs) in the extracellular N-terminal for facilitated copper import (Dancis et al., 1994). ScCtr3 on the other hand, has 11 cysteine residues, another Cu-binding ligand, throughout the sequence (Pena et al., 2000). The conserved M-xxx-M motif in the transmembrane domain is essential for copper ion translocation (Puig et al., 2002). In order to be internalized by Ctr proteins, environmental copper is reduced from Cu^{2+} to Cu$^+$ by cell surface metalloreductases ScFre1 and ScFre2 prior to uptake (Rees and Thiele, 2004; Rutherford and Bird, 2004). Cu$^+$ transport across membranes requires Ctr proteins to assemble as trimers and generate a pore in the plasma membrane (De Feo et al., 2009). Cu$^+$ transport by Ctr proteins does not require ATP hydrolysis (Lee et al., 2002), as Cu$^+$ enters the cell by a passive transport mechanism. Extracellular K$^+$ and the extremely low intracellular copper concentration facilitate copper import (Balamurugan and Schaffner, 2006). The knowledge gathered on these proteins has served as a reference for further studies.

The basic structural and functional features of Ctr proteins are highly conserved in fungi and this has enabled the identification of Ctr proteins in many species. For example, in *Cryptococcus neoformans*, an opportunistic pathogen responsible for meningoencephalitis in immunocompromised individuals, high affinity Cu uptake is achieved by two Ctr proteins, denominated CnCtr1 and CnCtr4. Strains defective in copper uptake show defective melanization and reduced virulence (Ding et al., 2011; Waterman et al., 2012; Zhang et al., 2016). Melanin is a recognized virulence factor in *C. neoformans* and the laccases involved in melanin biosynthesis require Cu$^+$ as a cofactor, thus copper acquisition from the host cell environment is necessary for virulence (Walton et al., 2005). Thus, besides its involvement in common cellular processes, the high affinity copper uptake has been proved to be a critical virulence factor in microbial pathogens.

For many years the study of the high affinity copper uptake system has been limited mostly to bacteria and yeast, while little was known about other organisms. However, in the last few years different manuscripts have been published in filamentous fungi. In *Aspergillus fumigatus*, a notorious opportunistic pathogen, the Ctr proteins AfCtrA2 and AfCtrC have been identified (Park et al., 2014). Studies also demonstrated that copper acquisition through the high affinity copper uptake machinery was critical for growth and conidiation in low Cu environments (Kusuya et al., 2017). As in many other pathogenic organisms, Cu uptake and virulence are also closely related in *A. fumigatus* (Cai et al., 2017). Expression of Ctr proteins is up-regulated when *A. fumigatus* conidia are challenged by human neutrophils (Sugui et al., 2008). Moreover, it has been reported that in the absence of the Ctr proteins *A. fumigatus* fails to grow in infected tissues (Cai et al., 2017), corroborating the importance of Ctr protein expression for virulence. While this research was ongoing Cai et al. (2019) published a paper describing the components of the copper uptake system in *A. nidulans*. This paper was mainly focused on the TF Mac1 and the presence of two copper transporter proteins termed, AnCtrA2 and AnCtrC, was reported.

The aim of this study was to gain insight on the effect of copper toxicity on gene expression, as well as to complement and expand the first characterization of the copper transport proteins by elucidating their role in general copper homeostasis in *Aspergillus nidulans*. For the first purpose, an RNA-seq experiment was performed which informed on gene expression changes in the most altered biological processes, structural components and molecular functions. For the second purpose, exhaustive functional analysis experiments permitted us to discern the individual roles of each Ctr protein in the copper uptake process. Apparently, AnCtrC plays a major role in high affinity copper uptake in mild copper deficiency conditions. Its deletion causes secondary level copper limitation effects like spore and pigmentation deficiencies, most likely due to Cu deficiency of the conidial laccase AnYA, which can be ascribed to limiting copper stores in the cells due to impaired copper uptake. On the other hand, AnCtrA prevails as the most effective copper uptake protein in conditions of more extreme copper deficiency. Its deletion causes primary copper limitation effects like growth limitation and lack of pigmentation. Nevertheless, individual deletion of either Ctr protein reveals that both function in a complementary manner. To further complement the characterization of the high affinity copper uptake system, a putative plasma membrane copper reductase is presented, AnFreC.

MATERIALS AND METHODS

Bioinformatics

Alignments were performed using the predicted protein sequences released in the National Centre for Biotechnology Information (NCBI) database. Multiple sequence alignments were performed and analyzed using Clustal Omega application in EBI[1]. Transmembrane domains were predicted using Hidden

---

[1]http://www.ebi.ac.uk/Tools/msa/clustalomega/

Markov Models (HMM) in the Institute Pasteur Mobyle server[2]. Phylogenetic analyses were carried out using the Molecular Evolutionary Genetics Analysis version 7 (MEGA 7) software[3].

Strains, Media and Growth Conditions

A list of all *Aspergillus nidulans* strains used in this study is presented in **Supplementary Table S1**. MAD1427 (wild-type, WT) strain was used to generate single and double knock-out and GFP-tagged strains. All colonies were grown in pH 6.8 buffered solid Aspergillus minimal medium (AMM) containing Käfer's trace elements (Kafer, 1965) 1% (w/v) D-glucose, 71 μM sodium nitrate and appropriately supplemented according to the procedure described in Pontecorvo et al. (1953). No agar was added to the medium for liquid AMM preparation. For low and high copper availability conditions, 100 μM bathocuproine disulfonic acid (BCS) Cu chelator and 100 μM $CuSO_4$ were added to AMM. For the oxidative stress condition, 2-methyl-1,4-naphthoquinone (menadione) was used. AMM media prepared with Käfer's trace elements contains 1.6 μM copper (copper-nutritional condition). For the 0 μM Cu AMM, copper was removed from the trace elements. Colony growth tests were carried out by inoculating conidiospores on solid AMM and incubating for 48 h at 37°C. Dry weight experiments were performed by inoculating conidiospores on liquid 0 μM Cu AMM, incubating for 16 h at 37°C.

Fungal growth tests were carried out in a 96-weel plate by inoculating 60 μl of a 1.10^6 spore/ml Tween 20 0.1% suspension on 160 μl liquid AMM or AMM + 100 μM BCS and incubating for 40 h at 37°C. For BCS addition after 16 h of incubation, the required volume was added from a 12.5 μM BCS solution. Measurements are averages of three biological replicates and three technical replicates of each condition. The error bars represent the standard deviation. OD_{600} was measured with an iMark^{TM} microplate absorbance reader (Bio-Rad).

To study the effect of gene deletion on conidia production, conidiospores of mutant strains were inoculated by point inoculation in solid AMM with and without 100 μM BCS. After incubation at 37°C for 3 days, colony diameter was measured using the Digimizer image analysis software. Thereafter, in order to collect the conidia, the agar including mycelia and produced spores was vortexed in 40 μL 0.2% Tween 20 solution for 3 min. Conidia were quantified using a hemocytometer. Four biological replicates and two technical replicates of each condition/strain were performed. Two-tailed Student's *t*-test for unpaired samples was used for the statistical analysis to compare quantitative counts of conidia (conidia/cm^2) between the WT and mutant strains.

Generation of Null and Tagged Strains

Deletion and C-terminally tagging cassettes were constructed following fusion-PCR technique described in Yang et al. (2004) and Markina-Inarrairaegui et al. (2011). Deletion cassettes were used for null mutant generation and contain the *Aspergillus fumigatus pyrG* or *riboB* selection marker which was amplified

using the plasmid p1439 (*pyrG^{Af}*) and p1548 (*riboB^{Af}*) as a template with oligonucleotides gsp2* and gsp3*. 1500 bp of the flanking 5′UTR and 3′UTR regions of the target gene were amplified from *A. nidulans* genomic DNA using specific primer pairs; gsp1-gsp2 (5′ UTR) and gsp3-gsp4 (3′ UTR). Hindsight, the fragments were fused using gsp1-gsp4 primers. The cassette for the generation of strains carrying C-terminally tagged fusion proteins were constructed as follow. The *gfp:riboB^{Af}* fragment from plasmid p1548 and *mrfp:pyrG^{Af}* fragment was amplified from plasmid p184 using oligonucleotides gsp6*-gsp3*. The 3′ end ($\sim$1500 bp) of the gene and the 3′UTR regions were amplified from gDNA using oligonucleotides gsp5-gsp6 and gsp3-gsp4, respectively. Finally, oligonucleotides gsp5 and gsp4 were used to fuse the fragments. Oligonucleotides used in this study are summarized in **Supplementary Table S2**.

The purified fused products were then used to transform *Aspergillus nidulans* MAD1427 recipient strain following the procedure detailed in Antsotegi-Uskola et al. (2017). *pyrG$^+$* and *riboB$^+$* transformants were isolated and single integration of construct was confirmed by Southern blot technique (**Supplementary Figure S1**). To generate the double knock-out, strains combining a deleted allele and C-terminally tagged expressing protein strain or a double tagged strain step-by-step transformation procedure was used with individual cassettes.

The strains carrying mutations in the last cysteines of the C-terminal domain, CtrC^{C213A,C214A} and AnCtrA^{C186A,C187A} were constructed as follows: For each gene two specific complementary primers were designed, carrying the necessary nucleotide modifications for cysteine modification. Two fragments were amplified using the GFP chimera of each gene as template; first fragment was gsp5-AAreverse and the second one AAforward-gsp4. Oligonucleotides gsp5 and gsp4 were used to fuse the fragments. In the case of the C-terminally truncated mutants, other two primers were designed for each gene. The C-reverse primer was placed upstream from the last amino-acid of interest and the *C-forward primer was placed in the next nucleotide of the stop codon of the gene (5′ tail complementary to the C-reverse primer). Using the GFP chimera of each gene as a template, two fragments were amplified gsp5-C-reverse and *C-forward-gsp4. Primers gsp5 and gsp4 were used for fragment fusion. The cysteine mutants and the C-terminal deletion strains were tested by sequencing.

RNA Isolation and RT-PCR Analysis

1.10^6 conidia/ml were inoculated into a two liter flask with air steam containing liquid AMM and incubated at 37°C for 16 h with magnetic stirring. RNA was extracted from cells harvested prior (0 min) and after transfer to fresh liquid AMM containing 100 μM BCS or 100 μM $CuSO_4$ for the indicated period. Mycelia was collected by filtration and ground in liquid nitrogen. Total RNA was isolated from one hundred milligrams of mycelia of three independent biological replicates using a RNA Isolation Kit, Nucleospin® RNA plant, following instructions from the manufacturer (Macherey-Nagel GmbH & Co. KG). The integrity of the RNA was examined by gel electrophoresis and concentration was calculated using a Nanodrop 2000c system

---

[2]http://mobyle.pasteur.fr/

[3]https://www.megasoftware.net/home

(Thermo Fisher Scientific, Waltham, MA, United States). First-strand cDNA of each sample was synthesized using the reverse transcriptase PrimeScript[TM] RT reagent Kit (Takara) and then cDNA was used for evaluating gene expression levels. Each cDNA sample was tested in duplicate. qPCR assays were performed in an ABI 7500 system according to the manufacturer's instructions (Applied Biosystems, Foster, CA) using 5x PyroTaq EvaGreen qPCR Mix Plus (CMB, Cultek Molecular Bioline). b*enA* was used as internal reference to normalize gene expression levels. The $2^{-\Delta CT}$ method was used to determine the relative expression level ratio. Oligonucleotides used in this assay are listed in **Supplementary Table S2**.

RNA-Seq

For the RNA-seq experiment 1:10 diluted supplemented AMM was used to grow MAD1427 strain. The transcriptome of vegetative hyphae grown for 16 h in liquid medium was compared with those cultured under identical conditions but shifted to 100 μM CuSO$_4$ medium (IC50 in 1:10 diluted media) 1 h before cell harvest. Three biological replicates were processed for each culture condition. RNA isolation, mRNA library construction, Illumina sequencing and data analysis was performed as described in Garzia et al. (2013). Briefly, total RNA was extracted based on TRIzol reagent (Invitrogen, Carlsbad, CA, United States), samples were purified using the RNeasy Mini Kit (QIAGEN, Valencia, CA, United States) and libraries were prepared following Illumina standard protocols (Illumina, San Diego, CA, United States). Sequencing was performed in a pair-end-read and 50-base mode on an Illumina HiSeq Sequencer running nine samples per lane (multiplexing). Sequences were demultiplexed and quality of reads was analyzed with FastQC v0.10.1. Reads with quality values higher than Q30 were introduced for mapping using CUTADAPT v1.2 and *Aspergillus nidulans* genome version s07-m02-r07 as the template[4]. TopHat version 2.0.6 was used for mapping reads and Cuffdiff version 2.0.2 to detect genes differentially expressed between different samples. For the determination of differentially expressed genes a *q*-value below 0.05 was used as a FDR threshold. RNA-seq results were visualized with CummeRbund version 1.99.2 software. Gene ontology (GO) terms for each *A. nidulans* gene were obtained from the *Aspergillus* genome database[5] and were related with terms downloaded from OBO[6]. The GO project provided a standardized set of terms describing the molecular functions of genes. We used the topGO software package from the Bioconductor project[7] to identify overrepresented GO terms from a set of differentially expressed genes. The Python programming language[8] was used to prepare the data, utilizing rpy2[9] to call R for the statistical analysis. The raw Illumina sequencing data were submitted to the NCBI

---

[4]http://www.aspergillusgenome.org/download/sequence/A_nidulans_FGSC_A4/archive/

[5]http://www.aspgd.org/download/go/gene_association.aspgd.gz

[6]http://www.geneontology.org/ontology/obo_format_1_2/gene_ontology_ext.obo

[7]http://www.bioconductor.org/packages/release/bioc/html/topGO.html

[8]http://www.python.org/

[9]http://rpy.sourceforge.net/rpy2.html

Sequence Read Archive (SRA) and deposited under Accession Number PRJNA623550.

Protein Isolation and Western Blot

1.10^6 conidia were inoculated in liquid AMM and incubated on a rotary shaker at 220 rpm and 37°C for 16 h. Cells were harvested (0 min), transferred to fresh liquid AMM followed by induction with 100 μM BCS and 100 μM CuSO$_4$ for the period indicated in the figures. Mycelia was collected, lyophilized for 16 h and ground in a minibeater. Protein samples were extracted by alkaline-lysis buffer (0.2 M NaOH, 0.2% β-mercaptoethanol), as described in Hervas-Aguilar and Penalva (2010).

Five micro liters of each protein sample were loaded into each well of 10% SDS-polyacrylamide gels and electrotransfered to Immun-Blot® PVDF membranes by TransBlot Turbo Transfer System (Bio-Rad). Ponceau S staining was used as a loading control (0.1% Ponceau S, 5% acetic acid). Ponceau staining was removed using a 20% acetonitrile, 200 μM NaOH solution. For Western blotting the following primary antibodies were used: monoclonal mouse anti-GFP antibody (1/5000; Roche). As secondary antibodies peroxidase-conjugated goat anti-mouse IgG immunoglobulin (1/4000 dilution; Jackson Immunoresearch Lab.) is used. Proteins were detected using Clarity[TM] Western ECL Substrate (Bio-Rad) in a Chemidoc + XRS system (Bio-Rad). Signal intensity was measured with Image Lab 3.0 software (Bio-Rad).

Fluorescence Microscopy

For localization of AnCtrA and AnCtrC, conidiospores of GFP-tagged strains were cultured in Ibidi μ-dishes, 35 μm high (Ibidi GmbH, Germany; 2 μl of medium per well) for 16 h at 30°C in liquid Aspergillus Minimal WATCH medium (Penalva, 2005) adequately supplemented and containing 0.1% D-glucose, 71 μM sodium nitrate, 25 μM sodium phosphate monobasic. For low copper availability conditions, 100 μM bathocuproine disulfonic acid (BCS) Cu chelator were added to the WATCH media.

Fluorescence microscopy was performed using a Zeiss Axio Observer Z1 inverted microscope (63 Plan Apochromat 1.4 oil immersion Lens) and Axiocam MRm Rev.3 camera. For observation of GFP, a filter set 38 HE (Ex BP 470/40; FT 495; Em BP 525/50) was used. The images shown are representative of at least five experiments repeats. Levels of fluorescence were analyzed using open source ImageJ software[10] (U. S. National Institutes of Health, Bethesda, MD, United States).

RESULTS

Gene Expression Analysis Under Copper Toxicity Conditions

An RNA-seq analysis was performed to compare the transcriptome of vegetative hyphae grown for 16 h in liquid medium (nutritional condition; acronym NC) with that of

---

[10]http://imagej.nih.gov/ij

a hyphae shifted to medium with 100 µM $CuSO_4$ -a high enough concentration to activate the copper toxicity response- (copper toxicity; acronym CT) 1 h before harvest. The reads of mRNAs expressed under NC and CT conditions mapped 87.4% and 89.7% of a total of 10,943 genes predicted by the AspGD, respectively. Fragments per kilobase of exon per million fragments mapped (FPKM) values for all predicted *A. nidulans* genes in each condition are shown in **Supplementary Table S3**. Based on the gene expression analysis criteria applied in this study ($\geq$2-fold change, *p*-value < 0.05) the expression of 13.7% (1494) of genes was modified between the two conditions: 7.3% (796) of the genes were up-regulated (higher transcript levels in CT than in NT), while 6.4% (698) were down-regulated. The copper toxicity response therefore

exhibited a balanced gene down-regulation and up-regulation rate (**Figure 1A**).

Table 1 shows the expression of most of the genes related to copper homeostasis, either characterized or predicted, and also some copper containing proteins. The TFs that orchestrate the copper homeostasis process, *AnaceA* and *Anmac1*, showed no significant variations in response to copper; however, the genes that code for copper mobilizing proteins, either uptake or detoxification, showed significant changes in their expression. The copper detoxification gene *AncrpA* was up-regulated in response to an external copper load. On the other hand, the already described Ctr protein coding genes *AnctrA* and *AnctrC* (elaborated on below) were significantly down-regulated under copper-toxicity condition; however, the putative Ctr protein

FIGURE 1 | Graphic representation of the RNA-seq results. **(A)** To exemplify the number of mapped genes in each condition, the 10.943 genes predicted by the AspGD were considered as 100% and data was presented in percentages. The differentially expressed genes are represented in the copper toxicity pie chart divided in two colors in proportion to the number of up-regulated and down-regulated genes. **(B)** Representation of the up-regulated and down-regulated genes of the most affected biological processes.
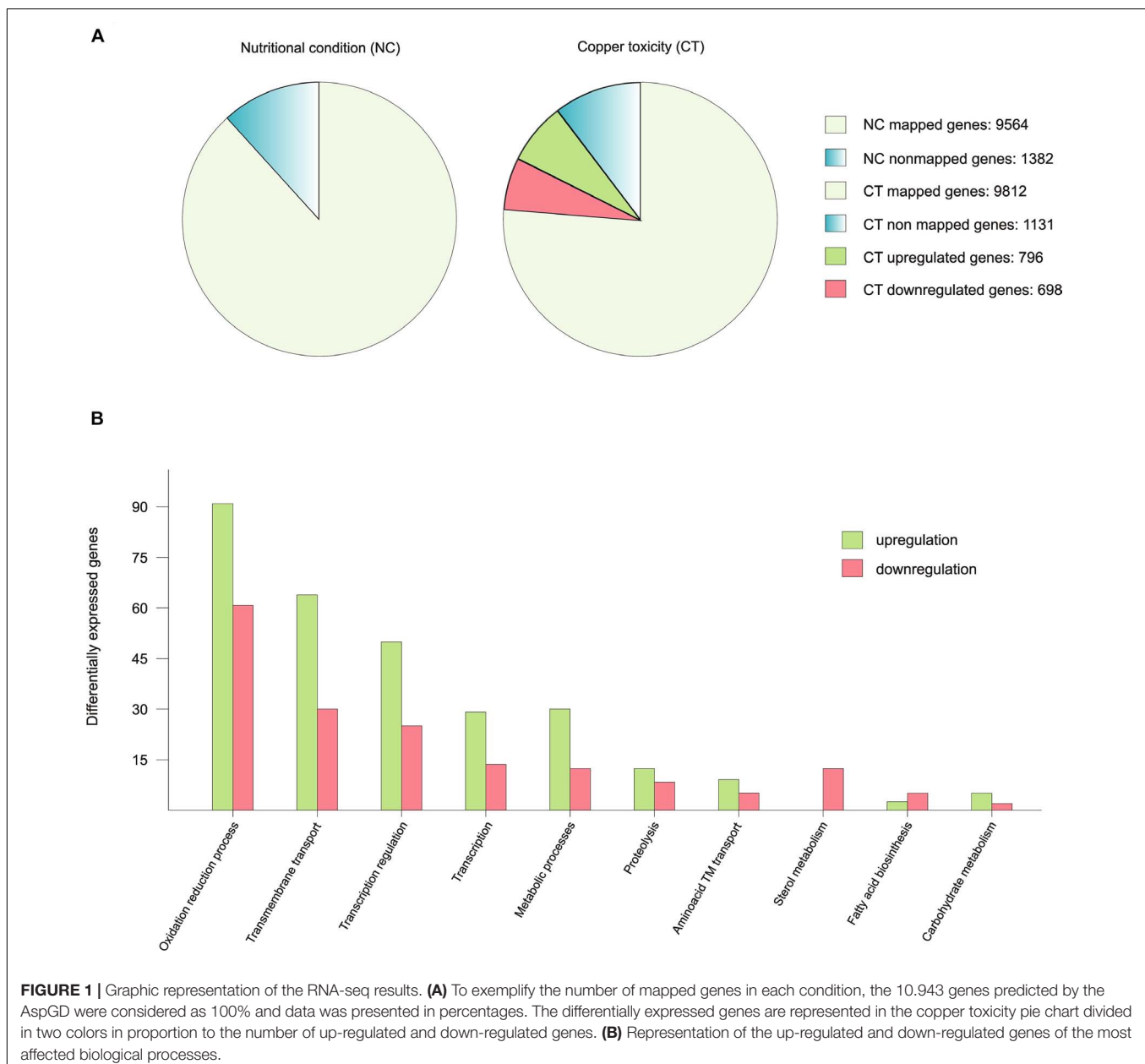
TABLE 1 | RNA-seq data of the copper homeostasis genes and the copper related protein coding genes.

Gene	Log2 fold change	Value_1	Value_2	*q*-Value	Significant	Description
AN1924	−0,554556	250,162	170,327	0,269576	No	*AnaceA*. Copper detoxification TF
AN0658	0,417535	20,518	27,4048	0,503204	No	*Anmac1*. Copper uptake TF
AN3117	6,4078	11,9725	1016,54	0	Yes	*AncrpA*. Copper-exporting P-type ATPase.
AN2934	−0,284851	71,0897	58,3523	0,686464	No	*AnctrB*. Copper ion transmembrane transporter activity.
AN3209	−4,18902	24,4975	1,34308	2,75E-08	Yes	*AnctrA*. High-affinity copper transporter
AN3813	−2,97333	134,667	17,1475	3,34E-12	Yes	*AnctrC*. High-affinity copper transporter.
AN3624	1,01501	20,1871	40,7964	0,015651	Yes	*AnygA*. ScCcc2 homolog. Predicted copper transporter.
AN6045	1,95069	76,4666	295,588	2,09E-07	Yes	Ccs1 SOD chaperone ortholog
AN1390	0,137135	110,504	121,523	0,853005	No	Atx1 chaperone homolog
AN4863	0,397399	78,3646	103,216	0,541532	No	Cox17 Cytochrome C oxidase chaperone homolog
AN7662	−1,11534	35,8567	16,5508	0,018818	Yes	*AnfreA*. Predicted iron metalloreductase
AN0773	−2,14409	114,6	25,9269	4,15E-08	Yes	Predicted metalloreductase
AN3208	−4,54749	14,5531	0,622335	2,56E-14	Yes	*AnfreC*. Predicted metalloreductase
AN0241	−0,342918	1361,11	1073,16	0,57373	No	*AnsodA*. Cu/Zn-superoxide dismutase
AN6635	−1,48008	4,56506	1,63643	0,034958	Yes	*AnyA*. Conidial laccase involved in green pigment production
AN6830	1,79e + 308	0	0,145851	1	No	*AnlccA*. Putative laccase
AN9170	0	0	0	1	No	*AnlccB*. Extracellular laccase
AN5379	−0,611597	0,055515	0,0363333	1	No	*AnlccC*. Extracellular laccase
AN0878	−1,92869	1,5301	0,401909	0,0384564	Yes	*AnlccD*. Extracellular laccase
AN0901	1,89527	6,9476	25,8445	6,10E-05	Yes	*AntilA*. Hyphal tip laccase

coding gene, *AnctrB* (elaborated on below), was unaltered. By homology searches the putative homologs of the *S. cerevisiae* Atx1, Cox17 and Ccs1 have been found. A very important element for proper copper uptake is the plasma membrane oxidoreductase that reduces copper prior to internalization. In this table we show a characterized metalloreductase, *AnfreA*, and two other predicted plasma membrane oxidoreductases AN0773 and *AnfreC* (elaborated on below) that are co-regulated with the Ctr proteins and thus, could be possible metalloreductase candidates. Finally, the expression of the intracellular copper trafficking P-type ATPase *AnygA* shows a significant up-regulation under excess copper conditions.

Besides copper homeostasis proteins, there are many other copper related proteins, as copper is a required cofactor of many enzymes (**Table 1**). The Cu/Zn superoxide dismutase *AnsodA* showed no difference in expression in response to the external copper load. On the other hand, laccases, a copper-containing enzyme-family required for melanin synthesis, displayed a divergent response: *AnyA* and *AnlccD* were down-regulated, while *AntilA* was up-regulated.

To interpret the biological significance of the registered changes in gene expression, we conducted a GO classification analysis of the results. The identified changes in gene expression occurring in response to toxic copper levels were indicative of modifications in various processes (**Figure 1B**). Red-ox processes were the most affected. Copper has a relatively high reduction potential ($E^o_0 = -0.34V$), thus, it may interfere with ongoing oxidation-reduction processes, leading to changes in the expression levels of the corresponding enzymes. For example, seven oxidoreductases with predicted roles in sterol metabolism were significantly down-regulated (AN8907, AN4094, AN6506, AN6973, AN3638, AN10648, and AN3817). Catalases *AncatB*,

AncatC and *AncpeA/AncatD* were slightly up-regulated. On the other hand, the expression of superoxide dismutases and the oxidative stress transcription factors *AnnapA* and *AnatfA* was not altered. Transmembrane transport of various substrates, as sugars, oligopeptides and metals was modified: the xylose transporters *AnxtrA* and *AnxtrB*, the putative high affinity nickel uptake protein AN6115, the putative Cation Diffusion Facilitator (CDF) transporter. Finally, transcriptional regulation was also notably altered, based on the changes in the expression of transcription factors. Most of them were unidentified.

Analyzing the repercussion of copper-toxicity on gene expression we found that certain gene clusters were affected by copper addition. For example, the siderophore biosynthesis gene cluster (*AnsidA*, *AnsidC, AnsidD, AnsidF, AnsidG, AnsidH,* and *AnsidI*) was notably down-regulated, together with the iron homeostasis TF, *AnhapX*. Besides the siderophore biosynthesis cluster, most members of the Emericellamide antibiotic biosynthesis gene cluster were down-regulated (*AneasB, AneasC,* and *AneasD*). A set of genes (AN2558, AN2559, AN2560, AN2561, and AN2562) with no confirmed function was drastically upregulated. However, by sequence analysis tools we found that AN2562 is the homolog of the *N*-acetylglucosamine transporter Ngt1 from *C. albicans;* AN2560 and is the homolog of the high-affinity methionine and cysteine transporter Mup1 from *S. cerevisiae* and *C. albicans*; AN2558 is the homolog of the flavin-containing monooxygenases CaIfk1 and ScFmo1; and AN2559 and AN2561 are a predicted oxidoreductase and a predicted methyltransferase, respectively (**Table 2**).

In summary, copper toxicity altered the expression of 13.7% of the genes with a balanced ratio between up-regulated and down-regulated genes (**Figure 1A**). Changes in copper concentration derived in a strong modification of the copper

TABLE 2 | RNA-seq data of differentially expressed genes.

Gene	Log2 fold change	NC	CT	q-Value	Significant	Description
AN8251	−2,29289	212,998	43,4658	2,21E-10	Yes	*AnhapX*. TF iron homeostasis
AN5823	−1,6464	2071,32	661,656	0,00046089	Yes	*AnsidA*. Siderophore biosynthetic gene cluster member
AN8751	0,252704	33,0097	39,329	0,68274	No	*AnsidB*. Siderophore biosynthetic gene cluster member
AN0607	−0,957512	17,4648	8,99339	0,0248114	Yes	*AnsidC*. Siderophore biosynthetic gene cluster member
AN6236	−1,68316	454,38	141,494	0,00026402	Yes	*AnsidD*. Siderophore biosynthetic gene cluster member
AN6234	−0,91275	248,15	131,81	0,0336505	Yes	*AnsidF*. Siderophore biosynthetic gene cluster member
AN8539	−1,19743	277,515	121,011	0,00473987	Yes	*AnsidG*. Siderophore biosynthetic gene cluster member
AN6235	−1,19947	157,372	68,5252	0,00438479	Yes	*AnsidH*. Siderophore biosynthetic gene cluster member
AN0609	−2,13608	394,676	89,7878	3,63E-09	Yes	*AnsidI*. Siderophore biosynthetic gene cluster member
AN10080	−0,216896	22,965	19,7594	0,777446	No	*AnsidL*. Siderophore biosynthetic gene cluster member
AN7800	−0,267815	48,5357	40,3126	0,702964	No	*AnmirA*. Siderophore iron transporter
AN8540	−1,24341	1759,6	743,208	0,0167845	Yes	*AnmirB*. Siderophore iron transporter
AN7485	−0,738315	101,585	60,894	0,103354	No	*AnmirC*. Siderophore iron transporter
AN8907	−3,85352	2257	156,138	0	Yes	Putative sterol methyl oxidase
AN4094	−2,81214	478,501	68,131	2,56E-14	Yes	Putative sterol reductase
AN6506	−2,63572	947,541	152,464	2,10E-11	Yes	Putative sterol methyl oxidase
AN6973	−1,72893	1740,29	525,004	5,21E-05	Yes	Putative sterol methyl oxidase
AN3638	−1,34834	382,258	150,129	0,00162595	Yes	Putative sterol methyl oxidase
AN10648	−0,960416	76,6647	39,3987	0,0282487	Yes	Sterol reductase activity, ergosterol biosynthetic process
AN3817	−0,929126	85,5385	44,9228	0,0288343	Yes	Putative reductase, predicted role in sterol metabolism
AN6412	1,75949	4,36251	14,7705	0,00418067	Yes	*AnxtrA*. Xylose transporter A
AN3264	1,44359	4,83779	13,1587	0,0126647	Yes	*AnxtrB.* Xylose transporter B
AN2911	−0,0516925	117,662	113,521	0,95033	No	*AnatfA*. TF for response of conidia to stress.
AN7513	0,53883	117,309	170,426	0,298838	No	*AnnapA*. TF required for resistance to oxidative stress
AN8637	−1,56595	4,86518	1,64324	0,0317285	Yes	*AncatA*. Catalase
AN9339	1,49778	18,7857	53,0525	0,00017666	Yes	*AncatB*. Catalase
AN5918	1,24056	25,0035	59,0807	0,00396133	Yes	*AncatC*. Catalase
AN7388	1,37382	12,0197	31,1495	0,00400481	Yes	*AncpeA/AncatD*. Catalase
AN6115	1,89337	35,271	131,032	1,45E-06	Yes	Cation Diffusion Facilitator (CDF) transporter
AN2545	−1,46337	0,478858	0,173655	1	No	*AneasA*. Emericellamide biosynthetic gene cluster
AN2547	−2,25667	1,10672	0,231587	0,001229	Yes	*AneasB*. Emericellamide biosynthetic gene cluster
AN2548	−4,52491	0,952086	0,0413563	0,0229756	Yes	*AneasC*. Emericellamide (eas) biosynthetic gene cluster
AN2549	−2,98507	14,804	1,86976	1,06E-07	Yes	*AneasD*. Emericellamide (eas) biosynthetic gene cluster
AN2558	6,95672	0,0388284	4,82314	5,62E-05	Yes	Calfk2 and ScFmo1 homolog
AN2559	8,11636	0,171753	47,662	2,56E-14	Yes	Predicted oxidoreductase activity
AN2560	7,69094	0,0580346	11,992	6,81E-07	Yes	ScMup1 and CaMup1 homolog
AN2561	7,98542	1,19049	301,7	0	Yes	Putative methyltransferase
AN2562	7,07374	0,0340531	4,58737	0,00125881	Yes	CaNgt1 homolog

homeostasis system, the copper dependent enzymes and multiple biological processes, especially oxidation reduction processes and predictably, in cellular components such as biological membrane composition. As a remarkable feature, in most of these processes, more genes were up-regulated than down-regulated (**Figure 1B**).

Screening for Potential Copper Transport Proteins

In order to select putative copper transporters we searched for putative orthologs of *Saccharomyces cerevisiae* Ctr transporters among down-regulated genes under copper toxicity. Blastp searches using the full-length of the ScCtr protein sequences yielded three results, the already identified AN3209 and

AN3813, and another putative copper transporter, AN2934, termed *AnctrB*. *AnctrB* is the top hit of the low affinity copper transporter ScCtr2, which encodes a vacuolar Cu transporter (Liu et al., 2012; Qi et al., 2012). Cai et al., 2019 recently identified AN3209 and AN3813 as copper uptake proteins in *A. nidulans*, and AnMac1 as the TF controlling their expression. In this work, AN3209 and AN3813 were named AnCtrA2 and AnCtrC, respectively, claiming they were AfCtrA2 and AfCtrC homologs, but the protein sequence analysis results support a different interpretation. BLASTp analyses revealed that AnCtrA and AnCtrC are significant hits of AfCtrC (42% and 60% protein identity, respectively); however, there is no significant hit of AfCtrA2 (24% and 22% protein identity, respectively) in the *A. nidulans* proteome.

Thus, instead of naming AN3209 as AnCtrA2, we considered the name AnCtrA.

Sequence data revealed that *AnctrA* and *AnctrC* share great similarity. Furthermore, out of the 127 species that possess an *AnctrA* ortholog, 94 also possess an *AnctrC* ortholog (**Figure 8**).

According to the phylogeny analyses shown in **Figure 2**, three major clusters can be differentiated. Most Ctr proteins of filamentous fungi are related to ScCtr3 (red); *A. fumigatus*, *A. nidulans*, and *A. niger* possess Ctr proteins closely related to the vacuole Cu transporter ScCtr2 (Blue); Out of the 27 proteins of the phylogeny test, only four proteins are related to ScCtr1 (Green). The results reflect that ScCtr3 orthologs comprise the biggest group of proteins and in this group we can find most Ctr proteins of filamentous fungi.

A multiple sequence alignment of *A. nidulans* Ctr proteins is shown in **Figure 3A**. Strong similarities in amino acid sequences could be observed, except for the loop between transmembrane domains (TMD) 1 and 2, which showed higher variability. Detailed sequence analysis showed the presence of common conserved motifs predicted to code for copper binding. AnCtrA, AnCtrC, AfCtrC and CnCtr4 contain a Met motif arranged as M-xx-M-x-M in the amino-terminal region (Nt) (Met motif shown in blue box). Three additional methionine residues are conserved among the Ctr protein sequences aligned: a methionine in the amino-terminal, located ~ 22 amino acids upstream from the TMD1 (M^{30} in AnCtrA, M^{23} in AnCtrC, M^{20} in ScCtr3, M^{58} in AfCtrC and M^{41} CnCtr4) and an M-xxx-M motif in the predicted TMD2 (M^{134}-M^{138} in AnCtrA, M^{168}-M^{172} in AnCtrC and M^{185}-M^{189} in ScCtr3, M^{197}-M^{201} in AfCtrC and M^{156}-M^{160} CnCtr4). The methionine residue located prior to TMD1 is equidistant in *A. nidulans* and other fungi, as noted by Puig et al. (2002). As shown in **Figure 3A**, there are two conserved cysteine residues flanking this functional residue (Cys residues are highlighted in red for their copper handling capacity). Additional methionine and cysteine residues are widespread within the sequence. Finally, in all the proteins analyzed, close to the terminus of the carboxy-terminal region a putative copper handling motif that could be involved in copper coordination and transport was observed; a di-cystine motif in the case of ScCtr3, CnCtr4, AnCtrA and AnCtrC, and a M-x-C motif in the case of AfCtrC. Based on computer algorithms (TMHMM and HMMTOP predictions), as shown in **Figure 3B**, AnCtrA was predicted to contain two transmembrane regions while AnCtrC contained three. According to these predictions, the amino tail would be oriented to the outside of the cell and the carboxyl tail into the cytosol, in the case of AnCtrC. In the case of AnCtrA, however, both protein ends would be oriented to the outside.

Functional Characterization of AnCtr Mutants

The function of AnCtrA and AnCtrC through mutant analysis was recently reported (Cai et al., 2019); however, the individual role of each protein and their hierarchy in copper homeostasis remained unspecified. To gain further insight into this matter, single and double knock-outs of *AnctrA* and *AnctrC* were generated by gene replacement techniques (see list of strains).

The capacity of these strains to grow at different copper availability conditions was tested. We first reproduced the experiment conducted by Cai et al. (2019), by testing all generated mutant strains in 0 µM Cu media with identical results: the single deletion mutants showed a WT-like phenotype and the only strain showing growth disruption was the double null mutant $\Delta AnctrA$-$\Delta AnctrC$ (**Figure 4A**). These results provided evidence that under copper deficiency condition, AnCtrA and AnCtrC complemented each other. Addition of copper to the medium rescued the double deletion mutant defective phenotype. Similar results were obtained in liquid media as only the double null mutant showed a significantly lower growth rate than the WT strain (**Figure 4B**).

The above results showed that removing Cu from the trace element solution did not help discern phenotypic differences between single null mutants. Thus, we used the copper chelator bathocuproine disulfonic acid (BCS) in our experiments. As shown in **Figure 4C**, null mutant colonies did not exhibit appreciable alterations in radial growth or conidial pigmentation on regular solid minimal medium. Under copper starvation conditions (AMM supplemented with BCS), $\Delta AnctrC$ exhibited secondary level copper limitation effects at 80 µM concentration, displaying yellowish conidia which could be a result of the inactivity of the copper-dependent conidial laccase AnYA due to Cu deficiency. In contrast, the $\Delta AnctrA$ mutant presented no appreciable copper limitation effects. When both mutations were combined, primary level copper limitation effects were visible. Radial growth of the double knock-out strain was reduced to 40% and no pigmentation was appreciated. Upon Cu^+ supplementation (100 µM BCS + 100 µM CuSO4), normal growth and morphology were restored. It has been described that copper and iron metabolism are related in fungi, and iron can recover $\Delta mac1$ colony morphology -very similar to the double knock-out strain shown in **Figure 4C**- to some extent in *A. fumigatus* (Cai et al., 2017). Therefore, we tested whether addition of FeSO4 could rescue the colony defects observed in $\Delta Anctr$ mutants grown under copper starvation conditions. Fe supplementation (100 µM BCS + 400 µM FeSO4) did not rescue the defects in null mutants (**Figure 4C**). Since SODs are also copper dependent enzymes, we hypothesized that a menadione (a widely used oxidative stress inducing agent) experiment could probably help clarify the nature of the differences observed so far between the two transporter null mutants. However, with 60 µM menadione, the phenotype was similar; the $\Delta AnctrC$ strain was visibly more affected by the oxidative damage generated by menadione, suggesting that in the condition tested SOD copper supply depended more on AnCtrC.

In addition to the above colony growth inhibition and pigmentation defects, hyphal growth in liquid medium and conidia production were also studied. To investigate the effect of the deletion of the *Anctr* coding genes on conidial production, we harvested and compared the number of conidiospores produced by each strain, under basal and low copper availability conditions (**Figure 4D**). Under basal conditions, single deletion of *Anctr* genes had no apparent effect on conidia production. Under copper deficiency conditions *AnctrA* deletion had a slight effect, but *AnctrC* deletion had a remarkable impact; conidia numbers

FIGURE 2 | Phylogenetic analysis of Ctr proteins. Using MEGA7, a phylogenetic tree was generated by the Neighbor-Joining method with the Bootstrap method as phylogeny test. Analyzed organisms: *Alternaria alternata* (Aa), *Aspergillus nidulans* (An), *Aspergillus fumigatus* (Af), *Aspergillus fischeri* (Afis), *Aspergillus flavus* (Afla), *Aspergillus niger* (Anig), *Aspergillus oryzae* (Ao) *Aspergillus clavatus* (Ac), *Aspergillus terreus* (At), *Botrytis cinerea* (Bc), *Fusarium oxysporum* (Fo), *Magnaporthe oryzae* (Mo), and *Saccharomyces cerevisiae* (Sc).

were halved by comparison to the wild-type strain. Numbers of conidia are connected with the amount of biomass and the ΔAnctrC colony grown in solid AMM medium with 100 μM BCS was not smaller than the colony grown in AMM. Thus, copper scarcity had no effect on colony expansion, but on colony density, an effect that has also been described under other stresses conditions such as carbon or nitrogen starvation (Richie et al., 2007). Deletion of both *Anctr* proteins had a

slight effect at control conditions. Under copper starvation conditions, conidia quantity was, 37-fold lower than the wild-type strain (**Figure 4D**).

Hyphal growth studies were conducted with the WT stain and the ΔAnctrA-ΔAnctrC strain. At 16 h both strains presented very similar growth rates under all tested conditions. However, after 40 h, the double deletion strain presented a dramatically lower growth rate in low copper availability conditions compared to

FIGURE 3 | Sequence analysis of *Aspergillus nidulans* high affinity copper transporters AnCtrA and AnCtrC. **(A)** Alignment of predicted full-length of *Saccharomyces cerevisiae* Ctr3, *Cryptococcus neoformans* Ctr4, *Aspergillus nidulans* CtrA and CtrC, and *Aspergillus fumigatus* CtrC sequences compared using the Clustal method. Identical residues are described with asterisk, and conservative and semi-conservative residues with double and single dots, respectively. Methionine residues are represented in green and cysteines in red. The length of each protein is indicated adjacent to the last amino acid. Protein accession numbers are reported as follows: ScCtr3 (Q06686), CnCtr4 (J9VLN4), AnCtrA (C8VIA1), AnCtrC (C8V6S8), and AfCtrC (Q4WHY8). **(B)** Proposed model of AnCtrA and AnCtrC describing the predicted membrane topology and the conserved methionine and cysteine residues. AnCtrA contains two transmembrane domains and AnCtrC three.

the WT and itself in basal copper conditions (28.1% and 35.2% compared to WT, for BCS and BCS* conditions, respectively) (**Figure 4E**). Thus, environmental copper deprivation had no apparent effect in the germination process but had a strong effect in the ensuing growth phase.

Since the addition of 100 μM BCS to media showed results for the *AnctrC* null mutant; however, but no characteristic phenotype with the null *AnctrA* mutant and the WT strain, we increased the BCS concentration (400–600 μM). In these extremely low copper availability conditions, the WT strain presented secondary copper limitation symptoms like pigmentation deficiency, similar to that of the Δ*AnctrC* strain. In addition, the Δ*AnctrA* strain displayed primary level copper limitation effects as a reduced radial growth and lack of pigmentation, similar to the double null strain albeit less aggravated (**Figure 4F**).

Taken together, the results support the interpretation that AnCtrA and AnCtrC are copper transporting proteins that complement each other. AnCtrC seems to be the principal copper transporting protein at nutritional and mild copper deficiency conditions, as the *AnctrC* deletion strain is more susceptible to oxidative damage and shows secondary copper limitation effects like defects in sporulation and spore pigmentation. However, the phenotypes of the WT strain and Δ*AnctrC* become very similar in extreme copper scarcity conditions, suggesting that the contribution of AnCtrC in those conditions is very limited. Although *AnctrA* deletion has no tangible effect under mild copper deficiency, primary level copper limitation effects are visible in extreme copper deficiency conditions. When both transporters were jointly deleted, pigmentation and colony growth defects were far greater than in the single null strains, as manifested by strongly reduced growth rate in liquid medium

under low copper availability. This would support the view that both transporters cover an extended concentration range for environmental copper uptake.

AnCtr Protein Expression Dynamics

After identifying the copper uptake proteins involved in copper homeostasis, their expression patterns were investigated, with special interest in AnCtrA, which remained uncharacterized. Hence, the expression profiles of AnCtrA and AnCtrC throughout Cu and BCS treatments, were examined in time course experiments.

We generated two fluorescent protein-tagged chimera strains: AnCtrA:GFP and AnCtrC:GFP. In order to test whether GFP tagging could alter protein function we verified that both strains followed wild-type like phenotypes under BCS treatments in plate experiments (**Figure 5A**).

RT-PCR experiments revealed that Cu and BCS addition caused opposite effects on *AnctrC* expression (**Figure 5B**). Shortly after 100 μM $CuSO_4$ addition, *AnctrC* transcript levels were reduced four-fold and this tendency was maintained throughout the experiment. On the other hand, upon addition of 100 μM BCS, initially presented lower relative expression of *AnctrC* transcript than at t_o, followed by a gradual increase, reaching the highest level at 120′ (2.5-fold). Western blot analyses were coherent with RT-PCR data. When BCS was added to the medium, a 50 kDa band coinciding with the AnCtrC:GFP monomer was visible. The signal detected at short incubation times was similar to the one detected at t_o. The signal grew stronger at longer exposures. After Cu addition, AnCtrC protein signal gradually faded through time.

FIGURE 4 | Functional analysis of *AnctrA* and *AnctrC* mutants. **(A)** Spores from the mutant strains were point-inoculated and images of colonies were taken after 48 h of incubation at 37°C in 0 µM Cu AMM (Aspergillus minimal medium) and 0 µM Cu AMM with 1, 2.5, and 5 µM Cu. **(B)** Dry weight measurements of the mutant strains incubated for 16 h at 37°C in 0 µM Cu AMM. **(C)** Spores from the mutant strains were point-inoculated and images of colonies were taken after 48 h of incubation at 37°C in AMM and AMM with 100 µM CuSO4, 100 µM BCS, 100 µM BCS with 100 µM CuSO4 and 100 µM BCS with 400 µM FeSO4. **(D)** Conidia production was determined by quantifying the number per unit of colony surface area (conidia/cm²). In order to facilitate data comparison, growth of the wt strain at basal level was designated 100%, data was normalized and presented as percentages.*Significant conidiospore number reduction $p < 0.05$. **(E)** In liquid medium culture experiments, 6×10^4 spores of the WT and $\Delta AnctrA \Delta AnctrC$ strains were inoculated for 16 h and 40 h at 37°C, under basal conditions (MMA), low copper availability conditions (BCS) and low copper availability conditions after 16 h of normal growth (BCS*). **(F)** Spores from the mutant strains were point-inoculated and images of colonies were taken after 48 h of incubation at 37°C in AMM and AMM with 200, 400, and 600 µM BCS.

The *AnctrA* transcript expression pattern showed a more specific pattern for copper deficiency conditions (**Figure 5C**). When copper was added, expression levels exhibited a five-fold decrease. However, upon BCS addition, expression increased up to 21.5-fold relative to the total RNA extract at t_o, substantially greater than observed in *AnctrC*. Western Blot

FIGURE 5 | AnCtrC and AnCtrA expression profiles with Cu and BCS. **(A)** Phenotypes of the strains used for expression analysis of AnCtrC and AnCtrA in AMM and AMM + BCS media. **(B)** Western Blot and RT-PCR data showing changes in AnCtrC and *AnctrC* expression levels after addition of 100 μM CuSO$_4$ or 100 μM BCS. **(C)** Western blot and RT-PCR data showing changes in AnCtrA and *AnctrA* expression levels after addition of 100 μM CuSO4 and 100 μM BCS. **(D)** Western blot and RT-PCR data showing changes in AnCtrC and *AnctrC* expression levels in a Δ*AnctrA* genetic background, after addition of 100 μM CuSO4 and 100 μM BCS. **(E)** Western Blot and RT-PCR data showing changes in AnCtrA and *AnctrA* expression levels in the Δ*AnctrC* genetic background, after addition of 100 μM CuSO4 and 100 μM BCS.
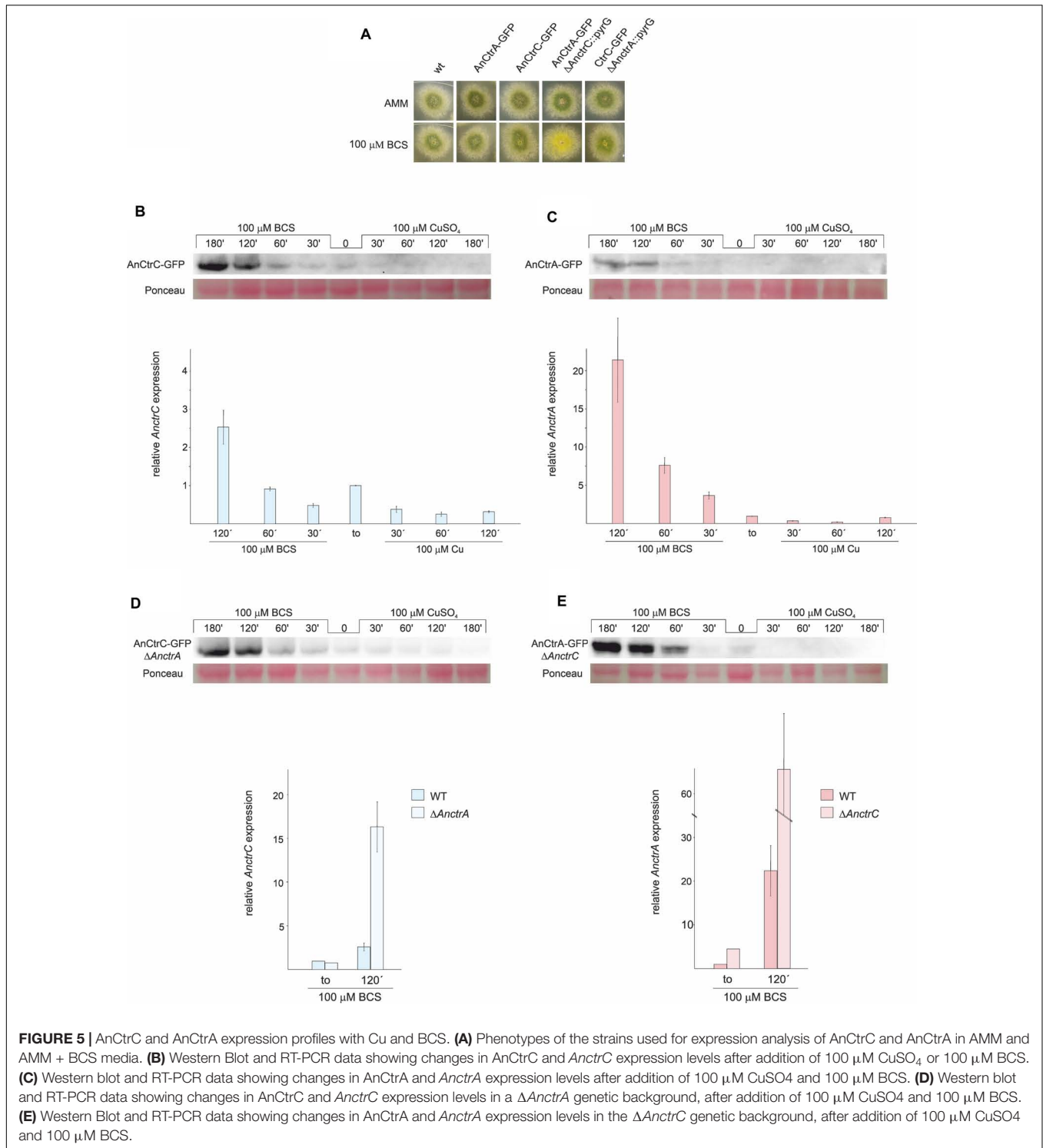
analyses exhibited a 47 kDa band only visible in samples treated with BCS. Although the observed band was very faint at early incubation times, it grew stronger with increasing incubation times.

Phenotypic observation of the mutants showed that AnCtrC is effective under copper sufficiency or and mild copper

deficiency conditions, while AnCtrA function gains relevance under extreme copper deficiency conditions. Taking this into account, we decided to study the behavior of *AnctrA* and *AnctrC*, RNA and protein, in their respective null mutants and compared them with WT strain levels. *AnctrC* expression in a Δ*AnctrA* background, was slightly lower at basal conditions.

FIGURE 6 | Fluorescence microscopy images of AnCtrC and AnCtrA chimeras. **(A)** AnCtrC:GFP-Hhoa:mRFP protein expressing strains were grown in selective WATCH medium for 16 h at 30°C. Images show the protein localization before BCS addition **(A1)** and 2 h after 100 μM BCS addition **(A2)**. Pictures A1.2–A2.2–A2.3 show a closer look at the most interesting features. **(B)** AnCtrA:GFP-HhoA:mRFP protein expressing strains were grown in selective WATCH medium for 16 h at 30°C. Images show the protein localization before BCS addition **(B1)** and 2 h after 100 μM BCS addition **(B2)**. Pictures B1.2–B1.3–B2.2–B2.3 show a closer look at the most interesting features.
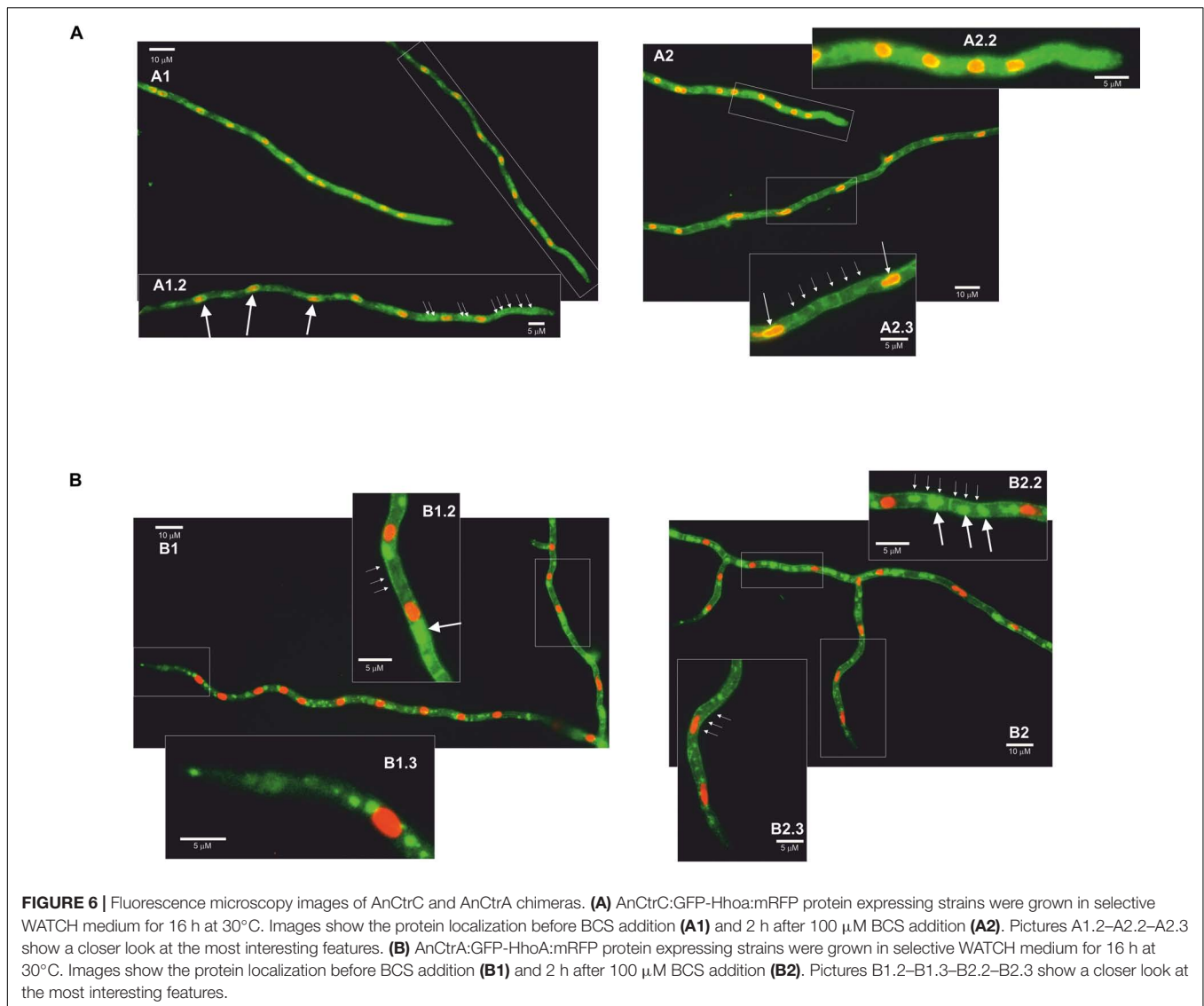
However, at later times, expression level grew 16.74-fold higher under copper deficiency conditions (**Figure 5D**). At the protein level, the expression profile was maintained. *AnctrA* expression on the other hand, was clearly different in a Δ*AnctrC* background. At basal levels *AnctrA* expression was 4.5-fold higher and 63.81-fold higher under copper starvations conditions (**Figure 5E**). At the protein level, t_o protein signal could be detected and with BCS incubation, the signal became considerably stronger compared to that in the wild-type background.

The results from this study demonstrated that *AnctrA* and *AnctrC* expression is copper dependent, albeit with some differences (**Figure 5**). *AnctrC* expression profile is more stable through time in line with a possible role of copper sup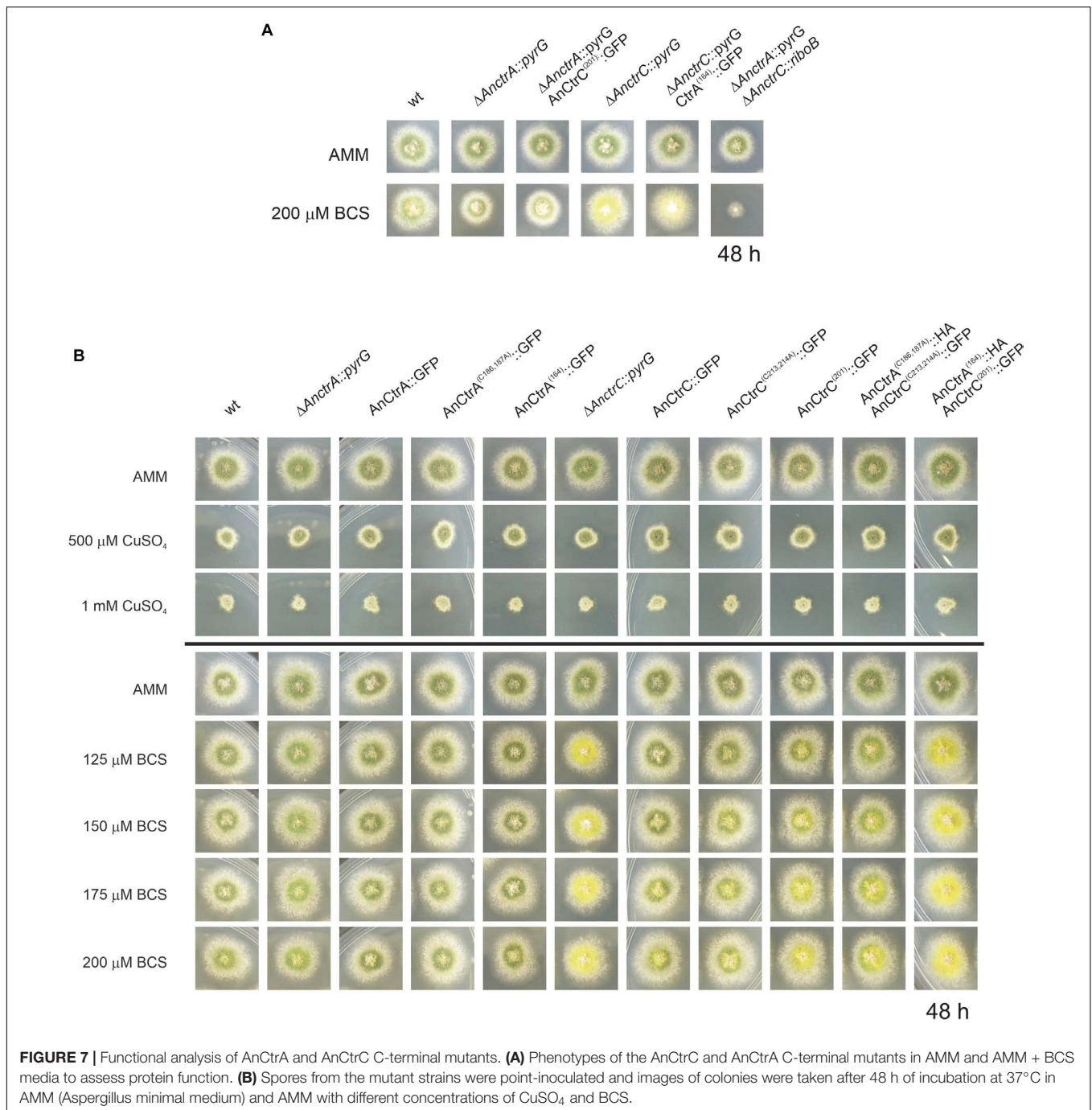ply in nutritional and mild copper deficiency conditions. *AnctrA* expression on the other hand, experiences an outstanding induction after BCS addition, a fitting expression pattern for an extreme copper deficiency copper transporter. The implications

of these results will be further elaborated when the relative contribution of each protein is discussed.

AnCtr Localization

AnCtrA and AnCtrC protein localization was conducted *in vivo* using strains expressing C-terminally GFP-tagged chimeric proteins, together with AnHhoA:mRFP marked strains. AnHhoA is Histone 1, a marker of the nuclear chromatin. Ctr proteins function as copper internalizing proteins. Considering the likely mobility upon changes in environmental copper concentration, we grew our GFP chimera expressing strains in regular WATCH medium, added BCS to the medium and observed protein dynamics within a 2 h period. In regular WATCH media without copper deprivation, AnCtrC:GFP was detected throughout the cytosol of hyphae (**Figure 6A1**). Many oval structures that colocalized with the red nuclei (white arrows) were distinguished, with some associated membranes displaying green fluorescence and the fluorescence signal was notably polarized (**Figure 6A1.2**).

FIGURE 7 | Functional analysis of AnCtrA and AnCtrC C-terminal mutants. **(A)** Phenotypes of the AnCtrC and AnCtrA C-terminal mutants in AMM and AMM + BCS media to assess protein function. **(B)** Spores from the mutant strains were point-inoculated and images of colonies were taken after 48 h of incubation at 37°C in AMM (Aspergillus minimal medium) and AMM with different concentrations of $CuSO_4$ and BCS.

After BCS addition fluorescence signal became more visible in the plasma membrane but no protein migration was appreciated. In the vicinity of the tip area, no fluorescence was localized in the plasma membrane and the signal inside the hyphae polarized toward the tip. After 2 h of BCS addition the presence of the protein in the plasma membrane became clearer along the hyphae but not in the tip region (**Figure 6A2**). Fluorescence signal was notably polarized in the tip region (**Figure 6A2.2**). Fluorescence was still visible in the perinuclear area and discrete fluorescence signals were detected elsewhere within

hyphae but the identity of the organelles could not be specified (**Figure 6A2.3**). In the case of AnCtrA, throughout the course of the experiment, a gradual increase in fluorescence intensity was observed but protein localization remained quite stable. Without copper deprivation, the protein was mainly localized in irregular granules dispersed along the hyphae (**Figure 6B1**). Disperse fluorescence patches could be detected in the plasma membrane (**Figure 6B1.2**) and as with AnCtrC, close to the tip region no protein was localized in the membrane (**Figure 6B1.3**). After 2 h of BCS addition, the signal in the plasma membrane became

more notorious (**Figure 6B2**). Besides the plasma membrane fluorescence signal numerous other structures were visible along the hyphae, possibly early endosomes (**Figure 6B2.2**). Even in copper deprivation conditions, no protein was localized in the tip region (**Figure 6B2.3**). The subcellular localization of each protein will be further discussed.

In conclusion, in case of AnCtrC, the signal accumulated around nuclei associated membranes, most likely the nuclear envelope (Markina-Inarrairaegui et al., 2013) and other structures; considering the polarization of the fluorescence signal possibly the peripheral ER. In low copper availability conditions, the fluorescence signal along the hyphae, except for the tip, partially shifted toward the membrane; nevertheless, most of the protein was still detected along the hyphae. In the case of AnCtrA the fluorescence signal was in the plasma membrane, but toward the tip region of the hyphae, the plasma membrane appeared free of fluorescence. The protein could be also detected in numerous morphologically heterogeneous compartments. These could be vacuolar compartments or early endosomes, considering the similarities between the role and expression pattern of AnCtrA and previously described copper uptake proteins.

C-Terminal Mutations of AnCtrA and AnCtrC

In organisms like *S. cerevisiae* and humans, Ctr protein C-terminals reportedly play a crucial role in shutting down copper uptake when intracellular copper concentrations reach a threshold (Schuller et al., 2013). Certain copper binding residues, namely cysteines and histidines, are specifically involved in the mechanism, which is separate from copper uptake (Wu et al., 2009; Clifford et al., 2016). In the C-terminal of AnCtrA and AnCtrC there are two adjacent cysteines that are conserved in many other orthologs, flagging them as copper binding residues. In order to test this hypothesis, single and double mutants of the mentioned cysteine residues AnCtrA^{C186,187A} and AnCtrC^{C213,214A} were generated by alanine substitution. C-terminally truncated mutants, AnCtrA^{164} and AnCtrC^{201}, were also generated, in order to check if there was any difference in copper susceptibility compared to the cysteine mutants. The mutants were checked for a possible loss of function due to the inserted mutations. All mutants were proven to be functional, as the outcome of the C-terminal mutation in combination with a Ctr deletion was not similar to the double null mutant (**Figure 7A**). The mutants were grown in AMM with different concentrations of CuSO$_4$ and BCS as shown in **Figure 7B**.

Neither the deletion of the C-terminal domain nor the mutation of the cysteine residues resulted in added susceptibility toward copper. However, the mutants presented secondary level copper limitation effects in copper scarcity conditions, especially the double C-terminal deletant strain. The AnCtrA$^{(164)}$:HA-AnCtrC$^{(201)}$:GFP strain phenotype was similar to the Δ*AnctrC* phenotype regarding conidial pigmentation deficiency at 125 µM BCS. The AnCtrC$^{(201)}$:GFP and AnCtrA$^{(C186,187A)}$:HA-AnCtrC$^{(C213,214A)}$:GFP also showed pigmentation deficiencies

but to a lower degree. The C-terminally truncated mutants were still functional as shown in **Figure 7A**.

Therefore, the broadly conserved di-cysteine motif was shown to have no impact on copper uptake shut-down under the conditions tested. However, this motif may be involved in copper uptake, since removing the C-terminal and the cysteine residues does appear to reduce uptake capacity as their deletion results in defective pigmentation, a secondary level copper limitation effect. This would mean that the copper uptake regulation mechanism of the *A. nidulans* Ctr proteins is different from the so far studied regulation mechanisms and that the contribution of the C-terminal is necessary for full capacity copper uptake.

Screening for Cupric Metalloreductases

As mentioned in the RNA-seq analysis, RNA-sec offered the opportunity to search for Plasma Membrane metalloreductases, homologs to the Fre protein family. The expression of the copper metalloreductases reportedly follow the same expression pattern as Ctr proteins since both are under control of the TF Mac1 (Yamaguchi-Iwai et al., 1997; Levitin and Whiteway, 2007). Our screen retrieved three candidates that were co-regulated with the Ctr protein out of ten members of the family of metalloreductases present in the *A. nidulans* genome: *AnfreA*, AN0773, and AN3208. *AnfreA* is a characterized iron reductase and it has no putative AnMac1 binding sequence. AN0773 and AN3208 are two uncharacterized putative copper reductases that possess a possible AnMac1 binding region in their respective promoter regions. However, a detail caught our attention. AN3208 is a putative cell surface metalloreductase adjacent to AnctrA and they share the promoter region where AnMac1 binds (**Figure 4**). This feature reinforces the idea that it may be a copper metalloreductase. Thus, it was named AnfreC. Synteny and multiple alignment data in the EnsemblFungi site revealed that the *AnctrA-AnfreC* ortholog's position and orientation is conserved in the majority of fungal species that contain an *AnctrA* ortholog. The majority of screened species (110/127) contain the putative plasma membrane high affinity copper transporter and a metalloreductase located in tandem (**Figure 8**).

In summary, AN0773 and *AnfreC* fulfill the conditions to be copper metalloreductases. However, due to the unique features of *AnfreC* mentioned above it is a suitable candidate to be the main cupric metalloreductase in *A. nidulans*.

DISCUSSION

This study provides additional information on the expression and function of the high affinity copper uptake system reported in yeast and filamentous fungi of clinical interest. The study of gene expression profiles under basal copper availability conditions, copper deprivation and copper toxicity has shed new light on the overall adaptation of *A. nidulans* to copper fluctuations, as well targeting the dynamics of copper transporters. The subsequent analysis through targeted mutagenesis of the principal copper transporters have enabled an interpretation of their individual contributions in the copper uptake process, their expression

FIGURE 8 | An image representing the chromosomal location of *AnfreC-AnctrA*, and a list of fungal organisms that possess an *AnctrA* ortholog are presented. (1) The organism possesses another Ctr protein ortholog of *AnctrC*. (2) The organism possesses an Ox-Red coding gene beside the *AnctrA* ortholog, just like *A. nidulans*. The color of the rectangles next to the organism represents: green (yes), red (no) and gray (unidentified).

patterns and their subcellular localization dynamics. In addition, new inquiries into the role of transporter C-terminal domains together with the identification of putative membrane copper reductases have been initiated.

The response to copper toxicity in *A. nidulans* involves the differential expression of 13.7% of its genes. Significant changes were recorded on recognized copper homeostasis genes. Even though the expression of the TFs regulating the process was not significantly altered, that of proteins responsible of copper uptake and detoxification was very notable. The gene coding for the copper exporting P-type ATPase AnCrpA (Antsotegi-Uskola et al., 2017), was up-regulated. On the other hand, the two characterized copper transporter genes *AnctrA* and *AnctrC* (Cai et al., 2019) were down-regulated, in line with the objective of reducing the copper uptake to the minimum. Finally, the notable upregulation of the intracellular copper trafficking P-type ATPase *AnygA* (Clutterbuck, 1990) might be a response to the presence of high amounts of copper ions within the cell that have to be distributed or compartmentalized. Out of the identified three putative copper chaperones only the putative Cu/Zn SOD chaperone AN6045 was significantly up-regulated. The functional counterpart in *S. cerevisiae*, chaperone Atx1, responsible for copper distribution within the cell, binds excess cytosolic copper (Lin and Culotta, 1995) and could act as a first level scavenger at low levels of toxicity. This effect may have been relevant under our experimental conditions, as discussed below.

Free cytoplasmic copper is known to produce ROS through Fenton-type reactions (Sutton and Winterbourn, 1989; Timoshnikov et al., 2019). Superoxide dismutases, accept electrons from reduced metals or superoxides, yielding hydrogen peroxide, which, along with small organic peroxides, is the substrate of catalases ($2\,H_2O_2 \rightarrow 2\,H_2O + O_2$) (Zamocky et al., 2008). Hence, the reported copper toxicity response involves the activation of both groups of enzymes (Wiemann et al., 2017). In our experiments, however, we observed that catalases *AncatB* (2.82-fold), *AncatC* (2.36-fold) and *AncpeA/AncatD* (2.59-fold) were up-regulated, but the expression of the Cu/Zn superoxide dismutase *AnsodA* (Holdom et al., 1996) (reported in **Table 1**), an enzyme activated in response to copper and zinc-derived ROS toxicity, remained unchanged, along with that of the ROS responsive transcription factors *AnatfA* and *AnnapA* (**Table 2**). These variations may stem from the differences in copper concentrations and the relative sensitivities of the strains used by Wiemann et al. (2017) and this study. In our experiments, 100 µM Cu concentrations were used, a dose that showed no visible effect in *A. nidulans* colony development (Antsotegi-Uskola et al., 2017). On the other hand, Wiemann et al. (2017) used a 200 µM copper concentration, in an organism at which 50 µM already compromised colony development. It is therefore likely that, under conditions which elicit no phenotypic symptoms of copper toxicity, the AnCrpA detoxification system could have removed the free cytosolic copper, rendering ROS neutralization unnecessary. On the other hand, Wiemann et al. (2017) combined higher copper concentrations and greater susceptibility may have overwhelmed the capacity of AfCrpA, thus triggering the upregulation catalases to quench ROS and H_2O_2. Both results may thus depict the response to two different

levels of copper toxicity. We hypothesize that catalases are heme-containing enzymes (Scherer et al., 2002) and it is well known that intracellular free copper ions can displace protein-bound iron. The selective up-regulation of the catalases in this case may be a response to this phenomenon, leading to the greater demand for functional catalases. More evidence will be required to confirm this interpretation.

Aside from catalases, the copper toxicity response also modified the expression of many other oxidoreductases. Laccases are blue–copper enzymes involved in lignin degradation or pigment biosynthesis (Scherer and Fischer, 2001). However, laccases don't show a specific expression pattern in response to copper toxicity (**Table 1**). Other oxidoreductases corresponded to membrane function-related metabolic processes such as sterol metabolism. Sterols, especially ergosterol, are the most abundant lipids in fungal cell membranes (Rodrigues, 2018), with roles in integral protein stabilization, membrane fluidity and permeability (Alvarez et al., 2007; Abe and Hiraki, 2009). Under copper toxicity, the expression of proteins involved in transmembrane traffic augmented; for example, many putative sugar transporters were up-regulated. This could be ascribed to a heightened requirement for energy (ATP) and reducing power (NADH), both principal products of aerobic sugar catabolism. For example, the ATP-dependent copper detoxification protein AnCrpA was highly up-regulated in this study, in line with earlier observations (Antsotegi-Uskola et al., 2017). Changes in differential expression of various heavy metal transporters may indicate that a change of copper concentration could cause an imbalance in heavy metal homeostasis, as described in *A. fumigatus* (Cai et al., 2017). Finally, a stress mechanism with such a wide ranging impact on cellular metabolism should also alter the regulation of a core regulatory process as transcription. A TF that experienced notable lower expression under copper toxicity conditions was *AnhapX* and this, in turn, is consistent with the down-regulation of the siderophore biosynthesis cluster that it has been reported to regulate (Schrettl et al., 2010). The same result was obtained with the antimicrobial compound emericellamide biosynthesis cluster (**Table 2**). Finally, analyzing the data of the RNA-seq we found out a highly up-regulated set of genes. The upregulation of an *N*-acetylglucosamide transporter, AN2562, could be an adaptive response to the high copper environment as this compound proves to be important for survival in the phagosome (Vesely et al., 2017) where copper toxicity is used to kill by the innate immune system (Li et al., 2019). Secondly, it is very convenient that a cysteine and methionine transporter, AN2560, would be upregulated in such conditions as they are two amino-acids that participate in copper binding motifs (Pena et al., 2000). The Flavin-containing monooxygenase might play an important role in creating an optimal redox environment threatened by the presence of copper in the cytosol (Suh et al., 2000). These three genes together with the predicted oxidoreductase AN2559 and the putative methyltransferase AN2561 might comprise a defensive gene cluster against copper toxicity.

The phylogenetic characteristics of two *A. nidulans* Ctr proteins, AnCtrA and AnCtrC, have been examined in this study. Although the reference Ctr sequence used to screen

for orthologs in fungi had been ScCtr1, none were found in the *A. nidulans* genome with that criterion. According to the Ensembl fungi ortholog predictions, homologs of ScCtr1 are only found in the Saccharomycetales order. Moreover, most Ctr proteins of filamentous fungi shared higher similarity with ScCtr3 (**Figure 2**). Unfortunately, *Scctr3* is poorly documented as it is disrupted by a Ty2 transposon in many laboratory strains (Knight et al., 1996). AnCtrC showed phylogenetic relationship with numerous Ctr orthologs in *A. fumigatus*, *S. cerevisiae* and various other fungi. On the other hand, AnCtrA showed similarity with other putative Ctr proteins that have not been characterized.

Both proteins possess the characteristic features of Ctr proteins (Zhou et al., 2003; Petris, 2004; Rees and Thiele, 2004). Ctr family members generally harbor three putative TMDs (Puig et al., 2002), but according to topology software predictions, AnCtrA has only two TMDs. This has also been reported in *A. fumigatus* and *C. neoformans* (Waterman et al., 2012; Park et al., 2014). Cysteine residues are present throughout the sequence and cysteines are known for their affinity to copper (Pena et al., 2000). Both proteins contain two cysteine residues flanking the methionine residue adjacent to TMD1. This soft Lewis base may be important to coordinate copper since it has been described that metal binding residues located close to the plasma membrane seem to play a more important role in copper transport (Puig et al., 2002).

Functional characterization analyses in this study showed that the two Ctr proteins worked independently and the range of copper concentrations they covered were partially complementary, as derived from the obtained phenotypes. The phenotypes observed were broadly interpreted in terms of acute or partial deficiencies as follows. Normal growth rates and WT-like green conidial pigmentation were interpreted as an indication of adequate copper supply for basic growth and developmental functions. Defects in spore pigmentation and sporulation that did not affect growth rate were interpreted as the result of a partial limitation in copper. Conidiogenesis is strongly reliant on autophagy-based resources (Kikuma et al., 2007; Richie et al., 2007). The yellowish spore pigmentation could be explained by the inactivity of the copper-dependent conidial laccase AnYA; the phenotype corresponds with the *yA2* phenotype (Hermann et al., 1983; Scherer and Fischer, 2001). On the other hand, acute copper deficiency was interpreted to affect extracellular copper transport with direct consequences on vegetative growth. Following these criteria, we surmised that AnCtrC functions as the principal copper uptake protein under copper sufficiency and mild copper deficiency conditions. AnCtrA may complement the lack of AnCtrC at moderate copper deficiencies but is specifically required for extreme copper deficiency scenarios.

As shown in this study, conditions of low copper availability induce a gradual up-regulation in Ctr expression, while high copper levels induce the opposite effect. The rapid shutdown of the copper uptake system under high extracellular copper concentrations is of great importance to avoid copper toxicity (Bertinato and L'Abbe, 2004; Dong et al., 2013). The expression patterns of AnCtrA and AnCtrC under similar testing conditions share certain similarities with *S. cerevisiae* Ctr proteins; a Ctr protein with a more stable expression pattern (ScCtr3)

and another one that is uniquely expressed under low copper availability conditions (ScCtr1) (Pena et al., 2000). AnCtrC is the only high-affinity copper transporter expressed at basal copper levels, which means it is likely to cover for copper intake under ordinary copper availability (**Figure 5B**). On the other hand, AnCtrA expression pattern seems to be designed for extreme copper scarcity conditions, when AnCtrC transport cannot meet the cell's copper requirements. These results are in line with the conclusions from phenotypic analyses of selective null mutants discussed above.

In terms of protein localization dynamics, Ctr proteins are known to follow a very dynamic trafficking pathway. Pena et al. (2000) described that ScCtr3 traveled to the plasma membrane through the Trans-Golgi network and the fluorescence signal of tagged proteins accumulated in the ER after inhibiting protein traffic from ER to Golgi. However, when copper concentration rose, Ctr proteins like ScCtr1, moved from the plasma membrane to the vacuole (Liu et al., 2007), or early endosomes, as in the case of hCtr1 (Eisses and Kaplan, 2002; Clifford et al., 2016). The predominant ER localization of AnCtrC (Markina-Inarrairaegui et al., 2013) and its partial migration to the plasma membrane in copper deficiency conditions support its role as a copper uptake protein covering transport under copper sufficiency or mildly limiting conditions. The predominant plasma membrane and vesicular localization of AnCtrA is in line with reported data of other proteins that respond to extreme copper deficiency scenarios such as described for ScCtr1 or hCtr1 (Eisses and Kaplan, 2002; Liu et al., 2007; Clifford et al., 2016).

The shutdown of copper transport as a measure to avoid toxicity has been documented many instances. Previous reports on this toxicity-preventing mechanism refer to certain residues, mostly cysteines, in the C-terminus of Ctr proteins as key elements in uptake modulation (Liu et al., 2007; Wu et al., 2009; Schuller et al., 2013). Copper has been postulated to bind C-terminal cysteines, purportedly triggering the mechanism. The possible role of the Ctr proteins' C-terminal in activity modulation has not been studied in filamentous fungi. However, the C-terminal di-cysteine motif, a common heavy metal binding sequence (Lekeux et al., 2018) can be found in Ctr proteins of *Alternaria alternata*, *Aspergillus fumigatus*, *Botrytis cinerea*, *Fusarium graminearum*, *Histoplasma capsulatum* and *Magnaporthe oryzae*. We first hypothesized that this di-cysteine motif could act as copper uptake modulator, as the ScCtr1 C-terminal cysteine residues or the hCtr1 HCH motif. However, our results do not indicate any copper dependent uptake modulation or internalization role. Moreover, unlike the C-terminus of ScCtr1, that is dispensable for full copper uptake capacity (Wu et al., 2009), deletion of AnCtrC C-terminus results in secondary copper deficiency effects manifested as a pigmentation deficiency (**Figure 2B**). Thus, the C-terminus of the Ctr proteins plays some role in the copper uptake process. Further studies will be needed to clarify this question.

Plasma membrane metalloreductases are crucial components of the copper uptake process as they provide Ctr transporting proteins with the substrate in a transport-compatible reduced state (Labbe et al., 1997; Petris, 2004). There are documented

reductases that reduce iron and also copper (Georgatsou et al., 1997); however, *AnfreA* was discarded for lacking a putative Mac1 binding sequence. *AN0773* and *AnfreC* both shared copper reductase features, but the phylogenetically preserved genomic location of *AnfreC* in tandem with *AnctrA* tipped the scales in its favor. The genes coding for the reductive iron assimilation complex composed by the oxidoreductase FetC and the iron transporter FtrA (Schrettl et al., 2004) are located in tandem, exactly like *AnfreC-AnctrA*, in Fusarium species (Park et al., 2007; Wiemann et al., 2012) and other Aspergillus species like *A. fumigatus, A. clavatus* and *A. fischeri* for example. This fact points out to *AnfreC* as the main copper oxidoreductase.

In conclusion, the RNA-seq experiments performed in this study have clearly shown that copper concentration has a notable impact on many cellular processes, especially the redox-state and transmembrane transport. The absence of phenotypic impact of the treatments used on colony development suggests that the concentration used for the RNA-seq experiment is within the range of concentrations covered by the P-type ATPase AnCrpA. The deep functional characterization of AnCtrA and AnCtrC has revealed that both Ctr proteins function in a complementary manner but each protein has a role in copper uptake. AnCtrC works in copper uptake under copper sufficiency conditions and AnCtrA is only activated under extreme copper deficiency. Both proteins display a copper-dependent expression but with different patterns that reinforce the above-mentioned hypothesis. Interestingly, both proteins are upregulated when the counterpart is missing but they are not able to fully complement each other. Both proteins are partially located in the plasma membrane; nevertheless, they are clearly dynamic proteins. The C-terminus CC motif neither the C-terminus itself are part of the copper uptake modulation mechanism in copper toxicity conditions but they do have a role in copper uptake. Finally, the putative plasma membrane metalloreductase *AnfreC* possesses very interesting features that make it a good candidate to be the main cupric metalloreductase.

DATA AVAILABILITY STATEMENT

The datasets presented in this study can be found in online repositories. The names of the repository/repositories and accession number(s) can be found below: https://www.ncbi.nlm.nih.gov/, PRJNA623550.

AUTHOR CONTRIBUTIONS

MA-U designed and conducted the experimental work, analyzed and interpreted the results, wrote the manuscript, and ensured the accuracy of the project as whole. AM-I made the concept and designed the work, analyzed data and contributed to the writing of the manuscript. UU con-conceived the work, ensured the scientific issue was appropriately investigated, ensured the integrity of the work, revised and approved the final version to be published. All authors contributed to the article and approved the submitted version.

FUNDING

SUPPLEMENTARY MATERIAL

The Supplementary Material for this article can be found online at: https://www.frontiersin.org/articles/10.3389/fmicb.2020.555306/full#supplementary-material

Supplementary Figure 1 | Southern-blot validation of the mutant strains generated in this study. AnHhoA:mRFP strains were validated by microscope.

REFERENCES

Abe, F., and Hiraki, T. (2009). Mechanistic role of ergosterol in membrane rigidity and cycloheximide resistance in Saccharomyces cerevisiae. *Biochim. Biophys. Acta* 1788, 743–752. doi: 10.1016/j.bbamem.2008.12.002

Alvarez, F. J., Douglas, L. M., and Konopka, J. B. (2007). Sterol-rich plasma membrane domains in fungi. *Eukaryot. Cell* 6, 755–763. doi: 10.1128/ec.00008-07

Antsotegi-Uskola, M., Markina-Inarrairaegui, A., and Ugalde, U. (2017). Copper resistance in *Aspergillus nidulans* relies on the PI-Type ATPase CrpA, regulated by the transcription factor AceA. *Front. Microbiol.* 8:912. doi: 10.3389/fmicb.2017.00912

Balamurugan, K., and Schaffner, W. (2006). Copper homeostasis in eukaryotes: teetering on a tightrope. *Biochim. Biophys. Acta* 1763, 737–746. doi: 10.1016/j.bbamcr.2006.05.001

Bertinato, J., and L'Abbe, M. R. (2004). Maintaining copper homeostasis: regulation of copper-trafficking proteins in response to copper deficiency or overload. *J. Nutr. Biochem.* 15, 316–322. doi: 10.1016/j.jnutbio.2004.02.004

Besold, A. N., Culbertson, E. M., and Culotta, V. C. (2016). The Yin and Yang of copper during infection. *J. Biol. Inorg. Chem.* 21, 137–144. doi: 10.1007/s00775-016-1335-1

Cai, Z., Du, W., Liu, L., Pan, D., and Lu, L. (2019). Molecular characteristics of the conserved *Aspergillus nidulans* transcription factor mac1 and its functions in response to copper starvation. *mSphere* 4:e00670-18.

Cai, Z., Du, W., Zeng, Q., Long, N., Dai, C., and Lu, L. (2017). Cu-sensing transcription factor Mac1 coordinates with the Ctr transporter family to regulate Cu acquisition and virulence in *Aspergillus fumigatus*. *Fungal Genet. Biol.* 107, 31–43. doi: 10.1016/j.fgb.2017.08.003

Clifford, R. J., Maryon, E. B., and Kaplan, J. H. (2016). Dynamic internalization and recycling of a metal ion transporter: Cu homeostasis and CTR1, the human Cu(+) uptake system. *J. Cell Sci.* 129, 1711–1721. doi: 10.1242/jcs.173351

Clutterbuck, A. J. (1990). The genetics of conidiophore pigmentation in *Aspergillus nidulans*. *J. Gen. Microbiol.* 136, 1731–1738. doi: 10.1099/00221287-136-9-1731

Culotta, V. C., Howard, W. R., and Liu, X. F. (1994). CRS5 encodes a metallothionein-like protein in *Saccharomyces cerevisiae*. *J. Biol. Chem.* 269, 25295–25302.

Dancis, A., Haile, D., Yuan, D. S., and Klausner, R. D. (1994). The Saccharomyces cerevisiae copper transport protein (Ctr1p). Biochemical characterization, regulation by copper, and physiologic role in copper uptake. *J. Biol. Chem.* 269, 25660–25667.

De Feo, C. J., Aller, S. G., Siluvai, G. S., Blackburn, N. J., and Unger, V. M. (2009). Three-dimensional structure of the human copper transporter hCTR1. *Proc. Natl. Acad. Sci. U.S.A* 106, 4237–4242. doi: 10.1073/pnas.0810286106

Ding, C., Yin, J., Tovar, E. M., Fitzpatrick, D. A., Higgins, D. G., and Thiele, D. J. (2011). The copper regulon of the human fungal pathogen *Cryptococcus neoformans* H99. *Mol. Microbiol.* 81, 1560–1576. doi: 10.1111/j.1365-2958.2011.07794.x

Dong, K., Addinall, S. G., Lydall, D., and Rutherford, J. C. (2013). The yeast copper response is regulated by DNA damage. *Mol. Cell Biol.* 33, 4041–4050. doi: 10.1128/mcb.00116-13

Eisses, J. F., and Kaplan, J. H. (2002). Molecular characterization of hCTR1, the human copper uptake protein. *J. Biol. Chem.* 277, 29162–29171. doi: 10.1074/jbc.m203652200

Fridovich, I. (1983). Superoxide radical: an endogenous toxicant. *Annu. Rev. Pharmacol. Toxicol.* 23, 239–257. doi: 10.1146/annurev.pa.23.040183.001323

Garzia, A., Etxebeste, O., Rodriguez-Romero, J., Fischer, R., Espeso, E. A., and Ugalde, U. (2013). Transcriptional changes in the transition from vegetative cells to asexual development in the model fungus *Aspergillus nidulans*. *Eukaryot. Cell* 12, 311–321. doi: 10.1128/ec.00274-12

Georgatsou, E., Mavrogiannis, L. A., Fragiadakis, G. S., and Alexandraki, D. (1997). The yeast Fre1p/Fre2p cupric reductases facilitate copper uptake and are regulated by the copper-modulated Mac1p activator. *J. Biol. Chem.* 272, 13786–13792. doi: 10.1074/jbc.272.21.13786

Hermann, T. E., Kurtz, M. B., and Champe, S. P. (1983). Laccase localized in hulle cells and cleistothecial primordia of *Aspergillus nidulans*. *J. Bacteriol.* 154, 955–964. doi: 10.1128/jb.154.2.955-964.1983

Hervas-Aguilar, A., and Penalva, M. A. (2010). Endocytic machinery protein SlaB is dispensable for polarity establishment but necessary for polarity maintenance in hyphal tip cells of *Aspergillus nidulans*. *Eukaryot. Cell* 9, 1504–1518. doi: 10.1128/ec.00119-10

Holdom, M. D., Hay, R. J., and Hamilton, A. J. (1996). The Cu, Zn superoxide dismutases of *Aspergillus flavus*, *Aspergillus niger*, *Aspergillus nidulans*, and *Aspergillus terreus*: purification and biochemical comparison with the *Aspergillus fumigatus* Cu, Zn superoxide dismutase. *Infect. Immun.* 64, 3326–3332. doi: 10.1128/iai.64.8.3326-3332.1996

Kafer, E. (1965). Origins of translocations in *Aspergillus nidulans*. *Genetics* 52, 217–232.

Keller, G., Bird, A., and Winge, D. R. (2005). Independent metalloregulation of Ace1 and Mac1 in *Saccharomyces cerevisiae*. *Eukaryot. Cell* 4, 1863–1871. doi: 10.1128/ec.4.11.1863-1871.2005

Kikuma, T., Arioka, M., and Kitamoto, K. (2007). Autophagy during conidiation and conidial germination in filamentous fungi. *Autophagy* 3, 128–129. doi: 10.4161/auto.3560

Knight, S. A., Labbe, S., Kwon, L. F., Kosman, D. J., and Thiele, D. J. (1996). A widespread transposable element masks expression of a yeast copper transport gene. *Genes Dev.* 10, 1917–1929. doi: 10.1101/gad.10.15.1917

Kusuya, Y., Hagiwara, D., Sakai, K., Yaguchi, T., Gonoi, T., and Takahashi, H. (2017). Transcription factor Afmac1 controls copper import machinery in *Aspergillus fumigatus*. *Curr. Genet.* 63, 777–789. doi: 10.1007/s00294-017-0681-z

Labbe, S., Zhu, Z., and Thiele, D. J. (1997). Copper-specific transcriptional repression of yeast genes encoding critical components in the copper transport pathway. *J. Biol. Chem.* 272, 15951–15958. doi: 10.1074/jbc.272.25.15951

Lee, J., Pena, M. M., Nose, Y., and Thiele, D. J. (2002). Biochemical characterization of the human copper transporter Ctr1. *J. Biol. Chem.* 277, 4380–4387. doi: 10.1074/jbc.m104728200

Lekeux, G., Laurent, C., Joris, M., Jadou, A., Jiang, D., and Bosman, B. (2018). di-Cysteine motifs in the C-terminus of plant HMA4 proteins confer nanomolar affinity for zinc and are essential for HMA4 function in vivo. *J. Exp. Bot.* 69, 5547–5560.

Levitin, A., and Whiteway, M. (2007). The effect of prostaglandin E2 on transcriptional responses of *Candida albicans*. *Microbiol. Res.* 162, 201–210. doi: 10.1016/j.micres.2007.02.001

Li, C., Li, Y., and Ding, C. (2019). The role of copper homeostasis at the host-pathogen axis: from bacteria to fungi. *Int. J. Mol. Sci.* 20:175. doi: 10.3390/ijms20010175

Lin, S. J., and Culotta, V. C. (1995). The ATX1 gene of *Saccharomyces cerevisiae* encodes a small metal homeostasis factor that protects cells against reactive oxygen toxicity. *Proc. Natl. Acad. Sci. U.S.A* 92, 3784–3788. doi: 10.1073/pnas.92.9.3784

Lin, S. J., Pufahl, R. A., Dancis, A., O'Halloran, T. V., and Culotta, V. C. (1997). A role for the *Saccharomyces cerevisiae* ATX1 gene in copper trafficking and iron transport. *J. Biol. Chem.* 272, 9215–9220.

Liu, L., Qi, J., Yang, Z., Peng, L., and Li, C. (2012). Low-affinity copper transporter CTR2 is regulated by copper-sensing transcription factor Mac1p in Saccharomyces cerevisiae. *Biochem. Biophys. Res. Commun.* 420, 600–604. doi: 10.1016/j.bbrc.2012.03.040

Liu, J., Sitaram, A., and Burd, C. G. (2007). Regulation of copper-dependent endocytosis and vacuolar degradation of the yeast copper transporter, Ctr1p, by the Rsp5 ubiquitin ligase. *Traffic* 8, 1375–1384. doi: 10.1111/j.1600-0854.2007.00616.x

Lutsenko, S. (2010). Human copper homeostasis: a network of interconnected pathways. *Curr. Opin. Chem. Biol.* 14, 211–217. doi: 10.1016/j.cbpa.2010.01.003

Macomber, L., and Imlay, J. A. (2009). The iron-sulfur clusters of dehydratases are primary intracellular targets of copper toxicity. *Proc. Natl. Acad. Sci. U.S.A* 106, 8344–8349. doi: 10.1073/pnas.0812808106

Markina-Inarrairaegui, A., Etxebeste, O., Herrero-Garcia, E., Araujo-Bazan, L., Fernandez-Martinez, J., Flores, J. A., et al. (2011). Nuclear transporters in a multinucleated organism: functional and localization analyses in *Aspergillus nidulans*. *Mol. Biol. Cell* 22, 3874–3886. doi: 10.1091/mbc.e11-03-0262

Markina-Inarrairaegui, A., Pantazopoulou, A., Espeso, E. A., and Penalva, M. A. (2013). The *Aspergillus nidulans* peripheral ER: disorganization by ER stress and persistence during mitosis. *PLoS One* 8:e67154. doi: 10.1371/journal.pone.0067154

Nevitt, T., Ohrvik, H., and Thiele, D. J. (2012). Charting the travels of copper in eukaryotes from yeast to mammals. *Biochim. Biophys. Acta* 1823, 1580–1593. doi: 10.1016/j.bbamcr.2012.02.011

Park, Y. S., Kim, J. H., Cho, J. H., Chang, H. I., Kim, S. W., Paik, H. D., et al. (2007). Physical and functional interaction of FgFtr1-FgFet1 and FgFtr2-FgFet2 is required for iron uptake in *Fusarium graminearum*. *Biochem. J.* 408, 97–104. doi: 10.1042/bj20070450

Park, Y. S., Lian, H., Chang, M., Kang, C. M., and Yun, C. W. (2014). Identification of high-affinity copper transporters in *Aspergillus fumigatus*. *Fungal Genet. Biol.* 73, 29–38. doi: 10.1016/j.fgb.2014.09.008

Pena, M. M., Koch, K. A., and Thiele, D. J. (1998). Dynamic regulation of copper uptake and detoxification genes in *Saccharomyces cerevisiae*. *Mol. Cell Biol.* 18, 2514–2523. doi: 10.1128/mcb.18.5.2514

Pena, M. M., Puig, S., and Thiele, D. J. (2000). Characterization of the Saccharomyces cerevisiae high affinity copper transporter Ctr3. *J. Biol. Chem.* 275, 33244–33251. doi: 10.1074/jbc.m005392200

Penalva, M. A. (2005). Tracing the endocytic pathway of *Aspergillus nidulans* with FM4-64. *Fungal Genet. Biol.* 42, 963–975. doi: 10.1016/j.fgb.2005.09.004

Petris, M. J. (2004). The SLC31 (Ctr) copper transporter family. *Pflugers. Arch.* 447, 752–755. doi: 10.1007/s00424-003-1092-1

Pontecorvo, G., Roper, J. A., Hemmons, L. M., Macdonald, K. D., and Bufton, A. W. (1953). The genetics of *Aspergillus nidulans*. *Adv. Genet.* 5, 141–238.

Puig, S., Lee, J., Lau, M., and Thiele, D. J. (2002). Biochemical and genetic analyses of yeast and human high affinity copper transporters suggest a conserved mechanism for copper uptake. *J. Biol. Chem.* 277, 26021–26030. doi: 10.1074/jbc.m202547200

Qi, J., Han, A., Yang, Z., and Li, C. (2012). Metal-sensing transcription factors Mac1p and Aft1p coordinately regulate vacuolar copper transporter *CTR2* in *Saccharomyces* cerevisiae. *Biochem. Biophys. Res. Commun.* 423, 424–428. doi: 10.1016/j.bbrc.2012.05.150

Rees, E. M., and Thiele, D. J. (2004). From aging to virulence: forging connections through the study of copper homeostasis in eukaryotic microorganisms. *Curr. Opin. Microbiol.* 7, 175–184. doi: 10.1016/j.mib.2004.02.004

Richie, D. L., Fuller, K. K., Fortwendel, J., Miley, M. D., McCarthy, J. W., Feldmesser, M., et al. (2007). Unexpected link between metal ion deficiency and autophagy in *Aspergillus fumigatus*. *Eukaryot. Cell* 6, 2437–2447. doi: 10.1128/ec.00224-07

Rodrigues, M. L. (2018). The multifunctional fungal ergosterol. *mBio* 9:e01755-18.

Rutherford, J. C., and Bird, A. J. (2004). Metal-responsive transcription factors that regulate iron, zinc, and copper homeostasis in eukaryotic cells. *Eukaryot. Cell* 3, 1–13. doi: 10.1128/ec.3.1.1-13.2004

Scherer, M., and Fischer, R. (2001). Molecular characterization of a blue-copper laccase, TILA, of *Aspergillus nidulans*. *FEMS Microbiol. Lett.* 199, 207–213. doi: 10.1111/j.1574-6968.2001.tb10676.x

Scherer, M., Wei, H., Liese, R., and Fischer, R. (2002). Aspergillus nidulans catalase-peroxidase gene (cpeA) is transcriptionally induced during sexual development through the transcription factor StuA. *Eukaryot. Cell* 1, 725–735. doi: 10.1128/ec.1.5.725-735.2002

Schrettl, M., Beckmann, N., Varga, J., Heinekamp, T., Jacobsen, I. D., Jöchl, C., et al. (2010). HapX-mediated adaption to iron starvation is crucial for virulence of *Aspergillus fumigatus*. *PLoS Pathog.* 6:e1001124. doi: 10.1371/journal.ppat.1001124

Schrettl, M., Bignell, E., Kragl, C., Joechl, C., Rogers, T., Arst, H. N., et al. (2004). Siderophore biosynthesis but not reductive iron assimilation is essential for *Aspergillus fumigatus* virulence. *J. Exp. Med.* 200, 1213–1219. doi: 10.1084/jem.20041242

Schuller, A., Auffermann, G., Zoschke, K., Schmidt, U., Ostermann, K., and Rodel, G. (2013). Overexpression of ctr1Delta300, a high-affinity copper transporter with deletion of the cytosolic C-terminus in *Saccharomyces cerevisiae* under excess copper, leads to disruption of transition metal homeostasis and transcriptional remodelling of cellular processes. *Yeast* 30, 201–218. doi: 10.1002/yea.2953

Smith, A. D., Logeman, B. L., and Thiele, D. J. (2017). Copper acquisition and utilization in fungi. *Annu. Rev. Microbiol.* 71, 597–623. doi: 10.1146/annurev-micro-030117-020444

Sugui, J. A., Kim, H. S., Zarember, K. A., Chang, Y. C., Gallin, J. I., Nierman, W. C., et al. (2008). Genes differentially expressed in conidia and hyphae of *Aspergillus fumigatus* upon exposure to human neutrophils. *PLoS One* 3:e2655. doi: 10.1371/journal.pone.0002655

Suh, J. K., Poulsen, L. L., Ziegler, D. M., and Robertus, J. D. (2000). Redox regulation of yeast flavin-containing monooxygenase. *Arch. Biochem. Biophys.* 381, 317–322. doi: 10.1006/abbi.2000.1965

Sutton, H. C., and Winterbourn, C. C. (1989). On the participation of higher oxidation states of iron and copper in Fenton reactions. *Free Radic. Biol. Med.* 6, 53–60. doi: 10.1016/0891-5849(89)90160-3

Timoshnikov, V. A., Kobzeva, T., Selyutina, O. Y., Polyakov, N. E., and Kontoghiorghes, G. J. (2019). Effective inhibition of copper-catalyzed production of hydroxyl radicals by deferiprone. *J. Biol. Inorg. Chem.* 24, 331–341. doi: 10.1007/s00775-019-01650-9

Vesely, E. M., Williams, R. B., Konopka, J. B., and Lorenz, M. C. (2017). N-acetylglucosamine metabolism promotes survival of *Candida albicans* in the phagosome. *mSphere* 2:e00357-17.

Walton, F. J., Idnurm, A., and Heitman, J. (2005). Novel gene functions required for melanization of the human pathogen *Cryptococcus neoformans*. *Mol. Microbiol.* 57, 1381–1396. doi: 10.1111/j.1365-2958.2005.04779.x

Waterman, S. R., Park, Y. D., Raja, M., Qiu, J., Hammoud, D. A., O'Halloran, T. V., et al. (2012). Role of CTR4 in the virulence of *Cryptococcus neoformans*. *mBio* 3:e00285-12.

Wiemann, P., Albermann, S., Niehaus, E. M., Studt, L., von Bargen, K. W., Brock, N. L., et al. (2012). The Sfp-type 4'-phosphopantetheinyl transferase Ppt1 of *Fusarium fujikuroi* controls development, secondary metabolism and pathogenicity. *PLoS One* 7:e37519. doi: 10.1371/journal.pone.0037519

Wiemann, P., Perevitsky, A., Lim, F. Y., Shadkchan, Y., Knox, B. P., Landero Figueora, J. A., et al. (2017). *Aspergillus fumigatus* copper export machinery and reactive oxygen intermediate defense counter host copper-mediated oxidative antimicrobial offense. *Cell. Rep.* 19, 2174–2176. doi: 10.1016/j.celrep.2017.05.075

Wu, X., Sinani, D., Kim, H., and Lee, J. (2009). Copper transport activity of yeast Ctr1 is down-regulated via its C terminus in response to excess copper. *J. Biol. Chem.* 284, 4112–4122. doi: 10.1074/jbc.m807909200

Yamaguchi-Iwai, Y., Serpe, M., Haile, D., Yang, W., Kosman, D. J., Klausner, R. D., et al. (1997). Homeostatic regulation of copper uptake in yeast via direct binding of MAC1 protein to upstream regulatory sequences of FRE1 and CTR1. *J. Biol. Chem.* 272, 17711–17718. doi: 10.1074/jbc.272.28.17711

Yang, L., Ukil, L., Osmani, A., Nahm, F., Davies, J., De Souza, C. P., et al. (2004). Rapid production of gene replacement constructs and generation of a green fluorescent protein-tagged centromeric marker in *Aspergillus nidulans*. *Eukaryot. Cell* 3, 1359–1362. doi: 10.1128/ec.3.5.1359-1362.2004

Zamocky, M., Furtmuller, P. G., and Obinger, C. (2008). Evolution of catalases from bacteria to humans. *Antioxid. Redox. Signal.* 10, 1527–1548. doi: 10.1089/ars.2008.2046

Zhang, P., Zhang, D., Zhao, X., Wei, D., Wang, Y., and Zhu, X. (2016). Effects of CTR4 deletion on virulence and stress response in *Cryptococcus neoformans*. *Antonie Van Leeuwenhoek* 109, 1081–1090. doi: 10.1007/s10482-016-0709-2

Zhou, H., Cadigan, K. M., and Thiele, D. J. (2003). A copper-regulated transporter required for copper acquisition, pigmentation, and specific stages of development in *Drosophila melanogaster*. *J. Biol. Chem.* 278, 48210–48218. doi: 10.1074/jbc.m309820200

Zhu, Z., Labbe, S., Pena, M. M., and Thiele, D. J. (1998). Copper differentially regulates the activity and degradation of yeast Mac1 transcription factor. *J. Biol. Chem.* 273, 1277–1280. doi: 10.1074/jbc.273.3.1277

Copper Resistance in *Aspergillus nidulans* Relies on the P$_I$-Type ATPase CrpA, Regulated by the Transcription Factor AceA

Martzel Antsotegi-Uskola, Ane Markina-Iñarrairaegui * and Unai Ugalde

Microbial Biochemistry Laboratory, Department of Applied Chemistry, Faculty of Chemistry, University of the Basque Country, San Sebastian, Spain

Copper homeostasis has been extensively studied in mammals, bacteria, and yeast, but it has not been well-documented in filamentous fungi. In this report, we investigated the basis of copper tolerance in the model fungus *Aspergillus nidulans*. Three genes involved in copper homeostasis have been characterized. First, *crpA* the *A. nidulans* ortholog of *Candida albicans CaCRP1* gene encoding a P$_I$-type ATPase was identified. The phenotype of *crpA* deletion led to a severe sensitivity to Cu^{+2} toxicity and a characteristic morphological growth defect in the presence of high copper concentration. CrpA displayed some promiscuity regarding metal species response. The expression pattern of *crpA* showed an initial strong elevation of mRNA and a low continuous gene expression in response to long term toxic copper levels. Coinciding with maximum protein expression level, CrpA was localized close to the cellular surface, however protein distribution across diverse organelles suggests a complex regulated trafficking process. Secondly, *aceA* gene, encoding a transcription factor was identified and deleted, resulting in an even more extreme copper sensitivity than the ∆crpA mutant. Protein expression assays corroborated that AceA was necessary for metal inducible expression of CrpA, but not CrdA, a putative metallothionein the function of which has yet to be elucidated.

Keywords: copper resistance, *Aspergillus nidulans*, copper homeostasis, P$_I$-type ATPase, transcription factor, metallothionein

INTRODUCTION

Copper (Cu) is an essential trace element that functions as cofactor of enzymes involved in a wide range of biochemical processes including cellular respiration (cytochrome-c oxidase), free radical detoxification (superoxide dismutase), pigmentation (tyrosinase), and collagen maturation (lysyl oxidase; Lutsenko, 2010; Nevitt et al., 2012). However, excess accumulation of copper promotes the generation of hydroxyl radicals that induce severe cellular damage (Halliwell and Gutteridge, 1990; Valko et al., 2005). Copper toxicity can also be triggered by displacement of other metals present in molecules leading to protein dysfunction (Macomber and Imlay, 2009; Lemire et al., 2013).

Because environmental copper availability may fluctuate in ecological niches (soil, pollutants, etc.), all biological systems have developed homeostatic mechanisms that sense copper levels and respond in order to maintain adequate cellular concentrations within the required threshold levels. To ensure this balance, cells tightly control copper uptake, cellular traffic, storage, and detoxification (reviewed in Nevitt et al., 2012).

In the model organism *Saccharomyces cerevisiae,* elevated environmental copper concentrations (>1 μM) result in a copper-dependent inactivation of the transcription factor (TF) ScMac1p (Graden and Winge, 1997). In consequence, the genes coding proteins implicated in copper uptake, two high affinity Cu^+ transporters (ScCtr1p and ScCtr3p) and a surface Cu^{+2}-metalloreductase (ScFre1p), are down-regulated (Graden and Winge, 1997; Labbé et al., 1997; Nevitt et al., 2012). Copper has the opposite effect on the transcriptional factor ScAce1p (Keller et al., 2005; Ehrensberger and Bird, 2011). Formation of a tetra-copper cluster in the regulatory domain of the TF results in a conformational change that leads to the activation of the inactive Apo-ScAce1p (Furst et al., 1988). As a result, ScAce1p is capable to bind the promoters and induce the expression of detoxification genes, *ScCUP1* and *ScCRS5*, which encode two Cu-metallothioneins (MTs; Thiele, 1988; Culotta et al., 1994). Metallothioneins, cysteine (C)-rich low molecular weight polypeptides characterized by high-affinity for diverse metals (Cu, Zn, Cd, Hg, etc.), are found in all eukaryotes and some prokaryotes (Balamurugan and Schaffner, 2006; Sutherland and Stillman, 2011). These proteins are induced in response to exposure to metals, buffering them and lowering their intracellular concentrations.

Other known intracellular copper level regulators are the *P*-type ATPases, which are heavy-metal translocators conserved through all biological kingdoms. These copper extrusion pumps are the major copper resistance determinant in bacteria (Odermatt et al., 1993; Solioz and Odermatt, 1995; Ladomersky and Petris, 2015), while in eukaryotes, in general, they are involved in copper compartmentalization into the secretory network for the subsequent metallation of newly synthesized Cu-dependent enzymes. In humans, hATP7A (MNK, Menkes disease protein) and hATP7B (WND, Wilson disease protein) copper ATPases carry out both, copper delivering and detoxification functions. At basal Cu conditions hATP7A and hATP7B deliver copper to cuproenzymes in the *trans*-Golgi compartment (TGN; Lutsenko et al., 2007) but in response to Cu level increase, ATPase pumps traffic from the TGN to the cell surface in order to efflux copper out of the cytoplasm, thus increasing resistance of cells to this transition metal (Petris et al., 1996; Suzuki and Gitlin, 1999). In contrast, in *Candida albicans,* each function is achieved by different P_I-type ATPases; CaCcc2p is involved in cuproenzyme biosynthesis (Weissman et al., 2002) while CaCrp1p is committed to copper export (Riggle and Kumamoto, 2000; Weissman et al., 2000). Indeed, CaCrp1p is mainly responsible for the unusual high copper tolerance of this dimorphic yeast, in contrast to other eukaryotes were copper detoxification relies significantly on MTs. Recently, it has been shown in *A. fumigatus* that histidine is also involved in copper detoxification (Dietl et al., 2016).

The great majority of studies in copper homeostasis have focused on mammalian, bacteria, and yeast cells, but not in filamentous fungi, a major group of microorganisms which includes species of agricultural, food, clinical and environmental interest. *Aspergillus nidulans* is one of the best characterized fungal species and offers the opportunity to study in detail the precise mechanisms involved in Cu balance. The present report describes the identification and characterization of the major copper resistance determinant in *A. nidulans*, the copper transporting P_I-type ATPase, CrpA. We show that CrpA expression is highly inducible and dynamic in response to prolonged copper exposure and localizes close to the cellular surface as a result of an organized trafficking process. In addition, we demonstrate that metal-dependent induction of CrpA is under the control of AceA, a transcription factor activator of genes involved in copper detoxification. A third gene encoding a metallothionein-like protein has been identified, CrdA, although further studies are needed to elucidate its function. Our results indicate that copper detoxification in *A. nidulans*, as in the dimorphic fungus *C. albicans,* relies mainly in copper excretion.

MATERIALS AND METHODS

Bioinformatic

Alignments were performed using the predicted protein sequences released in the National Centre for Biotechnology Information (NCBI) database. Multiple sequence alignments were performed using BLAST and Clustal Omega application in EBI (http://www.ebi.ac.uk/Tools/msa/clustalomega/). Alignments visualization and domain analysis were performed with Jalview program. Transmembrane domains were predicted using Hidden Markov Models (HMM) in the Institute Pasteur Mobyle server (http://mobyle.pasteur.fr/).

Strains, Media, and Growth Conditions

A. nidulans strains used in this study are listed in **Table 1**. Strain MAD1427 was used as a recipient for transformation and generation of single/double-null and GFP/HA$_3$-tagged strains. Appropriately supplemented Käfer's minimal (MMA) and complete (CMA) pH 6.8 buffered medium (Käfer, 1965) containing 1% (w/v) D-glucose and 71 mM sodium nitrate as main carbon and nitrogen source was used to cultivate *A. nidulans*. Liquid culture experiments were conducted with MMA without agar (liquid MMA). General molecular techniques followed (Sambrook et al., 1989).

Colony growth tests were carried out by inoculating conidiospores on solid MMA and incubating for 48 h at 37°C. Phenotypes caused by the deletion of genes were studied under an array of metal stresses induced by addition of CuSO$_4$ (50, 100, 150, 200, 400, 600 and 1000 μM), AgNO$_3$ (2.5 and 5 μM) and Cd(NO$_3$)$_2$ (100, 150, and 250 μM). Radial extension and colony morphology of mutant strains was always compared with that of the wild-type MAD1427 strain. Close-up views of colonies grown for 36, 48, and 72 h at 37°C were observed and photographed with a binocular microscope (Nikon SMZ800).

To quantify the effect of CuSO$_4$, AgNO$_3$, and Cd(NO$_3$)$_2$, on biomass production liquid culture experiments were carried out. 1.10^6 spores were inoculated in liquid MMA (30 ml medium in 100 ml flask) with or without metal agents and incubated for 24 h at 37°C in a rotary incubator at 200 rpm. The cultures were collected, dried for 24 h at 100°C, and their dry weight measured. Three technical replicates were performed. Two-tailed Student's *t*-test for unpaired samples was used for the statistical analysis to compare the cellular growth between two strains in different conditions.

RNA and protein extracts were isolated from mycelium of strains cultivated in a fermenter for 16 h at 37°C. Cells were harvested before (0 min) and after adding the metal agent to fresh MMA and incubating for the period indicated in the figures. Mycelia was collected by filtration through Miracloth (Calbiochem), squeezed to dry and frozen in liquid nitrogen. Samples for protein extraction were lyophilized for 16 h.

Generation of Null and Tagged Strains

Genomic cassettes for the generation of strains carrying null alleles and GFP or HA$_3$ C-terminally tagged fusion proteins were constructed following fusion-PCR technique described in Markina-Iñarrairaegui et al. (2011). Null mutants were generated by using deletion cassettes containing the *Aspergillus fumigatus pyrG* or *riboB* as prototrophic selection marker flanked by 1,500 bp of 5′ UTR and 3′ UTR regions of the target gene. Firstly, each fragment was amplified using specific oligonucleotide pairs; gsp1–gsp2 (5′ UTR), gsp3–gsp4 (3′ UTR), and gsp2∗–gsp3∗ (selectable marker). The gsp2∗, gsp3∗, and gsp6∗ (see below) hold, in addition of the selectable marker sequence, a 24 bp tail homologous to the gsp2, gsp3, and gsp6 gene specific primers. The fragments containing the selectable marker were amplified using a plasmid as a template. Afterwards, the three fragments were fused using gsp1-gsp4 primers. For the C-terminal tagging *ha$_3$::pyrG^{Af}* and *gfp::riboB^{Af}* fragments, the 3′ end (∼1,500 bp) of the gene and the 3′ UTR regions were amplified using oligonucleotides gsp6∗–gsp3∗, gsp5–gsp6, and gsp3–gsp4, respectively. Finally, the tagging cassettes were constructed using gsp5 and gsp4 oligonucleotides to fuse the fragments. Oligonucleotides used in this study are summarized in **Table 2**.

The *A. nidulans* transformation procedure followed in this study is an adaptation of the transformable protoplasts production protocol described in Szewczyk et al. (2006) and the protoplast transformation protocol described by Tilburn et al. (1983). The purified genomic casettes obtained above were used to transform *A. nidulans*. Between 7 and 15 transformants were obtained in each regeneration plate (4 plates/transformation). Among the *pyrG$^+$* and *riboB$^+$* transformants, Southern blot technique was used in order to identify homokaryotic recombinant strains carrying a single-copy integration event. Of the initially screened 4 transformants, 2 verified clones were characterized in this study. The double-null

TABLE 1 | *Aspergillus nidulans* strains used in this study.

Strains	Genotype	References
MAD1427	*pyrG89, pabaA1; argB2; ΔnkuA::argB; veA1, riboB2*	TN02A25 Oakley B.
MAD2731	*pabaA1; argB2; ΔnkuA::argB; veA1, riboB2*	Markina-Iñarrairaegui et al., 2011
MAD2733	*pabaA1; argB2; ΔnkuA::argB; veA1*	Markina-Iñarrairaegui et al., 2011
BD888	*pyrG89, pabaA1; argB2; ΔnkuA::argB; ΔcrpA::pyrG^{Af}; veA1, riboB2*	This study
BD892	*pyrG89, pabaA1; argB2; ΔnkuA::argB; crpA::gfp::riboB^{Af}; veA1, riboB2*	This study
BD894	*pyrG89, pabaA1; argB2; ΔnkuA::argB; crpA::ha$_3$::pyrG^{Af}; veA1, riboB2*	This study
BD896	*pyrG89, pabaA1; argB2; crdA::ha$_3$::pyrG^{Af}, ΔnkuA::argB; ΔcrpA::riboB^{Af}; veA1, riboB2*	This study
BD898	*pyrG89, pabaA1; argB2; ΔcrdA::pyrG^{Af}, ΔnkuA::argB; veA1, riboB2*	This study
BD900	*pyrG89, pabaA1; argB2; crdA::ha$_3$::pyrG^{Af}, ΔnkuA::argB; veA1, riboB2*	This study
BD961	*pyrG89, pabaA1; argB2; ΔnkuA::argB; crpA::ha$_3$::pyrG^{Af}; ΔaceA::riboB^{Af}; veA1, riboB2*	This study
BD963	*pyrG89, pabaA1; argB2; ΔcrdA::pyrG^{Af}, ΔnkuA::argB; ΔcrpA::riboB^{Af}; veA1, riboB2*	This study
BD965	*pyrG89, pabaA1; argB2; ΔnkuA::argB; ΔaceA::pyrG^{Af}; veA1, riboB2*	This study
BD1062	*pyrG89, pabaA1; argB2; crdA::ha$_3$::pyrG^{Af}, ΔnkuA::argB; ΔaceA::riboB^{Af}; veA1, riboB2*	This study
BD1073	*pyrG89, pabaA1; argB2; ΔnkuA::argB; crpA^{An} (ΔcrpA::pyrG^{Af}); veA1, riboB2*	This study

TABLE 2 | Oligonucleotides used in this study.

Oligo	Sequence (5′–3′)
CrpA-gsp1	CGTACATGGGTCTGGTCTTCCCC
CrpA-gsp2	GACGAGTGGCGGCTAGTGTTCC
CrpA-gsp3	TTATTTTTTTCTAGTTCCATGCATGC
CrpA-gsp4	CCCTGAGCAGTCTCGATGAG
CrpA-gsp5	CTTCAGCGGGTCGCAGATACG
CrpA-gsp6	CTCCTGTTGACGCGTAGTCCGG
CrpA-gsp2*	GGAACACTAGCCGCCACTCGTCACCGGTCGCCTCAA ACAATGCTCTTCA
CrpA-gsp3*	CATCGCATGCATGGAACTAGAAAAAAATAACTGTCTG AGAGGAGGCACTGATGC
CrpA-gsp6*	CCGGACTACGCGTCAACAGGAGGGAGCTGGTGCA GGCGCTGGAGCC
CrdA-gsp1	GGCTTCGAGAACTACCAGAACC
CrdA-gsp2	ATTGAATGTTGTTTGAATGGTAG
CrdA-gsp3	TGCGTTTGAATTCATGTTAATGAAGC
CrdA-gsp4	CCAATCCGAGGTCGAGTACG
CrdA-gsp5	ATGGTTCACCCCACCTCAACCTGCT
CrdA-gsp6	AGCCTTGGCCGTCGTAAAATCTGTCTC
CrdA-gsp2*	CTACCATTCAAACAACATTCAATACCGGTCGCCTCA AACAATGCTCT
CrdA-gsp3*	GCTTCATTAACATGAATTCAAACGCACTGTCTGAGAGG AGGCACTGATG
CrdA-gsp6*	GAGACAGATTTTACGACGGCCAAGGCTGGAGCTGGTG CAGGCGCTGGAGC
AceA-gsp1	CCGATGATTCCTTCCACTGCCCAGACATAC
AceA-gsp2	CGCCGCGGTTACTGGGATTGGCACATG
AceA-gsp3	GGACAGCAAGGGCCTTAGAATCTT
AceA-gsp4	ATACAAATAGAGAGGCGAAGGAATGGCG
AceA-gsp2*	CATGTGCCAATCCCAGTAACCGCGGCGACCGGTCGCCT CAAACAATGCTCT
AceA-gsp3*	AAGATTCTAAGGCCCTTGCTGTCCCTGTCTGAGAG GAGGCACTGAT

mutant and strains combining a null allele and HA$_3$-tagged protein were generated by step-by-step transformation with each fusion genomic cassette.

Revertant strain construction was achieved by transforming the null *crpA* strain (BD888) with a DNA cassette containing the *crpA* gene flanked by 1,500 bp up and downstream the corresponding ORF. gsp1 and gsp4 oligonucleotides were used to amplify the cassette using a WT strain genomic DNA as a template. Transformants containing the replacement of the null locus were selected by the ability to resist the 2 mg/ml 5-fluoro-orotic acid (5-FOA; Apollo Scientific, Stockport, United Kingdom) that was added in the medium.

RNA Isolation and Northern Blot

Total RNA was isolated using TRIzol reagent following the Invitrogen protocol (Invitrogen, Carlsbad, CA) as described in Garzia et al. (2013) and RNA concentration was calculated using a Nanodrop 2000 c system (Thermo Fisher Scientific, Waltham, MA). Ten micrograms of total RNA were loaded in 1.2% agarose gels, transferred to positively charged nylon filters, and analyzed by Northern blot which was carried out with a digoxigenin Northern starter kit (Roche) essentially following manufacturer's instructions and using the hybridization solution (1% BSA, 1 mM EDTA, 0.5 M NaPO$_4$, pH = 7.2, and 7% SDS; Church and Gilbert, 1984). Transcript of *crpA* was detected using a genomic probe amplified by PCR using oligonucleotides gsp5 and gsp6 listed in **Table 2**. Labeling of the probe was performed using DIG High Prime DNA Labeling Starter Kit (Roche) and covered 43% of the ORF. Equal loading of total RNA, which was used as internal control for normalization, was evaluated by ethidium bromide staining of rRNA. Digoxigenin bound probe was detected using CSDP (Roche) in a Chemidoc + XRS (Bio-Rad) system. Intensity of chemiluminescence signal of bands was measured with Image Lab 3.0 software (Bio-Rad).

Protein Isolation and Western Blot

Protein extraction from lyophilized samples was performed by two different methods. The alkaline-lysis extraction (AL) procedure was used for CrpA extraction, using Lysis buffer (0.2 M NaOH, 0.2% β-mercaptoethanol), as described in Hervás-Aguilar and Peñalva (2010). Protein concentration of extract was estimated loading 5 μl of each sample on polyacrylamide gels. CrdA was extracted as described in Drubin et al. (1988) using Drubin buffer (5 mM HEPES pH 7.5, 1 mM EDTA, 20 mM KCl, 0.1% NP-40, 0.5 mM DTT) supplemented with EDTA-free protease-inhibitor cocktail tablets (1 tablet/50 ml of buffer; Roche). Protein quantification was carried out by Bradford assay (Bradford, 1976) using Bradford dye reagent (Alfa Aesar) and following manufacturer's instructions 12.5 μg of total protein samples were loaded on gels.

Tagged protein expression was analyzed by Western blotting. Proteins were resolved in 8% (CrpA-HA$_3$) or 12% (CrdA-HA$_3$) SDS-polyacrylamide gels and electrotransfered to Immun-Blot® PVDF membranes by TransBlot® Turbo™ Transfer System (Bio-Rad). HA$_3$-tagged proteins were detected using anti-HA mouse antibody [1/10,000 (v/v) dilution for tagged CrpA and 1/1,000 for tagged CrdA detection; Santa Cruz

Biotechnology] and CrpA-GFP with mouse anti-GFP (1/5,000; Roche). Hexokinase, used as loading control, was detected with anti-hexokinase rabbit antibody (1/30,000; Chemicon Intemat Inc.). Peroxidase-conjugated goat anti-mouse IgG immunoglobulin (1/4,000 for CrpA and 1/2,500 for CrdA detection; Jackson Immunoresearch Lab) or donkey anti-rabbit (1/10,000; Sigma) cocktails were used as secondary antibodies. Peroxidase activity was detected using Clarity™ Western ECL Substrate (Bio-Rad). Chemiluminescence was observed using a Chemidoc + XRS system (Bio-Rad) and signal intensity was measured with Image Lab 3.0 software (Bio-Rad).

Fluorescence Microscopy

A. nidulans conidiospores were cultured in uncoated glass-bottom dishes (Ibidi GmbH, Germany; 2.5 ml of medium per well) for 16 h at 25°C in adequately supplemented pH 6.8 Käfer's minimal medium containing 0.1% D-glucose, 71 mM sodium nitrate and 25 mM sodium phosphate monobasic, similar to watch minimal medium (WMM; Peñalva, 2005). After this period, the medium was replaced with fresh medium supplemented with 100 μM CuSO$_4$ to induce CrpA-GFP expression.

Fluorescence images were acquired using a Zeiss Axio Observer Z1 inverted microscope equipped with a 63x Plan Apochromat 1.4 oil immersion Lens, Axiocam MRm Rev.3 camera, an Zeiss HXP 120C external light source for epifluorescence excitation and fitted with filter set 38HE for green fluorescence (Ex BP 470/40; FT 495; Em BP 525/50) and filter set 43HE for red fluorescence (Ex BP 545/25; FT 570; Em BP 605/70). Same exposure time and microscope settings were applied for all image acquirement. Numerous cells were observed for each time before taking representative images. Fluorescence levels were measured using ImageJ software (http://imagej.nih.gov/ij; U.S National Institutes of Health, Bethesda, Maryland, USA).

RESULTS

Identification of *Aspergillus nidulans* Genes Involved in Copper Homeostasis

In a RNA-seq experiment conducted in our lab (data not published) the expression of the AN3117 gene was significantly increased as a consequence of copper load. Blastp sequence analysis identified the 1,211 amino acid long protein encoded by AN3117 ORF (3,636 bp) as the putative ortholog of *C. albicans* copper-transporting P$_I$-type ATPase, CaCrp1p (Riggle and Kumamoto, 2000; Weissman et al., 2000). Based on sequence conservation (35% identity, 55% similarity, and 95% query cover) AN3117 was termed *crpA* (*copper resistance P-type ATPase*). The *A. nidulans* genome contains a second P$_I$-type ATPase coding gene, *ygA*, with high homology to CaCcc2p (37% identity; Weissman et al., 2002). YgA is predicted to transport Cu$^+$ to the secretory pathway and its absence results in conidial pigmentation impairment (Clutterbuck, 1990).

As shown in **Figure 1A**, bioinformatic analyses predicted in CrpA the presence of the distinctive domains described for well-studied copper-transporting ATPases of yeast, human,

FIGURE 1 | Sequence analysis of CrpA and CrdA. (A) Proposed two dimensional model of CrpA describing the predicted membrane topology and comparison of the conserved functional domains of P$_1$-type ATPases and their position among different species. GenBank accession numbers are given in parentheses: *Aspergillus nidulans* CrpA (CBF83376.1) and YgA (CBF75750.1); *Candida albicans* CaCrp1p (AAF78958.1) and CaCcc2p (XP_720761.1); *Saccharomyces cerevisieae* ScCcc2p (AAC37425.1); *Homo sapiens* Menkes disease protein hATP7A (AAA35580.1); *Escherichia coli* EcCopA (CDL39203.1); *Enterococcus hirae* EhCopA (AAA61835.1); *Legionella pneumophila* copper-translocating *P*-type ATPase (WP_010947353.1); *Archaeoglobus fulgidus* copper-exporting *P*-type ATPase AfCopA (KUJ93751.1). **(B)** Alignment of predicted full-length of CrdA and CaCrd2p sequences compared using Clustal method. Asterisks describe identical, *double* and *single dots*, conservative and semi-conservative residues, respectively. CxC repeats are boxed in light blue. Protein accession numbers are reported as follows: *Aspergillus nidulans* CrdA (CBF79264.1) and *Candida albicans* CaCrd2p (AAF78959.1).

bacteria and archaea (Solioz and Odermatt, 1995; Mandal et al., 2002; Barry et al., 2010; Rosenzweig and Argüello, 2012; Migocka, 2015; Smith et al., 2016; **Figure 1A**); 8 transmembrane domains (TM), a conserved CPC copper translocation motif placed in the 6th TM segment and cysteine rich metal binding motifs (MBD) in the cytoplasmic N-terminal. 5 N-MBD are predicted as tandem repeats, 2 CxxC motifs located closer to the amino terminus followed by 3 GMxCxxC classical heavy metal associated domains (HMA). This structure of Cu-binding domains in the NH$_2$-terminal extension is similar to *C. albicans* CaCrp1p (Riggle and Kumamoto, 2000; Weissman et al., 2000) but different from other homologs. In common with non-heavy metal P-type ATPases, CrpA shares characteristic features as an aspartyl kinase domain (DKTG) in a large cytoplasmic loop containing an aspartate residue that is transiently phosphorylated during the catalytic cycle, a phosphatase domain (TGES) and

a consensus domain for ATP binding and energy transduction (GDGVNDSP; Palmgren and Nissen, 2011; Inesi et al., 2014).

Earlier studies had shown that metallothioneins (MTs) play a significant role in copper tolerance. For this reason, *in silico* searches were carried out using *S. cerevisiae* (ScCup1p and ScCrs5p) and *C. albicans* (CaCup1p and CaCrd2p) sequences. Protein database searches revealed the existence of a single putative MT-like protein in *A. nidulans,* product of AN7011 and possible ortholog of Ca*CRD2,* named *crdA.* The 109 residues of CrdA are 44% similar and 36% identical to (84% query cover) CaCrd2p. CrdA is longer and has additional cysteine residues, which is not surprising due to the diversity in primary structure of this heterogeneous protein family (reviewed by Blindauer and Leszczyszyn, 2010). As shown in **Figure 1B** the 16 cysteine residues are scattered throughout the entire sequence, arranged in cysteine clusters which are essential for copper binding. CrdA

contains seven CxC clusters of which four shared the location of all CxC clusters identified in CaCrd2p. Besides, CrdA shares signature features of MTs; few aromatic amino acids (1 aa), lack of histidine and high Ser and Lys residue content (9 and 6%, respectively; Riggle and Kumamoto, 2000). Additional searches did not reveal any further known conserved functional domains.

Functional Analysis of CrpA and CrdA

To assess the role of *crpA* and *crdA* in copper tolerance, we generated single-knockout mutants for each locus by gene replacement technique (see Section Material and Methods). The mutant $\Delta crpA$ (BD888), $\Delta crdA$ (BD898), and wild-type (WT) strains were tested at different copper concentrations. As shown in **Figure 2A**, the *crpA* null strain showed reduced resistance to Cu^{+2}, exhibiting morphological defects at 100 µM $CuSO_4$ and a nearly total growth inhibition at 150 µM $CuSO_4$. At 100 µM $CuSO_4$ the *crpA* deletant exhibited similar colony radial growth compared to the wild-type strain, albeit with a significantly lower cellular density in the central region of the colony (**Figure 2B**). We named this cellular morphology "copper phenotype," to distinguish it from those obtained with other metal ions (see below). After additional 24 h of incubation the scarce cellular growth visualized gradually recovered resembling wild-type morphology (**Figure 2C**, magenta line). Close up views of strain BD888 inoculated in medium supplemented with 150 µM $CuSO_4$ revealed the presence of isolated hyphae with normal extension pattern across the whole colony (**Figure 2B**, magenta dotted line). No cellular recovery was observed after additional incubation, as described previously. The "copper phenotype" was rescued to wild-type by introduction of *A. nidulans crpA* gene in the $\Delta crpA$ strain, confirming the involvement of the P_I-ATPase pump in copper tolerance (**Supplementary Figure 1**). In contrast, the null *crdA* mutant was not abnormally susceptible to high Cu^{+2} concentrations, displaying wild-type phenotype over the concentration range tested (**Figure 2A**).

To ascertain the participation of the putative metallothionein in the copper detoxification pathway we generated a double null deletant strain (BD963) lacking CrdA and CrpA. The double null $\Delta crdA \Delta crpA$ and the single $\Delta crpA$ mutants, showed indistinguishable copper sensitivity (**Figure 2A**), denoting that *crdA* and *crpA* mutations were not additive. This result indicates that a functional form of CrdA is not required for resistance to toxic copper loads.

Bearing in mind the possibility that in *A. nidulans*, as it has been described in other organisms (Odermatt et al., 1994; Mandal et al., 2002), CrpA could catalyze diverse heavy-metal ion efflux, mutants were tested in plates with $AgNO_3$ and $Cd(NO_3)_2$. The extreme sensitivity of *A. nidulans* to silver in solid medium, range from 2.5 to 5 µM $AgNO_3$, did not allow us to determine accurate silver tolerance data. In the case of cadmium, the *crpA* null strain exhibited colony defects such as reduced (~50%) and compact growth at 150 µM of $Cd(NO_3)_2$. This colony morphology was distinct from the "copper phenotype" formerly described (**Figure 2A**). As previously, the *crdA* deletant did not manifest a phenotype related to heavy metal ion tolerance.

Sensitivity of mutant strains was also evaluated in liquid culture by measuring mycelial biomass. In agreement with the results obtained in solid medium cultures, it was observed that deletion of *crpA* strongly affected cellular growth in liquid medium in response to copper and cadmium, whereas a null mutation of *crdA* had no significant effect. As shown in **Figure 2D**, in the presence of 30 µM $CuSO_4$ and 60 µM $Cd(NO_3)_2$ $\Delta crpA$ and $\Delta crdA \Delta crpA$ mutant strains decreased biomass production significantly compared to WT, up to 15 and 14%, respectively. In line with previous observations, no significant differences were detected between the two strains carrying the *crpA* deletion. In the case of silver, all mutants were unable to grow at 0.75 µM $AgNO_3$.
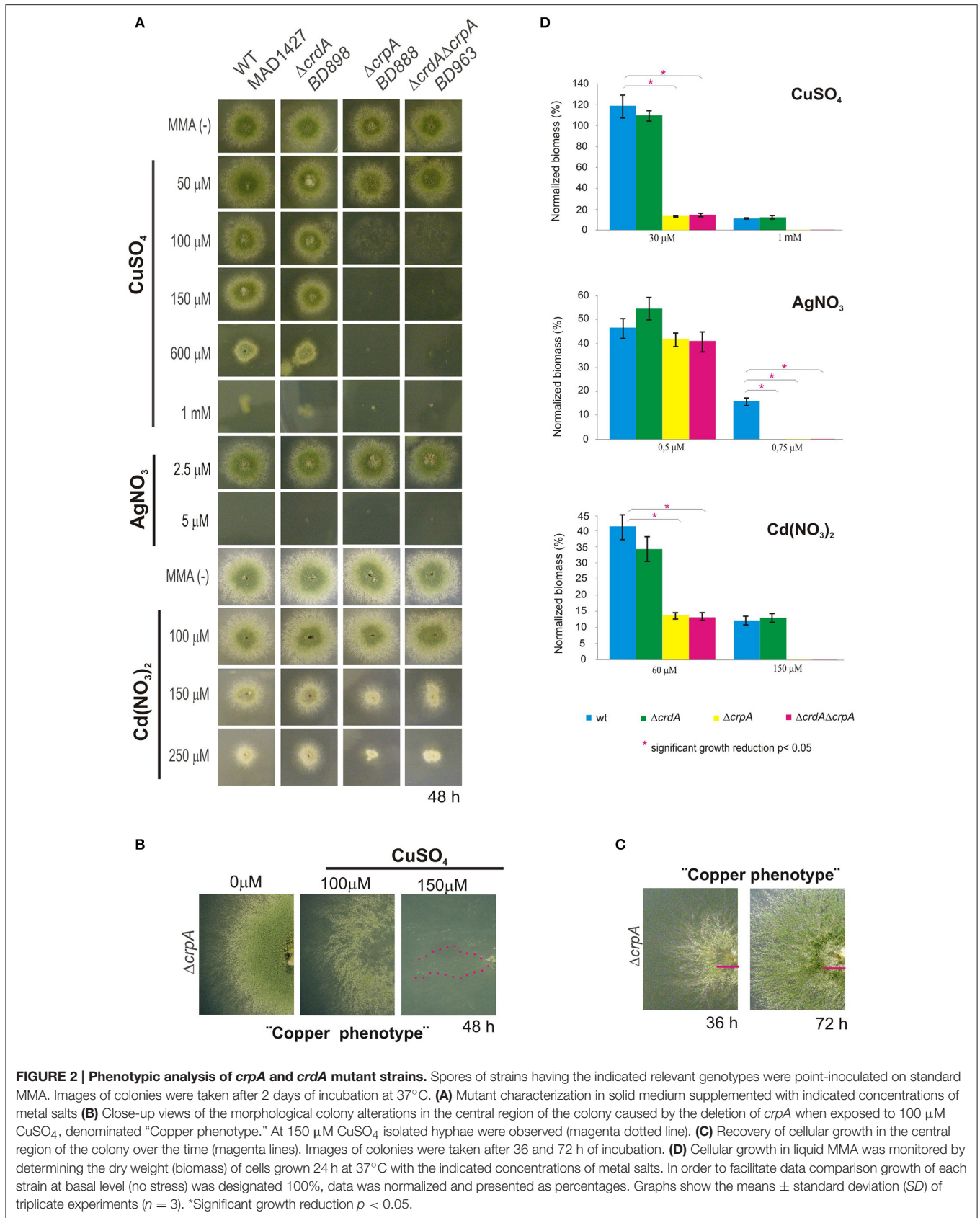
The results obtained with the comparison of the mutants highlight that the P_I-type pump CrpA, as a key factor in determining copper resistance in *A. nidulans* and its function may be extended to other metals. In contrast, the contribution of CrdA in tolerance to metal ion toxicity remains to be clarified.
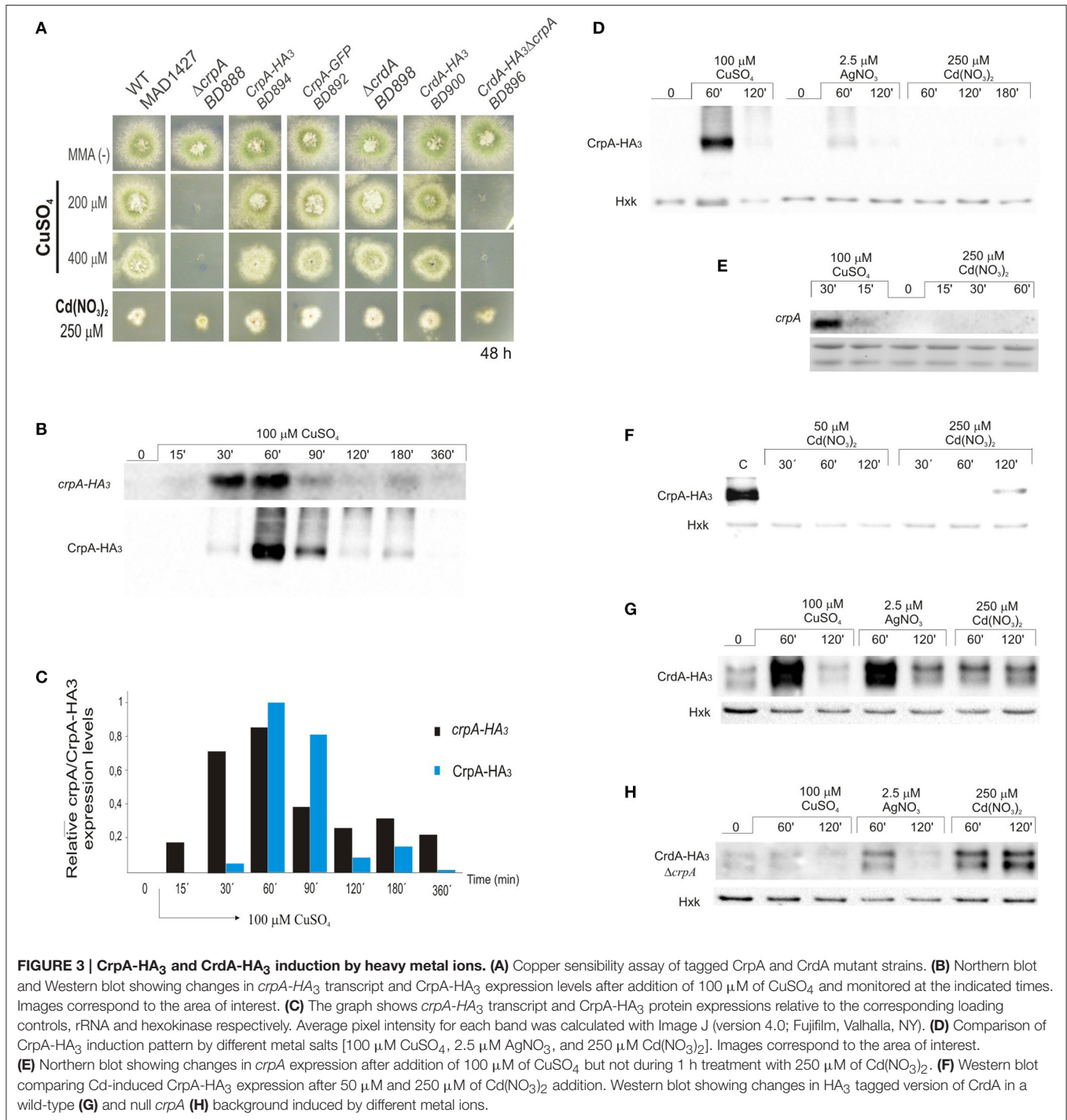
Dynamic Expression of CrpA and CrdA in Response to Metal Toxicity

Earlier studies had reported that after metal loading metallothionein production is increased (Liu and Thiele, 1997; Peña et al., 1998; García et al., 2002; Ehrensberger and Bird, 2011) and the detoxifying P_I-type ATPase activity is enhanced, either inducing expression (Riggle and Kumamoto, 2000; Weissman et al., 2000) or by modifying subcellular localization (Suzuki and Gitlin, 1999; Cobbold et al., 2002).

Here we confirmed that *crpA* expression is copper-inducible. Hence, to gain a better insight into CrpA regulation during prolonged copper treatment, extracts for gene and protein expression were prepared from same mycelium samples. We generated a strain expressing a CrpA-HA_3 fusion (BD894) and since HA_3 tagging might alter CrpA function we tested copper and cadmium tolerance on plates. BD894 displayed wild-type phenotype indicating that the CrpA-HA_3 chimera was functional at the copper concentrations used for gene and protein expression (**Figure 3A**). After spores were incubated for 16 h, cells were harvested at different times, before (0 min) and after addition of 100 µM of $CuSO_4$ (15–360 min). *CrpA-HA_3* and CrpA-HA_3 signals were measured and normalized with respect to rRNA and hexokinase signals.

Northern blot analysis revealed that the transcript of *crpA* was not detectable in total RNA extracts from resting cells (**Figure 3B**). After 15 min of Cu-addition to the culture *crpA* was quickly induced (6-fold), reaching maximum mRNA levels (57-fold) within 60 min. This was followed by a gradual repression to expression levels compared with those observed at 15 min (8-fold; **Figure 3C**). The mRNA levels were maintained during the 360 min that last the experiment. These results confirmed that *crpA* expression is transiently induced to high levels in response to copper toxicity, but in prolonged exposures, low basal levels are maintained. Northern blot expression patterns matched with CrpA-HA_3 fusion protein (~134 kDa) kinetics, despite the fact that the band corresponding to the chimera was first detected 30 min after copper addition (**Figure 3B**). Western blot analyses additionally revealed dispersed high-molecular weight

FIGURE 2 | Phenotypic analysis of *crpA* and *crdA* mutant strains. Spores of strains having the indicated relevant genotypes were point-inoculated on standard MMA. Images of colonies were taken after 2 days of incubation at 37°C. **(A)** Mutant characterization in solid medium supplemented with indicated concentrations of metal salts **(B)** Close-up views of the morphological colony alterations in the central region of the colony caused by the deletion of *crpA* when exposed to 100 μM CuSO$_4$, denominated "Copper phenotype." At 150 μM CuSO$_4$ isolated hyphae were observed (magenta dotted line). **(C)** Recovery of cellular growth in the central region of the colony over the time (magenta lines). Images of colonies were taken after 36 and 72 h of incubation. **(D)** Cellular growth in liquid MMA was monitored by determining the dry weight (biomass) of cells grown 24 h at 37°C with the indicated concentrations of metal salts. In order to facilitate data comparison growth of each strain at basal level (no stress) was designated 100%, data was normalized and presented as percentages. Graphs show the means ± standard deviation (*SD*) of triplicate experiments (*n* = 3). *Significant growth reduction *p* < 0.05.

FIGURE 3 | CrpA-HA₃ and CrdA-HA₃ induction by heavy metal ions. (A) Copper sensibility assay of tagged CrpA and CrdA mutant strains. **(B)** Northern blot and Western blot showing changes in *crpA-HA₃* transcript and CrpA-HA₃ expression levels after addition of 100 μM of CuSO₄ and monitored at the indicated times. Images correspond to the area of interest. **(C)** The graph shows *crpA-HA₃* transcript and CrpA-HA₃ protein expressions relative to the corresponding loading controls, rRNA and hexokinase respectively. Average pixel intensity for each band was calculated with Image J (version 4.0; Fujifilm, Valhalla, NY). **(D)** Comparison of CrpA-HA₃ induction pattern by different metal salts [100 μM CuSO₄, 2.5 μM AgNO₃, and 250 μM Cd(NO₃)₂]. Images correspond to the area of interest. **(E)** Northern blot showing changes in *crpA* expression after addition of 100 μM of CuSO₄ but not during 1 h treatment with 250 μM of Cd(NO₃)₂. **(F)** Western blot comparing Cd-induced CrpA-HA₃ expression after 50 μM and 250 μM of Cd(NO₃)₂ addition. Western blot showing changes in HA₃ tagged version of CrdA in a wild-type **(G)** and null *crpA* **(H)** background induced by different metal ions.

CrpA-HA₃ species and a barely detectable smaller band within 1 h, which may reflect post-translational modification events.

To further elucidate the role of CrpA in non-copper metal ion detoxification, protein induction was studied under silver and cadmium stress conditions. It was determined that, in the presence of 2.5 μM AgNO₃, CrpA-HA₃ followed the expression pattern observed with copper, reaching a maximal level within 60 min followed by a decline (**Figure 3D**). However, the amplitude

of the response was considerably lower. In contrast, 250 μM Cd(NO₃)₂ did not activate protein expression until 2 h after the treatment, being the band detected very faint. This finding was not consistent with the observation that the deletion of *crpA* rendered the cells more sensitive to cadmium. Therefore, we monitored protein expression in cells treated in longer period. It was then observed that protein levels were increased in the 120–180 min time range (**Figure 3D**).

It has been reported that high concentrations of heavy-metal ions can inhibit synthesis of certain proteins (Matts et al., 1991; Staneviciene et al., 2008). To test if this was the cause of the late CrpA detection, *crpA* expression in earlier time points was studied. The analyses showed that no Cd-induced *crpA* signal was detected after 1 h of exposure to the cation, while Cu-induced mRNA was visualized as early as 15 min after exposure (**Figure 3E**). To further explore this aspect, protein expression with lower cadmium concentration was studied and compared with that of high concentration. No CrpA-HA$_3$ was detected over the incubation period with 50 µM Cd(NO$_3$)$_2$. In contrast, the protein was detected after 2 h of treatment with 250 µM Cd(NO$_3$)$_2$ (**Figure 3F**).

Riggle and Kumamoto (2000) pointed out that CaCrd2 was implicated in the initial buffering of copper ions. Since the possible function of CrdA was studied after 2 days of culture in solid medium we decided to assess its role at earlier times by protein expression analysis. The putative metallothionein expression was observed even in the absence of metals. A band of ∼15 kDa, similar to the predicted size of the HA$_3$ tagged version of CrdA, and a second slower-migrating band of ∼17 kDa were detected. The relative levels of both bands varied under different conditions and experiments. As it is observed in **Figure 3G** protein levels were increased in response to all metal ions tested. Once more, CuSO$_4$ and AgNO$_3$ triggered a similar protein expression pattern, although the effect of silver on CrdA-HA$_3$ was more robust than on CrpA-HA$_3$, being comparable to copper induction. Unlike the previous case, cadmium elicited protein expression by the first hour of treatment and remained at same level throughout the time course of the experiment. This response was faster and stronger than the Cd-induction observed in copper ATPase.

We then hypothesized that the absence of CrpA, which plays the principal role in copper resistance and was highly expressed at this time point, may lead to an enhance of CrdA expression in order to augment Cu-buffering. To test this possibility, a Δ*crpA* mutant strain carrying *crdA-HA$_3$* construct was generated (BD896; **Figure 3A**). Comparing the signal of the bands corresponding to CrdA-HA$_3$ in the wild-type and null *crpA* background, in the last case, intensities detected were much lower for Cu^{+2} and Ag$^+$, and approximately similar for Cd^{+2} (**Figure 3H**). This result indicates that the absence of *crpA* negatively affect CrdA expression.

In summary, these data show that *crpA* expression fluctuates in a prolonged copper treatment, being strongly and transiently induced as an early response, but lightly and continuously maintained thereafter. In addition, the results strongly suggest that copper is the principal ion transported by CrpA but has a role in silver transport. In addition, CrdA is involved in the early response to metal toxicity, but its role remains to be further elucidated.

Localization of CrpA-GFP at the Cellular Surface

Considering that the biological activity of copper P$_I$-ATPase is likely to extrude copper from the cell, we hypothesized that CrpA localizes in the plasma membrane. Cellular distribution of CrpA protein was investigated with a C-terminus GFP-tagged protein. To determine whether the CrpA-GFP fusion protein was functional, the strain expressing it (BD892) was grown in standard minimal medium with copper and cadmium stress and, as expected, displayed wild-type phenotype (**Figure 3A**). Functionality was also assessed studying protein expression by Western blotting using mouse anti-GFP antibody (**Figure 4A**), showing HA$_3$-fusion protein kinetics.

For life image experiments, cells were grown in minimal liquid medium for microscopy without copper stress and shifted to media containing 100 µM CuSO$_4$. As observed by epifluorescence microscopy, upon 30 min of the shift CrpA localized to a reticulated network of interconnecting tubules, surrounding structures that likely represent nucleus (**Figures 4B.A1,A2**, arrowed), and strands associated to the plasma membrane that reminded to the ER (Markina-Iñarrairaegui et al., 2013). Close up views of the tip region (boxed area) showed (**Figures 4B.A2–B.A4**) a finger-like protrusion directed toward the tip. Thirty minutes later CrpA distribution was modified, showing a homogeneously dispersed localization in the cytoplasm and a strong fluorescence across the entire length of the cell periphery, suggesting CrpA-GFP protein predominated at the plasma membrane (PM; **Figures 4B.B1,B2**), consistent with its predicted function. In a large number of cells CrpA was polarized in the proximity of the tip of hyphae (**Figures 4B.B3, B4**). Fluorescence was measured and represented in graphs corresponding to the linescans across the indicated lines, verifying signal accumulation in the proximity of the plasma membrane and tip region.

Figures 4B.C1 illustrates that 2 h after copper load, even if a significant proportion of CrpA-GFP appears to remain at the PM, it was also distributed in dispersed structures of variable sizes and morphology, punctuated and ring-shaped structures, throughout the cytosol (**Figures 4B.C2,C3**, yellow arrowheads) akin to Golgi equivalents (Pantazopoulou and Peñalva, 2009). An hour later large aggregates were noticeable along the hyphae that look like vacuolar compartments (Pantazopoulou et al., 2007; **Figures 4B.C4**, magenta arrows). Nevertheless, the identity of these membrane organelles has to be elucidated and further studied by colocalization experiments.

Overall, these results suggest that *de novo* CrpA translocates to the cell surface, most certainly to efflux copper, leaves the plasma membrane and reaches different organelles as part of an orchestrated trafficking process.

Expression Regulation of CrpA and CrdA by the Transcription Factor AceA

The rapid and regulated copper-inducible transcription of *crpA* suggested that it is under the control of a copper-dependent transcription factor (TF). Blastp searches using *S. cerevisiae* ScAce1p (CAA96877.1; Dameron et al., 1991), *Candida glabrata* CgAmt1p (XP_447430.1; Zhou et al., 1992), and *Yarrowia lipolytica* YlCrf1p (XP_500631.1; García et al., 2002) amino acid sequences allowed the identification of the putative transcription factor homologous in *A. nidulans*, a 525 amino acid long protein
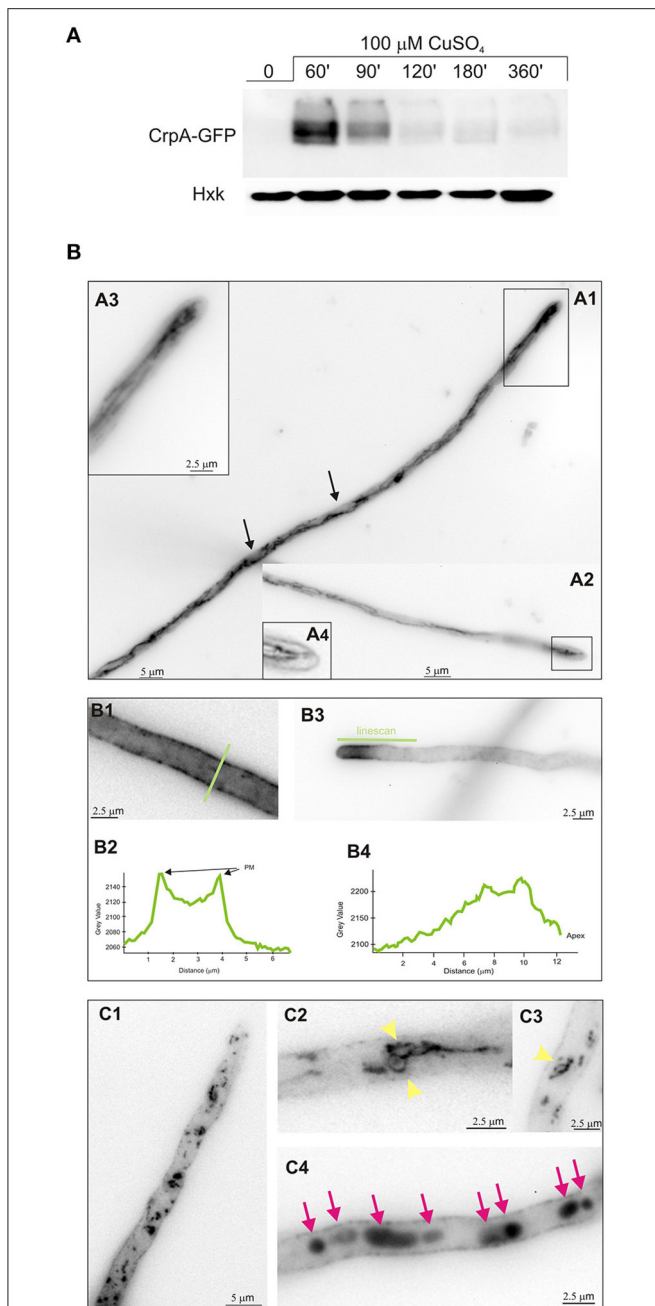
FIGURE 4 | Effect of copper in intracellular localization of CrpA-GFP.
(A) Western blot confirming CrpA-GFP normal expression kinetics after addition of 100 µM of CuSO$_4$ **(B)** Cells of a strain expressing a CrpA–GFP fusion were grown in selective medium for microscopy for 16 h at 25°C and shifted to medium containing 100 µM CuSO$_4$ for the indicated times. Images taken 30 min after the shift. **(A1,A2)** CrpA localized in a network of strands and tubules. **(A3,A4)** Images corresponds to the rectangular region indicated in **(A1,A3)** showing a magnification of the tip region. **(B1–B4)** Images corresponding to 1 h after the shift. GFP fluorescence was accumulated predominately in the PM **(B1)** and polarized in the tip region **(B3)**. Panels **(B2,B4)** corresponds to the line scans of CrpA-GFP signal across the indicated lines. **(C1–C4)** Images taken 2–3 h after shifting. Panels **(C1,C2,C3)** are examples of ring-shaped structures (yellow arrowheads) and **(C4)** of abnormal aggregates (magenta arrows). Images were treated with sharp filter, shown in inverted gray contrast and represent average intensity projections of z-stacks.

encoded by AN1924 ORF (1,689 bp) and referred to from now on as AceA.

AceA contains several features described for its orthologs, especially the N-terminal DNA-binding domain. This region (**Figure 5A**) showed the highest sequence conservation, especially the first subdomain (residues 1–39), copper-fist DNA-binding domain, which displayed 61% identity with 1–40 amino terminal amino acids of YlCrf1p (76% similarity), 55% with ScAce1p (73% similarity) and 45% identity with CgAmt1p (76% similarity). This whole region encompasses 11 of the 14 encoded cysteines arranged in CxC or CxxC clusters, conserved among the copper regulatory transcription factors mentioned. These cysteine residues are necessary for copper binding which induces a conformational change of the protein. This, in turn, allows the interaction of the copper-activated DNA-binding region with the Metal Regulatory Elements (MRE) of the promoter of the target genes (Peña et al., 1998). AceA exhibits a serine (14%) and proline (12%) rich composition and unusual distribution (SSxSS, SSS, PPP clusters), especially in the C-terminal half of the protein, similar to YlCrf1p of *Y. lipolytica* (García et al., 2002).

The conservation of motifs suggests that AceA may be the transcriptional factor involved in copper tolerance in *A. nidulans*. To investigate its role, a single-knockout mutant of *aceA* locus was generated (BD965) and tested in the same range of metal concentrations used before. Growth analyses demonstrated that not only did the *ΔaceA* strain display an identical "copper phenotype" to that observed in *ΔcrpA*, but it also exhibited a more pronounced sensitivity response to CuSO$_4$, since colony defects were observed at lower concentration (**Figure 5B**). Elevated cadmium content provoked a reduction of colony growth, nevertheless in a similar degree to the previously observed in the *ΔcrpA* strain. Biomass measurements supported these results (**Figure 5C**). The *ΔaceA* mutant strain was significantly more sensitive to CuSO$_4$ than *ΔcrpA* strain ($P < 0.05$). In contrast, the tolerance to Cd^{+2} and Ag$^+$ was almost identical in both strains. These results confirm the implication of AceA in metal tolerance, playing a key role in copper resistance.

We hypothesized that AceA was the copper dependent transcriptional activator of genes involved in copper detoxification, thus the strain bearing a mutation in the *aceA* gene should be sensitive to copper primarily due to a defect in copper-inducible transcription. In order to prove this hypothesis, we analyzed by Western blot extracts of strain BD961, which expressed the CrpA-HA$_3$ fusion protein in an *aceA*-deletant background (**Figure 5B**). Using anti-HA$_3$ antibody, we did not detect the 134 kDa band observed previously, as in extracts from the strain expressing CrpA-HA$_3$ and loaded as control (**Figure 5D**). The lack of CrpA-HA$_3$ detection demonstrated that AceA is necessary for metal induction of the P$_I$-type pump transcription. Subsequently, the HA$_3$ tagged metallothionein-like protein in response to metal salts in the absence of *aceA* allele (BD1062) was analyzed. CrdA-HA$_3$ was detected in the *ΔaceA*-deleted strain (**Figure 5E**). Moreover, results indicated that CrdA expression levels and kinetics in the null *ΔcrpA* and *ΔaceA* mutant strains were comparable. This result indicates
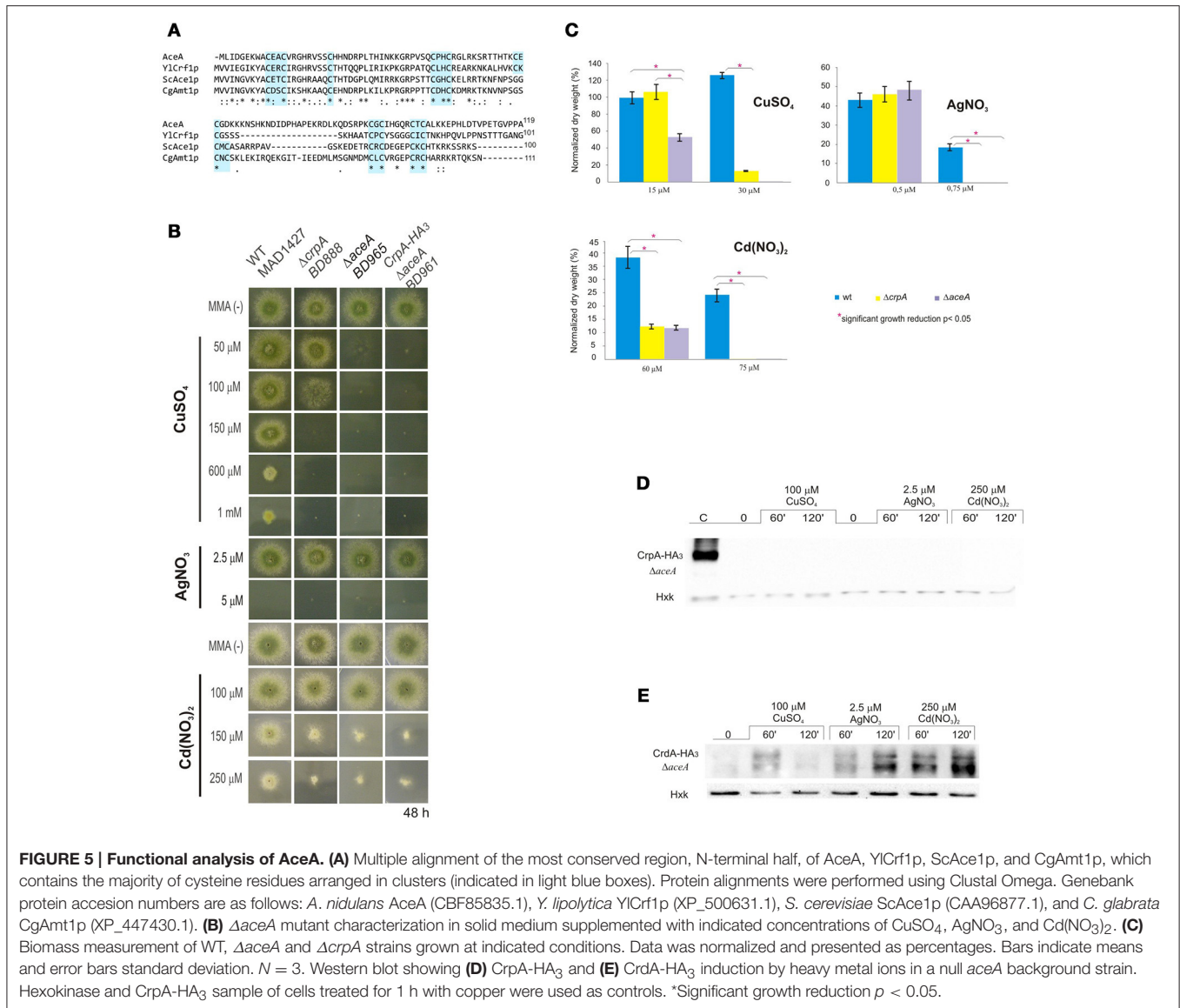
FIGURE 5 | Functional analysis of AceA. (A) Multiple alignment of the most conserved region, N-terminal half, of AceA, YlCrf1p, ScAce1p, and CgAmt1p, which contains the majority of cysteine residues arranged in clusters (indicated in light blue boxes). Protein alignments were performed using Clustal Omega. Genebank protein accesion numbers are as follows: *A. nidulans* AceA (CBF85835.1), *Y. lipolytica* YlCrf1p (XP_500631.1), *S. cerevisiae* ScAce1p (CAA96877.1), and *C. glabrata* CgAmt1p (XP_447430.1). **(B)** Δ*aceA* mutant characterization in solid medium supplemented with indicated concentrations of $CuSO_4$, $AgNO_3$, and $Cd(NO_3)_2$. **(C)** Biomass measurement of WT, Δ*aceA* and Δ*crpA* strains grown at indicated conditions. Data was normalized and presented as percentages. Bars indicate means and error bars standard deviation. $N = 3$. Western blot showing **(D)** CrpA-HA$_3$ and **(E)** CrdA-HA$_3$ induction by heavy metal ions in a null *aceA* background strain. Hexokinase and CrpA-HA$_3$ sample of cells treated for 1 h with copper were used as controls. *Significant growth reduction $p < 0.05$.

that AceA is not essential for metal-induced activation of *crdA* and supports the possibility of a role different from metal ion detoxification.

Taken together, these results confirm that AceA is the transcription factor responsible of regulating genes involved in copper detoxification, as CrpA, and suggest the existence of an as yet unidentified gene responsible for the residual copper resistance in *A. nidulans*.

DISCUSSION

Eukaryotes maintain physiological copper levels by regulating the balance between copper uptake, compartmentalization and detoxification. In this study, we identified and characterized two key operators of the copper detoxification system of *A. nidulans*, which relies principally in excretion.

CrpA Is a Putative Copper P$_I$-Type ATPase

Sequence analysis identified CrpA as the putative homolog of *C. albicans* CaCrp1p, which had been reported to confer high resistance to copper by ion extrusion (Riggle and Kumamoto, 2000; Weissman et al., 2000). CrpA and CaCrp1p share an atypical structure and distribution of the N-terminal metal binding domains (MDB). Since these motifs are likely involved in regulation, we postulate that CrpA and CaCrp1p have similar ion specificities and biological function. Studies carried out in *Y. lipolytica* strongly support the idea that copper resistance is not mediated by MT related Cu buffering but by efflux (García et al., 2002; Ito et al., 2007). Additional blast searches in this dimorphic fungus revealed a putative homolog, YALI0B02684p (GeneBank accession number XP_500433.1), which displayed a similar NH$_2$-terminal extension. These results indicate that this feature is not unique to *A. nidulans* and *C. albicans* and it could be characteristic to fungal species that utilize the

described ATPase-based extrusion system as the primary way to overcome high copper loads. It is also important to underscore the crucial role of copper resistance for virulence of clinically important fungal pathogens as *C. albicans* (Mackie et al., 2016), *Cryptococcus neoformans* (Samanovic et al., 2012; Ding et al., 2013) and *A. fumigatus* (Dietl et al., 2016; Wiemann et al., 2017).

Copper Detoxification Relies on the P$_I$-Type ATpase CrpA

Evidence of the direct participation of CrpA in copper resistance was obtained by the extreme sensitivity exhibited by CrpA null mutants. An atypical aspect of the phenotype of the null *crpA* mutation was the poor growth in the central region of the colony that overcame toxicity with time. This adaptive behavior could be partially explained by the growth pattern described by Valix et al. (2001). As the colony matures, copper may bind to new cellular material locally, resulting in reduction of free copper concentration, and increased growth.

Besides copper, *ΔcrpA* also exhibited sensitivity to cadmium, however the divergent phenotype reflected either affinity of metals for different targets and/or distinct detoxification paths (Mendoza-Cózatl et al., 2010). Neither *crpA* Cd-induction nor Cd-protein expression under low Cd concentration were observed. In addition, CrpA was detected only in the presence of high cadmium loads. Together, these results support an indirect P$_I$-type ATPase activation taking place, possibly due to the saturation of the main cadmium detoxification system, a Cd^{+2} pump (Shiraishi et al., 2000; Thorsen et al., 2009) or glutathione-derived peptides denominated phytochelatins (Mendoza-Cózatl et al., 2005, 2010).

Regarding silver toxicity, our data showed that *A. nidulans* is sensitive to this metal at a very low (2.5–5 µM) concentration range. Biomass measurements indicate that CrpA may participate in silver resistance. On the other hand, it was observed that silver induced expression of CrpA which matched copper kinetics, although to a lesser extent. Based on these results, we propose that copper is the principal substrate of the *A. nidulans* ATPase, however silver can also be transported. Indeed, this is consistent with the fact that orthologs described above are also reported Cu$^+$/Ag$^+$ transporters. Although we did not ascertain it in this study, CrpA likely exports Cu$^+$ and not Cu^{+2} since; (a) in the reduced cytosolic environment Cu^{+2} is found in Cu$^+$ form and (b) substitution of Cu$^+$ by Ag$^+$ is possible in proteins with CxxC containing MBDs, but not Cu^{+2} (Petris et al., 1996).

Long term copper exposure induces an early, strong, and transient expression followed by a basal maintenance expression level of CrpA. Considering the effect of copper exposure on *crpA* expression over time, we demonstrated that *crpA* induction is rapid (within 15 min), transiently strong (57-fold increase in 1 h) and sustained throughout the exposure to copper, since mRNA levels were detectable along the whole experiment. Hypothesizing that *crpA* mRNA levels may reflect intracellular ion concentrations, we consider that under long term high copper exposure, cells would firstly synthesize an elevated amount of

Cu-exporter in order to rapidly reduce the initial burst of copper incorporated via high affinity transporters. Subsequently, pump levels would be downregulated and then maintained at a certain level during the period in which copper continues to enter chronically to the cell via low affinity transporters, similar to *S. cerevisiae* (Yu et al., 1996). Regulation studies are ongoing at present in our laboratory to verify whether CrpA post-translational modifications (PTM) are involved in CrpA activity control besides the transcriptional regulation described in this work.

CrpA Localizes in the Plasma Membrane

CrpA localization close to the cell surface in response to copper addition sustains the expected copper extrusion role of this ATPase. Detailed evaluation of the subcellular distribution indicated that CrpA is under the control of a highly orchestrated trafficking process that resembles membrane transporter regulation (Pantazopoulou and Diallinas, 2007; Lauwers et al., 2010). We speculate, that in response to increased cytosolic Cu$^+$, *de novo* synthesized CrpA traffics from the ER to the Golgi compartment and then to the plasma membrane (PM). Upon a purported decrease in cytosolic copper concentration, a fraction of PM CrpA would be endocytically internalized and sorted to the multivesicular body (MVB). CrpA could then be recycled back to the PM via the TGN as reported in human cells (Pase et al., 2004), where PM CrpA could be the result of two different protein pools; a newly synthesized and a recycled CrpA pool. Post-traslational modification and organelle trafficking mutant studies would be required to establish a model of CrpA sorting and regulation. Solving the molecular mechanism of the P$_I$-type ATPase trafficking in *A. nidulans* could provide novel insights into how cells with a polarized architecture regulate copper ATPase activity.

The Transcription Factor AceA Regulates Metal-Responsive CrpA Expression

The active role of AceA in copper resistance gene regulation was demonstrated by the extreme copper-sensitive phenotype of the knock-out mutant and the absence of expression of CrpA in the *ΔaceA* strain. In fact, the increased sensitivity of *ΔaceA* with respect to *ΔcrpA* mutants highlighted two major points: firstly, the participation of an additional element in the copper detoxification path and secondly, the predominant role of CrpA over the minor participation of the other player in the system. This second participant could be either a copper-metallothionein (MT) that has not been identified or a copper scavenging phytochelatin, like in *Schizosaccahoromyces pombe* (Clemens et al., 1999). Identification of new metallothioneins, since the primary structure is highly diverse, could be a laborious task. It may be worthy to attempt a different approach. The characterization of the AceA binding metal-response element (MRE) on the CrpA promoter might propose a consensus MRE sequence for *A. nidulans* copper detoxification genes that could facilitate new searches.

CrdA, a Putative Metallothionein with Undefined Function

CrdA expression was induced by copper, silver and cadmium within 1 h, indicating a role in metal homeostasis. In summary, we found that: (a) a $\Delta crdA$ strain did not exhibit a metal sensitivity phenotype, (b) a non-additive effect of *crpA* and *crdA* deletion was observed, (c) the deletion of *crpA* did not increase *crdA* transcription, and (d) AceA was not required to activate CrdA expression. Taken together, these results do not support the participation of CrdA in CrpA-mediated metal detoxification. A likely role for this putative metallothionein may be as an antioxidant (Palmiter, 1998; Blindauer and Leszczyszyn, 2010). Further studies will confirm whether the principal AceA-regulated P_I-type ATPase (CrpA) system is connected with CrdA mechanisms in response to metal stress.

AUTHOR CONTRIBUTIONS

MA conducted the experimental work, analyzed data, and contributed to the writing of the paper. AM made the concept and designed the work, analyzed, and interpreted the results, wrote the manuscript, and ensured the accuracy of the project as whole. UU co-conceived the work, ensured the scientific issue was appropriately investigated, ensured the integrity of the work, revised, and approved the final version to be published.

FUNDING

SUPPLEMENTARY MATERIAL

The Supplementary Material for this article can be found online at: http://journal.frontiersin.org/article/10.3389/fmicb.2017.00912/full#supplementary-material

Supplementary Figure 1 | *crpA* rescue phenotype. WT, $\Delta crpA$, and $crpA^+$ complemented mutant strain characterization in solid medium supplemented with the indicated $CuSO_4$ concentrations.

REFERENCES

Balamurugan, K., and Schaffner, W. (2006). Copper homeostasis in eukaryotes: teetering on a tightrope. *Biochim. Biophys. Acta* 1763, 737–746. doi: 10.1016/j.bbamcr.2006.05.001

Barry, A. N., Shinde, U., and Lutsenko, S. (2010). Structural organization of human Cu-transporting ATPases: learning from building blocks. *J. Biol. Inorg. Chem.* 15, 47–59. doi: 10.1007/s00775-009-0595-4

Blindauer, C. A., and Leszczyszyn, O. I. (2010). Metallothioneins: unparalleled diversity in structures and functions for metal ion homeostasis and more. *Nat. Prod. Rep.* 27, 720–741. doi: 10.1039/b906685n

Bradford, M. M. (1976). A rapid and sensitive method for the quantitation of microgram quantities of protein utilizing the principle of protein-dye binding. *Anal. Biochem.* 72, 248–254. doi: 10.1016/0003-2697(76)90527-3a

Church, G. M., and Gilbert, W. (1984). Genomic sequencing. *Proc. Natl. Acad. Sci. U.S.A.* 81, 1991–1995.

Clemens, S., Kim, E. J., Neumann, D., and Schroeder, J. I. (1999). Tolerance to toxic metals by a gene family of phytochelatin synthases from plants and yeast. *EMBO J.* 18, 3325–3333. doi: 10.1093/emboj/18.12.3325

Clutterbuck, A. J. (1990). The genetics of conidiophore pigmentation in *Aspergillus nidulans*. *J. Gen. Microbiol.* 136, 1731–1738. doi: 10.1099/00221287-136-9-1731

Cobbold, C., Ponnambalam, S., Francis, M. J., and Monaco, A. P. (2002). Novel membrane traffic steps regulate the exocytosis of the Menkes disease ATPase. *Hum. Mol. Genet.* 11, 2855–2866. doi: 10.1093/hmg/11.23.2855

Culotta, V. C., Howard, W. R., and Liu, X. F. (1994). CRS5 encodes a metallothionein-like protein in *Saccharomyces cerevisiae*. *J. Biol. Chem.* 269, 25295–25302.

Dameron, C. T., Winge, D. R., George, G. N., Sansone, M., Hu, S., and Hamer, D. (1991). A copper-thiolate polynuclear cluster in the ACE1 transcription factor. *Proc. Natl. Acad. Sci. U.S.A.* 88, 6127–6131. doi: 10.1073/pnas.88.14.6127

Dietl, A. M., Amich, J., Leal, S., Beckmann, N., Binder, U., Beilhack, A., et al. (2016). Histidine biosynthesis plays a crucial role in metal homeostasis and virulence of *Aspergillus fumigatus*. *Virulence* 7, 465–476. doi: 10.1080/21505594.2016.1146848

Ding, C., Festa, R. A., Chen, Y. L., Espart, A., Palacios, Ò., Espin, J., et al. (2013). *Cryptococcus neoformans* copper detoxification machinery is critical for fungal virulence. *Cell Host. Microbe* 13, 265–276. doi: 10.1016/j.chom.2013.02.002

Drubin, D. G., Miller, K. G., and Botstein, D. (1988). Yeast actin-binding proteins: evidence for a role in morphogenesis. *J. Cell Biol.* 107, 2551–2561. doi: 10.1083/jcb.107.6.2551

Ehrensberger, K. M., and Bird, A. J. (2011). Hammering out details: regulating metal levels in eukaryotes. *Trends Biochem. Sci.* 36, 524–531. doi: 10.1016/j.tibs.2011.07.002

Furst, P., Hu, S., Hackett, R., and Hamer, D. (1988). Copper activates metallothionein gene transcription by altering the conformation of a specific DNA binding protein. *Cell* 55, 705–717. doi: 10.1016/0092-8674(88)90229-2

García, S., Prado, M., Dégano, R., and Domínguez, A. (2002). A copper-responsive transcription factor, CRF1, mediates copper and cadmium resistance in *Yarrowia lipolytica*. *J. Biol. Chem.* 277, 37359–37368. doi: 10.1074/jbc.M201091200

Garzia, A., Etxebeste, O., Rodriguez-Romero, J., Fischer, R., Espeso, E. A., and Ugalde, U. (2013). Transcriptional changes in the transition from vegetative cells to asexual development in the model fungus *Aspergillus nidulans*. *Eukaryot. Cell* 12, 311–321. doi: 10.1128/EC.00274-12

Graden, J. A., and Winge, D. R. (1997). Copper-mediated repression of the activation domain in the yeast Mac1p transcription factor. *Proc. Natl. Acad. Sci. U.S.A.* 94, 5550–5555. doi: 10.1073/pnas.94.11.5550

Halliwell, B., and Gutteridge, J. M. (1990). Role of free radicals and catalytic metal ions in human disease: an overview. *Methods Enzymol.* 186, 1–85. doi: 10.1016/0076-6879(90)86093-B

Hervás-Aguilar, A., and Peñalva, M. A. (2010). Endocytic machinery protein SlaB is dispensable for polarity establishment but necessary for polarity maintenance in hyphal tip cells of *Aspergillus nidulans*. *Eukaryot. Cell* 9, 1504–1518. doi: 10.1128/EC.00119-10

Inesi, G., Pilankatta, R., and Tadini-Buoninsegni, F. (2014). Biochemical characterization of P-type copper ATPases. *Biochem. J.* 463, 167–176. doi: 10.1042/BJ20140741

Ito, H., Inouhe, M., Tohoyama, H., and Joho, M. (2007). Characteristics of copper tolerance in *Yarrowia lipolytica*. *Biometals* 20, 773–780. doi: 10.1007/s10534-006-9040-0

Käfer, E. (1965). Origins of translocations in *Aspergillus nidulans*. *Genetics* 52, 217–232.

Keller, G., Bird, A., and Winge, D. R. (2005). Independent metalloregulation of Ace1 and Mac1 in *Saccharomyces cerevisiae*. *Eukaryot. Cell* 4, 1863–1871. doi: 10.1128/EC.4.11.1863-1871.2005

Labbé, S., Zhu, Z., and Thiele, D. J. (1997). Copper-specific transcriptional repression of yeast genes encoding critical components in the copper transport pathway. *J. Biol. Chem.* 272, 15951–15958. doi: 10.1074/jbc.272.25.15951

Ladomersky, E., and Petris, M. J. (2015). Copper tolerance and virulence in bacteria. *Metallomics* 7, 957–964. doi: 10.1039/C4MT00327F

Lauwers, E., Erpapazoglou, Z., Haguenauer-Tsapis, R., and André, B. (2010). The ubiquitin code of yeast permease trafficking. *Trends Cell Biol.* 20, 196–204. doi: 10.1016/j.tcb.2010.01.004

Lemire, J. A., Harrison, J. J., and Turner, R. J. (2013). Antimicrobial activity of metals: mechanisms, molecular targets and applications. *Nat. Rev. Microbiol.* 11, 371–384. doi: 10.1038/nrmicro3028

Liu, X. D., and Thiele, D. J. (1997). Yeast metallothionein gene expression in response to metals and oxidative stress. *Methods* 11, 289–299. doi: 10.1006/meth.1996.0423

Lutsenko, S. (2010). Human copper homeostasis: a network of interconnected pathways. *Curr. Opin. Chem. Biol.* 14, 211–217. doi: 10.1016/j.cbpa.2010.01.003

Lutsenko, S., Barnes, N. L., Bartee, M. Y., and Dmitriev, O. Y. (2007). Function and regulation of human copper-transporting ATPases. *Physiol Rev.* 87, 1011–1046. doi: 10.1152/physrev.00004.2006

Mackie, J., Szabo, E. K., Urgast, D. S., Ballou, E. R., Childers, D. S., MacCallum, D. M., et al. (2016). Host-imposed copper poisoning impacts fungal micronutrient acquisition during systemic *Candida albicans* infections. *PLoS ONE* 11:e0158683. doi: 10.1371/journal.pone.0158683

Macomber, L., and Imlay, J. A. (2009). The iron-sulfur clusters of dehydratases are primary intracellular targets of copper toxicity. *Proc. Natl. Acad. Sci. U.S.A.* 106, 8344–8349. doi: 10.1073/pnas.0812808106

Mandal, A. K., Cheung, W. D., and Arguello, J. M. (2002). Characterization of a thermophilic P-type Ag$^+$/Cu$^+$-ATPase from the extremophile *Archaeoglobus fulgidus*. *J. Biol. Chem.* 277, 7201–7208. doi: 10.1074/jbc.M109964200

Markina-Iñarrairaegui, A., Etxebeste, O., Herrero-Garcia, E., Araújo-Bazán, L., Fernández-Martínez, J., Flores, J. A., et al. (2011). Nuclear transporters in a multinucleated organism: functional and localization analyses in *Aspergillus nidulans*. *Mol. Biol. Cell* 22, 3874–3886. doi: 10.1091/mbc.E11-03-0262

Markina-Iñarrairaegui, A., Pantazopoulou, A., Espeso, E. A., and Peñalva, M. A. (2013). The *Aspergillus nidulans* peripheral ER: disorganization by ER stress and persistence during mitosis. *PLoS ONE* 8:e67154. doi: 10.1371/journal.pone.0067154

Matts, R. L., Schatz, J. R., Hurst, R., and Kagen, R. (1991). Toxic heavy metal ions activate the heme-regulated eukaryotic initiation factor-2 alpha kinase by inhibiting the capacity of hemin-supplemented reticulocyte lysates to reduce disulfide bonds. *J. Biol. Chem.* 266, 12695–12702.

Mendoza-Cózatl, D. G., Zhai, Z., Jobe, T. O., Akmakjian, G. Z., Song, W. Y., Limbo, O., et al. (2010). Tonoplast-localized Abc2 transporter mediates phytochelatin accumulation in vacuoles and confers cadmium tolerance. *J. Biol. Chem.* 285, 40416–40426. doi: 10.1074/jbc.M110.155408

Mendoza-Cózatl, D., Loza-Tavera, H., Hernandez-Navarro, A., and Moreno-Sanchez, R. (2005). Sulfur assimilation and glutathione metabolism under cadmium stress in yeast, protists and plants. *FEMS Microbiol. Rev.* 29, 653–671. doi: 10.1016/j.femsre.2004.09.004

Migocka, M. (2015). Copper-transporting ATPases: the evolutionarily conserved machineries for balancing copper in living systems. *IUBMB Life* 67, 737–745. doi: 10.1002/iub.1437

Nevitt, T., Ohrvik, H., and Thiele, D. J. (2012). Charting the travels of copper in eukaryotes from yeast to mammals. *Biochim. Biophys. Acta* 1823, 1580–1593. doi: 10.1016/j.bbamcr.2012.02.011

Odermatt, A., Krapf, R., and Solioz, M. (1994). Induction of the putative copper ATPases, CopA and CopB, of Enterococcus hirae by Ag$^+$ and Cu^{2+}, and Ag$^+$ extrusion by CopB. *Biochem. Biophys. Res. Commun.* 202, 44–48. doi: 10.1006/bbrc.1994.1891

Odermatt, A., Suter, H., Krapf, R., and Solioz, M. (1993). Primary structure of two P-type ATPases involved in copper homeostasis in *Enterococcus hirae*. *J. Biol. Chem.* 268, 12775–12779.

Palmgren, M. G., and Nissen, P. (2011). P-type ATPases. *Annu. Rev. Biophys.* 40, 243–266. doi: 10.1146/annurev.biophys.093008.131331

Palmiter, R. D. (1998). The elusive function of metallothioneins. *Proc. Natl. Acad. Sci. U.S.A.* 95, 8428–8430. doi: 10.1073/pnas.95.15.8428

Pantazopoulou, A., and Diallinas, G. (2007). Fungal nucleobase transporters. *FEMS Microbiol. Rev.* 31, 657–675. doi: 10.1111/j.1574-6976.2007.00083.x

Pantazopoulou, A., Lemuh, N. D., Hatzinikolaou, D. G., Drevet, C., Cecchetto, G., Scazzocchio, C., et al. (2007). Differential physiological and developmental expression of the UapA and AzgA purine transporters in *Aspergillus nidulans*. *Fungal Genet. Biol.* 44, 627–640. doi: 10.1016/j.fgb.2006.10.003

Pantazopoulou, A., and Peñalva, M. A. (2009). Organization and dynamics of the *Aspergillus nidulans* Golgi during apical extension and mitosis. *Mol. Biol. Cell* 20, 4335–4347. doi: 10.1091/mbc.E09-03-0254

Pase, L., Voskoboinik, I., Greenough, M., and Camakaris, J. (2004). Copper stimulates trafficking of a distinct pool of the Menkes copper ATPase (ATP7A) to the plasma membrane and diverts it into a rapid recycling pool. *Biochem. J.* 378, 1031–1037. doi: 10.1042/bj20031181

Peña, M. M., Koch, K. A., and Thiele, D. J. (1998). Dynamic regulation of copper uptake and detoxification genes in *Saccharomyces cerevisiae*. *Mol. Cell Biol.* 18, 2514–2523. doi: 10.1128/MCB.18.5.2514

Peñalva, M. A. (2005). Tracing the endocytic pathway of *Aspergillus nidulans* with FM4-64. *Fungal. Genet. Biol.* 42, 963–975. doi: 10.1016/j.fgb.2005.09.004

Petris, M. J., Mercer, J. F., Culvenor, J. G., Lockhart, P., Gleeson, P. A., and Camakaris, J. (1996). Ligand-regulated transport of the Menkes copper P-type ATPase efflux pump from the Golgi apparatus to the plasma membrane: a novel mechanism of regulated trafficking. *EMBO J.* 15, 6084–6095.

Riggle, P. J., and Kumamoto, C. A. (2000). Role of a *Candida albicans* P1-type ATPase in resistance to copper and silver ion toxicity. *J. Bacteriol.* 182, 4899–4905. doi: 10.1128/JB.182.17.4899-4905.2000

Rosenzweig, A. C., and Argüello, J. M. (2012). Toward a molecular understanding of metal transport by P(1B)-type ATPases. *Curr. Top. Membr.* 69, 113–136. doi: 10.1016/B978-0-12-394390-3.00005-7

Samanovic, M. I., Ding, C., Thiele, D. J., and Darwin, K. H. (2012). Copper in microbial pathogenesis: meddling with the metal. *Cell Host. Microbe* 11, 106–115. doi: 10.1016/j.chom.2012.01.009

Sambrook, J., Fritsch, E. F., and Maniatis, T. (1989). *Molecular Cloning: A Laboratory Manual*. New York, NY: Cold Spring Harbor Laboratory Press.

Shiraishi, E., Inouhe, M., Joho, M., and Tohoyama, H. (2000). The cadmium-resistant gene, CAD2, which is a mutated putative copper-transporter gene (PCA1), controls the intracellular cadmium-level in the yeast S. cerevisiae. *Curr. Genet.* 37, 79–86. doi: 10.1007/s002940050013

Smith, N., Wei, W., Zhao, M., Qin, X., Seravalli, J., Kim, H., et al. (2016). Cadmium and secondary structure-dependent function of a degron in the Pca1p cadmium exporter. *J. Biol. Chem.* 291, 12420–12431. doi: 10.1074/jbc.M116.724930

Solioz, M., and Odermatt, A. (1995). Copper and silver transport by CopB-ATPase in membrane vesicles of *Enterococcus hirae*. *J. Biol. Chem.* 270, 9217–9221. doi: 10.1074/jbc.270.16.9217

Staneviciene, I., Sadauskiene, I., Lesauskaite, V., Ivanoviene, L., Kasauskas, A., and Ivanov, L. (2008). Subacute effects of cadmium and zinc ions on protein synthesis and cell death in mouse liver. *Medicina* 44, 131–138.

Sutherland, D. E., and Stillman, M. J. (2011). The "magic numbers" of metallothionein. *Metallomics* 3, 444–463. doi: 10.1039/c0mt00102c

Suzuki, M., and Gitlin, J. D. (1999). Intracellular localization of the Menkes and Wilson's disease proteins and their role in intracellular copper transport. *Pediatr. Int.* 41, 436–442. doi: 10.1046/j.1442-200x.1999.01090.x

Szewczyk, E., Nayak, T., Oakley, C. E., Edgerton, H., Xiong, Y., Taheri-Talesh, N., et al. (2006). Fusion PCR and gene targeting in *Aspergillus nidulans*. *Nat. Protoc.* 1, 3111–3120. doi: 10.1038/nprot.2006.405

Thiele, D. J. (1988). ACE1 regulates expression of the *Saccharomyces cerevisiae* metallothionein gene. *Mol. Cell Biol.* 8, 2745–2752. doi: 10.1128/MCB.8.7.2745

Thorsen, M., Perrone, G. G., Kristiansson, E., Traini, M., Ye, T., Dawes, I. W., et al. (2009). Genetic basis of arsenite and cadmium tolerance in *Saccharomyces cerevisiae*. *BMC Genomics* 10:105. doi: 10.1186/1471-2164-10-105

Tilburn, J., Scazzocchio, C., Taylor, G. G., Zabicky-Zissman, J. H., Lockington, R. A., and Davies, R. W. (1983). Transformation by integration in *Aspergillus nidulans*. *Gene* 26, 205–221. doi: 10.1016/0378-1119(83)90191-9

Valix, M., Tang, J. Y., and Malik, R. (2001). Heavy metal tolerance of fungi. *Miner. Eng.* 14, 499–505. doi: 10.1016/S0892-6875(01)00037-1

Valko, M., Morris, H., and Cronin, M. T. (2005). Metals, toxicity and oxidative stress. *Curr. Med. Chem.* 12, 1161–1208. doi: 10.2174/0929867053764635

Weissman, Z., Berdicevsky, I., Cavari, B. Z., and Kornitzer, D. (2000). The high copper tolerance of *Candida albicans* is mediated by a P-type ATPase. *Proc. Natl. Acad. Sci. U.S.A.* 97, 3520–3525. doi: 10.1073/pnas.97.7.3520

Weissman, Z., Shemer, R., and Kornitzer, D. (2002). Deletion of the copper transporter CaCCC2 reveals two distinct pathways for iron acquisition in *Candida albicans*. *Mol. Microbiol.* 44, 1551–1560. doi: 10.1046/j.1365-2958.2002.02976.x

Wiemann, P., Perevitsky, A., Lim, F. Y., Shadkchan, Y., Knox, B. P., Landero Figueora, J. A., et al. (2017). *Aspergillus fumigatus* copper export machinery and reactive oxygen intermediate defense counter host copper-mediated oxidative antimicrobial offense. *Cell Rep.* 19, 1008–1021. doi: 10.1016/j.celrep.2017.04.019

Yu, W., Farrell, R. A., Stillman, D. J., and Winge, D. R. (1996). Identification of SLF1 as a new copper homeostasis gene involved in copper sulfide mineralization in *Saccharomyces cerevisiae*. *Mol. Cell Biol.* 16, 2464–2472. doi: 10.1128/MCB.16.5.2464

Zhou, P., Szczypka, M. S., Sosinowski, T., and Thiele, D. J. (1992). Expression of a yeast metallothionein gene family is activated by a single metalloregulatory transcription factor. *Mol. Cell Biol.* 12, 3766–3775. doi: 10.1128/MCB.12.9.3766

REVIEW

New insights into copper homeostasis in filamentous fungi

Martzel Antsotegi-Uskola [1] · **Ane Markina-Iñarrairaegui** [1] · **Unai Ugalde** [1]

Abstract

Copper is a metal ion that is required as a micronutrient for growth and proliferation. However, copper accumulation generates toxicity by multiple mechanisms, potentially leading to cell death. Due to its toxic nature at high concentrations, different chemical variants of copper have been extensively used as antifungal agents in agriculture and medicine. Most studies on copper homeostasis have been carried out in bacteria, yeast, and mammalian organisms. However, knowledge on filamentous fungi is less well documented. This review summarizes the knowledge gathered in the last few years about copper homeostasis in the filamentous fungi *Aspergillus fumigatu*s and *Aspergillus nidulans*: The mechanism of action of copper, the uptake and detoxification systems, their regulation at the transcriptional level, and the role of copper homeostasis in fungal pathogenicity are presented.

Keywords Copper · Homeostasis · Ctr · P-type ATPase · Transcription factor

Introduction

Virtually, all organisms depend on metal ions as catalysts, as structural elements in proteins, in electron transfer reactions, or as messengers. The first-row transition metals, cobalt (Co), copper (Cu), iron (Fe), manganese (Mn), and nickel (Ni), possess specific redox potential characteristics which are unavoidably required in key biological processes (Gerwien et al. 2018; Nevitt et al. 2012).

The availability of these metals must be maintained within a narrow range of concentrations, as an excess can easily result in metal toxicity (Blatzer and Latge 2017). All organisms have developed precise mechanisms to respond to fluctuations in extracellular metal availability enabling homeostatic regulation for each metal ion species. This is achieved by accurate sensing of extracellular and intracellular levels, and the activation of stimulus-response pathways that maintain intracellular levels within the safety range (Nevitt et al. 2012).

Copper functions as a cofactor in enzymes involved in processes such as cellular respiration (cytochrome-c oxidase), free radical detoxification (superoxide dismutase), pigmentation (tyrosinase), collagen maturation (lysyl oxidase), and iron acquisition (Ding et al. 2014; Lutsenko 2010; Nevitt et al. 2012). However, accumulation of copper beyond homeostatic capacity generates toxicity. An excess of free cytosolic copper ions leads to the inactivation of other metalloenzymes by metal displacement, the inappropriate engagement with intracellular metalophilic ligands such as Fe-S clusters, and the generation of reactive oxygen species (ROS) through Fenton chemistry (Fridovich 1983; Macomber and Imlay 2009). The essential, yet toxic, nature of copper demands for sensitive control mechanisms over intracellular Cu levels.

Most studies in copper homeostasis have been carried out on mammalian, bacteria, and yeast model systems. The model yeast *Saccharomyces cerevisiae* has served as an important reference for other lower eukaryotes (Balamurugan and Schaffner 2006), including pathogens like *Cryptococcus neoformans* and *Candida albicans* (Ballou and Wilson 2016). In these models, copper is also a recognized virulence factor (Zhang et al. 2016). A number of recent publications have described copper import and export mechanisms in *Aspergillus fumigatus*, a common airborne fungal pathogen (Blatzer and Latge 2017), responsible of severe invasive aspergillosis in immunocompromised patients (Cai et al. 2017).

In this review, we present an overview of recently published findings on different aspects of copper homeostasis in filamentous fungi, which constitute a major group of microorganisms associated with agricultural, food, clinical, and

✉ Unai Ugalde
 unaiona.ugalde@ehu.eus

1   Microbial Biochemistry Laboratory, Department of Applied
    Chemistry, Faculty of Chemistry, University of the Basque Country,
    San Sebastian, Spain

environmental issues. We will pay special attention to *Aspergillus fumigatus*, the model organism *Aspegillus nidulans*, and the plant pathogen *Botrytis cinerea*.

Copper import across membranes

Fungal hyphae must acquire copper from the environment and maintain intracellular concentration within the micromolar range. Copper is generally internalized through low- and high-affinity uptake systems, depending on extracellular copper concentration. The most studied copper transport system is that of *S. cerevisiae*, and studies in other fungi have been shown to be considerably similar (Balamurugan and Schaffner 2006).

The membrane-associated copper transporting protein (Ctr) family is omnipresent in all eukaryotes and they all share high specificity for copper. Ctr proteins are relatively small (18–30 kDa) and can contain up to three transmembrane domains (Petris 2004; Puig et al. 2002). Copper binding or acquisition motifs (Mets) are located in the extracellular N-terminal region and are rich in methionine (MxxM or MxM) (Jiang et al. 2005). Another methionine-rich motif MxxxM, located in a transmembrane domain, has been proved to be essential for copper ion (Cu^+) transport through the membrane (Puig et al. 2002). Ctr monomers assemble forming a trimer, as Cu^+ transport requires Ctr protein multimerization to create a pore that drives the copper ion through the membrane (De Feo et al. 2009). Cu^+ enters the cell by passive transport, facilitated by an extremely low intracellular copper concentration (Balamurugan and Schaffner 2006). Copper is normally present in the environment in two oxidation forms: Cu^{2+} and Cu^+. However, only Cu^+ is recognized as a substrate by the transporters. The extracellular Cu^{2+} is reduced by plasma membrane reductases prior to internalization. These plasma membrane reductases are equally widespread in eukaryotes (Garcia-Santamarina et al. 2018; Marvin et al. 2004).

The high-affinity copper uptake system in filamentous fungi contains all the elements mentioned above. In *Aspergillus fumigatus*, four Ctr proteins have been identified, AfCtrA1, AfCtrA2, AfCtrB, and AfCtrC. Phylogenetic analysis showed that these four proteins are closely related to *S. cerevisiae* Ctr1. AfCtrB showed higher homology to ScCtr2 (Park et al. 2014), a copper transporter that pumps copper ions out of the vacuoles in conditions of copper scarcity (Rees et al. 2004). Each protein has at least two transmembrane domains, four in the case of AfCtrB. All of them resemble the characteristic N-terminal Mets motifs for copper uptake and the MxxxM motif in one transmembrane domain, responsible of ion translocation (Park et al. 2014). In *A. nidulans*, three Ctr proteins have been identified, AnCtrA and AnCtrB and AnCtrC. AnCtrB is the putative ortholog of ScCtr2. The other two proteins possess the characteristic features of the copper

transporting proteins. However, orthology studies of each Ctr protein reveal very different results. AnCtrC is related to many other Ctr proteins that have already been characterized, for example, ScCtr3 and the abovementioned AfCtrC. On the other hand, AnCtrA is related to no characterized protein so far (Antsotegi-Uskola et al., unpublished). Even though they have not been characterized, *A. nidulans* and *A. fumigatus* possess several putative plasma membrane reductases, responsible of iron and copper reduction prior to uptake. Two putative plasma membrane reductases are phylogenetically related to ScFre1 in *A. nidulans* and only one in *A. fumigatus*. In conclusion, both organisms possess all the components of the high-affinity copper uptake system described in *S. cerevisiae*: multiple Ctr proteins and the plasma membrane reductases (Antsotegi-Uskola et al., unpublished) (Fig. 1).

Out of all the Ctr proteins identified in each organism, usually, two function as copper uptake proteins. Although the contribution of each protein to the high-affinity copper uptake system varies, functional complementation between the activities is a general trait. In *A. fumigatus*, only *AfctrA2* and *AfctrC* were able to complement the disruption of *ctr1* in *S. cerevisiae* (Park et al. 2014). The same authors claim that both proteins are equally functional, since individual deletion mutants of *AfctrA2* and *AfctrC* exhibited a wild type–like phenotype with 100 μM BCS (Bathocuproinedisulfonic acid disodium salt, a copper chelator). According to Cai et al. (2017), however, the *AfctrC* deletion mutant showed defective colony morphology with 100 μM BCS, suggesting that this protein plays a dominant role in copper homeostasis.

Expression of Ctr proteins is copper-dependent, as expression of *AfctrA2* and *AfctrC* increases under copper deficiency conditions and progressively decreases as extracellular copper concentrations rise. According to Park and collaborators (Park et al. 2014), the expression of either *AfctrC* or *AfctrA2* is upregulated when the other is missing. Cai and collaborators (Cai et al. 2017), on the other hand, claim that only *AfctrC* expression is upregulated when the counterpart is deleted. Taken together, the data obtained by Cai and collaborators suggest that AfCtrC plays a dominant role in copper uptake. In both cases, the double deletion mutant displayed severe growth defects with 100 μM BCS, suggesting that AfCtrA2 and AfCtrC, the two Ctr proteins that work as copper internalization proteins, function in a complementary manner.

In *A. nidulans*, the *AnctrC* deletion mutant displayed a defect in pigmentation with 100 μM BCS (copper is required for the formation of conidiospores and colony pigmentation). On the other hand, *AnctrA* deletion had no visible effect on colony phenotype. The double deletion mutant showed a very aggravated growth defect in 100 μM BCS, suggesting a synergistic relationship between *AnctrA* and *AnctrC*. The short-term response, from basal condition to 3 h of exposure to copper and BCS of these proteins, has been studied and they show a different expression profile. The *AnctrC* transcript, as
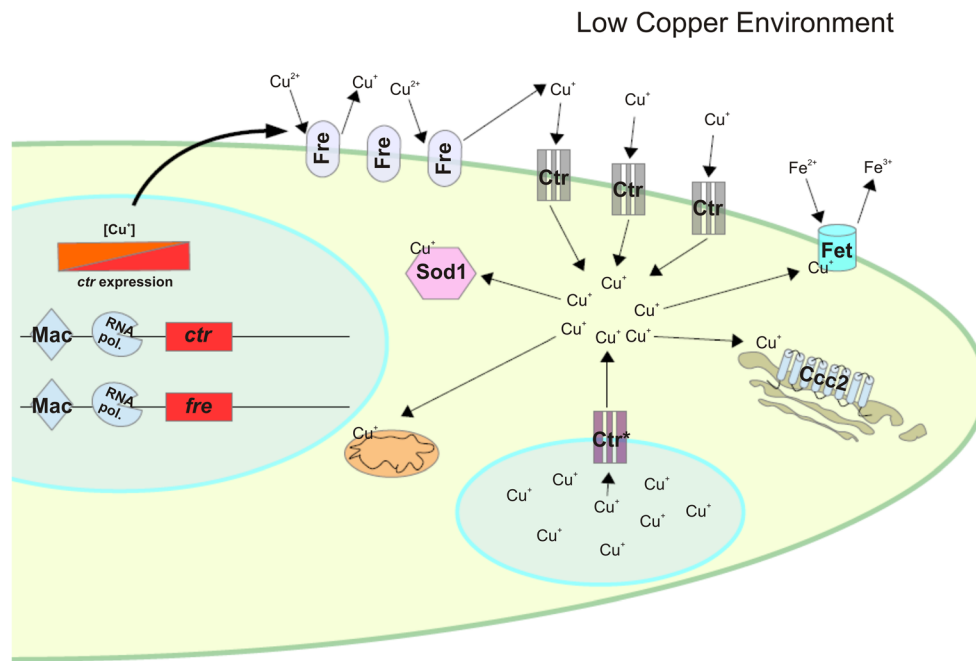
Low Copper Environment

Fig. 1 Copper homeostasis scheme for *A. nidulans* and *A. fumigatus*, under conditions of low copper availability. TF MacA binds to DNA enabling the transcription of the copper transporting proteins (*ctr*) and the plasma membrane copper reductase (*fre*) coding genes. The plasma membrane copper reductases (Fre) reduce environmental copper from Cu^{2+} to Cu^+. Subsequently, the copper transporting proteins (Ctr) introduce copper to the cell. Within the cell, Cu^+ ions are distributed to the

mitochondria as cofactor of the electron transport chain enzymes, the superoxide dismutase Sod1 or the ferroxidase Fet, essential for Reductive Iron Assimilation (RIA). Copper is also distributed to the P-type ATPase Ccc2, responsible of Cu^+ mobilization to the secretory compartment. (*) The Ctr protein identified as the ScCtr2 ortholog is regulated in a MacA-independent manner and pumps copper ions to the cytosol from the vacuole compartment in copper scarcity conditions

well as the protein, was present at copper satiety conditions, and expression increases with addition of BCS. The expression pattern of *AnctrA*, on the other hand, was different; the *AnctrA* transcript was present at copper satiety conditions, but the protein was not present. Upon addition of BCS, *AnctrA* transcript levels rose dramatically and the protein was first detected after 2 h of exposure to the copper chelator. The expression of both copper transporters was upregulated when the other one was missing, supporting the complementary role observed in protein function. In the case of *AnctrC*, the upregulation amounted to almost 17-fold, while in the case of *AnctrA*, it reached 64-fold. Despite this increase, *AnctrA* expression alone could not overcome the copper deficiency phenotype generated with 100 μM BCS. Correspondingly, the *AnctrC* deletant strain showed a pigmentation defect under copper starvation conditions. All together, these data suggest a dominant role of AnCtrC in *A. nidulans* high-affinity copper uptake system (Antsotegi-Uskola et al., unpublished).

The high-affinity copper uptake systems of *A. fumigatus* and *A. nidulans* share indeed many similar features with *S. cerevisiae*. Usually, more than one Ctr proteins are found in each organism but only one or two of them have a direct role in copper internalization. In both organisms, one of the Ctr proteins has a dominant role over the other one, but the deletion of both Ctr proteins proves the complementary relationship between both proteins.

Copper detoxification

Even if copper import is a strictly controlled process, there are circumstances in which intracellular copper levels surpass the toxicity threshold. In response to an excessive intracellular copper concentration, detoxification/sequestration mechanisms are activated in order to restore cellular copper balance. In contrast to the similarity in proteins and mechanisms described for copper uptake, two major mechanisms have been reported for copper detoxification processes, marking an important division between filamentous fungi, as detailed below.

Two major mechanisms for copper detoxification have been described in fungi. One of them relies on copper sequestration by metallothioneins (MTs) and exhaustively described in *S. cerevisiae*. It involves two copper-specific MTs, Cup1 and Crs5, and these two proteins are responsible of copper resistance (Culotta et al. 1994; Jensen et al. 1996). This mechanism has not been described in *Aspergillus* species, but for example in *C. albicans*, metallothioneins do contribute to copper detoxification (Weissman et al. 2000).

The second mechanism, detoxification, has been described in other filamentous fungi studied so far. It relies on P_{IB}-type ATPases, ATP-dependent heavy metal translocators that are deeply conserved from archaea to mammals. P_{IB}-type ATPases have peculiar terminal extensions (N- or C-terminal) which contain metal (copper) binding domains (MBDs), rich

in Cys and sometimes His. P_{IB}-ATPases possess 6 to 8 transmembrane domains (TMDs), metal binding sequences in their TMDs, regulatory MBDs, a structure involved in enzyme phosphorilation (P-domain), a nucleotide binding domain (N-domain), and an energy transduction domain (A-domain) (Palmgren and Nissen 2011).

These copper extrusion pumps represent the main detoxification mechanism in bacteria (Ladomersky and Petris 2015), and in eukaryotes, they are also involved in copper compartmentalization into the secretory network where copper is incorporated into different Cu-dependent proteins as a cofactor. In humans, two P_{IB}-ATPases ATP7A (Menkes disease protein) and ATP7B (Wilson disease protein) are responsible of delivery of copper to the *trans*-Golgi compartment (TGN) (Lutsenko et al. 2007). In response to Cu toxicity, both transporters change their location from the TGN to the cell membrane to act as detoxification (export) pumps conferring copper resistance to the cell (Suzuki and Gitlin 1999). In the dimorphic fungus *C. albicans*, each task is fulfilled by a different P_{IB}-ATPase; CaCcc2 is involved in copper compartmentalization into the TGN and CaCrp1p is responsible of copper detoxification at the plasma membrane (Riggle and Kumamoto 2000; Weissman et al. 2000). It has recently been described that some species of the *Aspergillus spp*. possess two CaCrp1p homologs involved in copper detoxification (Yang et al. 2018).

This divergence in the mechanism of metal detoxification by different fungal species may be the result of an adaptation to their respective ecological niches. *S. cerevisiae* has been isolated from a range of environments (Goddard and Greig 2015), many of which are specific, such as fruits and flowers. In contrast, *C. albicans*, like most filamentous fungi, is an all-rounder found in environments ranging from the digestive tracts of animals to soils, where competition and antagonism are common. In these environments, P_{IB}-ATPase (CaCrp1p) mediated copper export confers superior tolerance with respect to MTs, despite the greater cost in energy required to produce it and operate it. MTs, on the other hand, may allow for the immobilization of greater amounts of copper, as a resource, in media which may be especially poor in copper, such as flower nectar. In the same medium and growing conditions, *S. cerevisiae* is able to grow in up to 2 mM of $CuSO_4$, whereas *C. albicans* tolerates 20 mM $CuSO_4$ (Weissman et al. 2000).

C. albicans has become a benchmark for recent studies in filamentous fungi, such as the Aspergilli. Copper detoxification in *A. nidulans* relies on a P_{IB}-type ATPase termed CrpA (Antsotegi-Uskola et al. 2017). AnCrpA contains all the characteristic domains described in a P_{IB}-type ATPase: 8 TMDs, an ion translocation motif (CPC) in the sixth TMD and cysteine-rich MBDs in the cytoplasmic N-terminal domain. Five N-terminal MBDs are present as tandem repeats, and two CxxxC motifs are followed by three GMxCxxC classic

heavy metal–associated domains (HMA). Copper detoxification in *A. fumigatus* also depends on a P_{IB}-type ATPase termed AfCrpA (Wiemann et al. 2017).

Deletion of *crpA* resulted in acute susceptibility to copper in *A. nidulans* and *A. fumigatus*. Susceptibility towards other metals was also observed in the *A. nidulans crpA* deletant strain, albeit not comparably with Cu susceptibility. Expression analysis corroborated the copper detoxification role of AnCrpA. Exposure to copper had a dramatic effect on *AncrpA* expression, while other metals barely induced expression. The *AncrpA* deletant strain manifested reduced resistance to Cu compared with the wild type strain in solid medium (~ 10-fold). With 100 μM $CuSO_4$, the colony exhibited morphological defects and at 150 μM $CuSO_4$, an almost complete growth inhibition. At 100 μM $CuSO_4$, the colony exhibited a typical wild type radial growth pattern, but with very slight cellular density. This cellular morphology was named the "copper phenotype." The *AncrpA* deletant strain showed some sensitivity to Cd and Ag, but far lower than to Cu (Antsotegi-Uskola et al. 2017).

AncrpA expression analysis revealed that it is principally expressed in the presence of copper (100 μM $CuSO_4$), showing strong transient induction shortly upon exposure. mRNA appears 15 min after copper addition and the protein, after 30 min. The expression maximum is reached at 60 min followed by a gradual repression over time. The pattern of AnCrpA expression with Ag and Cd toxicities is similar, albeit several times weaker. In the case of Cd, with 250 μM $Cd(NO_3)_2$, a very faint band was visible at 120′ after exposure. It has recently been reported that AfCrpA also contributes to Zn resistance in *A. fumigatus* (Cai et al. 2018). These results indicate that even if it might have some role in other heavy metal detoxification, copper is the principal ion transported by CrpA (Antsotegi-Uskola et al. 2017).

AnCrpA is localized at the plasma membrane under copper stress conditions; however, depending on the level of stress, AnCrpA localization and function can change. After half an hour of copper addition to induce AnCrpA expression, subcellular localization studies show that fluorescence was localized at a reticulated network (highly likely the endoplasmic reticulum), surrounding structures that resemble the nucleus and strands associated to the plasma membrane under nontoxic copper loads. An hour after copper addition, AnCrpA appeared homogeneously dispersed in the cytoplasm and primarily distributed at the cell periphery, most likely at the plasma membrane. In numerous cells, fluorescence was polarized to the tip of hyphae. Approximately 2 h after copper addition, the protein mostly remained at the periphery, but fluorescent aggregates gradually appeared throughout the cytosol. After 3 h of copper exposure, large aggregates on vesicles resembling vacuolar compartments became visible (Antsotegi-Uskola et al. 2017). The authors hypothesized that de novo synthesized AnCrpA was translocated from the Golgi

compartment to the plasma membrane upon copper toxicity. Once the detoxification process decreased intracellular copper levels, part of the AnCrpA localized to the PM may have been recycled by endocytosis and redistributed to the multivesicular body. It is also possible that AnCrpA could be recycled back to the PM (Pase et al. 2004). As a result of this, the fluorescent protein detected at the plasma membrane could represent a mixed pool of the de novo synthesized and recycled protein (Fig. 2).

The P-type ATPase termed CrpA exerts the main detoxification mechanism found in *A. nidulans* and *A. fumigatus*. Deletion of *AncrpA* resulted in hypersensitivity to Cu and a slight susceptibility to other metals. AnCrpA is mostly localized at the plasma membrane under copper toxicity conditions. However, AnCrpA localization varies throughout the detoxification process. Most filamentous fungi possess an ortholog of the above-described CrpA protein, meaning that their detoxification mechanisms could be P$_{IB}$-ATPase-dependent.

Genetic regulation of copper homeostasis

Copper homeostasis is principally regulated at the transcriptional level. Metal responsive transcription factors are able to sense the copper concentration within the cell and orchestrate a response by activating the copper import or copper detoxification, as required. These two regulatory paths are under the control of two separate transcription factors (Keller et al. 2005) which were first discovered in *S. cerevisiae* as Mac1 and Ace1 (Balamurugan and Schaffner 2006), and later described in *A. nidulans* and *A. fumigatus* (Antsotegi-Uskola et al. 2017; Cai et al. 2019; Kusuya et al. 2017; Wiemann et al. 2017).

The high-affinity copper uptake system is controlled by the transcription factor MacA. All ascomycetes possess the characteristic functional domains of this copper sensing TF. The N-terminal region contains a RGHR and GRP motifs and the "Cu fist" domain, all together, they are responsible of the Cu-dependent DNA binding of the TF (Cai et al. 2017). A C-terminal copper binding domain with two cysteine-rich motifs is responsible for copper sensing (Kusuya et al. 2017). Site-directed mutagenesis studies in *A. fumigatus* and *A. nidulans* have demonstrated that Cys residues of the N-terminal "Cu fist" domain are essential for MacA DNA binding (Cai et al. 2019). Under copper limitation, AfMacA binds copper response elements 5′-TGTGCTCA-3′ in the gene promoter regions and enables the transcription of the Ctr proteins for copper uptake (Park et al. 2017). On the other hand, copper accumulation leads to AfMacA inactivation. The C-terminal copper binding domain acts as an auto-inhibitory domain (Park et al. 2017). Different studies have demonstrated that AfMacA is necessary for Ctr protein expression, Cu^{2+} metalloreductase expression, SOD activity, and many other
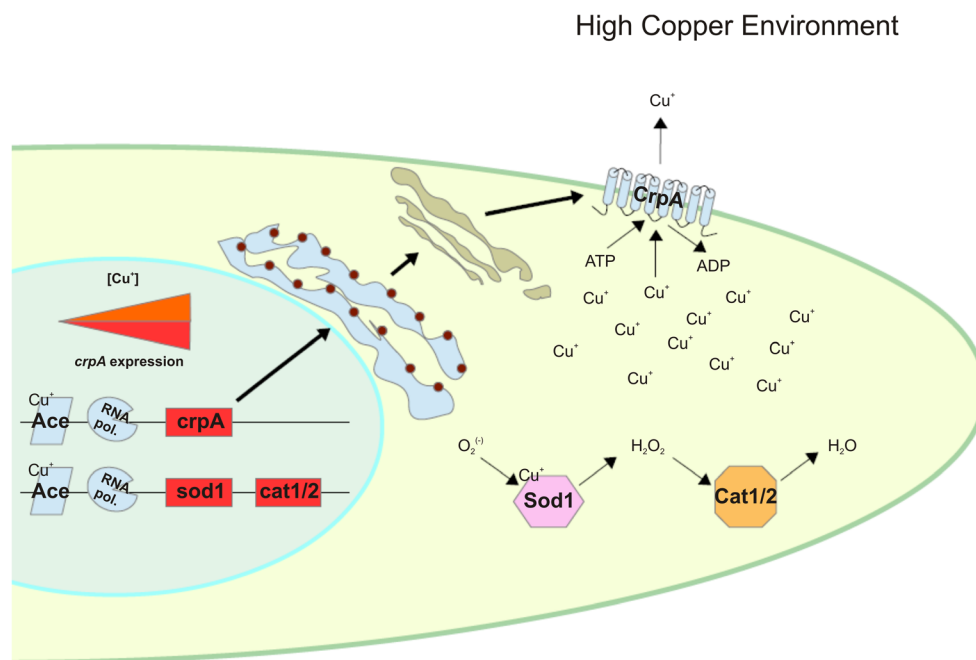

Fig. 2 Copper homeostasis scheme for *A. nidulans* and *A. fumigatus*, under copper toxicity conditions. The TF AceA binds copper forming a tetra-copper-thiolate cluster, thereby changing its conformation. By changing conformation, AceA is able to bind DNA and enables the transcription of the P-type ATPase *crpA* coding gene. The P-type ATPase CrpA is first synthesized in the endoplasmic reticulum and migrates to the plasma membrane passing through the Golgi apparatus. Once stabilized in the plasma membrane, CrpA pumps Cu^+ ions out of the cell in order to reduce copper toxicity within the cell. Meanwhile, the superoxide dismutase *sod1* and catalase *cat1/2* coding genes experiment AceA-mediated activation. Sod1 and Cat1/2 neutralize ROS generated by Cu^+ toxicity or host organism defense mechanisms

copper-dependent cellular processes (Fig. 1). It has recently been reported that AfMacA also regulates iron homeostasis and its localization in the cell varies depending on copper and iron concentration (Park et al. 2018). *AfmacA* disruption generated a copper starvation phenotype with manifest growth defects in copper depletion conditions (Cai et al. 2017; Kusuya et al. 2017; Park et al. 2017).

The copper detoxification process is orchestrated by the transcription factor AceA. In *A. fumigatus*, AfAceA is also involved in zinc detoxification (Cai et al. 2018). The characteristic domains that identify this TF are the "Cu fist" DNA binding domain, and the numerous cysteine residues arranged in CxC-CxxC segments through the protein sequence, identified as necessary for function in *S. cerevisiae* (Hu et al. 1990). Within the DNA binding domain, two different motifs are found, a 3 x Cys-His zinc finger and the KGRP motif for DNA binding stabilization. A single cysteine-rich domain is located downstream of the DNA binding domain. Under excess copper conditions, four Cu^+ atoms bind the Cys-rich domain to form a tetra-copper-thiolate cluster (Dameron et al. 1991). Cluster formation leads to a conformational change that enables AceA-DNA binding. In this way, AceA enables the transcription of the copper detoxification machinery, principally *crpA*. AfAceA also regulates ROS detoxification genes *sod1*, *cat1*, and *cat2* (Wiemann et al. 2017), as well as the TFs *AftA* and *Yap1* mediating ROS defense (Hagiwara et al. 2016) (Fig. 2). *aceA* deletion resulted in a defective phenotype with severe growth defects under copper excess conditions in *A. fumigatus* and *A. nidulans* (Antsotegi-Uskola et al. 2017; Cai et al. 2018).

In summary, even though copper homeostasis is transcriptionally regulated by a single transcription factor in some organisms, such as *C. neoformans*, in most filamentous fungi, it is orchestrated by two transcription factors. The TF-termed MacA is responsible of conducting the copper internalization process and AceA does the same with copper detoxification. The characteristic features of these transcription factors are well conserved in filamentous fungi.

Copper as a virulence factor

A. fumigatus is one of the most lethal airborne fungal pathogens responsible of severe invasive aspergillosis (IA), especially in immunocompromised individuals (Cai et al. 2017). Copper is a recognized virulence factor, as it is the cofactor of many enzymes that contribute to virulence, such as laccases or SOD. On the other hand, host organisms have developed defense strategies against fungal pathogens that target copper availability. By scavenging all Cu^+ in the infection area, copper deprivation can be induced in the pathogen. On the contrary, host innate immune cells, such as macrophages, are able to mobilize copper to invading fungal tissue as a defense

mechanism (Garcia-Santamarina and Thiele 2015). The generation of Reactive Oxidative Species (ROS) is another defense mechanism employed by the innate immune system. The superoxide dismutase (SOD) enzymes are copper-dependent enzymes responsible of neutralizing ROS, so the SOD enzyme is considered as an important virulence factor in organisms, like *C. albicans* and *C. neoformans* (Frohner et al. 2009; Narasipura et al. 2005). In conclusion, copper homeostasis plays a key role to overcome host barriers and the development of pathogenesis.

Disruption of any of the abovementioned TFs responsible for copper homeostasis has a direct effect on virulence. Recent studies revealed that AfMacA is necessary for normal virulence in *A. fumigatus* (Cai et al. 2017). *AfmacA* deletion results in delayed growth and pigmentation deficiency by DHN melanin synthesis inhibition. Laccases AfAbr1 and AfAbr2 are involved in melanin biosynthesis and they are copper-dependent proteins (Upadhyay et al. 2013). When copper uptake is impaired, laccase activity is substantially reduced (Park et al. 2014). Melanin confers a non-immunogenic status to the fungus. Inappropriately melanized conidia therefore become immunoreactive (Pihet et al. 2009). Melanin also provides a protective layer to the action of host-derived ROS (Jahn et al. 2000). *A. fumigatus* copper transporting protein expression is upregulated in the presence of human neutrophils (Sugui et al. 2008). This underscores the importance of copper uptake for pathogen viability within the host.

AfAceA has also been shown to be an important virulence factor. As detailed above, this TF controls the expression of the P_{IB}-type ATPase *AfcrpA* responsible of copper detoxification in *A. fumigatus*. Moreover, AfAceA regulates the expression of catalases such as *Afcat1* and *Afcat2* involved in ROS neutralization and the TF *AfatfA* involved in ROS-response (Hagiwara et al. 2014). It has been reported that *AfatfA* deletion renders *A. fumigatus* avirulent (Pereira et al. 2017). *AfaceA* deletion represses *AfatfA* expression considerably, together with *Afcat1* and *Afcat2*, making the fungus more vulnerable to oxidative stress (Wiemann et al. 2017). Deletion of *AfaceA* inhibits the expression *AfcrpA*, the main copper detoxification system in *A. fumigatus*, leaving the fungus exposed to copper mobilization to fungal tissue by host innate immune system cells. Thus, the copper detoxification machinery is a key factor in pathogen viability during infection.

Botrytis cinerea is a necrotrophic fungal plant pathogen of worldwide distribution, capable of infecting a wide range of hosts. It is probably the best studied necrotrophic plant pathogen. Copper-dependent proteins play a central role in many aspects of the *B. cinerea*, including pathogenesis. The P-type ATPase BcCcc2, an ortholog of the *S. cerevisiae* Ccc2 copper transporting P-type ATPase that delivers Cu to the secretory compartment for subsequent protein modification (Smith et al. 2017), is crucial for virulence in *B. cinerea* (Saitoh et al. 2010). The *Bcccc2* deletion strain presented melanization

and morphogenesis defects. Moreover, the deletion strain was not able to penetrate and infect host organisms (Saitoh et al. 2010). The most probable reason for this could be that the BcCcc2 targeted proteins could get no copper, and for this reason, all these cellular processes were impaired (Saitoh et al. 2010). *B. cinerea* is able to break through healthy tissue and secrete enzymes and toxins that generate necrosis (van Kan 2006). Lopez-Cruz and collaborators (Lopez-Cruz et al. 2017) revealed the importance of the Cu-Zn SOD in this process. The host oxidative burst (O⁻), a plant defense mechanism against pathogen organisms, plays an active role in *Botrytis* infection (Rossi et al. 2017). The O_2^-/H_2O_2 ratio in the necrotic lesion area is very significant for infection development. Higher concentration of H_2O_2 favors infection. BcSod1 actively generates H_2O_2, which damages plant tissue and reduces plant defense. The absence BcSod1 reduces the capacity to generate necrotic lesions in plant tissues as the oxidative environment is not appropriate for *Botrytis* infection development. The measured O^-/H_2O_2 ratio in necrotic lesions caused by a $\Delta Bcsod1$ strain is too high for infection. Incorrect function of BcCcc2 results in a defective BcSod1 function, as well as other proteins, proving the importance of the copper homeostasis system for *B. cinerea* virulence.

In summary, copper homeostasis plays an essential role in *A. fumigatus* virulence development. The high-affinity copper uptake system and the copper detoxification system are key factors in the infection mechanism. The high-affinity copper uptake system enables the maturation of many copper-dependent enzymes for virulence. On the other hand, the detoxification system confers the organism the necessary resistance for survival. In the necrotrophic fungus *B. cinerea*, the copper transporting P-type ATPase BcCcc2 is necessary for successful virulence development. Hence, copper homeostasis appears to be required for the development of infection in every major pathogenic fungus described thus far.

Conclusions

The study of copper homeostasis in filamentous fungi has unveiled the relevance of this cation in growth, development, and pathogenicity. In the last years, there have been some contributions in the pathogenic fungus *A. fumigatus* and the model organism *A. nidulans*, but many details remain to be uncovered. Considering the repercussion of copper homeostasis on fungal biology, it is a topic worth studying in more depth, and in a wider range of species. The copper uptake and detoxification mechanisms and their respective transcription factors have been the focus of recent publications, identifying the principal participants of each process, but the copper buffering and intracellular distribution mechanisms remain practically unknown. Phylogenetic analyses have revealed the presence of proteins that act as copper scavenging

and trafficking vehicles in other organisms (Ding et al. 2014), but so far, those proteins have not been investigated. Up to date, there is no evidence of CrpA homolog–dependent virulence in a phytopathogenic fungus. However, the BcCcc2 P-type ATPase, responsible of Cu traffic to the secretory compartment, in *Botrytis cinerea* has been proved to be essential for virulence. This evidence calls for further investigation covering intracellular copper trafficking and storage in oncoming years.

Copper has long been used as an antimicrobial agent in many different areas (Judet-Correia et al. 2011); however, it has often been applied in doses which cause severe impact on the environment. This excessive use has also brought about increasing levels of copper resistance in microbial pathogens. The mechanisms involved in fungal copper resistance are now in need of a thorough assessment in order to find new and effective methods to complement or replace copper in the control of fungal disease. New details on the mechanism of copper toxicity on fungal cells may shed light on the potential use of synergists affecting copper homeostasis that could help lower the currently required copper dose. The acquisition of copper by fungi in the soil, and its exchange between microorganisms and plants in symbiotic relationship, is another aspect which should be considered, to ensure sustainable agricultural and environmental conservation programs.

Compliance with ethical standards

References

Antsotegi-Uskola M, Markina-Inarrairaegui A, Ugalde U (2017) Copper resistance in Aspergillus nidulans relies on the PI-type ATPase CrpA, regulated by the transcription factor AceA. Front Microbiol 8:912

Balamurugan K, Schaffner W (2006) Copper homeostasis in eukaryotes: teetering on a tightrope. Biochim Biophys Acta 1763:737–746

Ballou ER, Wilson D (2016) The roles of zinc and copper sensing in fungal pathogenesis. Curr Opin Microbiol 32:128–134

Blatzer M, Latge JP (2017) Metal-homeostasis in the pathobiology of the opportunistic human fungal pathogen Aspergillus fumigatus. Curr Opin Microbiol 40:152–159

Cai Z, Du W, Liu L, Pan D, Lu L (2019) Molecular characteristics of the conserved Aspergillus nidulans transcription factor Mac1 and its functions in response to copper starvation. mSphere. 4:e00670-18

Cai Z, Du W, Zeng Q, Long N, Dai C, Lu L (2017) Cu-sensing transcription factor Mac1 coordinates with the Ctr transporter family to regulate Cu acquisition and virulence in Aspergillus fumigatus. Fungal Genet Biol 107:31–43

Cai Z, Du W, Zhang Z, Guan L, Zeng Q, Chai Y, Dai C, Lu L (2018) The Aspergillus fumigatus transcription factor AceA is involved not only in Cu but also in Zn detoxification through regulating transporters CrpA and ZrcA. Cell Microbiol 20:e12864

Culotta VC, Howard WR, Liu XF (1994) CRS5 encodes a metallothionein-like protein in Saccharomyces cerevisiae. J Biol Chem 269:25295–25302

Dameron CT, Winge DR, George GN, Sansone M, Hu S, Hamer D (1991) A copper-thiolate polynuclear cluster in the ACE1 transcription factor. Proc Natl Acad Sci U S A 88:6127–6131

De Feo CJ, Aller SG, Siluvai GS, Blackburn NJ, Unger VM (2009) Three-dimensional structure of the human copper transporter hCTR1. Proc Natl Acad Sci U S A 106:4237–4242

Ding C, Festa RA, Sun TS, Wang ZY (2014) Iron and copper as virulence modulators in human fungal pathogens. Mol Microbiol 93:10–23

Fridovich I (1983) Superoxide radical: an endogenous toxicant. Annu Rev Pharmacol Toxicol 23:239–257

Frohner IE, Bourgeois C, Yatsyk K, Majer O, Kuchler K (2009) Candida albicans cell surface superoxide dismutases degrade host-derived reactive oxygen species to escape innate immune surveillance. Mol Microbiol 71:240–252

Garcia-Santamarina S, Festa RA, Smith AD, Yu CH, Probst C, Ding C, Homer CM, Yin J, Noonan JP, Madhani H, Perfect JR, Thiele DJ (2018) Genome-wide analysis of the regulation of Cu metabolism in Cryptococcus neoformans. Mol Microbiol 108:473–494

Garcia-Santamarina S, Thiele DJ (2015) Copper at the fungal pathogen-host axis. J Biol Chem 290:18945–18953

Gerwien F, Skrahina V, Kasper L, Hube B, Brunke S (2018) Metals in fungal virulence. FEMS Microbiol Rev 42

Goddard MR, Greig D (2015) Saccharomyces cerevisiae: a nomadic yeast with no niche?. FEMS Yeast Res 15

Hagiwara D, Suzuki S, Kamei K, Gonoi T, Kawamoto S (2014) The role of AtfA and HOG MAPK pathway in stress tolerance in conidia of Aspergillus fumigatus. Fungal Genet Biol 73:138–149

Hagiwara D, Takahashi H, Kusuya Y, Kawamoto S, Kamei K, Gonoi T (2016) Comparative transcriptome analysis revealing dormant conidia and germination associated genes in Aspergillus species: an essential role for AtfA in conidial dormancy. BMC Genomics 17:358

Hu S, Furst P, Hamer D (1990) The DNA and Cu binding functions of ACE1 are interdigitated within a single domain. New Biol 2:544–555

Jahn B, Boukhallouk F, Lotz J, Langfelder K, Wanner G, Brakhage AA (2000) Interaction of human phagocytes with pigmentless Aspergillus conidia. Infect Immun 68:3736–3739

Jensen LT, Howard WR, Strain JJ, Winge DR, Culotta VC (1996) Enhanced effectiveness of copper ion buffering by CUP1 metallothionein compared with CRS5 metallothionein in Saccharomyces cerevisiae. J Biol Chem 271:18514–18519

Jiang J, Nadas IA, Kim MA, Franz KJ (2005) A Mets motif peptide found in copper transport proteins selectively binds Cu(I) with methionine-only coordination. Inorg Chem 44:9787–9794

Judet-Correia D, Charpentier C, Bensoussan M, Dantigny P (2011) Modelling the inhibitory effect of copper sulfate on the growth of Penicillium expansum and Botrytis cinerea. Lett Appl Microbiol 53:558–564

Keller G, Bird A, Winge DR (2005) Independent metalloregulation of Ace1 and Mac1 in Saccharomyces cerevisiae. Eukaryot Cell 4:1863–1871

Kusuya Y, Hagiwara D, Sakai K, Yaguchi T, Gonoi T, Takahashi H (2017) Transcription factor Afmac1 controls copper import machinery in Aspergillus fumigatus. Curr Genet 63:777–789

Ladomersky E, Petris MJ (2015) Copper tolerance and virulence in bacteria. Metallomics. 7:957–964

Lopez-Cruz J, Oscar CS, Emma FC, Pilar GA, Carmen GB (2017) Absence of Cu-Zn superoxide dismutase BCSOD1 reduces Botrytis cinerea virulence in Arabidopsis and tomato plants, revealing interplay among reactive oxygen species, callose and signalling pathways. Mol Plant Pathol 18:16–31

Lutsenko S (2010) Human copper homeostasis: a network of interconnected pathways. Curr Opin Chem Biol 14:211–217

Lutsenko S, Barnes NL, Bartee MY, Dmitriev OY (2007) Function and regulation of human copper-transporting ATPases. Physiol Rev 87:1011–1046

Macomber L, Imlay JA (2009) The iron-sulfur clusters of dehydratases are primary intracellular targets of copper toxicity. Proc Natl Acad Sci U S A 106:8344–8349

Marvin ME, Mason RP, Cashmore AM (2004) The CaCTR1 gene is required for high-affinity iron uptake and is transcriptionally controlled by a copper-sensing transactivator encoded by CaMAC1. Microbiology 150:2197–2208

Narasipura SD, Chaturvedi V, Chaturvedi S (2005) Characterization of Cryptococcus neoformans variety gattii SOD2 reveals distinct roles of the two superoxide dismutases in fungal biology and virulence. Mol Microbiol 55:1782–1800

Nevitt T, Ohrvik H, Thiele DJ (2012) Charting the travels of copper in eukaryotes from yeast to mammals. Biochim Biophys Acta 1823:1580–1593

Palmgren MG, Nissen P (2011) P-type ATPases. Annu Rev Biophys 40:243–266

Park YS, Kang S, Seo H, Yun CW (2018) A copper transcription factor, AfMac1, regulates both iron and copper homeostasis in the opportunistic fungal pathogen Aspergillus fumigatus. Biochem J 475:2831–2845

Park YS, Kim TH, Yun CW (2017) Functional characterization of the copper transcription factor AfMac1 from Aspergillus fumigatus. Biochem J 474:2365–2378

Park YS, Lian H, Chang M, Kang CM, Yun CW (2014) Identification of high-affinity copper transporters in Aspergillus fumigatus. Fungal Genet Biol 73:29–38

Pase L, Voskoboinik I, Greenough M, Camakaris J (2004) Copper stimulates trafficking of a distinct pool of the Menkes copper ATPase (ATP7A) to the plasma membrane and diverts it into a rapid recycling pool. Biochem J 378:1031–1037

Pereira SL, Alves de CP, Dos Reis TF, Paziani MH, Von Zeska Kress MR, Riano-Pachon DM, Hagiwara D, Ries LN, Brown NA, Goldman GH (2017) Genome-wide transcriptome analysis of Aspergillus fumigatus exposed to osmotic stress reveals regulators of osmotic and cell wall stresses that are SakA(HOG1) and MpkC dependent. Cell Microbiol 19:e12681

Petris MJ (2004) The SLC31 (Ctr) copper transporter family. Pflugers Arch 447:752–755

Pihet M, Vandeputte P, Tronchin G, Renier G, Saulnier P, Georgeault S, Mallet R, Chabasse D, Symoens F, Bouchara JP (2009) Melanin is an essential component for the integrity of the cell wall of Aspergillus fumigatus conidia. BMC Microbiol 9:177

Puig S, Lee J, Lau M, Thiele DJ (2002) Biochemical and genetic analyses of yeast and human high affinity copper transporters suggest a conserved mechanism for copper uptake. J Biol Chem 277:26021–26030

Rees EM, Lee J, Thiele DJ (2004) Mobilization of intracellular copper stores by the ctr2 vacuolar copper transporter. J Biol Chem 279:54221–54229

Riggle PJ, Kumamoto CA (2000) Role of a Candida albicans P1-type ATPase in resistance to copper and silver ion toxicity. J Bacteriol 182:4899–4905

Rossi FR, Krapp AR, Bisaro F, Maiale SJ, Pieckenstain FL, Carrillo N (2017) Reactive oxygen species generated in chloroplasts contribute to tobacco leaf infection by the necrotrophic fungus Botrytis cinerea. Plant J 92:761–773

Saitoh Y, Izumitsu K, Morita A, Tanaka C (2010) A copper-transporting ATPase BcCCC2 is necessary for pathogenicity of Botrytis cinerea. Mol Gen Genomics 284:33–43

Smith AD, Logeman BL, Thiele DJ (2017) Copper acquisition and utilization in Fungi. Annu Rev Microbiol 71:597–623

Sugui JA, Kim HS, Zarember KA, Chang YC, Gallin JI, Nierman WC, Kwon-Chung KJ (2008) Genes differentially expressed in conidia and hyphae of Aspergillus fumigatus upon exposure to human neutrophils. PLoS One 3:e2655

Suzuki M, Gitlin JD (1999) Intracellular localization of the Menkes and Wilson's disease proteins and their role in intracellular copper transport. Pediatr Int 41:436–442

Upadhyay S, Torres G, Lin X (2013) Laccases involved in 1,8-dihydroxynaphthalene melanin biosynthesis in Aspergillus fumigatus are regulated by developmental factors and copper homeostasis. Eukaryot Cell 12:1641–1652

van Kan JA (2006) Licensed to kill: the lifestyle of a necrotrophic plant pathogen. Trends Plant Sci 11:247–253

Weissman Z, Berdicevsky I, Cavari BZ, Kornitzer D (2000) The high copper tolerance of Candida albicans is mediated by a P-type ATPase. Proc Natl Acad Sci U S A 97:3520–3525

Wiemann P, Perevitsky A, Lim FY, Shadkchan Y, Knox BP, Landero Figueora JA, Choera T, Niu M, Steinberger AJ, Wuthrich M, Idol RA, Klein BS, Dinauer MC, Huttenlocher A, Osherov N, Keller NP (2017) Aspergillus fumigatus copper export machinery and reactive oxygen intermediate defense counter host copper-mediated oxidative antimicrobial offense. Cell Rep 19:2174–2176

Yang K, Shadkchan Y, Tannous J, Landero Figueroa JA, Wiemann P, Osherov N, Wang S, Keller NP (2018) Contribution of ATPase copper transporters in animal but not plant virulence of the crossover pathogen Aspergillus flavus. Virulence. 9:1273–1286

Zhang P, Zhang D, Zhao X, Wei D, Wang Y, Zhu X (2016) Effects of CTR4 deletion on virulence and stress response in Cryptococcus neoformans. Antonie Van Leeuwenhoek 109:1081–1090